Architecture of the Spore Envelope – Germination and Outgrowth in *Clostridium sporogenes*

By Hannah Fisher

Submitted for the degree of Doctor of Philosophy

School of Biosciences

The University of Sheffield, United Kingdom

September 2022

Abstract

Clostridium botulinum is an anaerobic spore-forming bacterium that produces a potent neurotoxin causing botulism. It poses a significant concern to the food industry and is considered a bioterrorism threat. *Clostridium sporogenes* is widely used as a surrogate for the study of Group I *C. botulinum*. The production of highly resilient dormant spores and their subsequent germination is important for transmission and survival, particularly through aerobic environments.

The outermost layer of the spore, the exosporium, is the first point of contact between the spore and the environment. It is composed of a para-crystalline basal layer decorated with a hairy nap. A variety of proteins are associated with the exosporium, including cysteine-rich proteins, CsxA, CsxB, and CsxC, and collagen-like proteins, BclA and BclB. CsxA is a major structural component of the exosporium, however, the roles of the other proteins remain unknown. The exosporium is thought to modulate the germination process. Germinant molecules trigger a dramatic morphological change within the spore resulting in vegetative cell emergence. Despite the importance of this transition our understanding remains limited.

The work described in this thesis aimed to characterise the process of germination and outgrowth in *C. sporogenes* and understand the structural and functional roles of exosporium associated proteins.

Through the use of microscopy techniques we observed the morphological changes that underpin the transition from dormant spore to vegetative cell. This included swelling of the spore body which was coupled with cortex expansion. It also revealed the presence of striations within the cortex that could facilitate polar cell emergence.

Generation of exosporium mutants enabled the potential role of CsxC in parasporal layer formation to be elucidated using ultrastructural analysis and electron crystallography. AFM showed that BclA was a major constituent of the hairy nap.

Furthermore, the exosporium was not essential for germination or heat tolerance of *C. sporogenes* spores. However, the lack of individual exosporium associated proteins was shown to modulate the germination process. Overall these findings led to the development of a model for the ultrastructural changes that accompany the germination and outgrowth process in *C. sporogenes*.

Acknowledgements

It is safe to say that this thesis would not have been possible without the support of a huge number of people. First of all I would like to thank my supervisors, Prof. Per Bullough and Dr. Robert Fagan, for the opportunity to discover the world of bacterial spores and electron microscopy. Your advice and support has been invaluable throughout this project. I would also like to thank the BBSRC for funding this project.

A huge thanks must also go to Svet Tzokov for all the training and assistance in all aspects of electron microscopy and to Chris Hill for all his help with chemical fixation and thin sectioning. I would also like to thank Nic Mullin (University of Sheffield, UK) for conducting the AFM research.

A special thanks goes to Ainhoa Dafis-Sagarmendi for all your help with image processing and laying down a lot of the groundwork for this project. I am very grateful to Jason Wilson for his continuous support and willingness to help, especially when it came to troubleshooting computer problems. A huge thank you goes to (Dr) Joe Kirk for teaching me all things molecular biology but most importantly for his constant support, friendship, and provision of many laughs. A massive thank you also goes to Laurence de Lussy-Kubisa for being an excellent shift buddy during covid and providing me with fantastic science and life advice, particularly over this writing up period. Jessie Davis and Becky Menday, I genuinely don't know what I would have done without you two, especially in these last few months. Thank you for all your support, encouragement and therapeutic climbing sessions. Thank you also to Jess Buddle for all her help and enthusiasm and to Shauna O'Beirne for always being a listening ear.

On a more personal note I would like to say a huge thank you to my parents for always being there for me no matter what hour of the day and for supporting me and encouraging me in everything that I do. Likewise to Rebecca, thank you for all your sound sisterly advise and for always finding a way to make me laugh! And to Katy, thank you for your constant friendship over so many years, I am extremely grateful for all the support, advice, and encouragement you have provided through the numerous highs and lows.

Last, but definitely not least, to James. I am immensely thankful for your continuous support and patience with me, particularly over the last 4 years. There have been many ups, downs and changes over the years but you have always been there to remind me of what was truly important. I am forever grateful.

Abbreviations

2D	Two-dimensional
3D	Three-dimensional
Å	Angstrom
AFM	Atomic Force Microscopy
ATCC	American type culture collection
BHI	Brain Heart Infusion
BSA	Bovine Serum Albumin
CEMOVIS	Cryo-electron microscopy of vitreous sections
CFU	Colony forming units
CTF	Contrast transfer function
Cryo-EM	Cryogenic electron microscopy
Cryo-ET	Cryogenic electron tomography
Cryo FIB-ET	Cryogenic focused ion beam milling and electron tomography
DMSO	Dimethyl sulphoxide
DPA	Dipicolinic acid
EC	Electron crystallography
EDTA	Ethylenediaminetetraacetic acid
EM	Electron microscopy
ET	Electron tomography
gDNA	Genomic DNA
HPF	High pressure freezing
LB	Luria-Bertani broth
FT	Fourier transform
FFT	Fast Fourier transform
GUI	Graphical user interface
IPTG	Isopropyl-beta-D-thiogalactoside
IQ	Signal to noise ratio representation (Henderson et al. 1986)
kDa	Kilodalton
keV	Kiloelectron volts
NAM	N-acetyl muramic acid

NAG	N-acetyl glucosamine
NCIMB	National Collection of Industrial, Food and Marine Bacteria
NEB	New England Biolabs
OD	Optical density
O/N	Overnight
PBS	Phosphate buffered saline
PCR	Polymerase chain reaction
PLG	Phase lock gel tube
RT	Room temperature
SASP	Small acid-soluble proteins
SDS	Sodium dodecyl sulphate
SDS-PAGE	Sodium dodecyl sulphate polyacrylamide gel electrophoresis
SEM	Scanning electron microscopy
SIRT	Simultaneous iterative reconstruction technique
SNR	Signal to noise ratio
SOC	Superoptimal broth with catabolite repression
TBS	Tris buffer saline
TEM	Transmission electron microscopy
TGY	Tryptose Glucose Yeast extract
TY	Tryptose Yeast extract
Tris	Tris (hydroxymethyl) aminomethane
UA, UF	Uranyl Acetate/Formate
w/v, v/v	Weight/Volume, Volume/Volume
WBP	Weighted back projection
WT	Wild type

Contents

Table of Figures

Table of Tables

Table of Movies

Movie 3.1: Timelapse of *C. sporogenes* Germination (Scale bar 6 µm)

Movie 3.2: Tomogram of a Germinating *C. sporogenes* Spore 2 h Post Germination Initiation (Scale bar 200 nm)

Movie 3.3: Tomogram of *C. sporogenes* Spore Shell Post Germination (Scale bar 200 nm)

1 Introduction

1.1 Clostridia and Bacilli

1.1.1 General Introduction to Clostridia and Bacilli

The Clostridia and Bacilli are Gram-positive rod-shaped bacteria of which many species are pathogenic including *Clostridium botulinum*, *Clostridioides difficile* and *Bacillus anthracis*. Bacillus species often reside in soils and are generally aerobic bacteria but can also be facultative anaerobes. Clostridia on the other hand are obligate anaerobes and are found to reside in anaerobic environments such as the mammalian intestinal tracts. What links these two genera of bacteria in the phylum *Firmicutes* is their ability to produce endospores. Endospores are morphologically distinct from vegetative cells and are extremely robust as well as metabolically dormant. In the case of pathogenic species endospores are the primary infectious agent and can persist in the environment for prolonged periods of time. To date, the majority of research on endospores has been carried out in Bacillus species, mainly *Bacillus subtilis*. Although many parallels exist between *B. subtilis* and Clostridia it is becoming increasingly clear that there are significant differences between them.

1.1.2 *Clostridium botulinum* and *Clostridium sporogenes*

C. botulinum is a dangerous pathogen capable of producing the most potent neurotoxin known, of which just 30-100 ng can be fatal to humans (Peck 2009). The neurotoxins block acetylcholine transmission in neurons, leading to floppy paralysis known as botulism (Brunt et al. 2014). The most common forms of human botulism are foodborne, infant, and wound botulism. Foodborne botulism is caused by consumption of the neurotoxin in food that has been contaminated with germinated

endospores, whilst infant and wound botulism are caused by ingestion or wound contamination with *C. botulinum* endospores that subsequently germinate and grow to produce neurotoxin within the gut or deep wound (Peck, Stringer, and Carter 2011). All these forms of botulism are caused by strains of Group 1 *C. botulinum* that produce one (or multiple) of type A, B, F or H neurotoxin (Brunt et al. 2014). Since *C. botulinum* has the ability to produce potent neurotoxins and is relatively easy to produce, it is considered a bioterrorism threat (Olguín-Araneda et al. 2015). Due to the risk level posed by *C. botulinum* it is rarely used in the laboratory. Instead, *Clostridium sporogenes* is used as a surrogate for Group 1 *C. botulinum*. It has been found to have similarity both physiologically and phylogenetically (Ihekwaba et al. 2016), but importantly, does not produce the potent neurotoxin.

C. sporogenes itself is a major cause of food spoilage, especially in vacuum packed meat and dairy products (Lorenzo et al. 2018). The eradication of endospores from food products poses a significant and costly challenge for the food industry. On a more positive note, *C. sporogenes* endospores are being considered as a potential vector for delivering drugs to tumour cells for cancer treatment due to its ability to survive in low oxygen environments such as those found within tumours (Nuyts et al. 2002). A better understanding of their germination process could also facilitate developments in this application.

1.2 Endospores

Endospores (spores) are most commonly produced under harsh conditions such as nutrient limitation, but they can also be produced stochastically. Spores are formed by vegetive cells differentiating in a process known as sporulation resulting in the formation of a metabolically dormant and highly resistant spore. Spores can remain dormant yet viable in the environment for hundreds of years and this is mainly due to their multi-layered structure. Each layer within a spore contributes to its ability to survive in harsh conditions and plays an important role in longevity.

1.2.1 Sporulation

Sporulation is a dynamic and tightly regulated process (Fig: 1.1) initiated by Spo0A activation (Stage I) and involves the asymmetric division of a cell to form the mother cell and the forespore (Stage II). The forespore is subsequently engulfed by the mother cell (Stage III) where assembly of the spore outer layers is co-ordinated (Stages IV-V) resulting in the assembly of a highly ordered mature spore (Stage VI). This is released from the mother cell into the environment (Stage VII). Sporulation is controlled across the mother cell and forespore by a cascade of events involving a multitude of sigma factors, transcription factors, proteases and phosphatases. Most of our understanding of the sporulation process comes from *B. subtilis* (Piggot and Hilbert 2004), however, studies conducted in species of Clostridia have revealed both similarities and differences, not only between *B. subtilis* and Clostridia, but also between individual Clostridia species (Al-Hinai, Jones, and Papoutsakis 2015). The key regulators include: Spo0A, σ^H, σ^F, σ^E, σ^G, and σ^K.
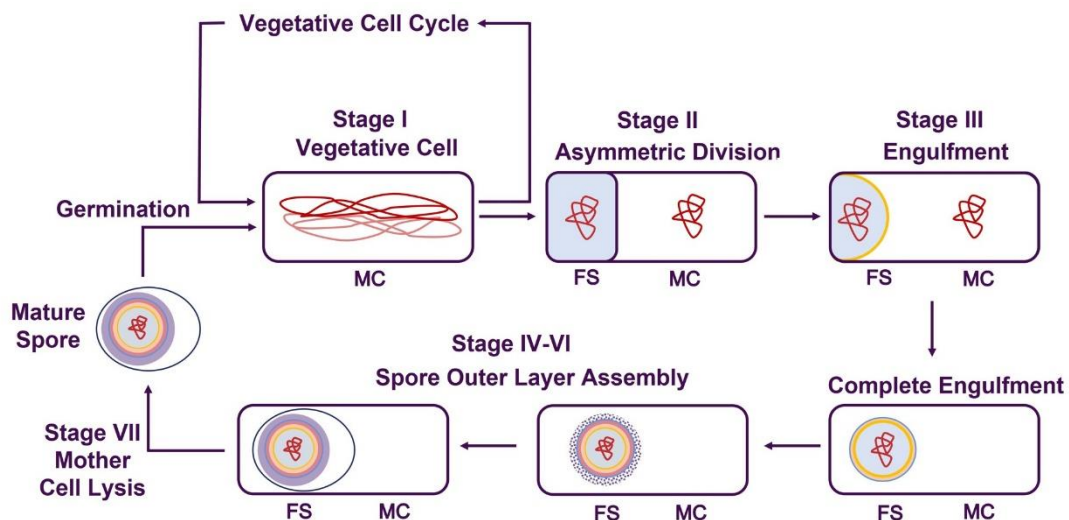
Figure 1.1: The Sporulation Process

Vegetative cells undergo the normal vegetative cycle until encountering conditions of stress which triggers the sporulation process. This begins with the replication of the genome (Stage I) and the asymmetric cell division of a vegetative cell to form a mother cell (MC) and a forespore (FS)(Stage II). Following the translocation of the forespore chromosome the mother cell engulfs the forespore (Stage III). Once within the mother cell the outer layers of the spore are assembled (Stages IV-VI), and, once complete, the mother cell lyses releasing the mature spore into the environment (Stage VII). Under favourable conditions the spore will then germinate to give rise to a vegetative cell.

Stage I – Sporulation Initiation

Sporulation is initiated by the activation of the transcription factor Spo0A. In *B. subtilis* this is activated by an elaborate phosphorelay system that results in the phosphorylation of Spo0A and the initiation of sporulation (Piggot and Hilbert 2004). In some Clostridia histidine kinases have been identified that directly phosphorylate Spo0A triggering the sporulation process (Al-Hinai et al. 2015). Additionally, in *C. botulinum*, σ^K has been implicated in the activation of Spo0A in addition to its later role in co-ordinating spore maturation (Kirk et al. 2012). It has been estimated that Spo0A regulates around 121 genes including those encoding the sigma factors σ^F and σ^E located within the forespore and mother cell respectively (Piggot and Hilbert 2004).

Stage II – Asymmetric Division

Asymmetric cell division involves the formation of a polar septum resulting in a mother cell and a smaller forespore. Polar septum formation is under the control of Spo0A and involves a relocalisation of the machinery used in vegetative septum formation (Khanna, Lopez-Garrido, and Pogliano 2020). FtsZ filaments form a Z-ring which facilitates the septum formation (Bisson-Filho et al. 2017). Cryo electron tomography (Cryo-ET) showed that the polar septum is approximately half the thickness of vegetative septum and that this correlates with there being half the number of FtsZ filaments present at the division site (Khanna et al. 2021).

Prior to asymmetric division the chromosome is replicated and adopts an elongated structure termed an axial filament that runs from pole to pole within the cell (Khanna et al. 2020). Upon septum formation 30% of the chromosome is located within the forespore and the remaining 70% within the mother cell (Wu and Errington 1994, 1998). The remainder of the chromosome is translocated into the forespore by a SpoIIIE complex that assembles at the midpoint of the septum

4

and uses ATP hydrolysis to actively transport the chromosome from the mother cell into the forespore (Khanna et al. 2020). This process causes an increase in the osmotic pressure within the forespore resulting in a swelling and reshaping of the forespore to form an ovoid (Lopez-Garrido et al. 2018).

After the establishment of the forespore and mother cell, compartment specific transcription occurs regulated by σ^F (forespore) and σ^E (mother cell). σ^E is thought to regulate up to 253 genes some of which are vital for forespore engulfment (Al-Hinai et al. 2015). In *C. botulinum* σ^F has also been implicated in regulating the asymmetric division process, with thin sections of σ^F mutants showing sporulating cells blocked at stage II (Kirk et al. 2014).

Stage III – Engulfment

Following asymmetric cell division, the mother cell engulfs the forespore in a process akin to phagocytosis, encapsulating the forespore in a second (outer) membrane. The entire process of engulfment in *B. subtilis* has recently been observed in unprecedented detail through the use of cryo focused ion beam milling and electron tomography (Cryo FIB-ET), revealing ultrastructural changes occurring within the sporangium (Khanna et al. 2019). Engulfment begins with the enlargement of the forespore, which stretches the septum and bends it towards the mother cell (Khanna et al. 2019). The leading edges of the mother cell membrane then migrate around the edges of the forespore towards the tip, forming small finger-like projections (Khanna et al. 2019). This process relies heavily on peptidoglycan remodelling machinery regulated by both the mother cell (σ^E) and the forespore (σ^F). Peptidoglycan degradation is mostly carried out by the mother cell regulated protein complex whilst peptidoglycan synthesis is likely to be carried out by the forespore biosynthetic machinery found at the leading edge of the engulfing membrane (Khanna et al. 2020).

Eventually the leading edges of the mother cell membrane meet at the tip of the forespore and fuse, releasing the forespore into the cytoplasm of the mother cell. This process, termed engulfment membrane fission, is facilitated by the σ^E regulated FisB protein and is also thought to be reliant on SpoIIIE, although the role of SpoIIIE is poorly understood (Khanna et al. 2020).

Stage IV-VI – Spore Maturation

The latter stages of sporulation are focused around developing a mature spore capable of maintaining dormancy and withstanding harsh conditions. This involves the assembly of the proteinaceous coat and exosporium (species specific), as well as the formation of the cortex, a modified peptidoglycan layer, and the dehydration of the spore core.

The maturation process is coordinated by σ^G (forespore) and σ^K (mother cell). The mother cell is responsible for the assembly of spore coat proteins and exosporium (species specific) and is coordinated by σ^K (Al-Hinai et al. 2015; Piggot and Hilbert 2004). σ^K also regulates the production of DPA required for spore core dehydration which is transported into the core in a process coordinated by σ^G (Piggot and Hilbert 2004).

Stage VII – Mother Cell Lysis

The final stage of sporulation involves mother cell lysis which releases the mature spore into the environment where the spore will remain dormant until conditions are appropriate for germination.

1.3 Spore Architecture and Function

Spores are complex structures made up of many layers all of which play key roles in making the spores highly robust and providing protection against environmental insults. They do this whilst also maintaining the ability of the spores to detect key molecules crucial for triggering the germination process. The general spore architecture is maintained across Bacilli and Clostridia and includes membranes, polysaccharide layers, a proteinaceous coat and in some cases an exosporium (Fig: 1.2).
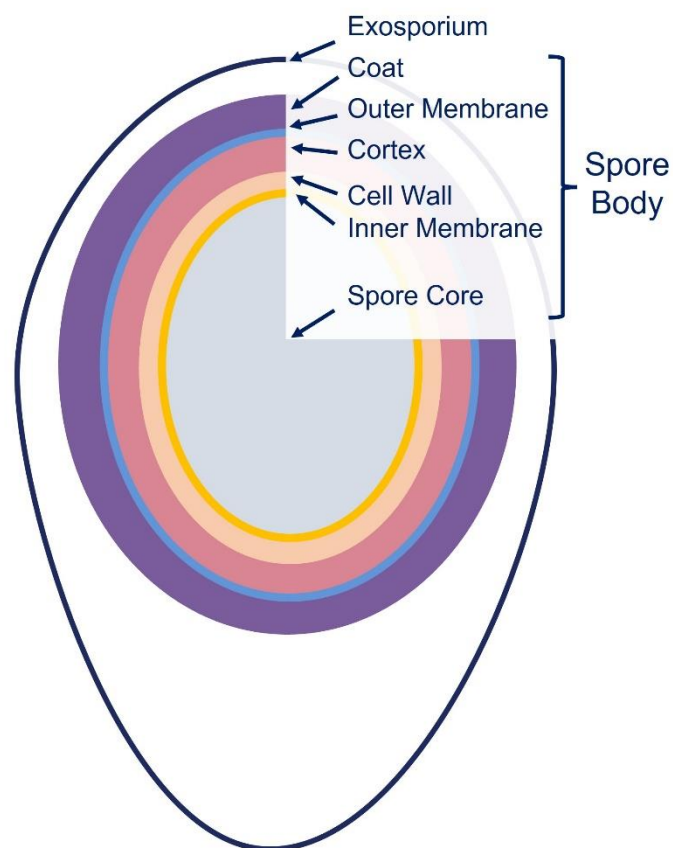
Figure 1.2: General Spore Architecture

In the centre of the spore is the spore core containing the spore DNA. This is surrounded by an inner membrane and two peptidoglycan layers, the cell wall and the chemically distinct cortex. The outer membrane separates the cortex from the multi-layered proteinaceous spore coat. Together these layers compose the spore body. In some species the spore body is surrounded be a baggy exosporium separated from the spore coat by an interspace region.

1.3.1 Core

The spore core is the innermost structure of the dormant spore and houses the chromosome, ribosomes and many proteins vital for the propagation of a new vegetative cell. The water content of the core is extremely low due to high levels of DPA in complex with Ca^{2+} cations (~25% of spore core dry weight)(Setlow 2006, 2007). The low water content is important in providing wet heat resistance. DPA has also been shown to have key roles in dry heat resistance and in protecting against loss of spore viability due to DNA damage during desiccation (Setlow et al. 2006). DPA is rapidly released during germination to allow for the rehydration of the spore core (Setlow 2006). α/β-type SASPs saturate spore DNA and are a major factor contributing to the UV resistance of the spores (Setlow 2007). Binding of SASPs to the DNA changes the UV photochemistry protecting against UV induced DNA damage in the form of mutations (Setlow 2007).

1.3.2 Inner Membrane

The inner membrane surrounds the spore core and is compositionally very similar to that of a vegetative cell membrane (Cortezzo and Setlow 2005). However, the lipids of the membrane are largely immobile which means the passive permeability of the membrane is extremely low, even to small molecules such as water and methylamine (Cowan et al. 2004; Setlow 2006). This is important in the spore's resistance to chemicals as well as preserving the low water content of the spore core and maintaining dormancy. In many species of Bacilli and Clostridia the inner membrane also houses the germinant receptors crucial for triggering the germination process (Barlass et al. 2002; Brunt et al. 2014; Moir, Corfe, and Behravan 2002; Setlow 2014) along with SpoVA thought to be a channel through which DPA is released (Vepachedu and Setlow 2007).

During the germination process the inner membrane rapidly expands in size to accommodate the rehydration of the spore core. Cryo-electron microscopy of vitreous sections (CEMOVIS) of *B. subtilis* spores revealed the presence of membrane reservoirs within the spore core (Laue et al. 2018). These are thought to insert into the plasma membrane during the early stages of germination allowing the expansion of the spore core. Similar structures have also been observed in *C. difficile* and *C. botulinum* (Laue et al. 2018)*.*

1.3.3   Cell Wall, Cortex and Outer Membrane

The cell wall and the cortex are composed of peptidoglycan and are contained between the inner and outer spore membranes. The cell wall has the same chemical structure as that of a vegetative cell consisting of alternating N-acetyl glucosamine (NAG) and N-acetyl muramic acid (NAM) residues and is heavily crosslinked via peptide stems attached to the NAM residues (Meador-Parton and Popham 2000; Popham 2002). The cell wall is not thought to have any specific role in spore resistance but instead seems to play a major role in maintaining the integrity of the cell after germination and serving as a template for new cell wall production during outgrowth (Atrih and Foster 1999; Popham 2002; Setlow 2006).

Unlike the cell wall, the cortex has been implicated in spore heat resistance as well as maintaining dormancy. Heat resistance and dormancy are linked to the water content of the core and it is thought that the cortex plays a role in maintaining core dehydration. It does this by applying directed pressure on the spore core, particularly during sporulation, allowing the efflux of water and the accumulation of DPA in the spore core, thereby maintaining a dehydrated state within the core (Warth 1978). The cortex peptidoglycan is chemically distinct from the cell wall in several ways; almost 50% of the muramic acid residues are converted to muramic-δ-lactam, approximately 25% of

N-acetylmuramic acid peptide side chains are replaced with atypical short peptides resulting in less crosslinking, and roughly 20% of N-acetyl muramic acid residues have a single L-alanine residue (Atrih and Foster 1999). Although the chemical modifications are not thought to directly contribute to the resistance properties of the spore, they are crucial for programmed hydrolysis of the cortex during germination. More specifically the δ-lactam residues are thought to act as substrates for cortex lytic enzymes activated during the early stages of germination, allowing targeted degradation of the cortex without compromising the underlying cell wall.

The outer membrane surrounds the cortex layer and is essential for spore formation although it is thought to have very little role in spore resistance. There have been suggestions that the outer membrane may contain pigments contributing to the UV resistance of spores (Khaneja et al. 2010).

1.3.4   Coat

1.3.4.1 Coat Structure and Assembly

The proteinaceous spore coat is composed of an abundance of proteins that are highly crosslinked and form distinct layers surrounding the inner layers of the spore. In some species, such as *B. subtilis*, the coat forms the outermost layer of the spore. The spore coat is thought to contain 30% of total spore proteins with over 70 coat proteins having been identified in *B. subtilis* (Henriques and Moran, Jr. 2007). At least 50 of these proteins are found in other Bacillus species, however, only 20 have been found to have homologues in Clostridia (Henriques and Moran, Jr. 2007). The diversity in coat proteins across species is likely to reflect species specific adaptations and account for the varying coat structures observed in thin sectioning (Driks and Eichenberger 2016). In *B. subtilis* three distinct layers were seen, including an undercoat that likely bridges the gap between the cortex and the coat, an inner coat, and a thick electron dense outer coat (Henriques and Moran, Jr. 2007). Thin

sectioning data from *C. sporogenes* suggests that the coat is composed of just two well defined layers, the inner and outer coat (Brunt et al., 2015; Dafis-Sagarmendi, 2021; Hoeniger and Headley, 1969; Panessa-Warren et al., 1994; 1997). The *C. sporogenes* spore coat has not been well characterised but homologues of some Bacillus coat proteins have been identified suggesting some similarity between the genera (Janganan et al. 2016).

2D electron crystallography of fragments from the outer layers of *B. cereus* and *B. thuringiensis* spores identified a crystal type that could correspond to an outer coat layer (Ball et al. 2008). It was composed of an assembly of hexagonal rings with *p6* symmetry that formed a 'pitted layer' with a central pore that was ~60Å in diameter (Ball et al., 2008). Likewise, in *B. subtilis*, a similar structure is observed when the cysteine rich coat protein CotY is over expressed in *E. coli* where it self-assembles to form a hexagonal crystalline array (Jiang et al. 2015).

The assembly of the spore coat spans a considerable amount of the sporulation period and is exclusively co-ordinated by the mother cell. The expression of 50% of the spore coat proteins in *B. subtilis* is under the control of σ^E, which is active shortly after asymmetric division within the mother cell (Driks and Eichenberger 2016). This includes the protein SpoIVA which is essential for spore coat formation and is conserved across Bacilli and Clostridia (Henriques and Moran, Jr. 2007). Most of the σ^E-regulated proteins are involved in the initialisation of coat assembly and the formation of the inner coat layers. A further 75 proteins are regulated by σ^K and therefore expressed later in sporulation (Driks and Eichenberger 2016; Henriques and Moran, Jr. 2007). The majority of these proteins compose the outer layers of the spore coat. However, some contribute to the maturation of the inner coat by either carrying out modifications to already assembled proteins or providing an additional structural role (Henriques and Moran, Jr. 2007). Once assembled, the spore coat undergoes an extensive maturation period during which a variety of post-translational modifications

are carried out such as crosslinking, glycosylation and proteolytic processing (Henriques and Moran 2000).

1.3.4.2 Coat Function

The multi-layered nature of the coat is thought to act as a physical barrier that to some extent passively excludes degradative enzymes, such as lysozyme, as well as toxic molecules (Driks and Eichenberger 2016; Henriques and Moran, Jr. 2007). However, the coat is not completely impermeable as it must also allow for the passage of germinant molecules into the spore. The presence of catalases within the coat also suggests that the coat plays an active role in detoxifying oxidative compounds (Driks and Eichenberger 2016; Henriques and Moran, Jr. 2007).

The coat is also thought to have a role in modulating the germination process. GerP is thought to reside within the coat and facilitate the passage of germinant molecules into the inner layers of the spore (Driks and Eichenberger 2016). However, the exact mechanism by which this occurs has yet to be determined. In addition, the cortex hydrolysis enzyme, CwlJ, is present within the inner coat of *B. subtilis* and thought to remain there until required during the germination process (Driks and Eichenberger 2016). Alanine racemases have also been found in association with the spore coat in *B. subtilis* which may be involved in the conversion of the germinant molecule L-alanine to D-alanine thereby delaying the germination process. Although this role has been seen for exosporium associated alanine racemase in *B. anthracis* (Chesnokova et al. 2009) it has not been confirmed for coat associated racemases.

It has further been suggested that the coat plays a role in adapting to changes in humidity (Driks 2003). Folds in the spore coat are thought to allow for expansion of the spore cortex during high

humidity conditions as well as allow for the expansion of the spore core during the early stages of germination (Driks 2003; Westphal et al. 2003).

1.3.5 Interspace

The interspace lies between the coat and the exosporium and is seen in thin sectioning data from many species across the Bacilli and Clostridia (Fig: 1.3A, B, and C) (Ball et al. 2008; Brunt et al. 2015; Dafis-Sagarmendi 2021; Ebersold et al. 1981; Hoeniger and Headley 1969; Portinha et al. 2022; Waller et al. 2004; Wehrli, Scherrer, and Kuebler 1980). The sectioning data revealed the presence of layers within the interspace in some species which have been termed 'parasporal layers'. In *B. thuringiensis* the layers are seen to stack forming distinct lamellae within the interspace (Fig: 1.3A) (Ebersold et al. 1981). Freeze-fracture studies demonstrated that these layers were in fact para-crystalline arrays (Ebersold et al. 1981; Wehrli et al. 1980). Electron crystallography conducted on fragments of the outer layers of *B. cereus* and *B. thuringiensis* revealed a crystal type proposed to correspond to the parasporal layers (Ball et al. 2008; Kailas et al. 2011). In both *C. sporogenes* (Dafis-Sagarmendi, 2021; Brunt et al., 2015; Hoeniger and Headley, 1969) and *C. botulinum* (Portinha et al. 2022; Stevenson, Vaughn, and Crisan 1972) parasporal layers have been observed within the interspace region. By electron crystallography of *C. sporogenes* a crystal type has been observed that could correspond to the parasporal layers (Dafis-Sagarmendi, 2021), however, composition and function remains unknown.
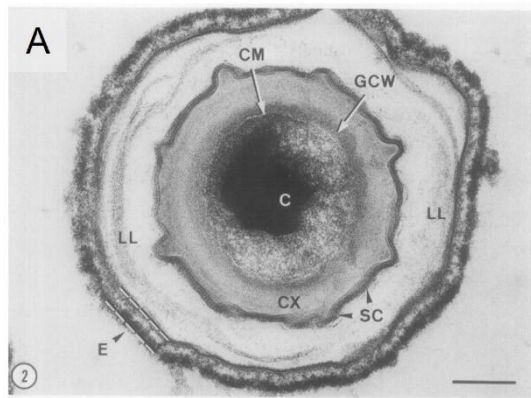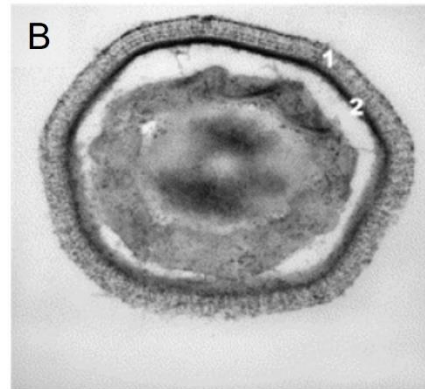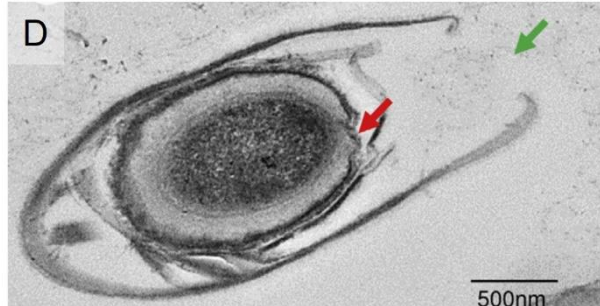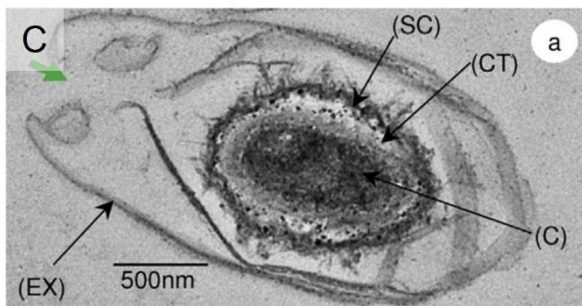
Figure 1.3: Thin Sections of Spores from Various Species of Bacilli and Clostridia

A) Thin section of a dormant *B. thuringiensis* spore. C – core, CM – cell membrane, GCW – germ cell wall, CX – cortex, SC – spore coat, LL – laminated layers, E – exosporium. Scale bar 160 nm. Reproduced with permission (Ebersold et al. 1981) B) Thin section of a dormant *B. anthracis* spore. 1 – hairy nap layer, 2 – exosporium basal layer. Reproduced with permission (Waller et al. 2004) C) *C. sporogenes* dormant spore. C – core, CT – cortex, SC – spore coat, Ex - exosporium. D) Germinating *C. sporogenes* spore. Green arrow shows opening in the exosporium pole. Pink arrow indicates coat disruption. Reproduced with permission (Brunt et al. 2015)

In *B. anthracis* it has been proposed that the interspace contains two distinct layers of

polysaccharide (Lehmann et al. 2022). An inner polysaccharide layer is thought to assemble around

the forespore during engulfment, prior to coat formation. The coat is assembled beneath this

polysaccharide layer. The outer polysaccharide layer accumulates at the mother cell-proximal pole

between the exosporium cap and the inner polysaccharide layer and is gradually distributed laterally

around the spore, guiding the formation of the exosporium around the spore body (Lehmann et al.

2022). These polysaccharide layers are thought to be degraded during the early stages of germination as an energy source for the developing cell. It is important to further note that parasporal layers have not been described within *B. anthracis* and how these would be assembled alongside the polysaccharide layers has not been investigated.

1.3.6   Exosporium

The exosporium is the outermost spore layer found in some species of Bacilli and Clostridia. This layer is not ubiquitous across all spore formers, for example it is not present in *B. subtilis* the organism that has been the primary focus of much spore research. Because of this there is limited knowledge on the structure and function of the exosporium layer.

As the first point of contact between the dormant spore and the environment or host, understanding the exosporium is essential. The interactions it makes are important for its role in surface adherence, protection, host cell interactions and germination (Henriques and Moran, Jr. 2007). Early studies of both Bacilli and Clostridia exosporium showed it to be composed of a basal layer with a honeycomb-like para-crystalline array (Gerhardt and Ribi 1964; Wehrli et al. 1980). In some species the basal layer is uniformly decorated with short filaments termed the hairy nap.

The majority of research into exosporium structure and assembly has been carried out within the *Bacillus cereus* group which includes *B. cereus*, *B. thuringiensis* and *B. anthracis*. More recently structural analysis of the *C. sporogenes* exosporium has revealed a similar structural nature between the species.

1.3.6.1 Exosporium within the *Bacillus cereus* group

Members of the *B. cereus* group possess a baggy exosporium that is often elongated at one pole and is separated from the coat layer by an interspace. Fragments of the outermost layers from these spores were analysed using electron crystallography which revealed the presence of three different crystal types (Ball et al. 2008). Types I, II and III were found in *B. cereus* and *B. thuringiensis* strains whilst just Types II and III in the *B. anthracis* strains (Ball et al. 2008). Type II crystal is common to all three species and corresponds to the basal layer of the exosporium, confirmed by the presence of the hairy nap on crystals from *B. cereus* seen by both EM and atomic force microscopy (AFM) (Ball et al. 2008; Kailas et al. 2011). The type II crystal is composed of a hexagonal array of crown like rings connected by threefold linkers with a unit cell $a = b = $ ~80 Å $\gamma = 120°$ and has phases consistent with *p6* symmetry (Ball et al. 2008; Kailas et al. 2011; Terry et al. 2017).

Type I and type III crystals are thought to correspond to layers deeper within the spore. Type I crystals found in *B. cereus* and *B. thuringiensis* are similar in structure to type II crystals however they have a smaller unit cell and phases consistent with *p3* symmetry (Ball et al. 2008; Kailas et al. 2011). This crystal is thought to make up a parasporal layer within the interspace of the spore (Ball et al. 2008). Type III crystal has a larger unit cell $a = b = $ ~100 Å and consists of a ring structure with *p6* symmetry. This crystal likely corresponds to an outer spore coat layer (Ball et al. 2008). A schematic showing the structures and locations of the different crystals can be seen in Figure 1.4.

The 3D reconstruction of the exosporium basal layer from both *B. thuringiensis* and *B. cereus* showed that the crown like rings are in fact enclosed to form a cup like structure on one side and a domed structure on the other (Ball et al. 2008). AFM of both *B. cereus* and *B. thuringiensis* 4D11 (a napless strain) revealed the domed structure to correspond to the interior surface whilst the concave cups form the exterior facing surface (Ball et al. 2008; Kailas et al. 2011). Threefold linkers or spokes are seen to connect these cups together, the likely location for the attachment of the hairy

16

nap (Kailas et al. 2011; Terry et al. 2017). Cryo-EM of type II crystal yielded an 8 Å resolution

projection map of the underlying crystal structure (Kailas et al. 2011). This clearly showed the central

ring, much like the crown-like structure seen previously in 3D reconstructions, and clear densities

were identified suggesting a partially α-helical subunit (Kailas et al. 2011). This was further

confirmed by the use of circular dichroism spectroscopy showing a 75% α-helical content for

exosporium fragments (Kailas et al. 2011). The 6 subunits that compose the central rings are

surrounded by six peripheral pores, approximately 20 Å in diameter, large enough for small

molecules such as germinants to enter but small enough that large degradative enzymes and

antibodies would be excluded (Ball et al. 2008; Kailas et al. 2011).
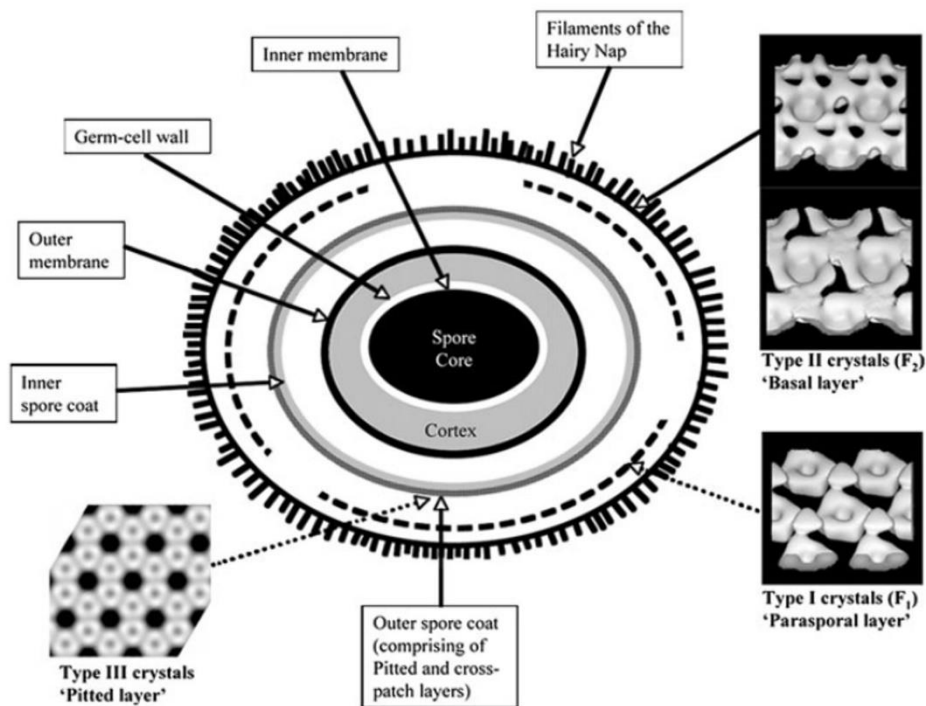
Figure 1.4: Proposed Crystalline Layer Locations Within the *B. cereus* Group Spores

Possible locations of Type I, Type II and Type III crystal lattices are indicated. Reproduced with
permission (Ball et al. 2008)

A large number of proteins associated with the exosporium of *B. cereus* group species have been

identified, including key structural proteins ExsY, CotY, BclA, BclB, ExsFA and ExsFB as well as

proteins likely to be adsorbed to the surface such as alanine racemase (Redmond et al. 2004; Todd

et al. 2003). ExsY and CotY are cysteine rich proteins and are homologues, sharing 90% amino acid sequence identity (Johnson et al. 2006). Mutagenesis studies in *B. cereus* showed that both CotY and ExsY play key roles in the formation of the exosporium (Johnson et al. 2006). Further to this, CotY has been implicated in forming the initial cap structure of the exosporium, from which the rest of the exosporium is rapidly assembled (Boone et al. 2018; Johnson et al. 2006). Heterologous expression of ExsY from *B. cereus* in *E. coli* yielded self-assembled 2D crystalline lattices with the same underlying crystal structure as that seen from native exosporium fragments (Terry et al. 2017). ExsY and CotY also have a 35% homology to the CotY coat crust protein in *B. subtilis*. Additionally, CotY from *B. subtilis* has also been shown to self-assemble when heterologously expressed in *E. coli* to form a structure not dissimilar to that of exosporium basal layer in the *B. cereus* group (Jiang et al. 2015). Taken together this suggests that despite low similarity there is likely a conserved assembly mechanism for not just exosporium proteins but also coat layers.

Both *B. cereus* and *B. anthracis* possess a hairy nap which is likely important for spore adhesion and surface interactions (Sylvestre, Couture-Tosi and Mock, 2002). The hairy nap is made up of glycosylated filaments of BclA and BclB proteins. The presence of BclA on the surface of *B. anthracis* has been associated with promoting spore persistence *in vivo* by mediating an immune inhibition mechanism (Wang et al. 2016). The BclA and BclB proteins are composed of a central collagen-like region containing ~70 GXX amino acid repeats and a C-terminal hydrophobic region (Sylvestre et al. 2002). The N-terminal of the Bcl proteins covalently binds ExsFA or ExsFB anchoring the protein to the exosporium layer (Kailas et al. 2011; Sylvestre, Couture-Tosi, and Mock 2005; Terry et al. 2017).

1.3.6.2 Exosporium of *C. sporogenes*

Much like the *Bacillus cereus* group discussed above, *C. sporogenes* possesses a baggy sac-like exosporium (Fig: 1.5A). Imaging by EM and AFM has revealed key structural details about the exosporium layer in *C. sporogenes*. Images show that the exosporium is extended at one pole of the

spore and that the outer surface appears uniformly covered in a hairy nap (Fig: 1.5) (Janganan et al.

2016). There are also several larger appendages including beaded fibrils that have beads at regular

70 nm intervals, intermediate fibrils, and a larger appendage approximately 20 nm in diameter and

up to 2 µm long (Fig: 1.5B)(Janganan et al. 2016). Whether the fibrils and the large appendages are

attached to the exosporium surface or emanate from deeper within the spore is unclear.
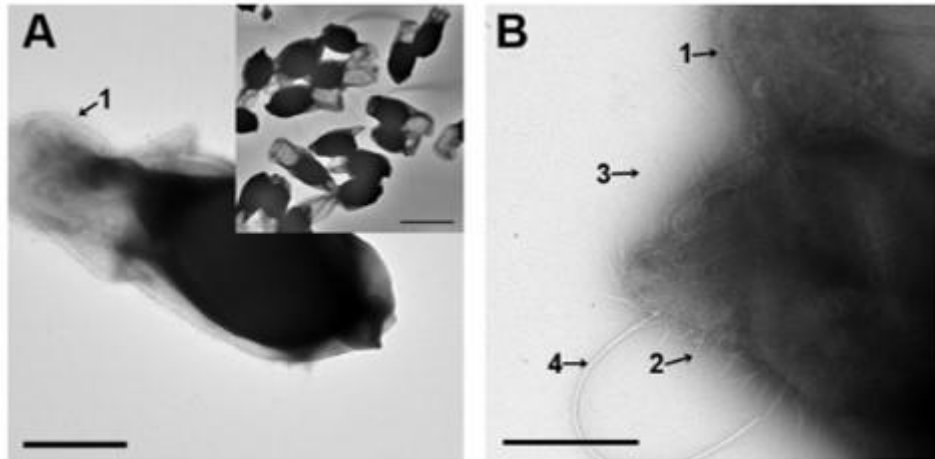
Figure 1.1: Negative Stain TEM of *C. sporogenes* Spores

A) *C. sporogenes* spore with an electron dense spore body with folded sac-like exosporium extended at one pole. Scale bar 0.5 µm. A hairy nap is present on the surface of the exosporium (arrow 1). Inlay shows a lower magnification view of spores. Scale bar 2 µm. B) High magnification of the exosporium surface edge showing various surface features. 1-hairy nap, 2-intermediate fibril; 3-beaded fibril, 4-large appendage. Scale bar 0.5 µm. Reproduced with permission (Janganan et al. 2016)

The proteins that compose or are associated with the exosporium layer were determined using mass

spectrometry of isolated exosporium fragments. The results indicated the presence of a number of

proteins including several cysteine rich proteins, CsxA, CsxB and CsxC, two proteins with collagen like

repeats, BclA and BclB (named by analogy not homology), and a variety of proteins containing

various enzymatic domains (Janganan et al. 2016). Homologues of the cysteine rich proteins have

been identified in other *C. sporogenes* strains as well as in Group I *C. botulinum*. A summary of these

proteins can be seen in table 1.1.

Table 1.1: Amino acid sequences of *C. sporogenes* exosporium associated proteins

Protein	Amino Acid Sequence	Molecular Weight (estimated)	Notes
CsxA	MAINSKDFIPRPGFVNKQGCLPDPVEICCIQVPKVFDQCLRKE CLKPTDDCEQLCKQIPNITDPSQVRCVGCCKNLKVIVNSVTKC PVSNGKPGYKKVTINYTITFDVDVDVEINGVTQTQTLSYSVNR TITASNLYCPDTIAKTIIGKECTSAEEVDQQFIKIEVVGDCLSTDI SKIDCGGGCNCGCTCPDDPNNGDNKVFLCITLGLFIIIKCEIVV QLMVPAYGYCPVPEECKCSHDPCKEFMERELPTLYPPQEMD NLFDEYDERQDDRHIHNEKHIEEEEERGNMITSSVITNN	34 kDa	7.1% Cys
CsxB	MSKSSEEKMENKEVLNINSFNISEFCNADEGSNFIHFKPCEICK RAILDPINVADTSRLLQVNVALRNVCIGKELTVGCILIDRTGTV LAFKSQTFTVGHGGSGCGCSEDKHGSPCTNTSRRFSFILPTRD LCSSMDLKVKIIANYTHPCN	16.6 kDa	6.6% Cys
CsxC	MMSMDEMRGNYDSNSYKSGNYDCHKDCGKVIESKTLPLCD GTDITPETVAPPVVAKIPVVIAEQEIQVDVEARMKLKEKYYEIK RIRKDVFLTQCELLPRAGVIEDGVPVTGKLFISGYVKKNIEYAT ADCVKHDAVSGDIKHTTEKIPFNCVTEVTYITPPIVSNRGIQRR TDLYCDEGLCDCSCREEKLGKLNCQEYLEDVVTYVEKPYCELM GARIFETDIQRKPCYEDGVKVYDELLEKMVVYVRVKVLQLQQ VAIDNGAGGLGCRSKEH	30 kDa	5.5% Cys
BclA	MVNNSLQLQRTTTGTISANTNVIFDNTLLSTGSDISYNGGTG VVTITKTGIYYVDWWVTTQSSFSATYISFAIKTSDNKTIKGESPI	64 kDa	186 XXG repeats

	KISQVSGNALLNVTTVPYTFSLINSNLDVSLAVNPTVKANLSVT		
	EETSTLGVTGPTGPQGITGATGPQGITGATGPQGVTGATGP		
	QGVTGTTGLQGVTGPTGPQGTTGPTGSQGVTGPTGPQGVT		
	GPTGPQGVTGATGPQGVTGATGPQGVTGATGPQGITGPTG		
	PQGITGPTGLQGVTGATGPQGITGTTGPQGTTGPTGPQGTT		
	GPTGPQGTTGPTGPQGTTGPTGPQGTTGPTGPQGTTGPTG		
	PQGTTGPTGVTGPTGIQGITGPTGVTGPTGIQGITGPTGVTG		
	PTGIQGITGPTGVTGPTGIQGITGPTGVTGPTGIQGITGPTGV		
	TGPTGIQGITGPTGVTGPTGIQGITGPTGVTGPTGIQGITGPT		
	GVTGPTGIQGITGPTGVTGPTGIQGITGPTGVTGPTGIQGITG		
	PTGVTGPTGIQGITGPTGVTGPTGIQGITGPTGVTGPTGIQGI		
	TGPTGVTGPTGIQGITGPTGVTGPTGIQGITGPTGVTGPTGIQ		
	GITGPTGVTGPTGIQGITGPTGVTGPTGIQGITGPTGVTGPTG		
	IQGITGPTGVTGPTGIQGITGPTGVTGPTGIQGITGPTGVTGP		
	TGIQGITGPTGVTGPTGP		
BclB	MSHRCKMICMPCCCNCTCPRGVTGPTGPRGITGPTGPTGVT	27.8 kDa	37 XXG repeats
	GPTGPIGITGPTGPIGITGPTGPIGITGPTGPIGITGPTGPIGITG		
	PTGPIGITGPTGPIGITGPTGPIGVTGPTGPIGITGPTGPTGASA		
	IIPFASGGPVALVTVLGGLANTGALLGFGSSFPGVTVSAGTITL		
	SPTVSDFAFVAPRTGTITSLAGFFSATIGVTLLSPVQIRLTIYTAP		
	AASNTFTPVGTPLLLTPALGIIAIGTTASGITAENIPVAAGDKILL		
	VADSDTLGVDLASVVTGYVSAGIAIS		

Electron crystallography of the native exosporium of *C. sporogenes* showed that it was formed of a hexagonally symmetric two-dimensional semipermeable lattice. A 3D reconstruction of the native exosporium showed the lattice was made up of a cog-like ring with 6-fold symmetry linked to adjacent rings through a small 3-fold linker (Fig: 1.6A)(Janganan et al. 2020). In the centre of the cog like ring there is a major pore and a further 6 smaller pores surrounding the ring between each of the 3-fold linkers. These pores fully permeate the exosporium layer and the largest central pore has a diameter of 55 Å. These pores would allow for movement of small molecules such as germinants into and out of the spore whilst excluding larger proteins, thereby acting as a molecular sieve (Janganan et al. 2020).

Based on the work in Bacillus, the cysteine rich proteins identified were thought to be the most likely candidates to compose the basal structure of the exosporium. Over-expression of CsxA in *E. coli* yielded self-assembling 2D crystals which when imaged had the same underlying structure as the native exosporium (Janganan et al. 2020). This suggests that the major protein composing the exosporium in *C. sporogenes* is CsxA and that it likely self assembles within the mother cell during sporulation.

One of the advantages of the recombinant CsxA crystals was that they were amenable to imaging using cryo-EM. This led to a much higher resolution projection map of the underlying crystal structure of the exosporium (Fig: 1.6B) (Janganan et al. 2020). The 9 Å map clearly shows a hexameric ring of 6 protein subunits surrounding a less dense central cavity. The hexameric rings appear to be connected together via a small 3-fold linker to form the crystalline lattice (Fig:1.6B) (Janganan et al. 2020). The addition of images from tilted crystals allowed for a 3D reconstruction of CsxA crystal to be generated (Dafis-Sagarmendi 2021). The 3D reconstruction showed that the central hexameric ring structure has a crown-like appearance and is connected to adjacent rings via 3-fold linkers that appear raised on one side of the crystal and form craters on the other (Fig:

1.6C)(Dafis-Sagarmendi 2021). The central pore within the crown-like ring has a diameter of ~ 40 Å

at its narrowest point (Dafis-Sagarmendi 2021). 6 peripheral ovoid shaped pores are also present

between the 3-fold linker regions (Dafis-Sagarmendi 2021).
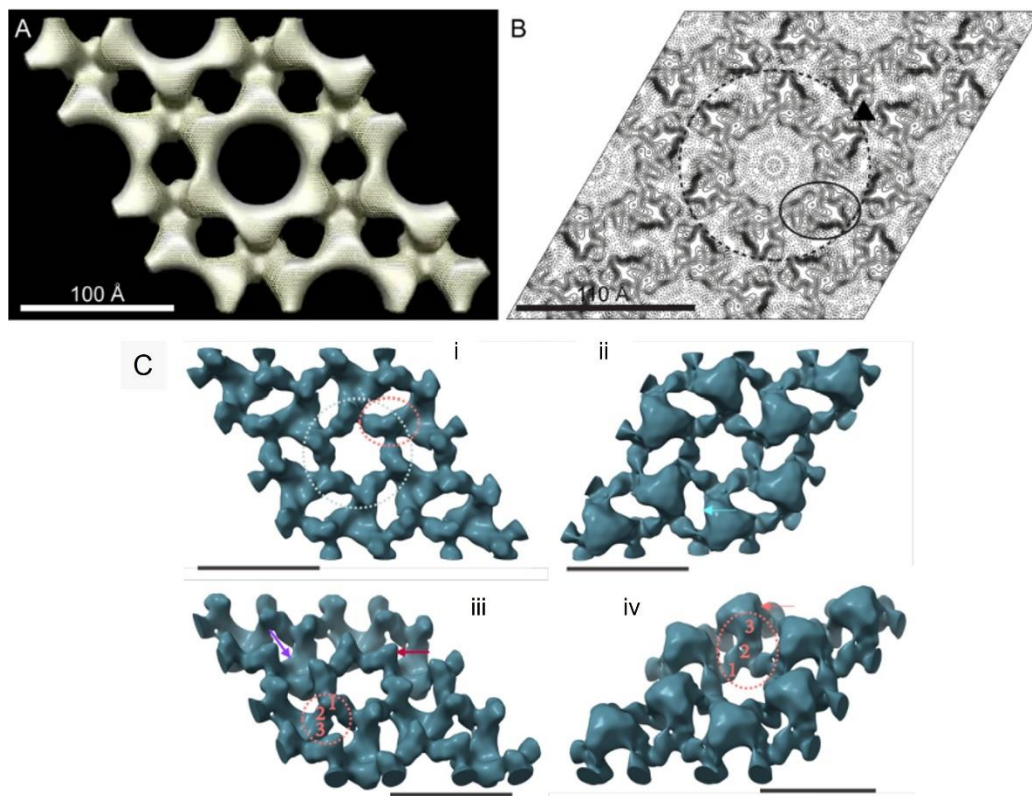
Figure 1.6: 3D Structure of CsxA Crystal and Native Exosporium

A) CsxA density (yellow) superimposed onto a 3D representation of the native exosporium in *C. sporogenes* (grey). B) 2D projection map from cryo-EC of CsxA crystal at 9 Å resolution. Solid contours represent density above the mean density whilst dashed lines represent density below the mean. The hexagonal ring of the unit cell is highlighted with a dashed circle, the threefold linker is marked with a triangle. A potential subunit is circled. A+B reproduced with permission (Janganan et al. 2020) C) Cryo 3D reconstruction of CsxA crystal. i+ii) views perpendicular to the plane iii+iv) tilted views showing opposite sides of the crystal lattice. Dotted circle (i) shows the central hexameric ring with a potential subunit highlighted with a pink dotted circle. Raised 3-fold linkers on one side of the crystal are labelled with a pink arrow (in iv and the craters with a purple arrow in iii. Red arrow (iii) indicated the pointed crown of the central ring. A peripheral pore is indicated by a light blue arrow (ii). Reproduced with permission (Dafis-Sagarmendi 2021)

AFM of the recombinant CsxA crystals alongside native exosporium fragments allowed for the allocation of the external and internal facing surfaces of the crystal (Janganan et al. 2020). The external surface appeared to be a hexameric assembly with petal like lobes whilst the internal surface possessed raised trimeric linkers joining the rings of the lattice together (Janganan et al. 2020). An additional important observation was that there were significant structural changes observed when the crystal samples were imaged in dehydrated and hydrated states. These changes appeared to be reversible and also representative of the differences seen between the 3D reconstructions obtained from negative stain (dehydrated) and cryo-EM (hydrated) (Fig: 1.6)(Dafis-Sagarmendi 2021; Janganan et al. 2020). This structural change could also be of significant biological importance in allowing the spore to adapt to changes in the environmental water content.

It is clear CsxA plays a major structural role in the formation of the exosporium. However, it remains to be determined what the roles of the other exosporium associated proteins are and how they contribute to the spore structure.

1.3.6.3 Exosporium Assembly

There is very limited knowledge about the assembly of the exosporium across Bacilli and Clostridia and it is thought to be a very complex and highly regulated process. Exosporium formation is closely linked to coat formation and signs of exosporium formation in Bacillus spp. have been seen as early in sporulation as engulfment. In *B. anthracis* the initial stage of exosporium assembly involves the formation of the cap and the generation of a sac that surrounds the spore acting as a scaffold onto which the exosporium is assembled (Boone et al. 2018). Proteins shown to be involved in this process include CotO and CotE with mutants showing mislocalisation of exosporium fragments and the loss of exosporium from spores (Boone et al. 2018). It has been shown in *B. anthracis* that CotO is required for exosporium cap formation. CotO itself is anchored to the spore coat via binding with CotE thereby anchoring the exosporium cap to the spore. It is thought that CotO and CotE are part of

the scaffold that surrounds the spore onto which the final exosporium is assembled (Boone et al. 2018). In addition to CotO and CotE there is also thought to be a layer of polysaccharide that surrounds the spore coat (Lehmann et al. 2022). CotY and ExsY proteins then assemble to form the exosporium structure that can be seen on native spores. The cap of the exosporium is laid down first and consists primarily of CotY protein (possibly with some ExsY present) whilst the remainder of the exosporium is composed primarily of ExsY (Fig: 1.7)(Terry et al. 2017). Exosporium assembly is thought to be guided around the spore by the formation of a second polysaccharide layer (Lehmann et al. 2022). This is initially formed at the mother cell proximal pole between the cap and the inner polysaccharide layer already present around the spore (Lehmann et al. 2022). As the exosporium is assembled around the spore the interaction between CotO and CotE is disrupted and the interspace, containing the polysaccharide layers, is formed between the exosporium and the coat (Boone et al. 2018; Lehmann et al. 2022).

In *B. anthracis* both the cap and the rest of the exosporium are covered in a hairy nap consisting exclusively of BclA on the cap region and a mixture of BclA and BclB around the rest of the exosporium (Thompson et al. 2012). The high structural similarity seen between Bacilli and Clostridia exosporium suggests that there may be an analogous assembly approach between the two, however, there is currently no evidence for a cap structure in Clostridia. In *C. sporogenes* an aperture has been observed at one pole, sometimes appearing to be covered, that could correspond to a cap but this is yet to be proven (Brunt et al. 2015).

There is substantial evidence for the role of self-assembly of CotY and ExsY in Bacilli and CsxA in *C. sporogenes* spores and it is likely that the crystal packing drives the exosporium assembly (Janganan et al. 2020; Jiang et al. 2015; Terry et al. 2017). However, as seen from work in *B. anthracis* it is still a controlled process likely involving chaperone proteins and scaffolds, such as CotO, CotE and polysaccharide layers, that direct the assembly process ensuring the progressive assembly of the

exosporium around the spore from the mother cell pole (Boone et al. 2018; Lehmann et al. 2022). This is further evidenced by the lack of patches of exosporium forming within the mother cell during sporulation. The high symmetry packing of the cysteine rich exosporium proteins provides favourable conditions for co-operative disulphide bond formation even in unfavourable conditions such as the reducing environment of the mother cell cytosol (Janganan et al. 2020). It seems that although some headway has been made in determining the assembly process of the exosporium the fundamental dynamics of the process are yet to be fully understood.

In addition to the major proteins CotY and ExsY in Bacillus the basal layer has several additional proteins, namely ExsFA (BxpB) and ExsFB that are incorporated to form the trimeric linkers between the hexameric rings (Fig: 1.7B)(Kailas et al. 2011). These proteins bind covalently with BclA and interact with BclB allowing for the formation of the hairy nap. Although a hairy nap has been observed in Clostridia the assembly process is yet to be determined as the additional proteins analogous to ExsFA and ExsFB do not appear to be present. A summary of the exosporium assembly process in *B. cereus* can be seen in Figure 1.7.
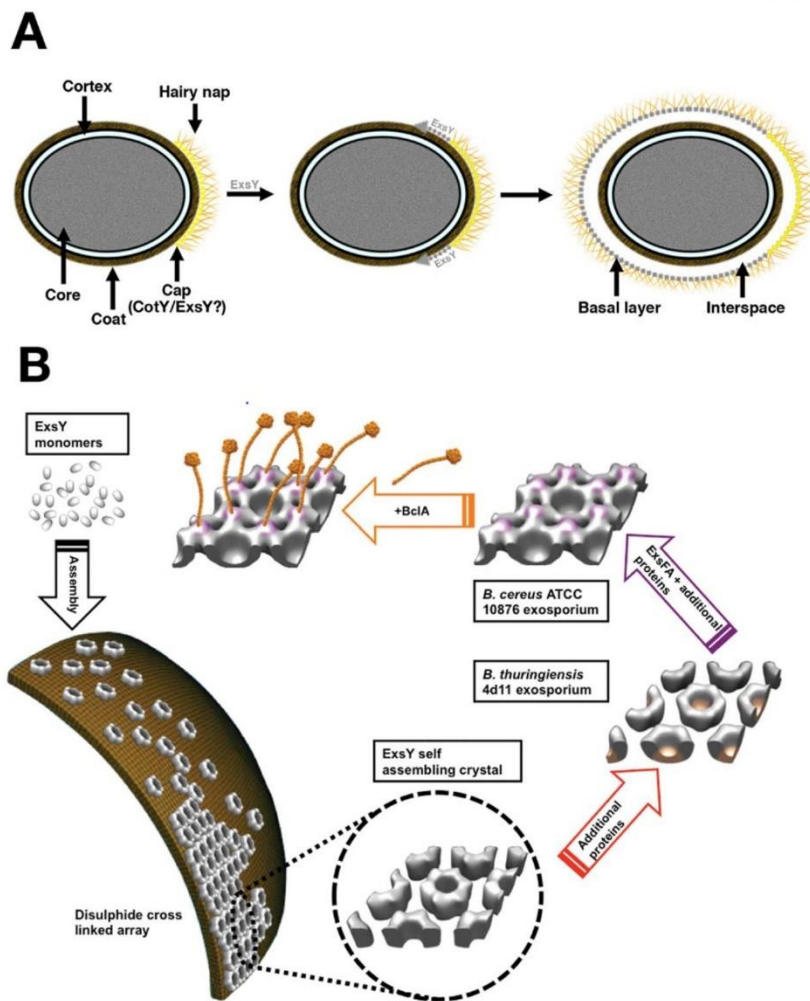
Figure 1.7: Assembly of Exosporium in the *B. cereus* Group

A) Main stages of assembly based on outline by Henriques and Moran (Henriques and Moran, Jr. 2007). An initial cap region is formed at one pole and then the assembly of the exosporium progresses around the spore. B) Monomeric ExsY self assembles into disuphide linked hexameric array. In *B. cereus* this is joined by ExsFA trimers that form an anchor for the BclA filaments to adhere to the exosporium surface forming the hairy nap. A+B reproduced with permission (Terry et al. 2017)

1.3.6.4   Role of the Exosporium

The exosporium is the outermost layer of the spore and as such is the first point of contact with the

environment or host. The hairy nap has been shown to play an important role in spore adhesion and

contributes significantly to spore hydrophobicity (Stewart 2015). Both of these spore qualities are

key to surface attachment including to food preparation surfaces such as stainless steel. The hairy nap protein BclA has been implicated in the process of spore uptake by phagocytic host cells specifically by interacting with host integrins (Reviewed in (Stewart 2015)).

The exosporium also has a protective role for the spore which is both active and passive. The exosporium itself is extremely resilient with crystals of both Bacilli and Clostridia exosporium proteins requiring particularly harsh reducing conditions to disassemble the crystal structure. For the *B. cereus* protein ExsY disassembly required subjecting the crystals to 8 M urea, 200 mM DTT, 2% (w/v) SDS at 90°C for 20 minutes (Terry et al. 2017) and for the *C. sporogenes* protein CsxA boiling the crystals in 2 M DTT for 60 minutes (Janganan et al. 2020). The exosporium structure is such that there are small pores present. These pores are small enough to impede the passage of large molecules such as digestive enzymes and antibodies but allow the passage of small molecules such as germinants (Ball et al. 2008; Janganan et al. 2020; Kailas et al. 2011). In this way the exosporium acts as a molecular sieve carefully selecting for required molecules and preventing inner spore layers from being degraded. The exosporium also acts as a matrix to which a large variety of enzymes are associated. In Bacilli this includes several superoxide dimutases (SODs) which may contribute towards protection against oxidative stress and increase pathogenicity (Steichen et al. 2003; Stewart 2015). In Clostridia, a ferrodoxin/flavodoxin oxidoreductase has been identified thought to be involved in the response to oxidative stress (Janganan et al. 2016).

The exosporium in *C. botulinum* has also been suggested to play a role in the heat resistant properties of the spore (Portinha et al. 2022). The thickness of the outermost exosporium layer varies between strains of *C. botulinum* and this appeared to correlate with the heat resistant properties displayed by the spores with strains with thinner or no exosporium being more susceptible to heat treatment (Portinha et al. 2022).

Finally, the exosporium has a role in spore germination. The observation of an exosporium cap structure in *B. anthracis* has led to the bottle cap model of germination where the outgrowing cell exploits the weak point created by the join between the cap and the rest of the exosporium (discussed in section 1.4.4)(Steichen, Kearney, and Turnbough 2007). Alanine racemase was also found to be present on the exosporium of *B. anthracis* and is thought to actively modulate the germination process by converting L-alanine, a germinant molecule, to D-alanine an inhibitor of germination (Chesnokova et al. 2009).

1.4 Germination

The process of spore germination allows dormant spores to return to active growth which is crucial to the pathogenesis of many species. The process of germination can be triggered by a variety of chemical and physical methods. However, the natural trigger is the presence of specific small molecules within the environment called germinants. Understanding the process of germination is of particular importance to the food industry where developing ways to either stimulate or prevent spore germination would help significantly in eliminating the threat posed by spores. The detailed mechanisms involved in the germination process are far from completely understood, however, by piecing together work from various species of both Bacilli and Clostridia a broad picture can be formed. Generally, germination involves three major stages: Stage I: germinant detection, commitment and Ca-DPA release, Stage II: cortex hydrolysis, Stage III: cell emergence and outgrowth.

1.4.1 Stage I: Germinant Exposure, Commitment and Ca-DPA Release

Germination is initiated by the recognition of small molecules (germinants) by germinant receptors (GRs) located within the inner membrane of the spore. The GRs encoded by each species determines their ability to germinate in response to specific germinants. Most species encode multiple GRs that bind a variety of small molecules that are effective in triggering germination (Olguín-Araneda et al. 2015). For the most part these germinant molecules tend to consist of amino acids, sugars, and other small organic molecules. The most effective combination of germinants varies across species, for example, in *B. subtilis* L-alanine and L-valine can individually trigger efficient germination and in *C. sporogenes* and *C. botulinum* a combination of L-cysteine and L-lactate has been shown to be the most effective (Brunt et al. 2014).

Germinant receptors that localise to the inner membrane of the spore belong to the Ger family of proteins. These are found in Bacilli as well as *C. botulinum* and *C. sporogenes*. Ger GRs are formed of three subunits A, B and C. Subunits A and B are integral membrane proteins which consist of transmembrane helices whilst subunit C is a peripheral membrane protein consisting of a hydrophilic domain which is anchored to the membrane by a diacylglycerylated cysteine residue. (Paredes-Sabja, Setlow, and Sarker 2011). The *C. botulinum* genome contains two tricistronic and one pentacistronic GR operons whilst *C. sporogenes* contains three tricistronic and one tetracistronic GR operon. It was shown through genetic manipulation of these operons that *C. botulinum* only requires two tricistronic encoded GRs for germination which cannot function independently of each other. *C. sporogenes* requires just one tricistronic GR for successful germination (Brunt et al. 2014). It is thought the other encoded GRs may form part of a complex involved in controlling the rate of amino acid stimulated germination.

After exposure to germinant molecules there comes a point of no return where the spores are committed to germination no matter what changes the spores are exposed to. Even germinant

dissociation by a strong competitive inhibitor or acidification no longer blocks the completion of germination after spore commitment (Yi and Setlow 2010). The specific mechanism of spore commitment is not well understood but it is thought that it could involve a change to the inner membrane of the spore with regards to its permeability that allows the release of monovalent cations from the spore core (Setlow 2014). What is clear is that spore commitment precedes core Ca-DPA release, often by several minutes.

Core Ca-DPA release is the final event of stage I of germination and is responsible for triggering entry to stage II. The release of Ca-DPA from the core is a rapid process and once initiated occurs within a matter of minutes. However, the process by which Ca-DPA is released is poorly understood. It is thought to be released via channels formed from spore specific SpoVA proteins (Vepachedu and Setlow 2007). The release of spore core Ca-DPA also leads to the partial rehydration of the spore core which can be visualised as change from phase bright to phase dark under a phase contrast microscope.

1.4.2   Stage II: Cortex Hydrolysis

During stage II of germination the cortex of the spore is degraded by cortex lytic enzymes (CLEs). In Bacilli and most Clostridia there are two major redundant CLEs, CwlJ and SleB, which degrade the cortex by recognition of the cortex specific δ-lactam residues. CwlJ and SleB both require additional proteins for proper localisation within spores (Chirakkal et al. 2002). CwlJ requires the GerQ protein and localises to the inner coat cortex boundary within the spore (Ragkousi et al. 2003). SleB requires the YpeB protein which is thought to localise to the inner membrane of the spore (Boland et al. 2000). CwlJ is known to be activated by Ca-DPA, however, whether this is through direct or indirect interaction is not known and how CwlJ is kept inactive during sporulation when Ca-DPA is being

accumulated within the spore remains a mystery (Paidhungat, Ragkousi, and Setlow 2001). SleB

activation is even more poorly understood, but, as the protein is associated with the inner

membrane, changes in pressure provided by the cortex as the spore Ca-DPA is released could cause

structural changes to the membrane triggering SleB activation (Olguín-Araneda et al. 2015). Despite

the limited knowledge on the mechanisms behind activation of the CLEs it is clear that the process of

cortex hydrolysis is essential for spore germination as knocking out both CLEs results in an arrest of

the germination process with spores unable to successfully release a vegetative cell (Chirakkal et al.

2002). The completion of cortex degradation allows for the germ cell wall to expand and for the core

of the spore to continue taking up water. Upon the completion of stage II the core water content has

risen to approximately 80% of the wet weight which is equal to that of a growing cell (Setlow 2014).

Thin sectioning of germinating spores in Bacillus species show the expanded nature of the spore core

and the apparent decrease in the thickness of the cortex layer consistent with its degradation

(Hashimoto and Conti 1971; Santo and Doi 1974). Although the process by which cortex hydrolysis

initiation is different in *C. difficile,* thin sectioning of spores undergoing germination clearly show the

cortex thickness decreasing from 130 nm to 40 nm and the spore core expanding to fill the space

within the coat (Baloh, Nerber, and Sorg 2022).

1.4.3   Stage III: Cell Emergence and Outgrowth

The final stage of germination involves the emergence of a vegetative cell from the outer layers of

the spore. Through the use of fluorescence microscopy it was discovered that one pole of the *B.*

anthracis exosporium is structurally different, forming a polar cap (Steichen et al. 2007). Imaging

throughout germination revealed that vegetative cell emergence occurred exclusively through this

polar cap region in the exosporium (Steichen et al. 2007). Emergence was often forceful enough to

allow the emerging cell to rapidly dissociate from the remaining spore layers completely (Steichen et al. 2007). All this evidence suggests that the emergence of vegetative cells in *B. anthracis* is via a programmed co-ordinated mechanism and that the structurally different cap may provide a weak point for vegetative cell emergence from the spore outer layers. This mode of emergence through a polar cap has been termed the bottle cap model of germination.

Some structural work has been carried out in *C. sporogenes* to visualise the emergence of cells from the spore outer layers. SEM and thin sectioning images have shown an aperture at one pole of the spore in the exosporium layer prior to cell emergence (Fig: 1.3C and D) (Brunt et al. 2015). This aperture aligns with visible ruptures in the spore coat layers further inside the spores (Brunt et al. 2015). The emerging cell is released through the polar aperture in the exosporium which could suggest a method of cell emergence analogous to that of *B. anthracis*. How and when this aperture is formed is unknown and the mechanism by which the protein coat is degraded is also unclear. There have been suggestions that the coat proteins may be broken down by lytic proteins released from the nascent cell (Hoeniger and Headley 1969).

The process of cell emergence observed in *C. sporogenes* appears to be a much slower and a less explosive process to that seen in some other species. The nascent cells can often remain partially within the spore outer layers, in some cases even to the point where the new cell begins to divide (Brunt et al. 2015; Hoeniger and Headley 1969). This observation would support the idea that cell emergence in *C. sporogenes* is controlled by slow degradation of the spore outer layers. A build-up of pressure that leads to the explosive release of the cell would usually result in cells completely dissociating from the spore remnants (Hoeniger and Headley 1969).

1.4.4 Superdormancy and Heterogeneity

The germination process is heterogeneous with individual spores having highly variable lag periods between germinant exposure and Ca-DPA release (Yi and Setlow 2010). Spores that take a prolonged period of time to begin the germination process, despite high germinant levels, are considered to be superdormant (Ghosh and Setlow 2009). The major reason for superdormancy is thought to be very low levels of GRs within the spore, however, recent findings from time-lapse fluorescence imaging suggests this may not be the case (Breedijk et al. 2020). Biologically the superdormant spores are thought to be a protective mechanism to allow for persistence in the case of premature germination. Superdormancy and heterogeneity is particularly problematic when trying to eradicate spores and is therefore an important area of further investigation.

1.4.5 Alternative Germination Triggers

Nutrient germinants are considered to be the natural triggers of germination, however, other conditions and molecules have been shown to trigger germination *in vitro*. These include high pressure (Sarker et al. 2015), dodecylamine (Rode and Foster 1961), and high concentrations of exogenous Ca-DPA (Riemann and John Ordal 1961). In all cases these methods bypass the initial stage of germinant detection by the GRs and cause the release of Ca-DPA from the spore core via alternative means.

During high pressure treatment of spores instead of germinants binding to the GRs the high pressure stimulates the GRs within the inner spore membrane triggering the germination process to occur (Black et al. 2005). This then proceeds in the same way as natural nutrient germination starting with the release of Ca-DPA from the spore core.

Dodecylamine triggers spore germination by interacting with the SpoVA channel located in the inner membrane of the spores. Upon interaction, the channels open allowing for the release of Ca-DPA from the spore core and subsequent germination steps to occur (Vepachedu and Setlow 2007).

High concentrations of exogenous Ca-DPA trigger the germination process by activating the cortex lytic enzyme CwlJ within the cortex of the spore (Paidhungat et al. 2001). This results in the breakdown of the cortex of the spore prior to Ca-DPA release from the spore core. The loss of cortex structure has a knock-on effect to the internal spore structure which ultimately leads to the release of spore core Ca-DPA and complete spore germination.

1.5 Electron Microscopy for Ultrastructural Analysis

Electron microscopy is a powerful method for conducting structural studies on biological samples. To begin with this relied heavily on the use of negative staining and chemical fixation (Brenner and Horne 1959). Thicker samples could also be embedded into resin blocks which were then thin sectioned using an ultramicrotome to provide samples amenable to TEM imaging. These techniques were crucial for beginning to understand the structural composition of biological samples, however, this methodology is limited to low resolution due to the use of heavy metal stains (Amos, Henderson, and Unwin 1982). Additionally, the harsh chemicals involved are also believed to have an impact on the structural integrity of the samples and can result in artefacts. Despite these limitations the use of these methods continues to this day and is the basis of the vast majority of our knowledge on bacterial ultrastructure.

In 1968 de Rosier and Klug published a ground-breaking paper on the 3D structure of the bacteriophage T4 tail using reconstructions generated from EM projections (de Rosier and Klug 1968). This laid down the fundamental principles of 3D reconstruction which paved the way to the

development of advanced electron microscopy techniques such as single particle analysis (SPA) and electron tomography (ET).

The limitations of staining however, still proved to be a barrier in obtaining high resolution structural information of biological specimens. In 1975 Unwin and Henderson presented a method for structure determination of unstained protein crystals using low dose imaging (Unwin and Henderson 1975). This used a glucose solution to preserve the crystalline sample which, unlike negative stain, did not limit the resolution to 20 Å. Low dose imaging was then used to collect data on the crystals to prevent sample destruction (Unwin and Henderson 1975). The low dose meant that SNR was reduced and therefore large areas had to be imaged in order to obtain a high enough SNR for analysis (Unwin and Henderson 1975). The use of this method produced a 7 Å projection map of the structure of purple membrane protein which enabled the allocation of helices within the structure (Henderson and Unwin 1975). In the 1980s a novel method of sample preparation was developed involving the plunge freezing of biological samples into liquid ethane at -195°C (Dubochet et al. 1988). This process, which suspends the sample in vitreous ice, not only removes the requirement for staining, but also preserves biological samples in a near native state. This opened up the possibilities for obtaining higher resolution structures, including the determination of the first atomic level model based on EM images with a resolution of 3.5 Å determined by cryo-electron crystallography (cryo-EC) (Henderson et al. 1990).

Despite improvements to specimen preparation, many samples are still too thick to be imaged by tomography and therefore several techniques have been developed to produce thin sections of vitrified samples. This allows for the biological context of the subcellular assemblies to be maintained whilst also providing a thin enough sample for TEM. Cryo electron microscopy of vitreous sections (CEMOVIS) is one such technique and involves the thin sectioning of frozen samples at cryogenic temperatures using a cryo-ultramicrotome (Al-Amoudi et al. 2004). This

technique enabled the imaging of membrane reservoirs in *B. subtilis* spores (Laue et al. 2018) and

has provided insights into the ultrastructure of *Staphylococcus aureus* cells (Matias and Beveridge

2007). In 2007 a more advanced method of obtaining thin cryo sections was developed. This uses a

gallium ion beam to mill away the surface of the sample to produce a thin lamella that can then be

used for tomography data collection (Marko et al. 2007). This technique is called focused ion beam

milling (FIB-milling) and is rapidly becoming the technique of choice for studying the ultrastructure

of both prokaryotic and eukaryotic cells, however, it remains technically challenging and low

throughput. This technique has recently been employed to provide unprecedented detail of the

process of engulfment during the sporulation of *B. subtilis* (Khanna et al. 2019).

There have been major advances in computational ability and with it the development of software

to streamline EM data processing making it more accessible and user friendly. There are now several

software packages available, specifically tailored towards different aspects of EM data processing,

such as Focus for EC (Biyani et al. 2017), IMOD for tomography (Mastronarde and Held 2017a), and

Cryo-sparc (Punjani et al. 2017) and Relion (Scheres 2012) for single particle analysis (SPA). The

processing of EM data remains heavily reliant on manual input and expertise and is therefore a key

area of current development is the automation of this process.

Although there have been many advances in sample preparation techniques, image processing

software, and the physical hardware of microscopes over the years, the major explosion in cryo-EM

usage came about over the last 10 years due to the so called "resolution revolution" (Callaway 2015;

Kühlbrandt 2014; Thompson et al. 2016). This is largely down to the development of the direct

electron detector (DED) which significantly improved the signal-to-noise ratio of the recorded

images (Thompson et al. 2016) as well as allowing for 'movie-mode' data collection. Movie-mode

collects a series of frames for each image allowing for the correction of beam induced motion that

would otherwise cause blurring and limit the resolution of structural information (McMullan et al. 2009).

There is no question that significant advancements have been made within the field of electron microscopy over the last 70 years, however, it is not without its shortcomings. Obtaining high resolution information is challenging and often requires extensive sample optimisation, particularly for cryo-EM (Thompson et al. 2016). In addition, exposure to the electron beam causes damage to biological samples and therefore has to be carefully controlled and monitored to prevent the loss of structural information and introduction of artefacts (Koning, Koster, and Sharp 2018).

This thesis includes the use of negative stain TEM, thin section TEM, EC and cryo-ET. A brief overview of the principles behind these techniques are provided below.

1.5.1   Negative stain and Thin Section TEM

Negative staining was one of the initial methods developed for imaging biological samples. It involves coating samples adsorbed to a grid in heavy metal compounds such as uranyl acetate or uranyl formate, and provides high levels of contrast (Amos et al. 1982; Thompson et al. 2016). Unfortunately, this method of sample preparation also requires the dehydration of the sample which can cause artifacts. In addition, staining caps the attainable resolution to ~20Å and is inadequate for revealing internal structure (Amos et al. 1982).

Chemical fixation and thin sectioning is a technique that allows for the imaging of thicker samples such as bacterial spores. Samples are fixed and dehydrated before being embedded into resin for thin sectioning. Sectioning involves the use of an ultramicrotome and produces thin sections between 80-200nm thick. Sections are loaded onto grids and post stained with uranyl acetate and Reynolds Lead Citrate which provides additional contrast to the samples. Imaging of thin sections

therefore allows for the visualisation of the internal structures within a cell or spore and therefore provides the basis for the majority of our ultrastructural understanding of biological systems. Like negative stain this technique requires use of harsh chemicals for fixing and staining the sample, which could introduce artefacts. Additionally, the sectioning process can sometimes lead to knife compression artefacts.

An alternative approach involves the use of high pressure freezing (HPF) and freeze substitution. During this process a sample is vitrified whilst under high pressure to preserve the native state of the specimen (McDonald and Auer 2006). The sample can then be gradually brought back up to room temperature in the presence of a solvent such as acetone which replaces the water within the sample in a process known as freeze substitution (McDonald and Auer 2006). These samples can then be stained and embedded in resin for sectioning. This process tends to introduce fewer artifacts than the traditional chemical fixation method (McDonald and Auer 2006; Thompson et al. 2016).

1.5.2 Electron Crystallography

Electron crystallography (EC) has been used to study both synthetic and naturally occurring crystals by EM. Synthetic crystals can be produced by packing membrane proteins into a lipid bilayer; a method that has proved vastly beneficial for determining their structure, particularly given that membrane proteins are notoriously challenging to purify for X-ray crystallography (Glaeser et al. 1986; Henderson et al. 1990; Stahlberg, Biyani, and Engel 2015). There are also many examples of native protein crystals whose structures have been solved by EC, including bacterial S-layers (Bharat et al. 2017; Lanzoni-Mangutchi et al. 2022) and exosporium (Ball et al. 2008; Janganan et al. 2020; Kailas et al. 2011; Terry et al. 2017).

2D crystals are composed of an array of repeating unit cells (Fig: 1.8). Each unit cell corresponds to the smallest repeating volume within the crystal lattice and can be described by the lengths a and b and the angle between them as y. Plane groups, of which 17 are possible for biological crystals, can be assigned to 2D crystals based on the symmetry present within the unit cell (Amos et al. 1982). As electrons pass through the crystal they obey Bragg's law, which results in the production of a diffraction pattern. A representation of this can be obtained by performing a Fourier transform (FT) on the images obtained. Within the FT are a series of bright spots (diffraction spots) that correspond to the reciprocal lattice of the 2D crystal. By assigning miller indices (h, k) to each spot within the lattice, it is possible to calculate the unit cell dimensions of the crystal, and extract amplitude and phase information (Amos et al. 1982). This information can then be used to produce a 2D projection map of the underlying crystal structure by following a processing pipeline detailed in chapter 2.7.2. By collecting data on tilted 2D crystals it is also possible to produce a 3D reconstruction of the underlying crystal structure (Stahlberg et al. 2015). This has been used to determine the exosporium structure in the *B. cereus* family (Ball et al. 2008; Terry et al. 2017) and *C. sporogenes* (Dafis-Sagarmendi 2021).
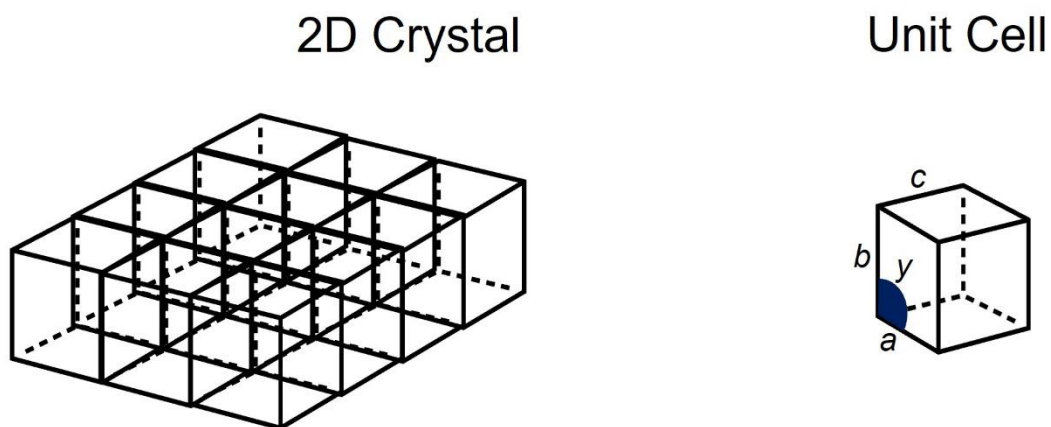
Figure 1.8: 2D Crystal Formed of Repeating Units

A 2D crystal is composed of repeating unit cells. A unit cell is described in terms of length, a and b, and the angle, y, between them.

1.5.3   Electron Tomography

Electron tomography provides 3D structural information on cellular complexes. It is important in providing biological context to complexes of interest. Used in combination with other techniques such as subtomogram averaging, (Reviewed in (Koning et al. 2018)) or single particle analysis (Reviewed in (Lyumkis 2019)), it can provide valuable insights into the roles of subcellular structures.

ET requires the collection of 2D projections of the sample from a range of angles, usually -60° to +60°. This is done by tilting the sample within the microscope to collect a tilt series (Fig: 1.9). These images can then be aligned and reconstructed to produce a tomogram, a process that is detailed in chapter 2.7.3.

For cyro-ET, samples are vitrified by plunge freezing. Samples thicker than ~500 nm typically require some form of sectioning for reliable or high resolution data collection (Koning et al. 2018). Hence the development of CEMOVIS and FIB-milling (Reviewed in (Koning et al. 2018)). Alignment of the raw tilt series is very important in tomography and must be done with accuracy to get a reliable reconstruction. In most cases electron dense gold fiducial markers, 5-25 nm in diameter are added to the sample prior to vitrification to aid in the tilt series alignment process (Mastronarde and Held 2017a; Walz et al. 1997). Although useful for alignment, gold fiducials can also result in artefacts within the final tomogram reconstruction and therefore need to be computationally erased prior to reconstruction (Mastronarde and Held 2017a).

Following tilt series alignment, the 2D projections can be merged to generate a 3D volume in a process termed tomogram reconstruction. This can be done by weighted back projection (WBP) or by the simultaneous iterative reconstruction technique (SIRT). As WBP is conducted in Fourier space it is not a very computationally intensive process, although it can produce tomograms with high levels of noise (Koning et al. 2018; Radermacher 1988). SIRT, on the other hand, is computed in real

space and, being an iterative process, can be extremely computationally intensive (Gilbert 1972; Koning et al. 2018), it does however, produces tomograms that have improved signal to noise ratio (SNR) when compared with WBP (Koning et al. 2018). The number of iterations required to produce an optimal tomogram also varies depending on the sample and can therefore require some trial and error to find an appropriate value. Alternatively, it is possible to use WBP with SIRT-like filters which combines the increased SNR of SIRT with the less computationally intensive process of WBP (Zeng 2012).

One of the major challenges for cryo-ET is sample damage. The requirement for multiple exposures of a delicate sample can often lead to radiation damage. To combat this, low doses are used, however, this means compromising on the SNR. The development of the DED made low dose imaging much more feasible and also led to an improved SNR (Thompson et al. 2016). Another consideration for ET is the missing wedge artefact resulting from the limited tilt range possible for data collection (highlighted in Fig: 1.9). The mechanical and optical constraints of the microscope as well as the projected thickness of the sample mean that data can only typically be collected between +/- 60° or 70°. This leads to a decrease in the resolution in the z direction in the final tomogram (Diebolder et al. 2015; Koning et al. 2018). The development of dual axis tomography, where the grid holder can rotate around two axes, increases the volume amenable to data collection (Mastronarde 1997). This changes the missing wedge artefact to become more like a missing cone and it also increases the exposure of the sample, therefore, lower doses have to be used so as not to damage the sample which leads to lower SNR (Mastronarde 1997).
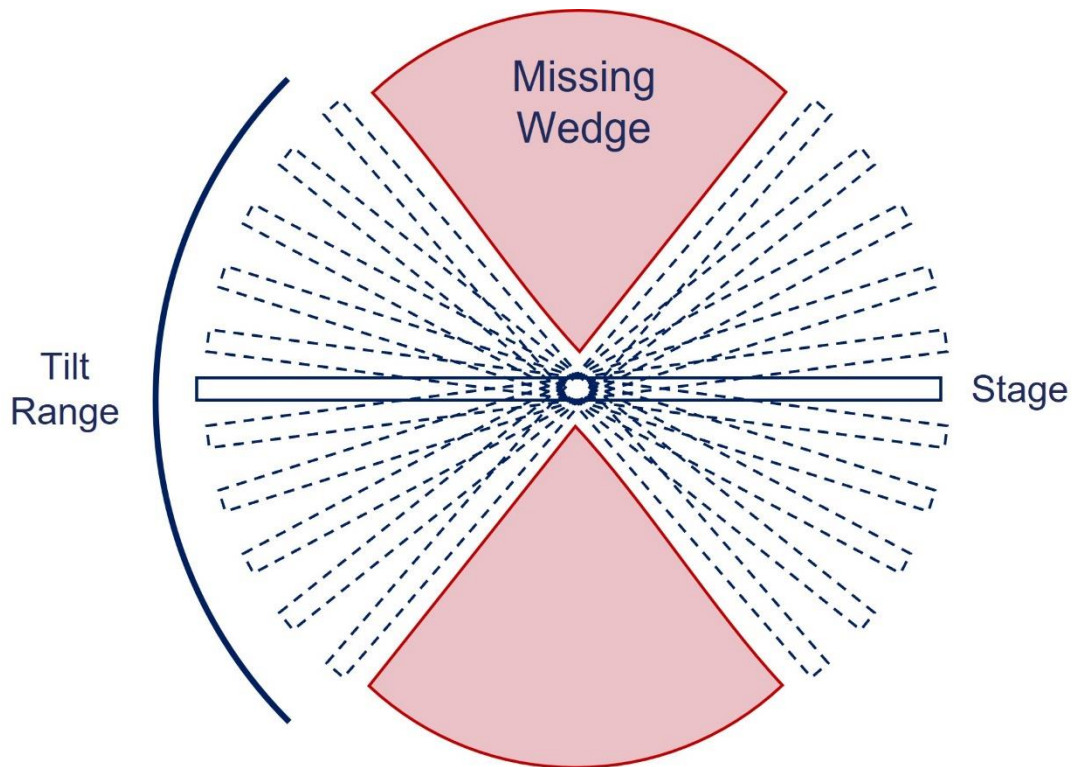
Figure 1.9: 3D Data Collection in EM

The grid holder is tiled to collect data across a range of angles. This is limited by the tilt range of the microscope and is usually +/- 60°. These limitations result in a missing wedge of information (red).

Despite these limitations, cryo-ET and cryo-FIB-ET are rapidly becoming the method of choice for

obtaining ultrastructural detail of biological samples. Advances in the automation of the sectioning

process are largely behind this, however, it is still some way from being a streamlined process. In

addition, the large amount of data produced from tomography would benefit from an automated

processing pipeline, and although some progress has been made, a lot of manual input and expertise

is still required (Reviewed in (Koning et al. 2018)).

1.6 Aims and Objectives

Our understanding of spore ultrastructure and germination has been developed through the study

of both Bacillus and Clostridium species. Previous research into the germination process has largely

been biochemical with the small amounts of structural work having been conducted prior to the major advances in EM imaging. Structural studies on the exosporium have been conducted in both the *B. cereus* group and *C. sporogenes* and have revealed the involvement of cysteine-rich proteins in their assembly. For *C. sporogenes* in particular, the cysteine-rich protein CsxA plays a major structural role in basal layer assembly. In addition to CsxA, a number of other cysteine-rich and collagen-like proteins were found associated with the *C. sporogenes* exosporium, however, their specific influence on spore ultrastructure remains undetermined. The aim of the project described here was to further our understanding of *C. sporogenes* spore ultrastructure with a focus on the outermost layers and the roles of cysteine-rich and collagen-like proteins. The aim was then to provide a detailed structural analysis of the germination process and the emergence of the vegetative cell from the confines of the spore outer layers.

The key research questions are as follows:

1. What are the fundamental morphological changes that underpin the germination and outgrowth process in *C. sporogenes*?

2. What role do the key exosporium associated proteins, CsxA, CsxB, CsxC, BclA and BclB play in *C. sporogenes* spore architecture?

3. Does the exosporium play an essential role in the germination process?

4. What impact does the lack of exosporium and its associated proteins have on fundamental spore properties such as heat resistance?

2 Materials and Methods

2.1 Bacterial Strains, Growth and Spores

2.1.1 Strains and Growth Conditions

Bacterial strains used are listed in table 2.1. *C. sporogenes* strains were grown on pre-reduced brain heart infusion (BHI) agar or TY agar (Table: 2.2). Liquid cultures were grown using pre-reduced TY broth (Table: 2.2). Cultures were supplemented with antibiotics where appropriate as listed in table 2.3. *C. sporogenes* was grown in an anaerobic work station (Don Whitley Scientific) containing an environment composed of 80% N_2, 10% CO_2, and 10% H_2 at 37°C.

E. coli strains were grown on LB agar, in LB broth or in 2xYT (Table: 2.2). Cultures were supplemented with appropriate antibiotics as required (Table 2.3). All cultures were grown with agitation (225 rpm) at 37°C.

All bacterial strains were stored in 20% glycerol at -80°C.

Table 1.2: Bacterial strains used in this study

Strain	Description	Source
C. sporogenes		
NCIMB 701792	WT strain	
csxA::ermB	NCIMB 701792 where *csxA* has been replaced with the *ermB* cassette via allelic exchange mutagenesis	This study
csxB::ermB	NCIMB 701792 where *csxB* has been replaced with the *ermB*	This study

	cassette via allelic exchange mutagenesis	
csxC::ermB	NCIMB 701792 where *csxC* has been replaced with the *ermB* cassette via allelic exchange mutagenesis	This study
bclA::ermB	NCIMB 701792 where *bclA* has been replaced with the *ermB* cassette via allelic exchange mutagenesis	This study
bclB::ermB	NCIMB 701792 where *bclB* has been replaced with the *ermB* cassette via allelic exchange mutagenesis	This study
E. coli		
NEB-5α	Chemically competent cells used for cloning and plasmid propagation	New England Biolabs
CA434	Strain HB101 with the IncPβ conjugative plasmid, R702. Used as a conjugation donor.	(Purdy et al. 2002)
Rosetta	BL21 derivative with universal translation not limited to	Novagen

| | *E. coli* codon usage. Genotype: F⁻ompT hsdS_B(r_B⁻ m_B⁻) gal dcm (DE3) pRARE (Cam^R) | |

Table 1.3: Growth media used in this study

Media	Contents	Quantities (1L)	Notes
LB	LB broth, Miller (Thermo Fisher)	25 g	*E. coli* cultures
TY	Tryptose (Bacto) Yeast Extract (Bacto)	30 g 20 g	*C. sporogenes* cultures
2xYT	Tryptone (Bacto) Yeast Extract (Bacto) NaCl (Sigma)	16 g 10 g 5 g	*E. coli* overexpression cultures
BHI agar	Brain Heart Infusion Agar (Sigma)	52 g	*C. sporogenes* growth
TY agar	Tryptose (Bacto) Yeast Extract (Bacto) Agar (Sigma)	30 g 20 g 15 g	*C. sporogenes* growth

Table 1.4: Antibiotics used in this study

Antibiotic	Concentration	Notes
Chloramphenicol	15 µg/ml in 70% ethanol	*E. coli* mutagenesis vectors
Thiamphenicol	15 µg/ml in methanol	*C. sporogenes* mutagenesis vectors
Colistin	50 µg/ml in H_2O	Against *E. coli*
Erythromycin	5 µg/ml in 70% ethanol	*C. sporogenes* selection of mutants
Kanamycin	50 µg/ml in H_2O	*E. coli* O/E vectors
Ampicillin	100 µg/ml in H_2O	*E. coli* O/E vectors

2.1.2 *C. sporogenes* Spore Isolation

5 ml TY broth was inoculated with a single colony of *C. sporogenes* and incubated overnight. The cultures were then sub-cultured to give OD_{600nm} 0.1 in 20 ml TY broth and incubated anaerobically for a minimum of 10 days. Cultures were harvested by centrifugation at 6,000 x g for 5 min. Pelleted material was washed in 10 ml ice-cold sterile water and then centrifuged at 5,000 x g for 1 min. The wash step was repeated a further 4 times. Pellets were then resuspended in 0.5 ml of 20% (w/v) HistoDenz (Sigma). This was then layered on top of 1 ml of 50% (w/v) HistoDenz and centrifuged at 15,000 x g for 15 mins. In this process the spores form a pellet while the vegetative cells and debris remain suspended in the HistoDenz density gradient. The HistoDenz was then removed by aspiration and the spores washed an additional 5 times in ice-cold sterile water as before. Purity of each preparation was checked by phase contrast microscopy. Purified spores were stored at 4°C.

2.2 Phenotypic Assays

2.2.1 Growth Analysis

O/N cultures of *C. sporogenes* were used to inoculate pre-reduced TY to an OD_{600nm} 0.05. Growth was measured by recording the OD_{600nm} every 30 min. Assays were conducted in technical triplicate and biological duplicate.

2.2.2 Sporulation Efficiency Assays

Sporulation assays were conducted based on methods developed for *C. difficile* (Dembek et al. 2015). Single colonies of *C. sporogenes* were used to inoculate a 5 ml pre-reduced TY and incubated O/N. The following morning. 5 ml of fresh pre-reduced TY media was inoculated to OD_{600nm} 0.01 and incubated for 12 h. This culture was then used to inoculate 20 ml of fresh pre-reduced TY media to an OD_{600nm} 0.0001. This was done to ensure that there was minimal carry over of spores from the original culture. The following morning (T_0), total CFU counts were obtained by serially diluting samples in PBS and plating 10 µl spots onto TY agar in triplicate. For total spore counts 500 µl samples of culture were heated to 65°C for 30 min to kill all vegetative cells in the sample. The heated samples were then serially diluted and plated onto TY agar. CFU enumeration was performed following 24 h incubation of plates at 37°C in the anaerobic cabinet. This process was repeated every day for a further 5 days (T_1-T_5).

2.2.3 Heat Resistance Assays

200 µl of spores at an OD_{600nm} 0.5 were heat treated at 65, 75, 85 and 95°C in a heat block for 30 min. Heated samples and a sample kept at RT were then serially diluted in MQ and 10 µl spots were plated onto TY agar in triplicate. CFU enumeration was carried out the following day to determine spore viability after heat treatment.

2.2.4   Germination Assays

5 ml pre-reduced TY media was inoculated with spores to an OD_{600nm} 0.5 and incubated for 20 min to allow the culture to equilibrate. The OD_{600nm} was measured every 15 min for the first 2 h and then every 30 min for another 6 h (until clear stationary phase). Data was obtained in biological duplicate and technical triplicate.

2.3   DNA Manipulation

2.3.1   Genomic DNA Isolation

Genomic DNA (gDNA) was isolated from *C. sporogenes*

1.5 ml of O/N *C. sporogenes* culture was harvested by centrifugation (2 min, 12,000 x g) and was resuspended in 200 µl lysis buffer (200 mM NaCl, 50 mM EDTA, 20 mM Tris-HCl pH 8.0). 10 µl of pronase (20 mg/ml) was then added and the mixture incubated at 55°C for 1 hr. 80 µl of 10% N-lauroylsarcosine was then added to the sample and incubated at 37°C for 1 hr. Finally, 200 µl of RNase solution (final concentration 0.2 mg/ml) was added and the sample was incubated at 37°C for 1 hr. Sample was transferred to a 1.5 ml Phase Lock Gel (PLG) tube and 500 µl of phenol:choloform:isoamyl alcohol (25:14:1) was added and gently mixed by inversion. The sample was then centrifuged (2 min, 13,000 x g) to allow separation of the organic phase and the DNA containing aqueous phase. The aqueous phase was then transferred to a new PLG tube and treated with phenol:choloform:isoamyl alcohol as before. The aqueous phase was again recovered and transferred to a new PLG tube. The sample was then treated with 500 µl choloform:isoamyl alcohol (24:1) to remove any excess phenol and centrifuged as before. The aqueous phase was again recovered and the choloform:isoamyl alcohol step repeated. The resulting aqueous phase was then transferred to a microfuge tube with an equal volume of ice-cold isopropanol and incubated at -20°C O/N to precipitate the gDNA. To harvest the gDNA the sample was centrifuged (15 min, 4,000 x g at

4°C) and washed once with 500 µl of 70% ethanol. Sample was centrifuged again (10 min, 4,000 x g at 4°C) and, after aspiration of the supernatant, the pellet left to air dry to remove any residual ethanol. gDNA was then resuspended in 50 µl nuclease free water and quantified using a Nanodrop and quality checked by agarose gel electrophoresis.

Low-quality gDNA preparations for PCR were also prepared using Chelex 100 resin (Sigma). Single colonies of *C. sporogenes* were resuspended in 100 µl nuclease free water containing a small amount of Chelex resin. Samples were briefly vortexed and then boiled for 10 min. The supernatant was then used as a template for PCR reactions. Fresh preparations were used for each PCR.

2.3.2 Polymerase Chain Reaction

2x Phusion polymerase high fidelity master mix (NEB) was used for reactions that required high accuracy. 20 µl reactions volumes were prepared with either 200 ng of *C. sporogenes* gDNA or 1 ng of plasmid DNA as the template plus 10 µM of the forward and reverse primers. 5% (v/v) DMSO was also added to most reactions. Initial denaturation was carried out at 98°C for 30 sec followed by 32 cycles of denaturation at 98°C for 30 sec, annealing at 50-65°C for 30 sec, and extension at 72°C for 20 sec per kb. A final extension at 72°C for 5 min was performed to complete any partial products.

Taq polymerase was used for colony PCRs where high fidelity was not required. A 2x master mix, prepared in house, was used. Each reaction contained 10 µl Taq polymerase mix, 1 µl of forward and reverse primer, 8 µl nuclease free water and 1 colony. Initial denaturation was carried out at 95°C for 3 mins followed by 35 cycles of denaturation at 95°C for 30 sec, annealing at 58°C for 30 sec, and extension at 72°C for 1 min per kb.

PCR reactions were performed using a T100 Thermo Cycler (Bio-rad). Primers were synthesised by Eurofins.

2.3.3 Agarose Gel Electrophoresis

0.8% (w/v) agarose in TAE buffer was melted in a microwave and cooled to approximately 55°C before being cast into a horizontal Perspex tray with the addition of SybrSafe DNA stain (1/10,000 final volume) (Invitrogen). Solidified gels were submerged in TAE buffer in an electrophoresis tank. DNA loading buffer was added to the DNA samples, either standard DNA loading buffer (New England Biolabs) or UView (Bio-rad) for gel extraction, and samples were loaded into the gel wells. Gels were subjected to electrophoresis at 110 V for 30 minutes.

2.3.4 Purification of PCR Products

PCR products were purified using a GeneJET Purification kit (Thermo) as per the manufacturer's instructions, or by gel extraction (see below). DNA was eluted in 20 µl nuclease free water and quantified using A_{260} spectroscopy.

2.3.5 Gel Extraction of DNA

DNA samples were resolved on agarose gels and the DNA was visualised using a UV transilluminator. Bands were excised using a scalpel and DNA was extracted from the gel using the GeneJET Gel Extraction kit (Thermo), as per the manufacturer's instructions. DNA was eluted in nuclease free water and quantified via A_{260} spectroscopy.

2.3.6 Restriction Endonuclease Digestion of DNA

Restriction enzymes were used to cleave DNA as per the manufacture guidelines (New England Biolabs). CutSmart buffer was required for use with all enzymes used in this study and was added at a 1:10 ratio to solutions of purified DNA and incubated at 37°C for 1 hr.

For removal of template plasmid DNA from completed Phusion PCR reactions, 2 µl of *Dpn*I was added to the PCR reaction mixture and incubated at 37°C for 2 hrs.

Digested DNA was purified via gel extraction (see above).

2.3.7   Ligation of DNA

DNA fragments were ligated using T4 DNA ligase (New England Biolabs) as described in the manufacturer's instructions. In short, reactions contained 1x T4 ligase buffer, 25 ng vector DNA, insert DNA in a molar ratio of 1:3 vector to insert, and nuclease free water to make a 10 µl final volume. Reactions were incubated at RT for 1 hr before being transformed into *E. coli* (see below).

2.3.8   Gibson Assembly of DNA Fragments

Gibson Assembly allows for the joining of multiple overlapping DNA fragments in a single reaction (Gibson et al. 2009). A 2x Gibson Master Mix was made according to protocol (Appendix 2).

Vector DNA was linearised using either Phusion PCR or by restriction endonuclease digestion. Insert fragments were amplified utilising primers that contained a 30 bp overlapping sequence with the adjacent DNA fragment. PCR fragments were isolated via gel extraction (see above). Reactions were performed in a final volume of 20 µl, with 40-50 ng of linearised vector and a vector:insert:insert ratio of 1:2:2 for a three fragment Gibson reaction. 10 µl of 2x Gibson Master Mix was added to the sample and the volume made up to 20 µl with nuclease free water. Samples were then incubated at 50°C for 4 hr before being used in *E. coli* transformations.

2.3.9   Production of Chemically Competent *E. coli*

O/N cultures of *E. coli* were sub-cultured 1:100 and incubated at 37°C shaking until they reached exponential growth phase (OD_{600nn} 0.4-0.6). Cells were then harvested by centrifugation (10 min, 4,000 x g at 4°C), resuspended in 5 ml ice-cold 100 mM $CaCl_2$ and were incubated on ice for 15 min. Cells were harvested as before and resuspended in 1 ml 100 mM $CaCl_2$ with 15% (v/v) glycerol prior to being incubated on ice for 2 hr. 50 µl aliquots were then snap frozen in liquid nitrogen before being stored at -80°C.

2.3.10 Transformation of *E. coli*

2 µl of ligation or Gibson Assembly reaction, or approximately 0.5 µl of a plasmid miniprep, was added to approximately 25 µl of competent *E. coli* cells (NEB5α or CA434) and incubated on ice for 30 min. Cells were then heat shocked at 42°C for 30 sec and incubated on ice for a further 2 min. 500 µl of SOC medium was then added and the mixture incubated at 37°C shaking for 1 hr. Following this 100 µl of mixture was spread onto LB agar plated containing appropriate antibiotic(s).

2.3.11 Isolation of Plasmid DNA

5 ml of *E. coli* O/N culture was harvested by centrifugation (10 min, 4,000 x g) and plasmid DNA was extracted using the GeneJET Plasmid Miniprep kit (Thermo) as per the manufacturer's instructions. DNA was eluted in 60 µl nuclease free water.

2.3.12 Sequencing of DNA

Sequencing of plasmid and PCR amplified DNA was carried out by using Genewiz Sanger Sequencing services. Geneious software was used for the analysis of sequencing data. Illumina sequencing of the *C. sporogenes* genome was carried out by MicrobesNG and genome assembly by Dr Roy Chaudhuri (University of Sheffield, UK).

2.3.13 Conjugation of Plasmid DNA into *C. sporogenes*

Conjugation of plasmid DNA into *C. sporogenes* was done using an adapted version of the method previously described (Kirk and Fagan 2016). 1 ml of O/N culture of plasmid containing *E. coli* strain CA434 was harvested gently by centrifugation (2 min, 4,000 x g). The pellet was then resuspended in 200 µl of *C. sporogenes* O/N culture. The resulting cell suspension was spotted onto a pre-reduced BHI plate and incubated for 8-24 hr. After incubation, growth was harvested using approximately 900 µl pre-reduced TY broth and an L-shaped spreader. Harvested growth was then spread onto plates containing colistin, to prevent *E. coli* growth, and thiamphenicol to select for the conjugated

plasmid. Transconjugants were restreaked onto BHI colistin thiamphenicol plates once more before further use to ensure purity.

2.3.14 Allele Exchange Mutagenesis in *C. sporogenes*

Allele exchange using the *codA* heterologous counterselection system was previously used for precise manipulation of the *C. difficile* genome (Cartman et al. 2012). A modified version of this system was used for the generation of knockouts in *C. sporogenes* where the *codA* gene was replaced with *mazF*, expression of which is controlled by a xylose inducible promoter. Genes of interest were to be replaced with *ermB* under the control of the *cwp2* promoter providing resistance to erythromycin and thus adding a selection marker to mutant strains.

600-1200 bp fragments upstream and downstream of the gene to be knocked out were amplified by PCR as well as the *ermB* resistance cassette and purified. PCR products were ligated into pHF012 using Gibson assembly. The resulting plasmids were transferred into *C. sporogenes* via conjugation.

Single recombination was confirmed by PCR and colonies restreaked on BHI agar supplemented with erythromycin and incubated for 72 hrs to allow for the second recombination event and plasmid loss.

Growth was then harvested using 1 ml pre-reduced TY media and the resulting cell suspension was used to inoculate 10 ml pre-reduced TY containing xylose to promote the expression of *mazF* used for counter-selection. Cultures were left for 8 h before being serially diluted in TY media and plated onto BHI containing erythromycin and 3% xylose.

Colonies were screened after 48-72 h using primers flanking the altered site and colonies restreaked onto BHI supplemented with thiamphenicol to confirm plasmid loss. The resulting fragment was then sequenced.

2.4 Protein Overexpression

2.4.1 Heterologous expression of Csx Proteins in *E. coli*

A single colony of transformed *E. coli* (Rosetta) was used to inoculate 5 ml LB supplemented with appropriate antibiotics. This was incubated at 37°C shaking for 8 hrs before subculturing into 50 ml 2xYT media at an OD 0.05 and left shaking at 37°C O/N. The O/N culture was used to inoculate 500 ml 2xYT supplemented with appropriate antibiotics to an OD 0.1 and was incubated at 37°C shaking until an OD 0.6-0.8 was reached. 500 µl of 1 M IPTG was then added to the culture to induce expression and cultures were placed at 37°C shaking 3 hrs (CsxA) and 25°C shaking 4 hrs (CsxB and CsxC). Cells were harvested by centrifugation at 4,000 x g for 10 mins. Cell pellets were stored at -20°C.

2.4.2 SDS-PAGE Analysis

SDS-PAGE analysis was used to determine the levels of Csx protein expression by resolving proteins from cell lysate based on molecular weight (Laemmli 1970). SDS-PAGE gels were prepared as detailed in Table 2.4 using a stacking gel of 5% and a resolving gel of 15%.

Table 1.5: SDS-PAGE gel recipe

15% Resolve Gel		5% Stacking Gel	
30% Acrylamide:bisacrylamide (37:5:1)	5 ml	30% Acrylamide:bisacrylamide (37:5:1)	833 µl
1.5 M Tris pH 8.8	2.5 ml	0.5% Tris pH 6.8	1.25 ml
MQ	2.4 ml	MQ	2.87 ml
10% SDS	100 µl	10% SDS	50 µl

10% APS	50 µl	10% APS	25 µl
TEMED	10 µl	TEMED	5 µl

2.4.2.1 Sample Preparation

Pre and post induction cell pellets were resuspended in 50 mM Tris pH 8 and samples were sonicated at 40% amplitude for 7 s x 3. Samples were centrifuged at 21,000 x g for 2 min. The supernatant was kept as the soluble fraction and the pellet was resuspended in 1 ml MQ to provide the insoluble fraction. Protein concentration was determined by Bradford Assay (Section 2.4.2.2). 20 µg of protein for each sample (as determined by Bradford Assay) was taken and made up to 15 µl in MQ for the soluble fraction and 4% SDS for the insoluble fraction. 5 µl of SDS loading dye (50 mM Tris pH 6.8, 2% SDS, 10% glycerol, 12.5 mM EDTA 0.02% bromophenol blue, 100 mM DTT) was then added to the samples. Where required samples were boiled for 5 min at 95°C. Samples were then loaded onto the SDS-PAGE gels and electrophoresis was performed at a constant voltage (200V) for 40 min or until the dye front approached the bottom of the gel. Gels were stained using Quick Coomassie Stain (Protein Ark) for 15 min.

2.4.2.2 Bradford Assay

Protein concentration was determined by Bradford assay (Bradford 1976). 1-10 µl of protein sample was added to a cuvette with 800 µl MQ and 200 µl Bradford reagent (BioRad) and was mixed by inversion. Absorbance readings were taken at OD_{595} and the protein concentration was determined using the following formula:

$$Protein\ concentration\ (mg/ml) = \frac{OD_{595} \times 15}{volume\ protein\ (\mu l)}$$

2.5   Light Microscopy

2.5.1   Cell Fixation

A fixation cocktail was used which consisted of 20 µl 1 M $NaPO_4$ (pH 7.4), 100 µl 16% (w/v) paraformaldehyde and 4 µl 25% (w/v) glutaraldehyde per 0.5 ml of cells (Ransom, Ellermeier, and Weiss 2015). 0.5 ml of sample was added to the cocktail and incubated for 30 min at 37°C then on ice for 15 min. Samples were centrifuged at 5,000 x g for 1 min and washed in 500 µl PBS or TBS. The wash step was repeated a further 2 times. The pellets were resuspended in 30 µl PBS or TBS and stored at 4°C.

2.5.2   Phase Contrast Microscopy

For phase contrast and fluorescence microscopy cells were fixed and resuspended in sterile water before being dried onto a glass slide. Slides were rinsed using distilled water and dried. Cover slips were mounted in 80% glycerol. Samples were visualised using a Nikon Ti Eclipse inverted microscope at the Wolfson Light Microscopy Facility at the University of Sheffield.

2.5.3   Live Cell Imaging

For live cell phase contrast imaging of *C. sporogenes* germination, 10 µl of an OD_{600nm} 10 spore suspension were placed under a pre-reduced 1% TY agarose gel pad in a glass bottomed petri dish. Petri dishes were sealed with parafilm before being removed from the anaerobic cabinet and imaged. Samples were visualised using a Nikon Ti Eclipse inverted microscope at the Wolfson Light Microscopy Facility at the University of Sheffield.

2.6 Electron Microscopy

2.6.1 Sample Preparation

Table 1.6: EM Reagents

Reagent	Components
Uranyl Formate (UF) 0.75%	0.035 g uranyl formate (polysciences Inc.) 5 ml distilled water 8 μl 5 M NaOH
Uranyl Acetate (UA) 2%	0.093 g uranyl acetate (Polysciences Inc.) 5 ml distilled water 8 μl 5 M NaOH
Reynold's Citrate	1.33 g lead nitrate 1.76 g sodium citrate 50 ml CO_2 free distilled water 7 ml 1 M NaOH pH12 +/- 0.1
3% Glutaraldehyde	50% glutaraldehyde 0.1 M sodium cacodylate buffer
2% aqueous OsO_4	Osmium tetroxide (Agar Scientific)
Araldite Resin	10 ml araldite resin CY212 (Agar Scientific)

| | 10 ml dodecenyl sunnic anhydride (DDSA, Agar Scientific) |
| | 1 ml benzyldimethylamine (BDMA, Agar Scientific) |

2.6.1.1   Negative Stain Grids

Negative stain samples were prepared on 300 mesh copper palladium grids (EM Resolutions) that had a carbon film applied to the surface to provide a hydrophilic layer for improved sample adherence. Carbon coating was carried out in house and involved evaporating high purity carbon (Agar Scientific) onto a sheet of mica (Agar Scientific) resting atop a sheet of filter paper. Evaporating carbon was done under vacuum using the Quorum Q150T. The thickness if the carbon film was determined visually and was approximately 150-300 Å thick. The carbon layer was then floated over the copper grids as previously described in (Harris 2007).

2.6.1.2   Negative Staining for TEM

Carbon coated grids were glow discharged for between 15-60 sec depending on the age of the grids. 5 µl of sample was applied to the carbon surface of the grids and left for 1 min. The grids were then blotted and washed in 2 drops of distilled water and blotted again. The grids were then dipped in uranyl formate (Table: 2.5) and blotted before being held in a final drop of uranyl formate for 20 sec and blotted to remove excess liquid. The grids were then dried using a vacuum pump.

2.6.1.3   Chemical Fixation for TEM

Spore pellets were fixed with 3% glutaraldehyde (Table: 2.5) and left O/N at 4°C. The pellet was washed with 0.1 M sodium cacodylate buffer and the supernatant discarded immediately. A further two washes with 0.1 M sodium cacodylate buffer were carried out leaving the sample for 20 minutes between each wash. The final pellet then underwent secondary fixation with 1% aqueous osmium

tetroxide (OsO_4) (Table: 2.5). This was left for 2 hours before being washed twice with 0.1 M sodium cacodylate buffer.

Samples were then dehydrated using a series of ethanol washes increasing in concentration each time: 50%, 75%, 95% and 100%. Each ethanol concentration was left on the sample for 15 minutes before it was removed and replaced. The final 100% ethanol wash was repeated twice followed by two further washes with propylene oxide.

The samples were then infiltrated with resin. A 1:1 mix of propylene oxide and araldite resin (Table: 2.5) was added to the samples and left at RT, 2 rpm O/N. The mix was then removed leaving just a thin layer on top of the samples and the propylene oxide was left to evaporate for 1 hr. Pure araldite resin was then added to the samples and left at RT, 2 rpm for 3-4 hrs. The resin was replaced with fresh and left again for a further 3-4 hrs. The final sample was then embedded in fresh araldite resin and left to polymerise for 48-72 hrs at 60°C.

2.6.1.4   Thin Sectioning and Post Staining

Plastic resin blocks were sectioned using the Reichert Ultramicrotome to generate 70-90 nm thin sections. Sections were loaded onto nickel grids and post stained with 3% UA for 30 min and Reynold's Lead Citrate for 5 min (Table: 2.5). Grids were washed in water after each stain and left to dry on filter paper before imaging.

2.6.1.5   Cryo Sample Preparation

Samples for tomography were prepared using the Leica EM GP plunge freezer that allows for automatisation of the plunge freezing process. The chamber was set to 10°C and 80% humidity. 10 μl of OD_{600nm} 20 spores 2h post germination initiation were combined with 10 μl BSA treated 10 nm gold fiducial markers. 3.5 μl of sample was then applied to Quantifoil R2/2 grids and incubated for 1 min before botting for 2 sec. This was carried out automatically by the blotting arm equipped with filter paper (Whatman no.1). This was swiftly followed by rapid plunging of the grid into liquid ethane. Grids were then transferred into grid holders and stored in liquid nitrogen.

2.6.2 Electron Microscopy Data Collection

2.6.2.1 TEM of Negatively Stained Samples

Negatively stained samples were imaged on a Philips CM100 Philips Transmission Electron Microscope (TEM), with a LaB_6 source operated at 100 kV. Images were acquired on a Gatan 1k x 1k Multiscan 794 CCD camera.

2.6.2.2 TEM of Thin Sections

Thin sections were screened on the FEI Tecnai T12 with a tungsten source operated at 80 kV. Images were acquired on a Gatan Orius SC1000B 2672 x 4008 pixels CCD camera.

2.6.2.3 Tomography

Tomography data were collected in-house on an Tecnai Arctica at 200 kV equipped with the Falcon III direct electron detector (Thermo Fisher Scientific). The tomo software (Themo Fisher Scientific) was used to operate the microscope and set up automated data collection. An atlas of the grid was collected to provide an overview of the entire grid to screen for ice thickness and identify areas for data collection. 9 positions were selected containing spores at varying stages of the germination process and the eucentric height and off-sample focus points were set. Tilt series were collected at a magnification of 16,600x (0.663 nm pixel size) from -20° to +60° and then from -20° to -60° at 3° increments with a total dose of 100 electrons/$Å^2$ across each tilt series.

2.7 Image Processing

2.7.1 Spore Measurements

Spore features were measured from thin sections using the 3dmod drawing tools. The width of the spore body was measured across the widest region of transverse spore sections from outer coat to outer coat. The spore body length was measured across the longest region of longitudinal sections.

The spore core was measured where clear staining within the spore body allowed. The core width was measured across the widest region of the darkly stained centre of transverse spore sections. The core length was measured across the longest region of longitudinal sections.

Cortex thickness was only measured in spores with clear staining of the spore body. 4 measurements were taken from each spore from the inside of the spore coat to the core outer core edge and averaged to provide a estimate of cortex thickness.

The interspace was measured at 3 points across each spore from the exosporium to the exterior of the coat. These were averaged to provide an estimate of interspace thickness. Measurements were not taken from the poles of the spores where the exosporium is extended. In the case of *csxA* spores the interspace was measured from the outermost parasporal layer to the exterior of the spore coat.

2.7.2 2D Crystal Data Processing

The 2dx software was used for processing electron crystallography data which is a user-friendly package based on the MRC suite of programmes (Crowther, Henderson, and Smith 1996; Gipson et al. 2007; Henderson and Unwin 1975; Renault et al. 2006; Valpuesta, Carrascosa, and Henderson 1994). The workflow for image processing is shown in figure 2.1. Details of the steps are described below.
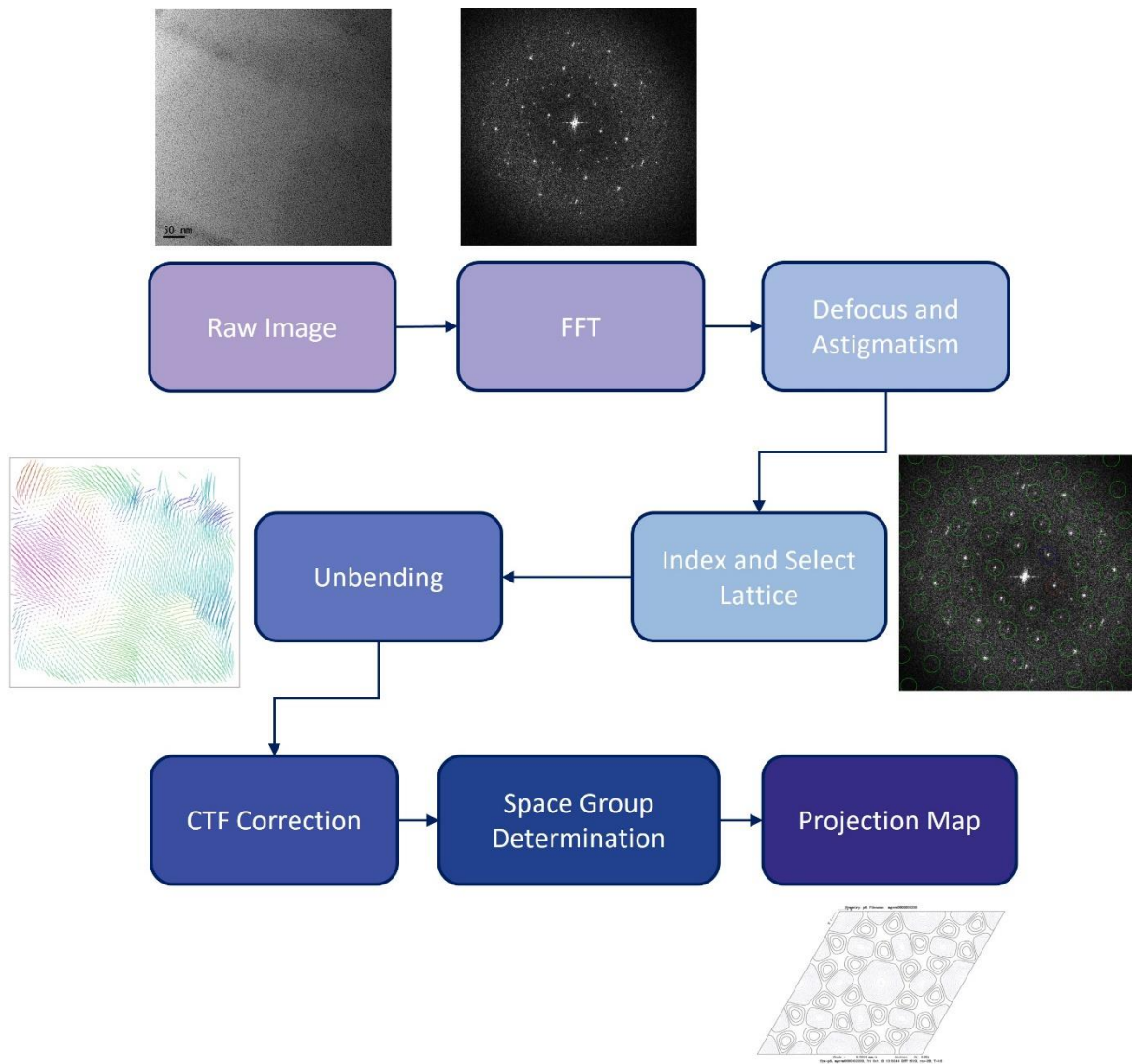
Figure 2.1: Workflow for Electron Crystallography Image Processing

2.7.2.1 Fast Fourier Transform (FFT) and Indexing

A Fourier transform of each raw micrograph was generated using the *FFTRANS* script. The FFT contained sharp peaks (diffraction pattern) resulting from the repeating units of the crystal lattice. Due to the nature of the biological sample these were often blurred due to distortions in the crystal lattice and background noise from the carbon film. The CTF can be seen in the FFT as dark and light concentric rings, Thon rings. These were not regularly seen in the negative stain data.

Micrographs were collected with defocus that allows for additional contrast within the image. This has to be accounted for during the processing. CFTFIND3 was used to calculate the defocus and astigmatism within the image which determines the CTF.

A first attempt at indexing the crystal lattice was done automatically by running GETLATTICE. The lattice defined could then be further refined manually. Alternatively the lattice was manually indexed from the start by identifying the Miller indices h and k. These correspond to the reciprocal lattice vectors 0,1 and 1,0. The FINDLAT script was then run to identify the rest of the lattice.

2.7.2.2 Unbending

Diffraction spots from the crystal lattice were selected using GETSPOTS1 which generates a spot list to be used during the unbending process. Unbending is an iterative process that corrects for translational crystal distortion and involves several steps. Firstly, the FFT is masked to remove noise and to isolate only the diffraction spots. A small reference patch was selected from the image that showed clear strong crystallinity. The reference patch was then cross correlated with the entire image and a displacement map was produced showing the distortions in the crystal compared to the reference patch. Distortions in the crystal lattice were corrected by interpolation and an FFT with sharper diffraction spots was produced indicating increased SNR. This was then used for a second round of unbending. After each round of unbending the IQ values of the image were checked. IQ values are an expression of SNR and give an idea of the image quality. An IQ value of 7 is considered background noise while an IQ value of 1 corresponds to a signal 7-fold higher than noise.

2.7.2.3 CTF Correction

Following unbending the phase contrast transfer function (CTF) was corrected for using the script CTFAPPLYK. This involves phase flipping and amplitude correction to bring high order spots beyond the first Thon ring into phase. For the magnification and defocus used for negative stain imaging the majority of the diffraction spots fall within the first Thon ring.

2.7.2.4 Space Group and 2D Projection Maps

Finally, the symmetry and phase origin of crystals was determined using ALLSPACE. This uses the lattice parameters, phase and amplitude information to determine which of the 17 plane groups possible for a 2D crystal are most likely for the imaged crystal. An internal phase residual is determined and compared to theoretical phase residuals for each plane group. All symmetry groups indicated as having low phase residuals are considered possible. The most appropriate symmetry is then imposed to enhance SNR of the final 2D projection map produced using generateSymMap.

2.7.2.5 Merging Processed Images

Processing individual images results in a list of spots containing their amplitudes and phases in Fourier space. 2D merging averages the Fourier components of the images together to produce a more reliable image. The process involves aligning images one by one to a reference. To begin with, an image was picked that had a high QVal or lots of good IQ value spots as an initial reference. Another image is then aligned to the reference by refining the phase origin. The refinement can be checked to ensure that the phase residual is low and that the cross-correlation plot shows a clear central peak. Providing this is the case the images can be merged to produce a new reference. This process was repeated until all suitable images were merged.

Merging involved the averaging of phase and amplitude values for each unique reflection. The script AVRGAMPHS weights each reflection based on its IQ value thereby ensuring that each diffraction spot of every image contributes to the average according to its SNR. This allows for images with majority bad IQ spots to be merged without compromising on the quality of the final 2D projection map. The list of averaged amplitudes and phases is then inverse Fourier transformed to produce the final merged 2D projection map.

2.7.3 Tomography Processing

For the processing of tomography data the IMOD software package was used (Mastronarde and Held 2017b). The workflow for processing is shown in figure 2.2. Details of the steps are described below.
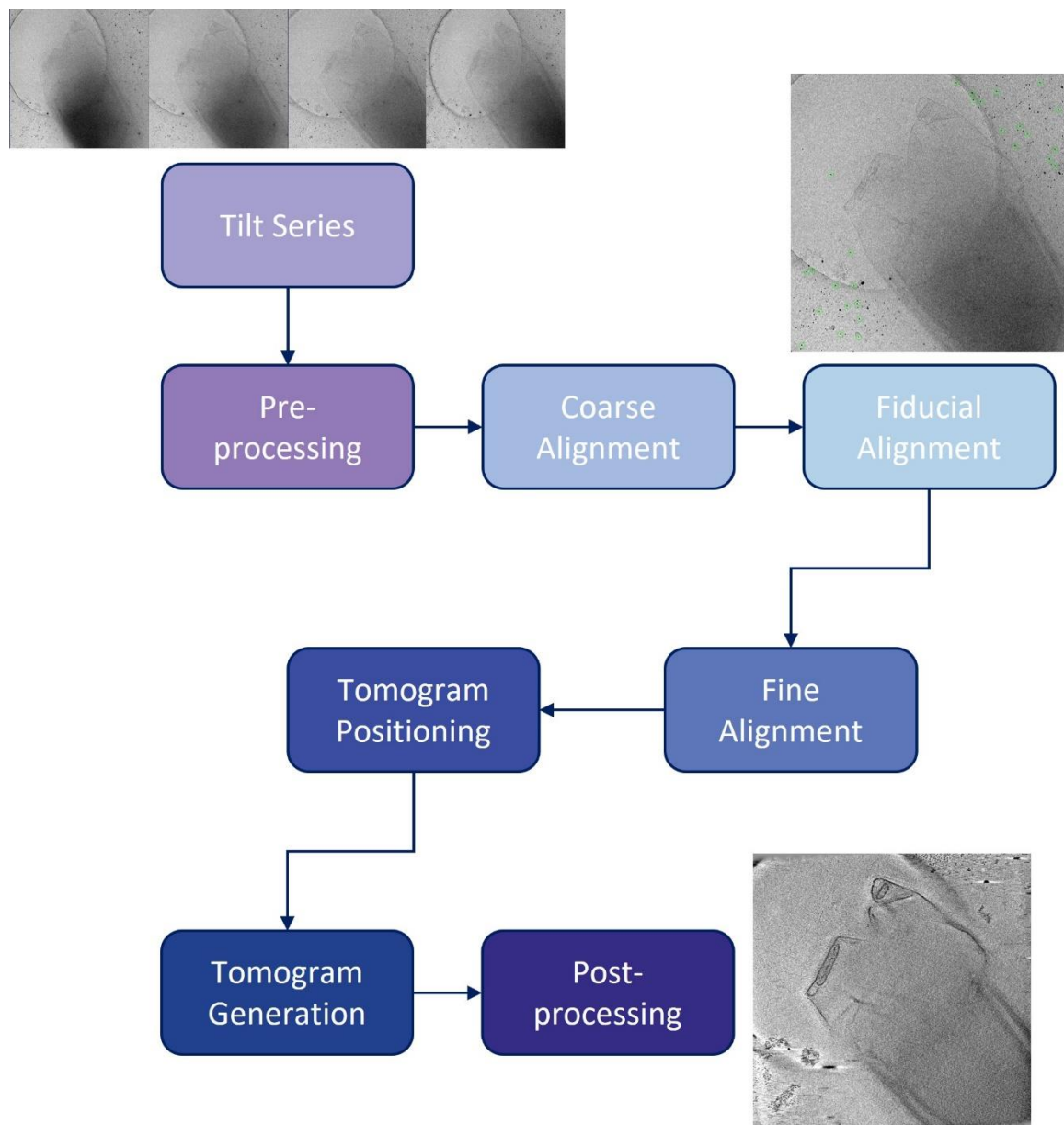
Figure 2.2: Workflow for Tomography Data Processing

2.7.3.1 Pre-processing

Prior to processing the dataset was screened for anomalous pixels corresponding to X-rays or flaws in the detector which can cause extreme high or low intensity pixels. These were identified and removed using CCDERASER.

2.7.3.2 Coarse Alignment

An initial course alignment of the tilt series was conducted using TILTXCORR. This determines the x and y translations required for aligning each image.

2.7.3.3 Alignment

Alignment of the tilt series is the most important step of generating tomogram reconstructions and relies on tracking of features within the tilt series. Gold fiducials were added to spore samples to aid this process. The fiducial markers were mapped automatically using AUTOFIDSEED, or picked manually. BEADTRACK was then used to track the fiducial markers throughout the tilt series.

2.7.3.4 Fine Alignment

The fiducial model produced during the 'alignment stage' was imposed on the full tilt series by running TILTALIGN. The COMPUTEALIGNMENT provides the mean residual error output from which the initial model can be adjusted in 3dmod to remove or adjust fiducials with large residual errors. This was a largely iterative process however the more robust the fine alignment the better the reconstruction at the end. The residual mean error for fiducial aligned tilt series was ~0.6 - 0.9 pixels.

2.7.3.5 Tomogram Positioning

Tomogram reconstruction is a computationally intensive process and therefore the volume that is reconstructed is made as small as possible prior to generation. The thickness of the tomogram is defined and the top, middle and bottom of the region of interest is defined in the y axis. Running TOMOPITCH analyses these boundaries and determines the shift required to make the section flat. TILTALIGN is then run to generate the final alignment.

2.7.3.6   Tomogram Generation

Tomogram reconstruction was done using WBP with SIRT-like filters which provided reduced noise

levels provided by SIRT without running the computationally intensive SIRT processes. This was done

by running the TILT script with FAKESIRTITERATIONS at 5 iterations.

2.7.3.7   Post-processing

After tomogram generation the final volume was trimmed and the contrast adjusted. Volume

trimming was performed to ensure that the tomogram contains only the sample of interest.

Boundaries were manually drawn and TRIMVOL was used to cut the volume to the specified

dimensions. It was also important to optimise the contrast to ensure this was based on biological

features. This was done by selecting a region of interest within the sample and running

FINDCONTRAST to find and apply the appropriate contrast values.

3   Ultrastructural Analysis of *Clostridium sporogenes* Germination

3.1   Introduction

The transition from spore to vegetative cell involves three major stages: germinant detection and DPA release, cortex hydrolysis, and cell emergence and outgrowth (Olguín-Araneda et al. 2015; Setlow 2014). Spores typically germinate in response to environmental cues, germinants, that indicate conditions favourable to vegetative cell survival. For *C. sporogenes* several key molecules have been proposed to trigger the germination process, but the precise conditions required for complete germination are currently unknown. In addition, previous work on germinants has focused purely on the initial stages of spore rehydration with work predominantly conducted in Tris buffer (Brunt et al. 2014). These conditions are unsuitable for the continued survival of the emerging cells, so further study into the entire germination process is required for a complete understanding.

Cortex hydrolysis is thought to be carried out by two enzymes CwlJ and SleB in *C. sporogenes*, activated by the release of DPA from the spore core (Tovar-Rojo et al. 2002). CwlJ is localised at the boundary between the cortex and coat (Bagyan and Setlow 2002) and SleB is thought to be localised to the inner membrane through interaction with YpeB (Boland et al. 2000). Cortex degradation has been observed in thin sections of germinating *C. difficile* (Baloh et al. 2022), however, *C. difficile* is known to have a different mechanism of germination to *C. sporogenes* and it remains to be seen if a similar process can be observed in *C. sporogenes*.

The structural composition of *B. anthracis* exosporium suggests a possible mechanism for cell emergence via the bottle cap model (Steichen et al. 2007). This model built on the evidence for a cap structure present within the exosporium concluding that the cap could provide a weak point from which the newly developed cell could emerge from the spore. A similar cap structure is also seen in the closely related *B. cereus* (Terry et al. 2017). Polar emergence through the cap has been observed in *B. anthracis* (Steichen et al. 2007); an aperture at the pole of the exosporium of *C. sporogenes*,

observed by SEM (Brunt et al. 2015), could imply a similar course of events in *C. sporogenes*. Thin sectioning of *C. sporogenes* also showed polar emergence of cells but clear ultrastructural details of the spores undergoing outgrowth were not distinguishable (Hoeniger and Headley 1969). Further investigation into the presence of a cap structure in *C. sporogenes* is required as well as detailed analysis of the ultrastructure of the spores undergoing germination to get a more complete picture of the germination and outgrowth process in *C. sporogenes*.

3.2   Aims

In order to understand the changes that occur structurally during germination it was initially important to consider dormant *C. sporogenes* spores. Negative stain TEM and thin sectioning of dormant spores was carried out to provide a basic structural understanding. Conditions for *C. sporogenes* germination were determined and live cell imaging was conducted to observe the germination process in real time and determine what changes occurred at the individual spore level. Negative stain TEM was used to gain an initial understanding of the phases of germination at higher resolution and electron crystallography was employed to determine if the crystallinity of the exosporium remained the same post germination. This was followed by thin sectioning of germinating spores to really understand the ultrastructural changes occurring within the spore during the germination process. Initial attempts were also made at moving towards gaining high resolution information through cryo electron tomography.

3.3 Results

3.3.1 *C. sporogenes* Endospore Morphology

3.3.1.1 General Spore Morphology

Samples of purified *C. sporogenes* NCIMB 701792 spores were negatively stained and screened by TEM. Micrographs showed a dense spore body (Fig: 3.1A pink arrows) completely surrounded by a baggy exosporium that extended further at one pole. High magnification micrographs of the exosporium revealed a para-crystalline organisation with a hairy nap decorating the surface, clearly visible at the edges of the para-crystalline layer (Fig: 3.1D and E). The spores also displayed several different types of appendage including beaded fibrils and thicker large appendages (Fig: 3.1C).

Atomic force microscopy (AFM) of whole spores (carried out by Dr. Nicholas Mullin, University of Sheffield) showed a gross spore morphology similar to that seen by TEM with the exosporium surrounding the spore body (Fig: 3.2). In some images it appeared that the pole of the exosporium was broken open (black arrow) with a cap-like structure folded back. The hairy nap was visible as a fringe on the surface of the exosporium and both beaded fibrils (light blue arrow) and large appendages (green arrow) were visible. The beaded fibrils appeared to be localised to the pole with the cap-like structure. The AFM images also revealed surface details across the spore body region including ridges in the exosporium as it enveloped around the spore body and traces of a large appendage present potentially beneath the surface of the exosporium (yellow arrow).
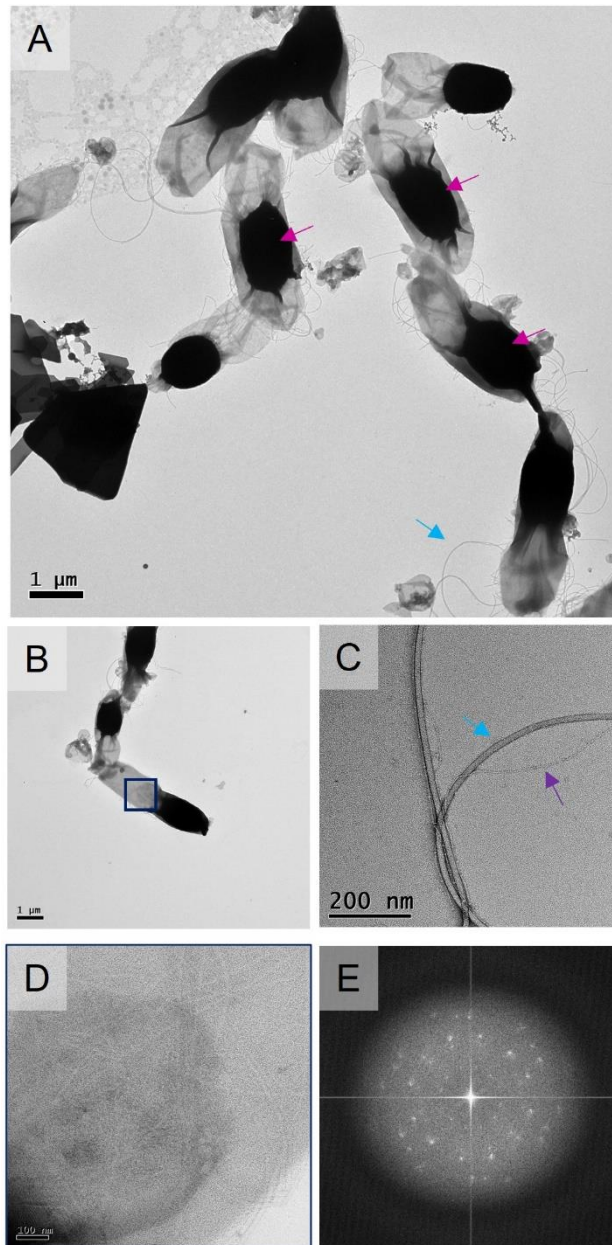
Figure 3.1: *C. sporogenes* **NCIMB 701792 Spores by Negative Stain TEM**

A) Low magnification of *C. sporogenes* spores, arrows indicate spore body (pink) and large appendages (light blue) B) Higher magnification of *C. sporogenes* spores show a dense spore body and baggy exosporium layer. Box highlights area shown in (D). C) High magnification of surface appendages, large appendage (light blue arrow) and beaded fibrils (purple arrow) D) High magnification of the exosporium area from (B) E) FFT of exosporium from (D) showing the crystalline nature of the exosporium. Unit cell dimensions $a = b = 110$ Å $y = 120°$
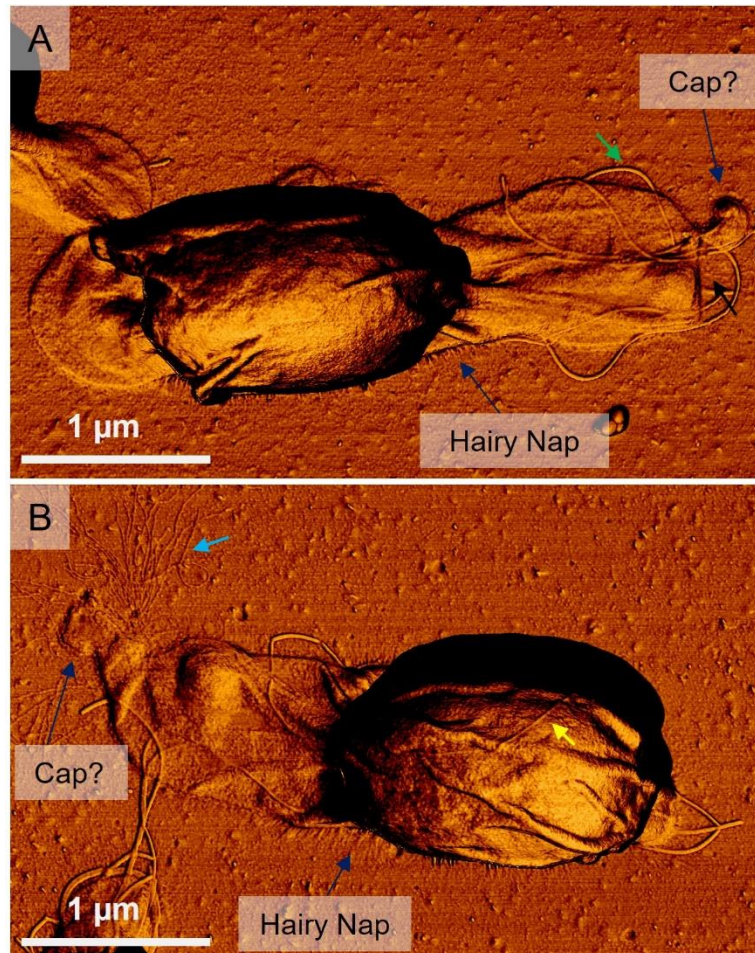
Figure 3.2: AFM of *C. sporogenes* Spores

A + B) Imaging shows a large spore body surrounded by a baggy exosporium that is extended towards one pole. A possible cap region is indicated at the pole of the extended exosporium. Arrows indicate beaded fibrils (light blue), flagella-like appendages (light green), appendage lying beneath the exosporium (yellow arrow) and a possible opening to the exosporium (black arrow).

Images provided by Dr Nic Mullin (Department of Physics and Astronomy, University of Sheffield, UK)

3.3.1.2   Internal Spore Structure

To gain a detailed view of the internal structure of the spore, samples were subjected to chemical

fixation, as detailed in (methods section 2.6.1.3), and thin sections (70-60 nm) were prepared and

imaged by TEM. The sections showed distinct variably stained layers constituting the ultrastructure

of the spore (Fig: 3.3). The central spore core was darkly stained with an average width of 480 nm ±

60 nm and length of 830 nm ± 90 nm (n = 15). It was possible to discern some details of internal

assemblies present within the core including ribosomes that were visible as darkly stained spots (Fig:

3.3 pink arrows). The plasma membrane and the germ cell wall were not clearly identifiable in these

sections. The cortex was present as a lightly stained region interior to the coat and surrounding the

central core, with an average thickness of 60 nm ± 40 nm. Within this region several darker stained
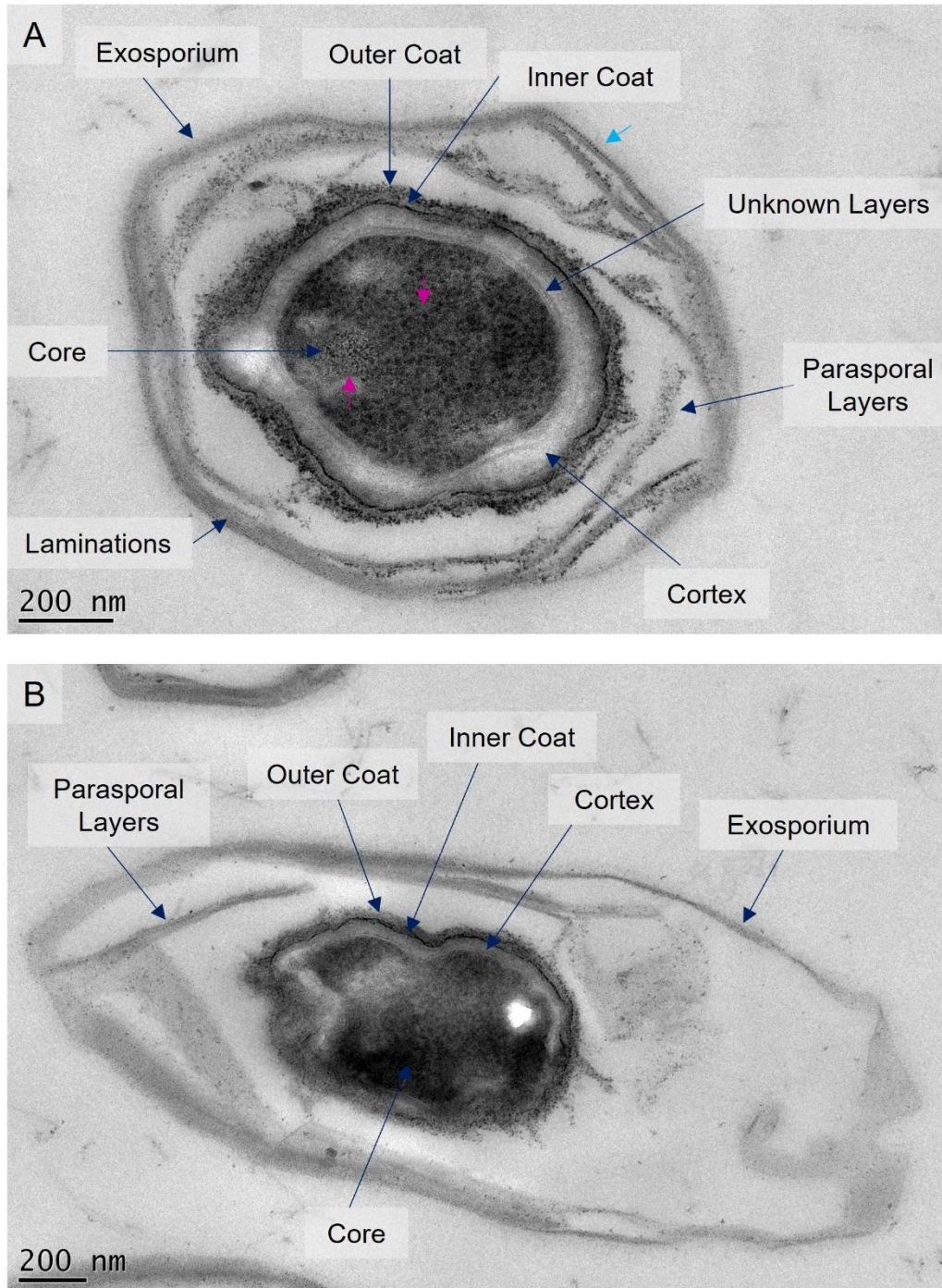
Figure 3.3: Thin sections of *C. sporogenes* Spores

A) traverse spore section displays the internal structure of the spore including parasporal layers
present in the interspace that often form laminations. Ribosomes can be seen in the core (pink
arrows) and individual units of the exosporium crystal lattice (light blue arrow) B) longitudinal spore
section displays extended exosporium and internal details of the spore body.

lamellae of unknown origin or composition were identified (Fig: 3.3A) similar to those observed in (Dafis-Sagarmendi 2021). The proteinaceous spore coat was heavily stained and outer and inner coat could be distinguished. The exosporium was identifiable as the densely stained outermost layer surrounding the spore. In some areas of the exosporium a crystal lattice was clearly visible as a regular array (Fig: 3.3A light blue arrow). The hairy nap on the surface was not visible in these thin sections. Parasporal layers were present between the coat and the exosporium, within the interspace of the spore, often stacking to form laminae.

3.3.2   Germination Conditions for *C. sporogenes*

The requirements for *C. sporogenes* germination were determined by testing a range of conditions based on (Brunt et al. 2014). By measuring the optical density of the sample at 600 nm it is possible to monitor the germination process within the population. Upon initiation of germination, the optical density of the spore suspension drops due to changes in the refractive properties of individual spores during DPA release and core rehydration (Setlow 2013). The optical density then increases as the vegetative cells emerge and outgrowth occurs. Figure 3.4A shows the initial stages of germination in a range of conditions. Germination in TY media alone showed a clear drop in OD_{600nm} followed by a short lag phase where the OD_{600nm} remained approximately constant . This was followed by a continuous rise in optical density corresponding to the outgrowth phase. Likewise, TY supplemented with 50 mM L-lactate as a germinant showed a similar profile, although the initial drop in OD_{600nm} appeared to occur marginally quicker than in unsupplemented TY. The lag phase and subsequent outgrowth remained consistent between the two conditions.

Figure 3.4: Germination Conditions for *C. sporogenes*

A) Germination was monitored by measuring the drop in OD_{600nm} due to spore rehydration and the subsequent increase due to outgrowth (condition dependent) for a variety of different conditions. TY media without supplementation proved adequate for germination. TY media supplemented with 50 mM L-lactate and 100 mM L-cysteine shows no increase in OD600nm during the course of the experiment. Experiments were conducted in triplicate on biological duplicates. The means ± standard deviations (error bars) are shown. B) Phase contrast microscopy of *C. sporogenes* spores 2 h and 4 h post germination initiation in the presence of 50 mM L-lactate and 100 mM L-cysteine. All spores appear phase dark indicating rehydration but very few free cells are seen. Scale bar = 6 μm

Tris buffer with no additional germinants showed no change in OD_{600nm} throughout the course of the experiment (Fig: 3.4A). Tris buffer supplemented with 50 mM L-lactate and 100 mM L-cysteine showed a clear drop in OD_{600nm} associated with the onset of germination but, due to lack of nutrients, showed no subsequent outgrowth. Interestingly, TY supplemented with 50 mM L-lactate and 100 mM L-cysteine showed no evidence of outgrowth within the time period of the experiment, despite showing a clear initial drop in OD_{600nm}. Phase contrast images 2 hr and 4 hr after germination with TY supplemented with L-lactate and L-cysteine showed phase dark spores and, in some cases, cells could be seen emerging from the pole of the spore (Fig: 3.4B). Very few free cells were observed in these samples.

As all the key features of the early stages of germination and outgrowth were observed in TY media this was used for all future germination experiments. A full germination assay, including subsequent outgrowth, in TY media was carried out over approximately 7 h (Fig: 3.5) and showed a clear initial drop in OD_{600nm} within the first 80 min. This was followed by a short lag phase of approximately 45 mins. Clear outgrowth was then observed as the OD_{600nm} began to rise due to exponential growth. After 300 min the cultures had reached the stationary phase.
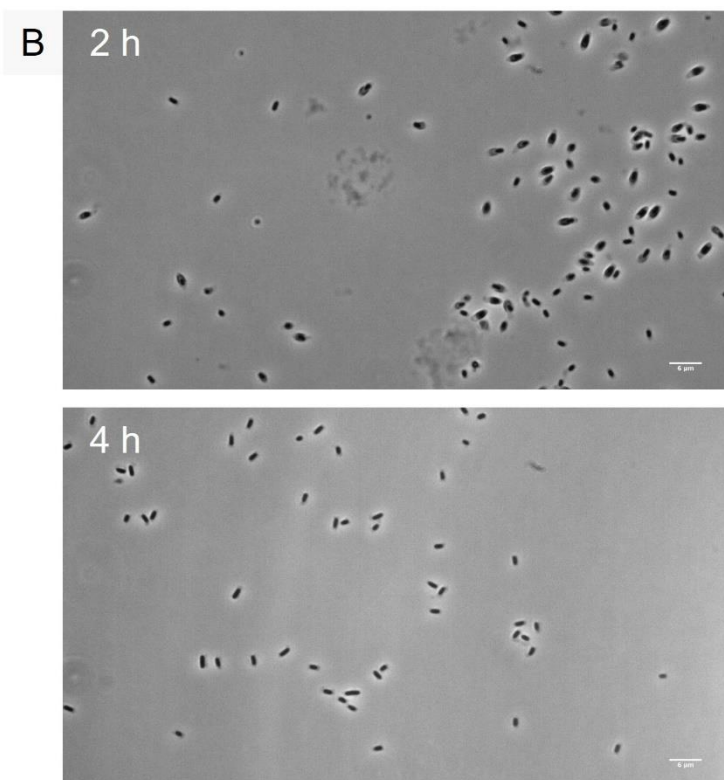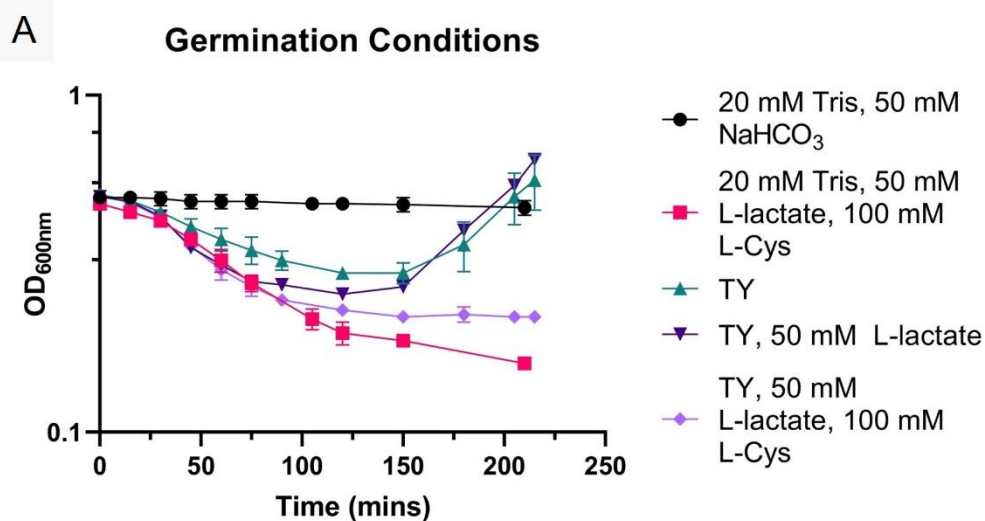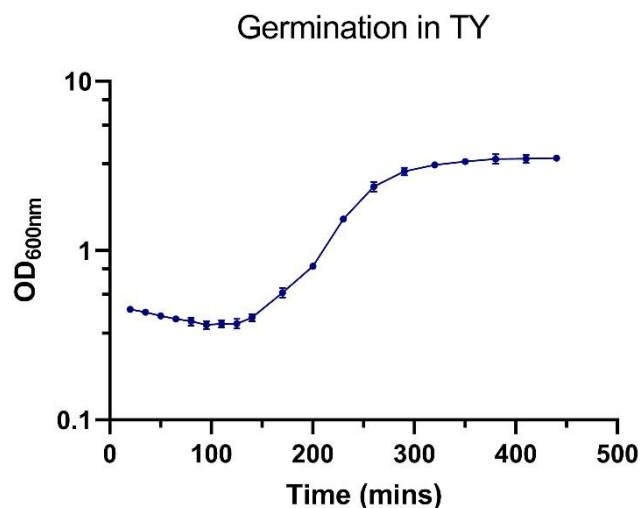

Figure 3.5: Germination of *C. sporogenes* in TY Media

Germination was monitored by measuring the drop in OD_{600nm} due to spore rehydration and the subsequent increase due to outgrowth. The assay was conducted in triplicate on biological duplicates. The means ± standard deviations (error bars) are shown.

3.3.3 *C. sporogenes* Germination is Asynchronous and Outgrowth is Polar

As OD_{600nm} measurements only provide a population average, live cell phase contrast microscopy was used to observe germination at the single spore level. A time course of *C. sporogenes* germination showed the transition from dormant spore to vegetative cell within a subset of the population over a 4 h time period (Movie 3.1, full time course in Appendix 3). The germination process was observed to be asynchronous across the population with 48 out of 53 spores showing changes associated with germination, for example cell emergence or a phase change within the spore body. The remaining 5 spores stayed phase bright throughout.

At T = 0 min 92% of spores were completely phase bright. Germinating spores gradually underwent a transition from phase bright to phase dark as they rehydrated (Fig: 3.6A). The spore body darkened from the outside in until the entirety became phase dark. At the individual spore level, this process took place over a period of 16 min ± 2 min (Fig: 3.6A pink arrows). A variable lag time between 18 and 80 min was then observed, consistent with what was observed at population level (Section 3.3.2), followed by the slow emergence of a vegetative cell from one pole of the spore body in 37 spores, out of 48 (Fig: 3.6A purple arrows). In some cases, the new cell appeared to be forcefully ejected from the spore shell (16 spores) (Fig: 3.6A light blue arrows). In several cases, first cell divisions of the newly emerged cell were seen (4 spores) (See Movie 3.1).

The emergence of a new vegetative cell always occurred from one pole of the spore. For 20 germinating spores it was possible to observe the exosporium surrounding the spore body during germination (See Appendix 4). Of those 20 spores, 18 had an extension to the exosporium at one pole. In 14 cases the new vegetative cell emerged from this extended pole (Fig: 3.6Bi). In 4 instances the cell emerged from the non extended pole (Fig: 3.6Bii) and in 2 instances there was polar emergence but the poles of the exosporium appeared similar in length (Fig: 3.6Biii). For 4 spores a phase change was observed but no outgrowth occurred (Fig: 3.6Biv) and 5 spores remained phase bright (Fig: 3.6Bv).
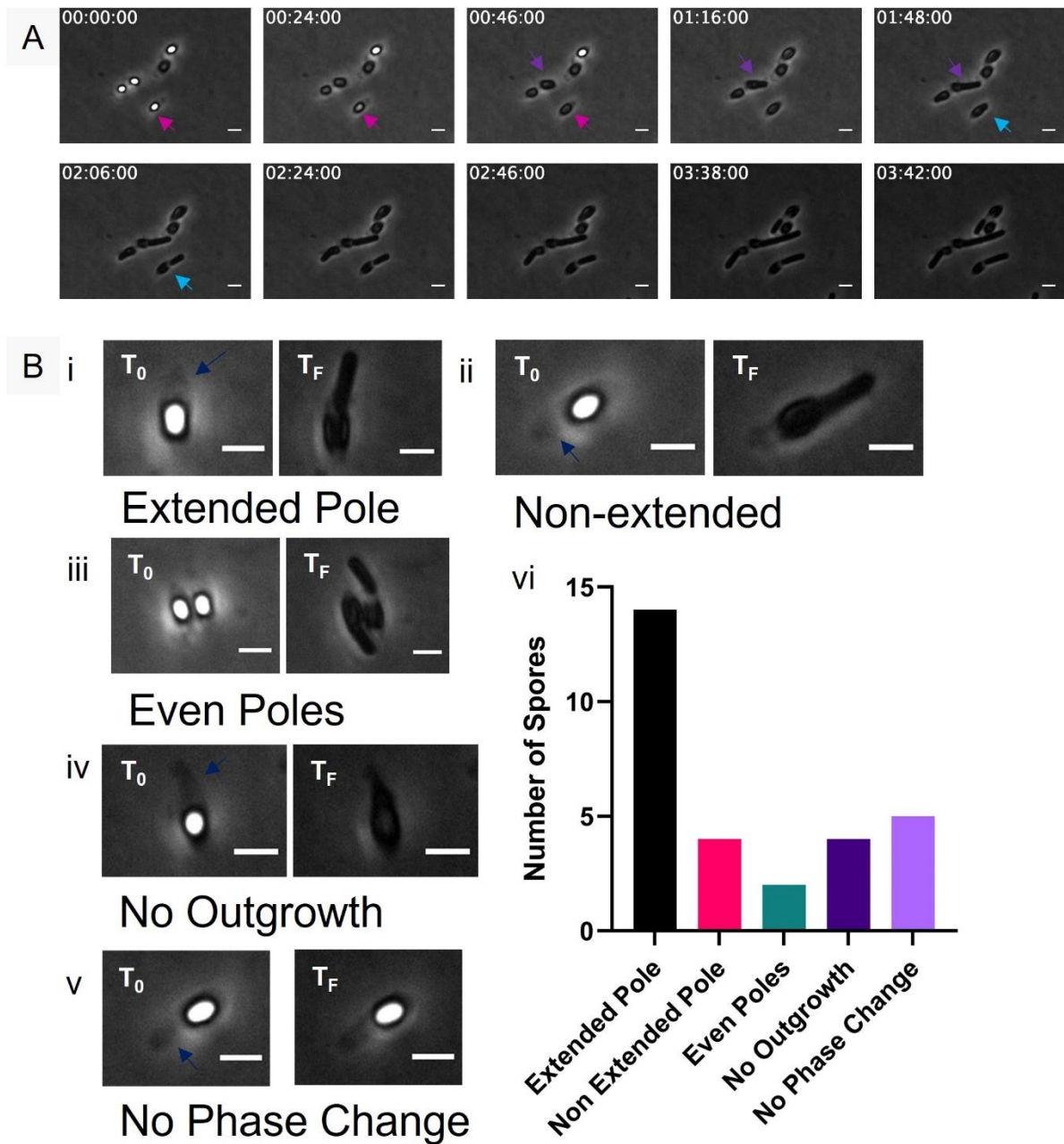
Figure 3.6: Phase Contrast Live Cell Imaging of *C. sporogenes* Germination and Outgrowth

A) Representative time points from Movie 3.1 shows the process of germination from the change from phase bright to phase dark to the emergence of new vegetative cells. Arrows indicate examples of the gradual change from phase bright to dark (pink arrows), the slow emergence of a vegetative cell (purple arrows), and the forceful emergence of a vegetative cell (light blue arrows). B) Final spore forms and polar emergence of cells i-iii) show examples of polar emergence of vegetative cells. iv) example of a spore that has undergone a phase change but not outgrown. v) example of a spore with no phase change. vi) summary of the emergence patterns within the imaged population. Dark blue arrows indicate extended pole of the exosporium.

3.3.4 Endospore Ultrastructure Changes During Germination and Outgrowth

3.3.4.1 Negative Stain

To gain an understanding of the structural changes that accompany germination, samples between 1 and 2.5 h post germination initiation were fixed, negatively stained, and imaged by TEM.

1 h post germination initiation

The sample consisted solely of intact spores with no obvious signs of germination (Fig: 3.7A-C). In 32% of observed spores, within the non-extended pole of the exosporium, electron dense structures could be seen emanating from the main spore body towards the exosporium (Fig: 3.7C blue arrows).

1.5 h post germination initiation

After a further half an hour 82% of spores appeared to be intact and showed no obvious sign of germination (Fig: 3.7D and F). The remaining 18% of spores showed vegetative cells emerging from one pole of the spore (Fig: 3.7E). These cells appeared to have remnants of the spore outer layers associated with the exposed surface of the cell.

2 h post germination initiation

2 h after triggering germination the sample consisted of a combination of three different spore germination phases; intact spores, emerging cells and empty spore shells. The dominant phase (65%) was that of cells emerging from the pole of the spore (Fig: 3.7H). Empty spore shells were frequently observed (22%), likely representing the remains of the outgrowth process (Fig: 3.7G). The exosporium surrounded the remnants of the spore body and possessed a clear opening at one pole from which the cell had emerged (Fig: 3.7I). Fourier transforms of the exosporium regions indicated that it remained crystalline post outgrowth (Fig: 3.7I inlay). Free cells were also observed of varying sizes (Fig: 3.7G). Intact spores that had no obvious signs of germination were present in low abundance (13%) (Fig: 3.7H).

2.5 h post germination initiation

At the final time point, there were predominantly free vegetative cells and empty spore shells

present (73%) (Fig: 3.7J and K). There were occasional intact spores present with no obvious signs of

germination (7%) (Fig: 3.7L) and the remaining 20% of spores had cells emerging from one pole.
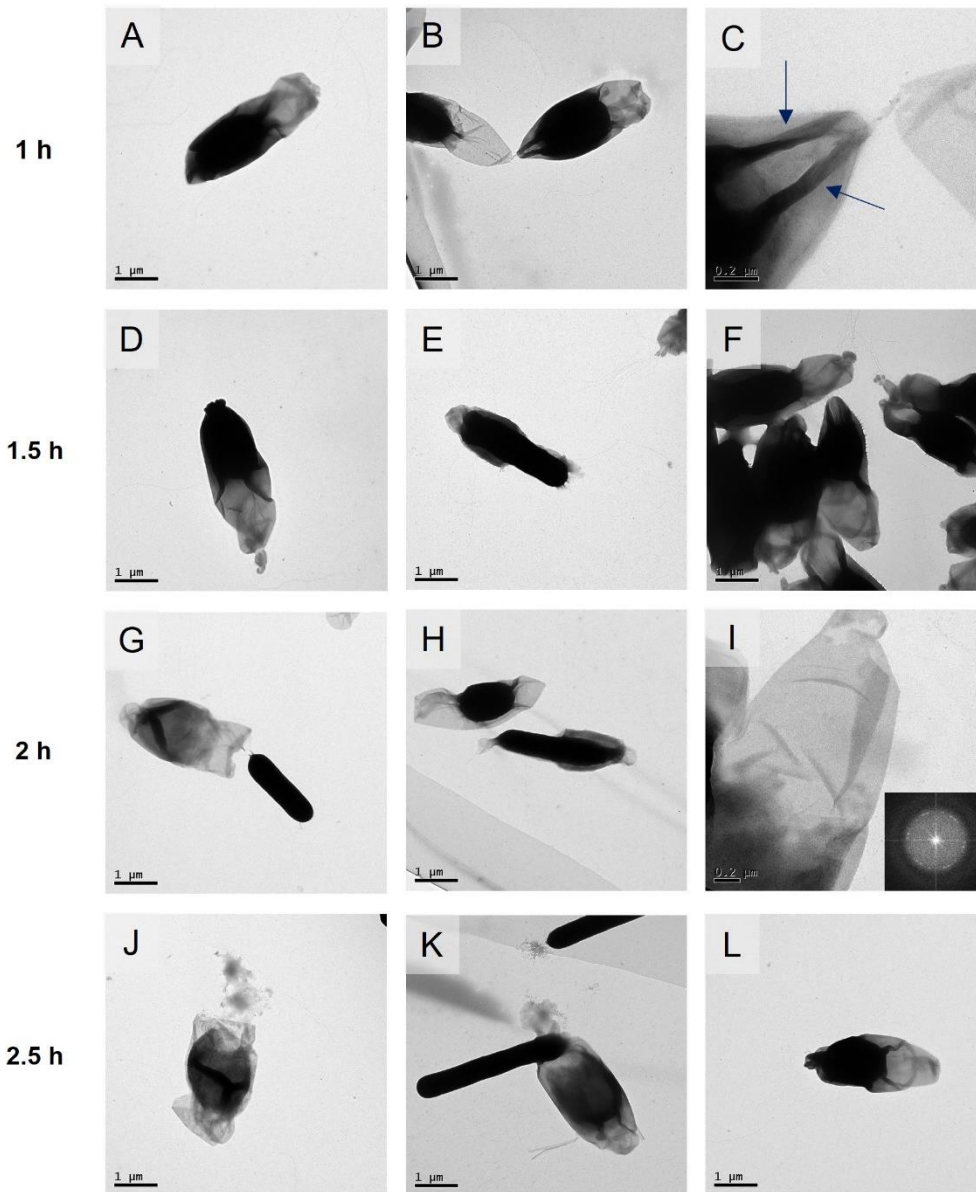
Figure 3.7: Germination of *C. sporogenes* by Negative Stain TEM

A-C) Spores 1 h after germination initiation. Dark blue arrow indicates electron dense features within the pole of the exosporium. D-F) Micrographs of spores 1.5 h after germination initiation with evidence of cell emergence (E). G-I) Micrographs 2 h after germination initiation show cells emerging from spore outer layers. Inlay (I) shows the crystalline nature of the exosporium post cell emergence. J-L) 2.5 h after germination initiation micrographs show spore shells (J), emerging cells (K) and some intact spores (L).

3.3.4.2 Ultrastructural Changes During Germination and Outgrowth

Building upon observations from negative stain TEM, samples of *C. sporogenes* were chemically fixed 2 h post germination initiation to allow imaging of thin sections (70-90 nm). The 2 h time point was chosen as the sample showed the biggest range of phases in spore germination by negative stain TEM. A low magnification overview of the sample showed the heterogeneity of the spore population (Fig: 3.8A), with micrographs depicting clear changes in spore morphology associated with different phases of the germination process (Fig: 3.8B-E).
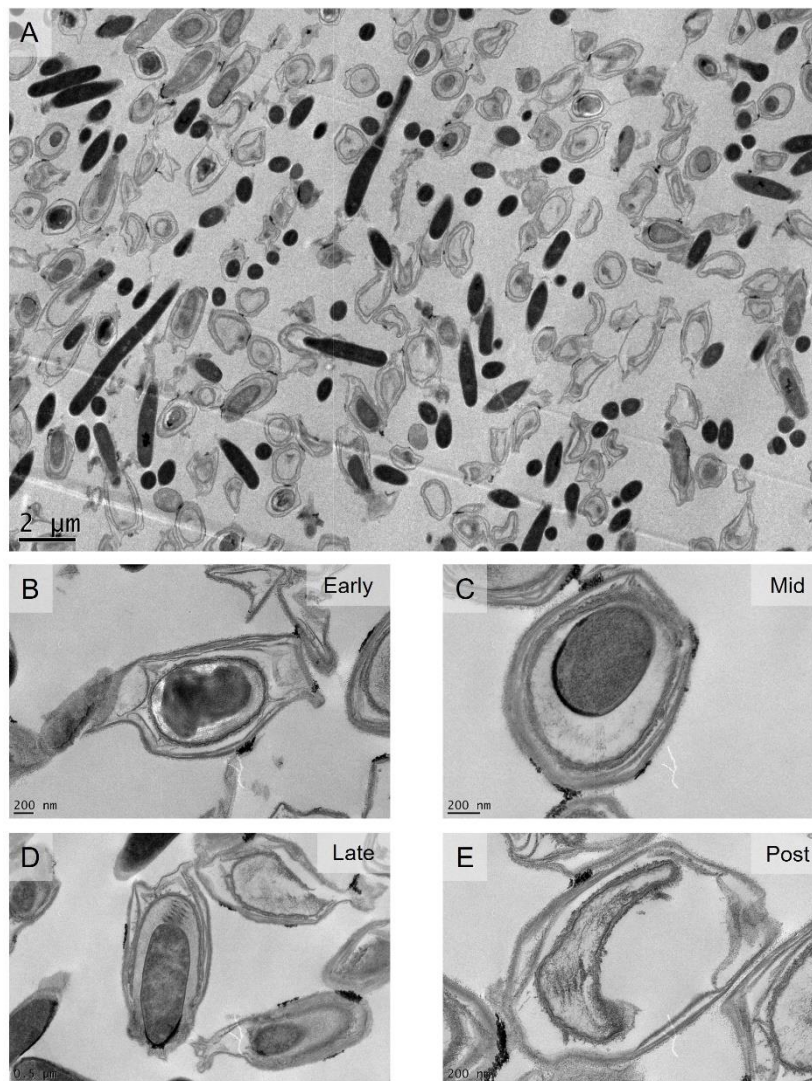
Figure 3.8: Overview of Thin Sectioning Data from *C. sporogenes* Spores

A) Low magnification overview of *C. sporogenes* 2 h post germination initiation displays the heterogeneity of the spore population. B-E) Examples of higher magnification micrographs of spores at early (B), mid (C), late (D), and post (E) germination.

Early Germination

Some spores within the sample appeared to be structurally similar to dormant spores displaying the

features outlined in Section 3.3.1.2 (Fig: 3.9). The core of these spores was often less defined, likely

due to poor infiltration of chemicals during the fixation process. In a small number of cases the spore

core was darkly stained and a clear pale region corresponding to the cortex was distinguishable (Fig:

3.9B transverse spore). From many of the longitudinal sections of spores early in germination it was

apparent that the exosporium was pointed at one pole (Fig: 3.9A and B pink arrows) and noticeably

flatter at the other (Fig: 3.9A and B blue arrows).
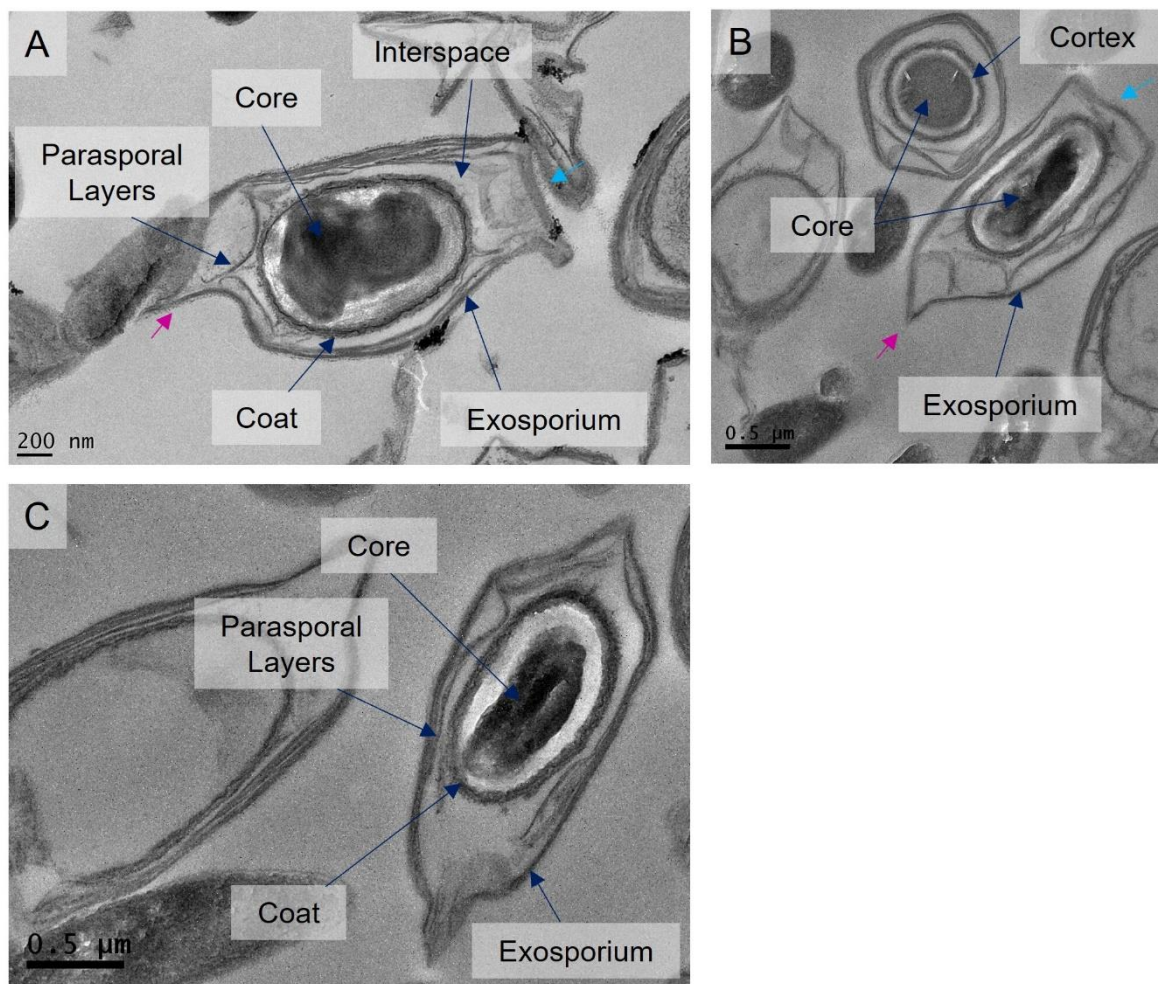
Figure 3.9: Thin Sections of *C. sporogenes* Spores in Early Germination

A-C) High magnification micrographs of spores in the early stages of germination. All layers
distinguishable are labelled. Additional arrows indicate the pointed (pink) and flat (light blue) poles
of the exosporium layer.

Mid Germination

The mid stage of germination was characterised by spores where the developing cell was uniformly darkly stained and was positioned in the centre of the spore body (Fig: 3.10). The width of the entire spore body measured 930 nm ± 110 nm compared to 690 nm ± 110 nm in dormant spores. The lightly stained cortex region of these spores was thicker than for dormant spores at an average of 180 nm ± 80 nm compared with 60 nm ± 40 nm. Interestingly the core of the germinating spore remained a similar width to that of dormant spores with an average of 540 nm ± 140 nm compared with 480 nm ± 60 nm. The interspace became almost indiscernible between the coat and the
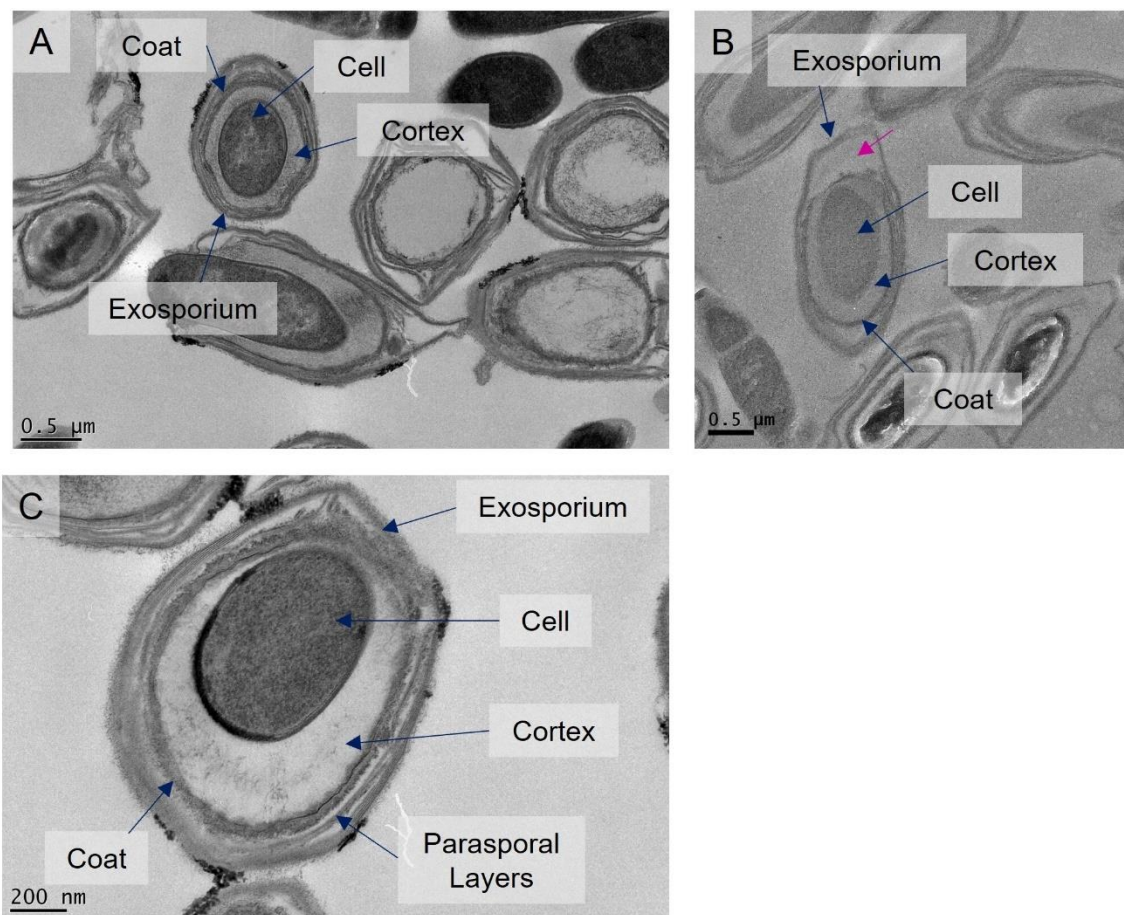
Figure 3.10: Thin Section of *C. sporogenes* Spores in Mid Germination

A-C) Spores in the mid stages of germination show an enlarged spore body and cortex region. Pink arrow indicates a polar interspace region devoid of parasporal layers.

exosporium. The distance between the coat and the exosporium, the interspace, measured 80 nm ± 10 nm compared with 160 nm ± 40 nm in dormant spores. Parasporal layers could be seen stacked between the coat and the exosporium layer along the sides of the spore body (Fig: 3.10C). It was evident in some cases that the area of interspace at one pole of the spore was devoid of parasporal layers (Fig: 3.10B pink arrow).

Late Germination

Spores that showed vegetative cells emerging were clearly in the latter stages of germination (Fig: 3.11). The vegetative cell was consistently observed emerging through one pole of the spore. The outer layers of the spore, the darkly stained exosporium and coat, remained closely associated with the emerging cell. The lightly stained cortex region surrounding the cell contained striations (pink arrows) regularly spaced 52 nm ± 5 nm apart (Fig: 3.11D).
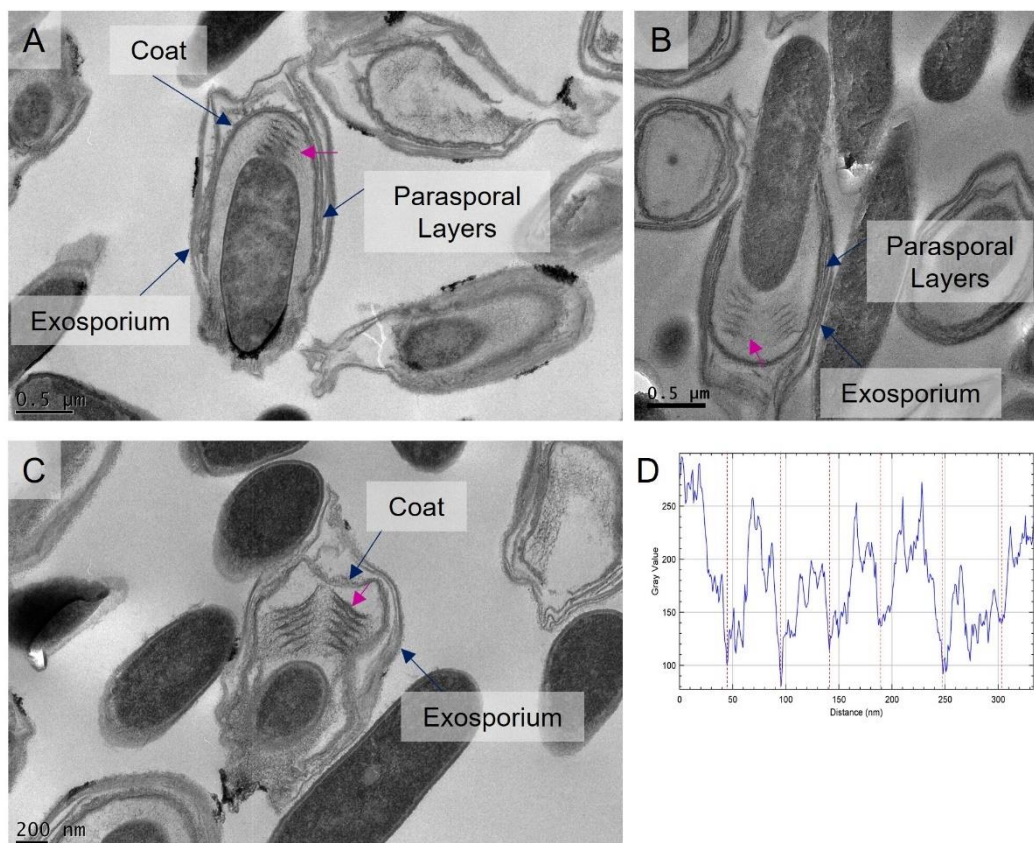
Figure 3.11: Thin Sections of *C. sporogenes* Spores in Late Germination

A-C) Spores in late germination show vegetative cells emerging from the outer layers of the spore. Pink arrows indicate striations present within the cortex region of the spores. D) Periodicity of the striations within the cortex region of C with an average spacing of 52 nm ± 5 nm.

Micrographs revealed spore shells consisting of the outer layers of the spore remaining after the vegetative cell has emerged (Fig: 3.12). Several features of the original spore were still identifiable: the outermost exosporium layer, parasporal layers mostly stacked between the exosporium and the coat along the edges, and the densely stained spore coat. The centre of these shells appeared to have some lightly stained disordered material remaining, likely the remnants of the cortex region (pink arrows) including a hint of the striations seen in late germination (Fig: 3.12A).
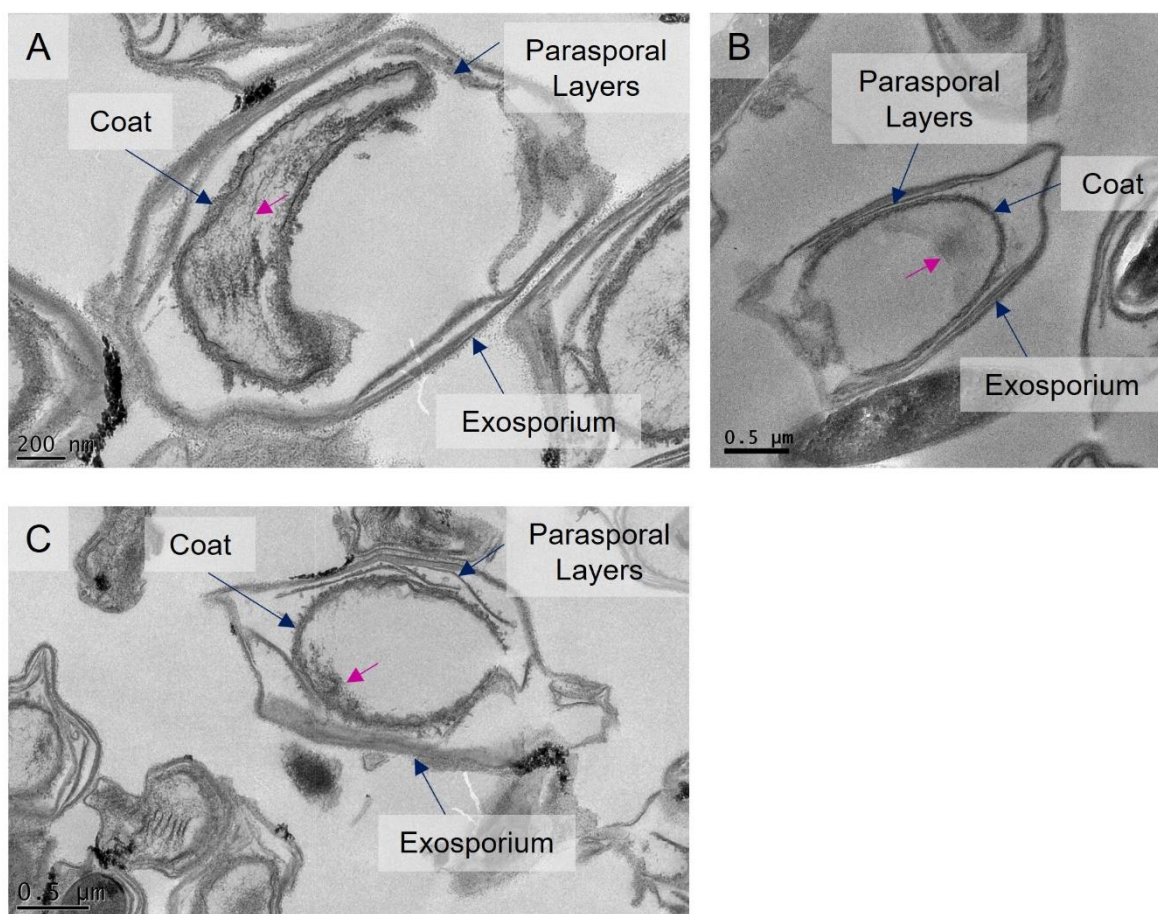
Figure 3.12: Thin Sections of *C. sporogenes* Spore Shells Post Germination

A-C) Spore shells composed of the outer layers of the spore including the exosporium, parasporal layers and the spore coat. Remnants of the cortex region are also present within the centre of the shell. Pink arrows indicate evidence of the striations seen within the cortex region in late germination.

3.3.5 Structure of the Exosporium Post Germination (Spore Shells)

To determine if any structural changes occur within the exosporium layer during the germination process, high magnification micrographs (21,000 x) of negatively stained samples were collected from across all areas of empty spore shells. Fourier transforms from areas within these micrographs showed the continuous crystalline nature of the exosporium across the entire spore shell.

Crystalline patches from across the spore shells, varying in their degree of crystallinity, were processed using *2dx* to produce individual 2D projection maps for each area (Fig: 3.13A). This
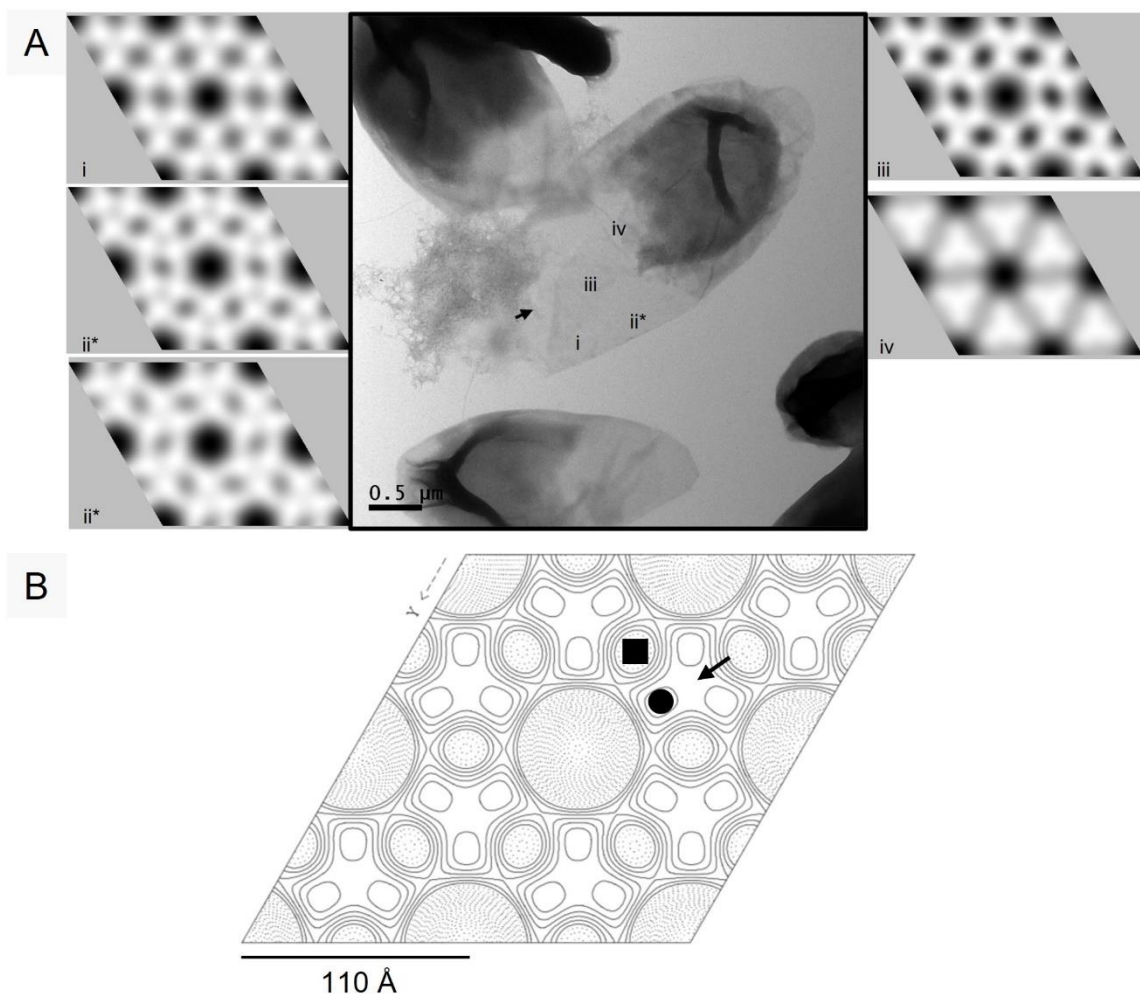
Figure 3.13: 2D Projection Maps of the Exosporium Crystal Structure Post Germination

A) 2D projection maps from areas of crystalline material across the spore shell. * indicates the presence of two lattices within the same image. Black arrow indicates opening in the exosporium and likely exit point of the vegetative cell. B) Merged 2D projection map from 21 images with *p6* symmetry imposed. Displays a clear area of low density corresponding to a central pore surrounded by 6 potential subunits (black circle) forming a hexagonal ring. The threefold linker region (black arrow) connects adjacent rings with a smaller pore present between each linker (black square).

demonstrated that the fundamental crystal lattice of the exosporium remained unchanged from previous dormant spore estimates of lattice parameters of $a = b = 105 \pm 1\text{Å}$ and $y = 119 \pm 1°$. A total of 21 image patches were merged to give a 2D projection map (Fig: 3.13B). This showed a clear hexagonal ring structure with a pore-like opening in the centre. Each ring is joined to the next via a 3-fold linker (Fig: 3.13B black arrow) forming a smaller pore along the edge of the central ring (Fig: 3.13B black square).

3.3.6   Advancing Towards High Resolution Ultrastructural Analysis Using Cryo-ET

3.3.6.1   Tilt Series

In order to gain some 3D information on spore ultrastructure during the germination process, spores 2 h post germination initiation were plunge-frozen onto EM grids. Grids were screened for ice thickness, revealing the ice around whole spores to be generally too thick for tomography, but empty spore shells had a suitable ice thickness. A total of 9 areas were chosen for tomography data collection. 7 of these were spore shells post germination and the remaining 2 were germinating spores where the developing cell remained within.

3.3.6.2   Data Processing

The tilt series was aligned using gold fiducials and tomograms were generated using the IMOD software. In several cases the spore body obstructed the tracking of gold fiducials which resulted in poor alignment and these tilt series could not be further processed. Where the developing cell remained within the spore, radiation damage was often observed after the initial -20° to +60° causing an expansion of the spore body. In these cases, an attempt was made at a reconstruction using a limited range of views. However, this increased the missing wedge artefact present in the final tomogram.

3.3.6.3 Tomograms

Slices through the tomographic volume of a spore in early germination showed that the developing

cell can be seen as an electron dense rod shape in the centre of the spore (Fig: 3.14A)(See also

Movie 3.2). The spore coat could still be seen surrounding the nascent cell. A clear space between

the developing cell and the coat was distinguishable corresponding to the spore cortex. Parasporal

layers could be seen within the interspace of the spore, although these were mostly at the sides and

towards one pole of the spore. The pole, orientated towards the bottom left of the tomogram,

appeared devoid of parasporal layers. The exosporium could be seen surrounding the entire spore

body.
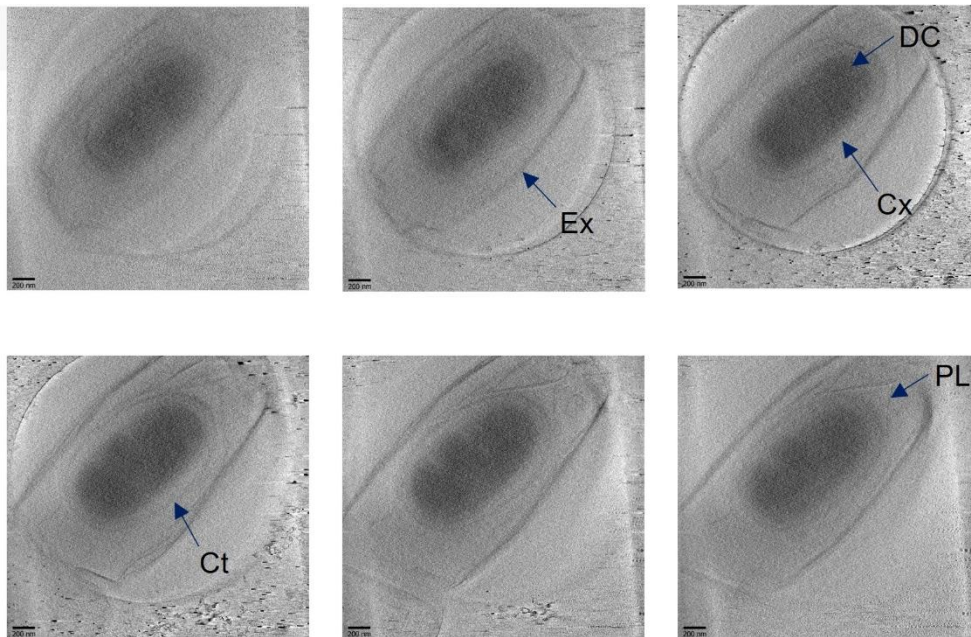
Figure 3.14: Slices Through a Tomogram of a *C. sporogenes* Spore 2 h Post Germination Initiation

Slices clearly show the exosporium (Ex) surrounding the spore body containing the developing cell
(DC). The cortex (Cx) was visible between the developing cell and the spore coat (Ct). Parasporal
layers (PL) were also visible within the interspace. Scale bar 200 nm

Slices are taken from Movie 3.2 – Scale Bar 200 nm

Slices from spore shell reconstructions (Movie 3.3) showed the clear presence of a crystalline

exosporium (Fig: 3.15C). At the pole of emergence the exosporium appeared to be folded back on

itself (Fig: 3.15A). The coat appeared to have a rough opening where the cell had emerged from the

spore. Parasporal layers were present pushed up along the edges against the exosporium. Beaded

fibrils could also be seen associated with the open pole of the exosporium (Fig:3.15A pink arrow and

B).
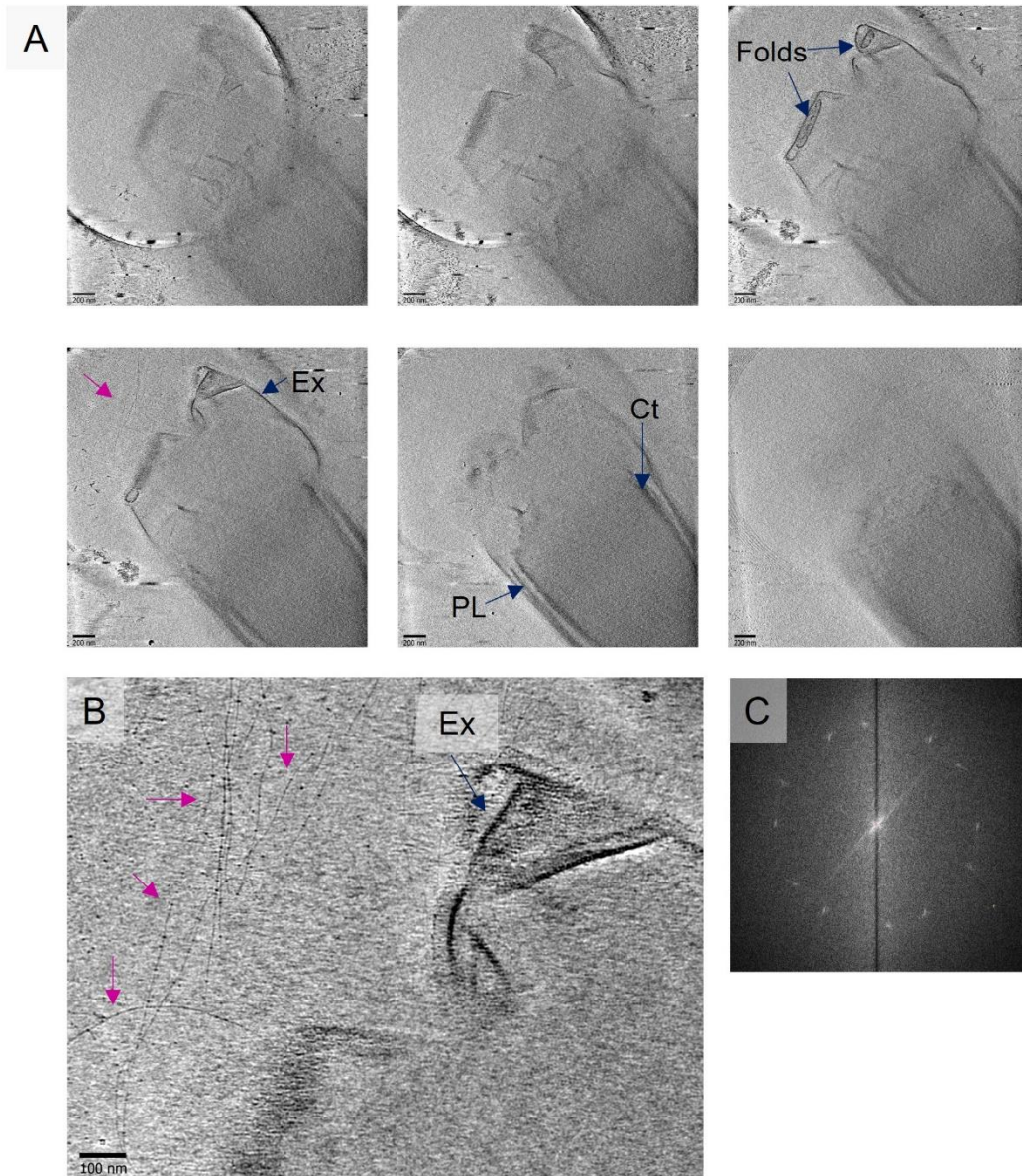
Figure 3.15: Slices Through a Tomogram of a *C. sporogenes* Spore Shell Post Germination

A) Slices clearly show the exosporium (Ex), parasporal layers (PL) and spore coat (Ct). Folds in the open end of the exosporium are highlighted. Pink arrow indicates location of beaded fibrils (B). Scale bars 200 nm. B) Zoomed in area showing the beaded fibrils. Scale bar 100 nm. C) FFT showing the crystallinity of the exosporium layer

Slices are taken from Movie 3.3 – Scale Bar 200 nm

3.4 Discussion

3.4.1 Dormant *C. sporogenes* Endospores

An understanding of dormant *C. sporogenes* ultrastructure was essential in order to interpret subsequent structural changes during germination. Negative stain TEM of NCIMB 70179 spores confirmed the previously seen *C. sporogenes* spore morphology with the distinctive large baggy outermost exosporium layer surrounding the spore body (Janganan et al. 2016, 2020). The exosporium was often extended at one of the poles and was heavily decorated with a dense hairy nap and additional appendages including beaded fibrils and large appendages. This is in contrast to the ATCC 15579 strain that possessed fewer decorations (Dafis-Sagarmendi 2021) highlighting the strain specific differences within the species. Despite differences in decoration, unit cell dimensions associated with the exosporium basal layer were consistent with those observed previously for ATCC 15579 as well as NCIMB 70179 (Janganan et al. 2020). This implies that the fundamental structural assembly of the exosporium layer is conserved between strains.

Thin sectioning of spores showed an ultrastructure with clear distinctions between many of the key spore layers. The exosporium, parasporal layers, coat, cortex and core were all clearly identifiable, however, the germ cell wall and the inner membrane were not possible distinguish. Regions thought to correspond to these layers were seen in thin sections by Hoeniger and Headley (Hoeniger and Headley 1969) although the resolution of these images are relatively poor making them hard to confidently assign. More recent work at higher resolution has shown these layers are present around the spore core as well as additional unknown darkly stained layers (Dafis-Sagarmendi 2021). These darkly stained unknown layers were also seen here (Fig: 3.3A Unknown Layers) and although their composition and role remains unclear, it is possible they are involved in forming a physical separation between the cortex and the cell wall.

AFM data from spores imaged in air revealed that ridges and folds are formed within the exosporium surface as it surrounds the spore body. These are likely formed as the exosporium collapses onto the spore body as it dehydrates. It is possible that these folds reflect the presence of structures below the exosporium surface such as the parasporal layers seen in the thin sectioning data or the spore coat. The spore coat is thought to form folds under desiccation conditions due to the contraction of the underlying cortex region (Driks 2003).

AFM images from several dormant spores appeared to show a potential cap region at one pole of the exosporium that was open and folded back (Fig: 3.2). This would align well with the terminal protrusions and open apertures seen at the pole of the exosporium in SEM imaging of dormant and germinating *C. sporogenes* spores (Brunt et al. 2015). The bottle cap model of germination established in *B. anthracis* predicts the presence of a cap structure formed at one pole of the exosporium that facilitates the germination process (Steichen et al. 2007). We would suggest that the potential cap region observed by AFM and SEM, along with the open polar apertures (Brunt et al. 2015) would correlate well with a cap structure that facilitated cell emergence during germination. It was also noted in the AFM data that the beaded fibrils appeared to be localised to the polar cap region of the exosporium, a feature that has not been observed by any other form of imaging in dormant *C. sporogenes* spores.

In addition, the AFM data seemed to show the presence of large appendages below the surface of the exosporium (Fig: 3.2B yellow arrow). These were seen mostly across the spore body where the thickness of the spore body rules out the possibility that the appendage is underneath the spore. However, if the appendages are present underneath the surface of the exosporium, within the interspace, they are not seen in any of the thin sectioning data and therefore it is possible that all the large appendages are actually located on the surface of the spore. Further higher resolution imaging of the spore surface would provide conclusive evidence as to the locality of these appendages.

3.4.2   Conditions Required for Germination of *C. sporogenes*

In order to structurally characterise the germination process in *C. sporogenes* it was vital to find reliable conditions that led to not only spore rehydration, but also to cellular outgrowth. Previous germination studies in *C. sporogenes* have focused on determining the specific germinant molecules required for the initial dip in optical density associated with spore rehydration (Brunt et al. 2014). These studies were carried out in Tris buffer where no outgrowth of the bacteria could be observed. We aimed to determine if supplementation of TY media with specific germinant molecules was required for efficient germination and outgrowth.

It was apparent that the components of rich media, such as TY, were ample for germination and subsequent outgrowth of *C. sporogenes*. As amino acids are known germinants for *C. sporogenes* (Brunt et al. 2014) it is likely that the presence of these molecules within TY media are responsible for triggering the germination process. Interestingly, we found that the addition of L-cysteine to TY resulted in an arrest in the outgrowth phase of germination (Fig: 3.4). The most probable explanation for these observations is that cellular growth is inhibited by the presence of high amounts of L-cysteine. A growth curve of *C. sporogenes* under these conditions would indicate whether there is a growth defect associated with them. Alternatively, it could suggest that commitment to germination after spore core rehydration may not be as straightforward as previously thought and that there are additional checkpoints throughout the germination process. Further analysis of germination and outgrowth in the presence of L-cysteine is required to develop our understanding. Thin sections of L-cysteine germinated spores, fixed during the germination process may provide an insight into any structural differences that are occurring.

3.4.3   Overview of Germination in *C. sporogenes*

Live cell imaging coupled with negative stain TEM of the *C. sporogenes* germination process at different timepoints provided an overview of the phases of spore germination. The germination process is asynchronous across the population. Indeed, some spores remained phase bright and seemingly dormant throughout. These phase bright spores could correspond to superdormant spores within the population (Ghosh and Setlow 2009). These are crucial for persistence within the native environment ensuring survival in the case of premature germination in unfavourable growth conditions or to protect against a rapid reversal of the favourable growth environment.

There was a remarkable consistency in the process by which the new vegetative cell emerged through the pole of the spore. This was typically from the pole with the large extension to the exosporium. This observation is consistent with the location of the potential cap structure seen in the AFM data (Discussed in 3.4.1) and with the bottle cap model of germination developed from research into *B. anthracis* (Steichen et al. 2007). The newly emerging cells could take advantage of the weakened or open cap at the pole of the exosporium to escape the outer layers of the spore leading to the clear polar emergence seen in the live cell imaging.

3.4.4   Exosporium Structure Post Germination

Post germination it was possible to image more areas of the exosporium by EM due to the lack of the dense spore body. For the same reason, spore shells also tended to lie flatter on the carbon surface on the grids, meaning larger areas of crystalline exosporium were amenable to imaging and processing.

The crystalline and cross-linked nature of the exosporium (Janganan et al. 2020) makes it extremely robust and not easily penetrable by an emerging cell. One hypothesis was that the exosporium lattice underwent a structural rearrangement during the germination process that would alter the properties of the layer allowing for the emerging cell to easily emerge from the exosporium. Electron crystallography of the spore shell post germination revealed no evidence of any such

rearrangement. The crystal had a unit cell of $a = b = 105 \pm 1$ Å and $y = 119 \pm 1°$ and the 2D projection

map showed an hexagonal ring structure connected by 3-fold trimeric linkers, identical to the

structure seen from intact dormant spores and CsxA crystals (Janganan et al. 2020) (Fig: 3.16). This

suggests that the likely mechanism for vegetative cell emergence does not include a structural

rearrangement of the exosporium. It is worth noting that negative stain electron crystallography is

limited to ~25 Å resolution. This resolution is not sufficient to identify small changes that might be

occurring within the structure, only that the overall lattice parameters do not change. In order to

probe this further higher resolution information would be required which could be obtained through

collection of additional data where spore shells are plunge frozen and imaged at cryogenic

temperatures.
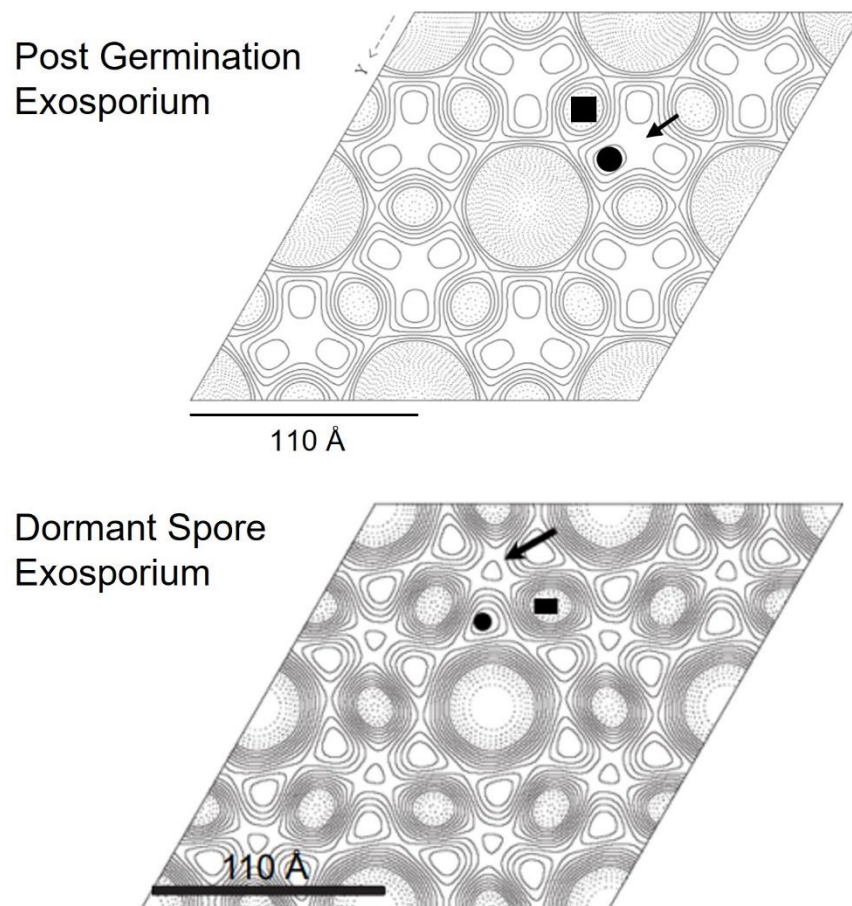
Figure 3.16: Comparison of Post Germination and Dormant *C. sporogenes* Exosporium

2D projection map of negatively stained exosporium post germination (top) and negatively stained dormant spore exosporium (bottom) from (Janganan et al. 2020). Black circle indicates potential subunit, square indicates a peripheral pore and the arrow indicates a 3-fold linker.

Dormant spore projection reproduced with permission from (Janganan et al. 2020)

Post germination TEM showed that the potential exosporium cap structure, seen by AFM of dormant spores, appeared to have dissociated from the spore shell during the germination process (Fig: 3.7G, J and 3.12B). Therefore it was not possible to further probe the structure of the cap regions to determine if they possessed an alternative basal layer structure that could contribute to a weakened interaction that can be exploited by the emerging cell. The location of the opening at the pole of the extended end of the exosporium does suggest that any cap structure present would have been easily amenable to imaging and processing on dormant spores. The structures obtained from dormant spore exosporium (Janganan et al. 2016), crystals of heterologously expressed CsxA (Janganan et al. 2020), and post germination exosporium are all identical. This could suggest that the basal layer of the cap is comprised of CsxA or a structurally similar protein that forms an identical lattice structure. Alternatively it is possible that the cap region is formed of a non-crystalline material and is therefore not amenable to structural analysis by EC.

3.4.5   Ultrastructural Information from Thin Sectioning Data

3.4.5.1   Evidence of Spore Core Rehydration

Micrographs depicting spores in the early stages of germination tended to show two spore subclasses; those with poorly stained cores and those with well stained cores (Fig: 3.17). The poor staining is likely the result of inadequate stain infiltration to the centre of the spore, however, as both subclasses occur within the same sample it may well indicate that subtle changes have occurred in those spores that are well stained. The well stained spores could correlate to small changes within the spore body structure that allowed for improved stain infiltration. These changes could include the opening of channels within the inner membrane that allow for the release of Ca-DPA leading to the uptake of water. The staining could reflect the early stages of spore core hydration with the darker staining reflecting a more hydrated state of the spore core.
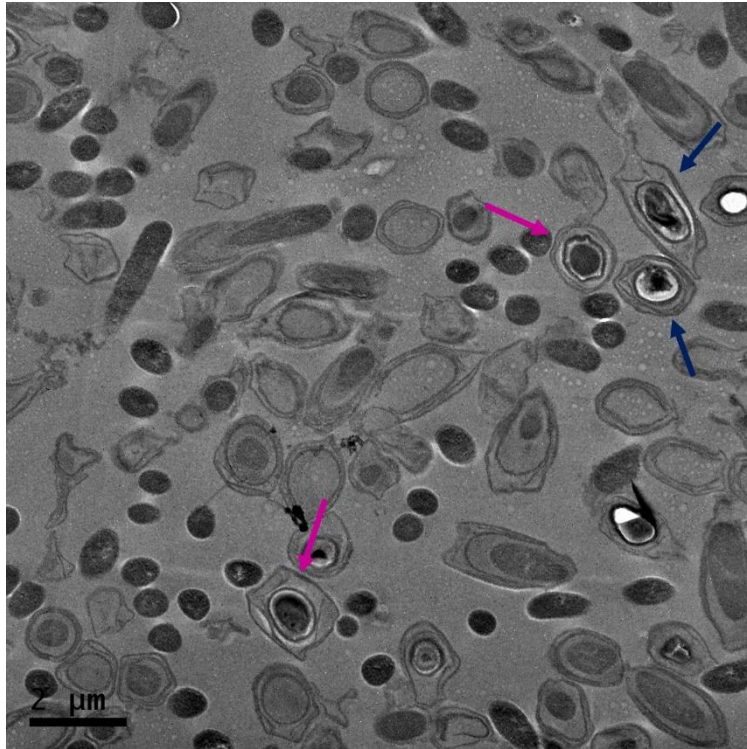
Figure 3.17: Staining Differences During Early Germination

Micrograph shows a thin section of *C. sporogenes* spores 2 h post germination initiation. Dark blue arrows indicate spores in early germination with poor spore body staining. Pink arrows indicate spores in early germination with distinct spore body staining.

3.4.5.2   Distortion of the Exosporium Early in Germination

Early in the germination process, the exosporium already starts to initiate changes that will lead to vegetative cell emergence. One pole of the exosporium appeared to come to a point whilst the other appeared flatter (Fig: 3.9A and B). A reduction in parasporal layers within the flatter pole of the spore would suggest that this is the subsequent pole of emergence (Discussed below in section 3.4.5.4). Further to this there are spores in the later stages of germination with markedly pointed exosporium at the pole distal from cell emergence (Fig: 3.11A and 3.12B). The reason for these morphological changes to the exosporium requires further investigation and would benefit from the use of fluorescent labelling of the exosporium during live cell imaging to monitor how the exosporium shape changes through the early stages of germination.

3.4.5.3   Expansion of the Spore Body

The spore body is seen to expand from 700 nm ± 100 nm to 950 nm ± 100 nm in diameter. This expansion is such that the spore coat pushes right up against the parasporal layers, stacking them with the outermost exosporium layer. The expansion of the entire spore body in response to germination has not previously been suggested in the literature. Expansion of the spore core has been alluded to during the rehydration process (Setlow, Wang, and Li 2017) and in *B. subtilis*, *B. thuringiensis* and *C. difficile* additional membrane reservoirs within the spore core have been observed in order to facilitate this expansion (Laue et al. 2018). However, the spore core of *C. sporogenes* itself appears to not undergo any dramatic expansion during the rehydration stage of germination.

The thin sectioning data suggest that an expansion of the cortex region throughout the germination process in *C. sporogenes* from 65 nm ± 35 nm to 180 nm ± 80 nm is responsible for the swelling of the spore body (Fig: 3.9 and 3.11). This is in stark contrast to what has been recently observed in *C. difficile* where the cortex region of germinating spores rapidly decreases in size from 130 nm 40 nm within the first 5 min of germination (Baloh et al. 2022). Swelling of the dormant spore body has been previously seen in *B. thuringiensis* in response to humidity levels within the environment (Westphal et al. 2003) and this has been attributed to an expansion of the cortex layer, accommodated by folds in the coat layer of the spores (Driks 2003). It is possible that the expansion of the cortex region seen throughout the germination process in *C. sporogenes* is due to the rehydration of the spore and the increased water content of the internal layers. In addition, the small waves and folds seen in the coat layer of dormant *C. sporogenes* spores were no longer apparent in the sections of germinating spores. This would suggest that the coat has been stretched out to accommodate the cortex expansion much like what was suggested to occur in *B. thuringiensis* (Driks 2003).

Alternatively, the cortex region could play a more active role in the emergence of the cell through a restructuring of the peptidoglycan layer. This could occur through enzymes already localised within the cortex of the spore and or proteins secreted from the developing cell. Cortex lytic enzymes, CwlJ and SleB, have been previously identified in *C. sporogenes* (Wang et al. 2017) but have mostly been studied in *B. subtilis*. They are thought to be activated by the release of DPA from the core of the spore (Tovar-Rojo et al. 2002) but the function of these enzymes in *C. sporogenes* is yet to be confirmed despite having been found to be essential for efficient germination (Wang et al. 2017). If these enzymes were acting to degrade the cortex layer we would expect the cortex region of the spores to decrease in size throughout the germination process. It is remarkable then that this is not seen to be the case and suggests that these enzymes have an alternative role within the spore, perhaps in restructuring the cortex layer. The SleB enzyme is thought to localise to the inner membrane through interaction with YpeB (Boland et al. 2000), it is possible then that SleB is involved in detaching the developing cell from the surrounding cortex allowing it to leave the confines of the spore body without the need for complete cortex degradation.

In addition to the expansion of the cortex region, the thin sectioning data also show the formation of darkly stained striations (Fig: 3.11). There features were always seen to form at the opposite pole to cell emergence and were not observed in any dormant spore thin sections. The formation of these structures would also be consistent with the idea that the cortex undergoes a restructuring during the germination process. The specific composition of the striations is unknown and their presence may well be the passive result of the pressure and stress the cortex is put under during the germination process. However, their location and association with the developing cell could suggest a molecular spring type mechanism actively involved in pushing the vegetative cell out through the pole of the spore. This would also align with the forceful ejection of vegetative cells from the spore outer layers seen in the live cell phase contrast microscopy (Movie 3.1).

3.4.5.4   Loss of Interspace Region and Polar Parasporal Layers

By mid germination the interspace of the spores is almost indiscernible, particularly around the sides

of the spore body (Fig: 3.10). Around the sides of the spore body the interspace decreased from 160

nm ± 40 nm to 80 nm ± 15 nm. Despite its name, the interspace is thought to be composed of two

distinct layers of polysaccharide formed during sporulation to guide the formation of the

exosporium (Lehmann et al. 2022). It is possible that the loss of interspace is associated with a

breakdown of these polysaccharide layers which would provide an energy source for the developing

cell.

The interspace region at the pole from which emergence occurs becomes devoid of parasporal

layers in the early stages of the germination process (Fig: 3.10B). Many layers can be seen along the

sides of the spore body as they get squashed between the spore coat and the exosporium when the

spore body expands. Within the sectioning data there are no obvious signs of parasporal layers being

degraded during the germination process. Therefore, it seems more likely that the parasporal layers

from the pole of the spore are pushed out through the opening in the exosporium pole. The

expansion of the spore body (discussed in section 3.4.5.3) could result in the movement of material

from within the interspace out into the environment which could include the parasporal layers

located within the pole region. Although no external debris was seen that could correspond to

parasporal layers being pushed out of the exosporium it is likely that any evidence of this would

have been washed away during the sample preparation.

3.4.5.5   Early Opening of the Exosporium Pole

From both thin sectioning and negative stain data it was clear that the pole of the exosporium from

which the cell emerges, opens prior to spore coat degradation (Fig: 3.9C and 3.10B). This would

correlate with the open aperture seen at the pole of *C. sporogenes* by SEM (Brunt et al. 2015). The

early opening of the exosporium suggests that the process is not reliant on pressure from the

emerging cell pushing its way out of the spore. However, the exosporium does not appear to be

degraded, even in the spore shells post germination. This coupled with the fact there are no structural changes to the exosporium (Section 3.4.4) points further to some form of cap structure that falls off or is cleaved at a specific location during germination.

3.4.5.6   Degradation of the Spore Coat

The thin sectioning data clearly show that spore coat degradation occurs in line with the opening in the exosporium (Fig: 3.10B and C). This is consistent with observations made previously by SEM (Brunt et al. 2015). The breakdown of the coat appears to be targeted only to this pole as the rest of the coat remains intact, even post germination in spore shells (Fig: 3.12). This would imply that the degrading enzymes are not free within the germinating spore but rather localised to the pole of emergence. The enzymes could be located within the coat itself where they become activated during the germination process, similar to the cortex lytic enzymes. If this is the case it may be possible to identify them by looking for possible coat degradation enzymes amongst the proteins expressed at the time of coat formation during sporulation.

Another hypothesis would be that coat degradation enzymes could be associated with the surface of the emerging cell. This would require the pole of the emerging cell to be in close proximity to the spore coat, and in several micrographs, this does appear to happen. In this case, any enzymes that are expressed in the early stages of cell development and are localised to the cell pole may be candidates for coat degradation.

3.4.6   Model of Germination and Outgrowth in *C. sporogenes*

The thin sectioning data provided detailed structural information concerning the changes occurring within the spore during the germination process. From this, it is possible to put together a model for germination in *C. sporogenes* (Fig: 3.18). I propose that, in the early stages of germination, the spore core starts to become rehydrated (Stage I) seen as a phase change in phase contrast microscopy

(Movie 3.1) and in altered staining patterns within the thin sectioning data (Fig: 3.17). The spore body then increases in size likely the result of rehydration and cortex expansion. This in turn pushed the coat up against the outer layers of the spore, sandwiching the parasporal layers between the exosporium and the coat, diminishing the interspace. At this point the exosporium is often open at the extended pole of the exosporium and striations are seen within the cortex layer of the spore at the distal pole to the exosporium opening. The appearance and locality of the striations suggest a potential role as a molecular spring to assist in the emergence of the vegetative cell in the latter stages of germination (Stage II). The coat of the spore is then degraded in line with the exosporium opening allowing the developing cell to begin emerging from the spore (Stage III). The cell then emerges through the pole of the exosporium into the environment, possibly mediated by the molecular spring within the cortex, completely dissociating from the outer layers of the spore leaving an empty spore shell (Stage IV).
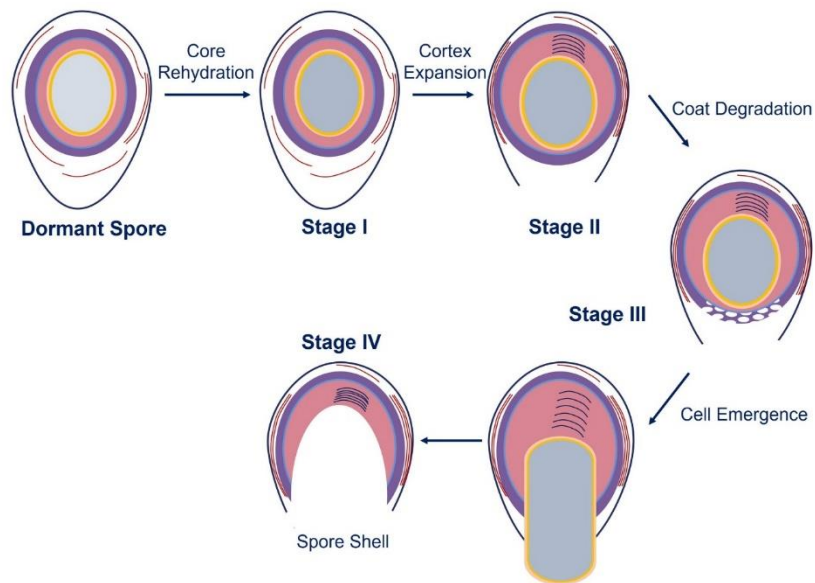
Figure 3.18: Model of Spore Restructuring During Germination and Outgrowth

The germination process begins with the rehydration of the spore core (Stage I). The spore body then swells, a process that is coupled with the expansion of the spore cortex. The expansion of the spore body sandwiches the parasporal layers between the exosporium and the coat. The exosporium is often open at one pole and striations can be seen within the expanded cortex region (Stage II). The coat of the spore is degraded in line with the opening at the pole of the exosporium allowing the vegetative cell to begin emerging (Stage III). The vegetative cell emerges through the open pole into the environment, possibly mediated by the striations within the cortex, leaving behind the outer spore layers as a spore shell (Stage IV).

3.4.7 High Resolution from Cryo-ET

The thin sectioning data provided a clear initial understanding of the coarse morphological changes that occur within the spore during the germination and outgrowth process. Higher resolution information and finer details of the spore structures were not distinguishable due to the staining required for this method. Sectioning of the samples also meant that only a small region of each spore was imaged rather than the entire 3D volume. Cryo-ET of germinating spores is not something that has been seen before in the literature and the initial attempts shown here aimed to provide valuable 3D structural information on the germination process.

Cryo-ET of spores was challenging and, in most cases, where the spore body still contained the developing cell, the ice was too thick for data collection or subsequent processing. The thinner spore shells proved to be more amenable to imaging. The low contrast from cryo-ET data meant that layers were quite hard to distinguish but the exosporium, parasporal layers, and the remnants of the coat were clearly visible. The presence of beaded fibrils decorating the outer surface of the exosporium were also clearly seen at the open pole of the spore shell (Fig: 3.15A and B, Movie 3.3). This is just one example of a feature that was not observed within the thin sectioning data. In addition, the tomography data showed the clear crystallinity of the exosporium layer post germination (Fig: 3.15C) and that the open end of the exosporium rolled back in on itself (Fig: 3.15A). Both of these features were not always evident within the thin sectioning data due to the 2D nature of the images.

The data presented here provide a good basis for further structural analysis of spores and the germination process. Details of the spore structure were clearly visible in these initial tomograms, however, it does appear that the spores are too thick for reliable tomography data collection. To harness the power of cryo-ET it would be necessary to generate thin lamellae by focused ion beam (FIB) milling (Marko et al. 2007) or cryo-sectioning (Al-Amoudi et al. 2004) followed by tomography

data collection. This would allow for high resolution imaging of internal areas of the germinating

spores and the opportunity for subtomogram averaging of features within the spore.

4 Structural Characterisation of Exosporium Mutants

4.1 Introduction

The exosporium of *C. sporogenes* consists partly of a para-crystalline array that forms the outermost layer of the spore. It forms the first point of contact between the dormant spore and the environment and is thought to play an important role in germination and contribute to spore resistance properties (Brunt et al., 2015; Panessa-Warren et al., 1994; 1997; Portinha et al., 2022). The structural organisation of the exosporium basal layer in *C. sporogenes* is similar to that seen in the *Bacillus cereus* family which is composed of a hexagonal array of protein (Kailas et al. 2011; Terry et al. 2017).

A large number of proteins have been identified that are associated with the exosporium in *C. sporogenes* both as potential structural proteins as well as decorative and accessory proteins (Janganan et al. 2016). Of particular interest are three cysteine-rich proteins, CsxA, CsxB and CsxC found to be highly conserved across *C. sporogenes* and Group I *C. botulinum* strains (Janganan et al. 2016). CsxA has since been found to self-assemble to form crystalline sheets identical in structure to the native exosporium basal layer (Janganan et al. 2020). CsxA is therefore thought to be the major structural protein of the exosporium in *C. sporogenes*. The roles of CsxB and CsxC remain uncertain although their high cysteine content is suggestive of potential structural roles within the spore.

In addition to the cysteine rich proteins, two collagen-like proteins, BclA and BclB, were identified (Janganan et al. 2016). In *B. anthracis* homologues of these proteins are found to form a hairy nap on the surface of the exosporium (Boydston et al. 2005; Thompson et al. 2012) where they have a significant impact on the adherence properties of the spores (Brahmbhatt et al. 2007). Based on these observations it seems likely that BclA and BclB are involved in the composition of the hairy nap present on the surface of *C. sporogenes* spores, however, their specific locality and function are yet to be fully determined.

4.2 Aims

The aim of the work described in this chapter was to investigate the roles of exosporium associated proteins in the ultrastructure of *C. sporogenes* spores. This included the three cysteine-rich proteins, CsxA, CsxB and CsxC that had previously been knocked out in a different strain of *C. sporogenes* as well as the two collagen-like proteins BclA and BclB.

Mutagenesis of *C. sporogenes* was carried out using a novel allelic exchange mutagenesis process that was refined for use in *C. sporogenes*. Mutant phenotypes were observed by negative stain EM and the roles of these proteins within the internal structure of the spores were further investigated through thin sectioning. Electron crystallography was used to classify two distinct crystal types from the layers enveloping the spores. Atomic force microscopy was also employed to probe the surface properties of the spores in more detail. By tying together information from multiple imaging techniques and data from all the mutants, we aimed to assign the roles of the exosporium associated proteins in the overall spore ultrastructure.

4.3 Results

4.3.1 Production of Exosporium Mutants

Mutagenesis of *C. sporogenes* was carried out using allelic exchange. Targets for knockout were picked based on the previous work done to identify exosporium associated proteins. The proteins of interest were the cysteine-rich proteins CsxA, CsxB and CsxC and the collagen-like proteins BclA and BclB. The genome of *C. sporogenes* NCIMB 701792 was sequenced using a combination of Illumina short-read and Oxford nanopore long-read sequencing (MicrobesNG) and assembled in house by Dr Roy Chaudhuri. The genes encoding our target proteins were identified within the genome and were found to be isolated genes not located within operons.

An initial construct was made to produce a clean knockout of *csxB* (Fig: 4.1). Approximately 1,200 bp either side of the target gene were amplified by PCR from the genome using primer pairs RF1686/RF1687 and RF1688/RF1689. The resulting homology arms were joined together in a Gibson Assembly reaction and inserted into pJAK184 linearised by inverse PCR using oligonucleotides RF311/RF312. pJAK184 contains the *mazF* gene under the control of the xylose inducible P$_{xyl}$ promoter for counter selection and *catP* for selection (Fig: 4.1). The resulting construct (pHF001) was then conjugated into *C. sporogenes* for mutagenesis. Colonies screened by PCR for first recombination showed integration of the plasmid into the genome as expected. However, when colonies were screened following second recombination no mutant genotypes were seen.

To select for favourable second recombination events, the erythromycin resistance gene, *ermB*, was used to replace the target gene. The *ermB* gene was amplified from pRPF215 using primers RF1877/RF1878. The fragment was then put under the control of the P$_{cwp2}$ promoter, a well characterised constitutive promoter in Clostridia, through insertion into pJAK014 using a BamHI SacI restriction ligation (pHF007). Primers RF1886 and RF1887 were then used to amplify the P$_{cwp2}$-*ermB* region in pHF007 for insertion between the homology arms of pHF001. pHF001 was linearised using primers RF1885/RF1825 and a Gibson Assembly reaction performed to insert the P$_{cwp2}$-*ermB* fragment (Fig: 4.1). The resulting construct (pHF009) was conjugated into *C. sporogenes* for mutagenesis. *csxB* mutants were selected for by resistance to erythromycin and sensitivity to thiamphenicol (signified plasmid loss) and confirmed by PCR and sequencing.
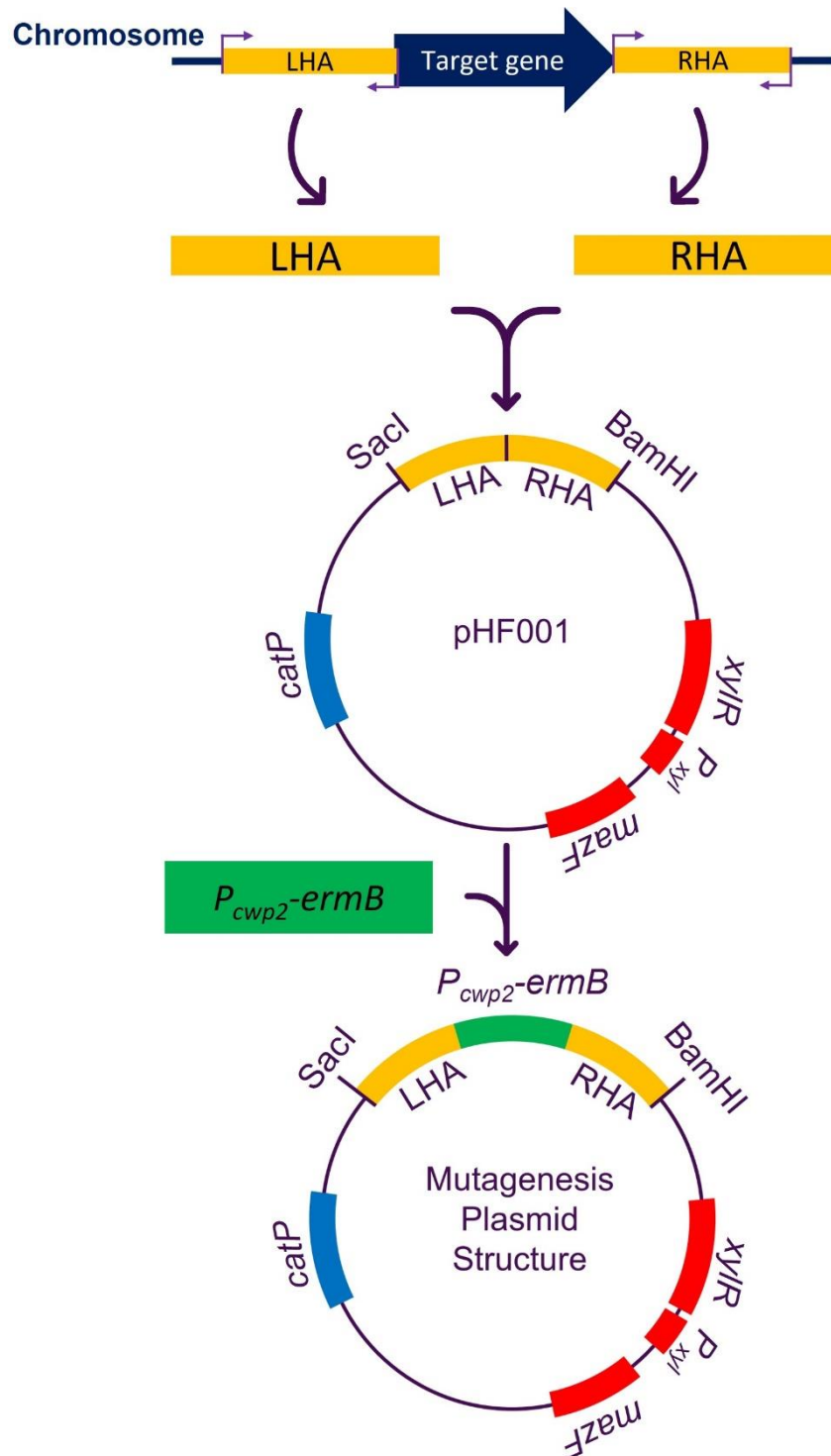
Figure 4.1: Mutagenesis Plasmid Generation

1.2 kb fragments either side of the target gene were amplified to produce homology arms. A Gibson Assembly reaction was used to insert these fragments into the mutagenesis plasmid backbone containing *mazF* under an inducible xylose promoter for counter selection and *catP* for selection. P$_{cwp2}$-ermB was later inserted between the homology arms by conducting a further Gibson Assembly reaction. Mutagenesis with this plasmid construct would result in the replacement of the target gene with the *ermB* resistance cassette.

For convenience, fragments containing homology arms with P*cwp2*-*ermB* between them for the 4 remaining constructs (*csxA*, *csxC*, *bclA*, *bclB*) were synthesised by Genewiz. Fragments were inserted into pJAK188 (*csxA*) or pHF012 (*csxC*, *bclA*, *bclB*) by restriction ligation. pJAK188 is similar to pJAK184 but contains an additional terminator after the *catP* gene to prevent readthrough into the homology arms and a small insertion between the xylose promoter and the *mazF* gene. pHF012 has this small insertion removed. The resulting constructs (Table 4.1) were conjugated into *C. sporogenes* for mutagenesis. Mutants were selected for by resistance to erythromycin and sensitivity to thiamphenicol and confirmed by PCR and sequencing.

Table 1.7: Knockout strains produced in *C. sporogenes* strain NCIMB 701792

Knockout	Backbone	Made By	Final Construct
ΔcsxA::ermB (*csxA*)	pJAK188	Synthesis by Genewiz followed by restriction ligation	pHF010
ΔcsxB::ermB (*csxB*)	pJAK184	RF1886/RF1887 P*cwp2*-*ermB* amplification. Gibson Assembly into RF1885/1825 linearised pHF001	pHF009
ΔcsxC::ermB (*csxC*)	pHF012	Synthesis by Genewiz followed by restriction ligation	pHF013
ΔbclA::ermB (*bclA*)	pHF012	Synthesis by Genewiz followed by restriction ligation	pHF015
ΔbclB::ermB (*bclB*)	pHF012	Synthesis by Genewiz followed by restriction ligation	pHF014

4.3.2   Morphology of Mutant Spores

In order to determine whether there were any substantial morphological differences, spores of each mutant were negatively stained and screened by TEM. A summary of the crystal types found can be found in table 4.2.

Table 1.8: Summary of Crystal Types Found Across *C. sporogenes* Mutant Spores

Crystal Type	Unit Cell Parameters	Symmetry	Comments
Type I	$a = b = 110$ Å ± 5 Å, $y = 120°$	*p6*	Found associated with the exosporium of WT (Janganan et al. 2020), *csxB*, *csxC*, *bclA* and *bclB* spores.
Type II	$a = b = 65$ Å ± 1 Å, $y = 120°$	*p3*	Found associated with outermost layers of *csxA* spores and close to the spore body on *bclA* and *bclB* spores.

4.3.2.1   *csxA*

Micrographs showed *csxA* mutant spores that lacked the continuous outermost exosporium layer of the spore (Fig: 4.2). The spore body was surrounded by patches of crystalline material that were broken and frayed at the edges (Fig: 4.2 pink arrows). Image processing of the crystalline patches revealed a crystal type (Type II) with a unit cell length of $a = b = 65 \pm 1$ Å, $y = 119° \pm 1°$, markedly different from that seen on WT spores (Type I). An indexed FFT can be seen in figure 4.2D. No hairy nap was present on the surface of these layers, however, some of the large appendages were still observed (Fig: 4.2 light blue arrows).

Figure 4.2: Negative Stain TEM of *csxA* Spores

A+B) Low magnification micrographs of negatively stained *csxA* spores C) Higher magnification micrograph showing the crystalline layers associated with the surface of *csxA* spores. Pink arrows indicate crystalline layers. Light blue arrows indicate large appendages. D) Indexed FFT of the crystalline layers present on *csxA* spores corresponding to Type II crystal, unit cell $a = b = 65$ Å and $y = 119°$

4.3.2.2   *csxB*

Micrographs of *csxB* mutant spores showed that there was morphologically very little difference between these and WT spores (Fig: 4.3). The exosporium surrounded the entire spore body, however, for ~65% of the spores observed, the spore body appeared to be more centrally located within the exosporium compared to WT. High magnification micrographs of the exosporium layer revealed a clear hairy nap on the surface of the exosporium (Fig: 4.3D pink arrow) as well as the presence of large appendages (Fig: 4.3 light blue arrows). Crystalline areas of the exosporium

revealed a crystal type identical to Type I crystal seen in WT spores with a unit cell length of $a = b =$ 105 ± 2 Å, y = 119° ± 1° (Indexed FFT Fig: 4.3E). No other crystal types were observed.

Figure 4.3: Negative Stain TEM of *csxB* Spores

A+B) Low magnification micrographs of negatively stained *csxB* spores show a baggy exosporium surrounding the spore dense spore body. C+D) Higher magnification micrograph showing the exosporium. The hairy nap can be seen decorating the surface of the exosporium (pink arrow) as well as large appendages (light blue arrow) E) Indexed FFT of the crystalline exosporium layer surrounding the spore corresponding to Type I crystal, unit cell $a = b$ = 105 Å and y = 119°.

4.3.2.3   *csxC*

csxC mutant spores were morphologically distinct. All spores possessed a clear exosporium often protruding significantly from one pole of the spore (Fig: 4.4A and B). The exosporium appeared to be very closely associated with the lateral sides of the spore body. High magnification micrographs confirmed the presence of a hairy nap on the surface of the exosporium (Fig: 4.4C and D pink arrows) along with the presence of large appendages and beaded fibrils (Fig:4.4B and D light blue arrows). Processing of crystalline areas of the exosporium proved challenging. In many cases the first order spots were absent or very hard to index suggesting that the crystal is more disordered than in WT (Fig: 4.4F). Of the small number of areas amenable to processing a crystal type with unit cell length of $a = b = 105 \pm 2$ Å, $y = 118° \pm 1°$ was found, similar to that of Type I crystal found on WT spores.

4.3.2.4   *bclA*

At low magnification *bclA* mutant spores showed a morphology very similar to that of WT spores. Micrographs showed a clear baggy exosporium completely surrounded the spore body (Fig: 4.5A and B) and was often extended at one pole of the spore. High magnification micrographs showed no evidence of a hairy nap on the surface of the exosporium. The crystal lattice of the exosporium was clearly visible by eye in many of the high magnification micrographs (Fig: 4.5D). Several micrographs of the extended region of the exosporium clearly showed areas of darker staining which appeared to be associated with patches of another material located within the exosporium (Fig: 4.5C pink arrow). FFTs of these areas revealed multiple crystal lattices were present. Processing of crystalline patches gave two distinct crystal types. The first had a unit cell length of $a = b = 110 \pm 3$ Å, $y = 118° \pm 1°$ similar to that of Type I crystal associated with native exosporium (Indexed FFT Fig: 4.5E) and the second had a unit cell length of $a = b = 64 \pm 1$ Å, $y = 118° \pm 1°$ (Indexed FFT Fig: 4.5F). The second lattice matched the Type II crystal that was found on the *csxA* mutant spores.
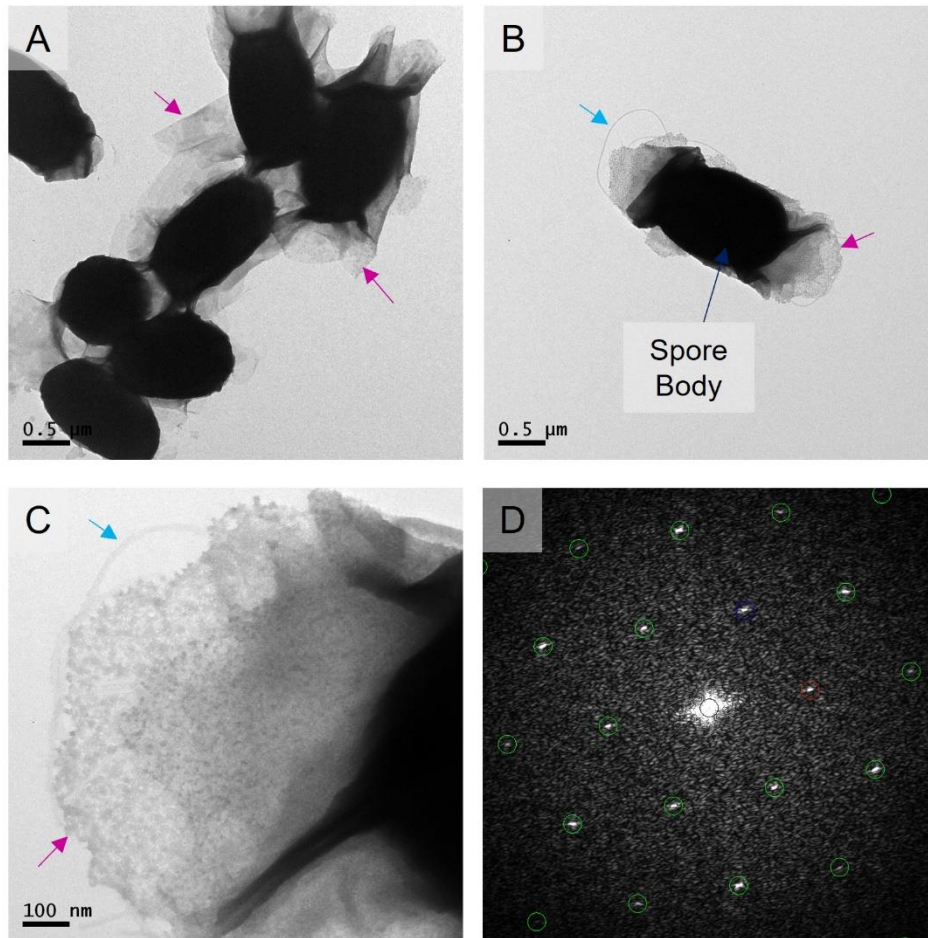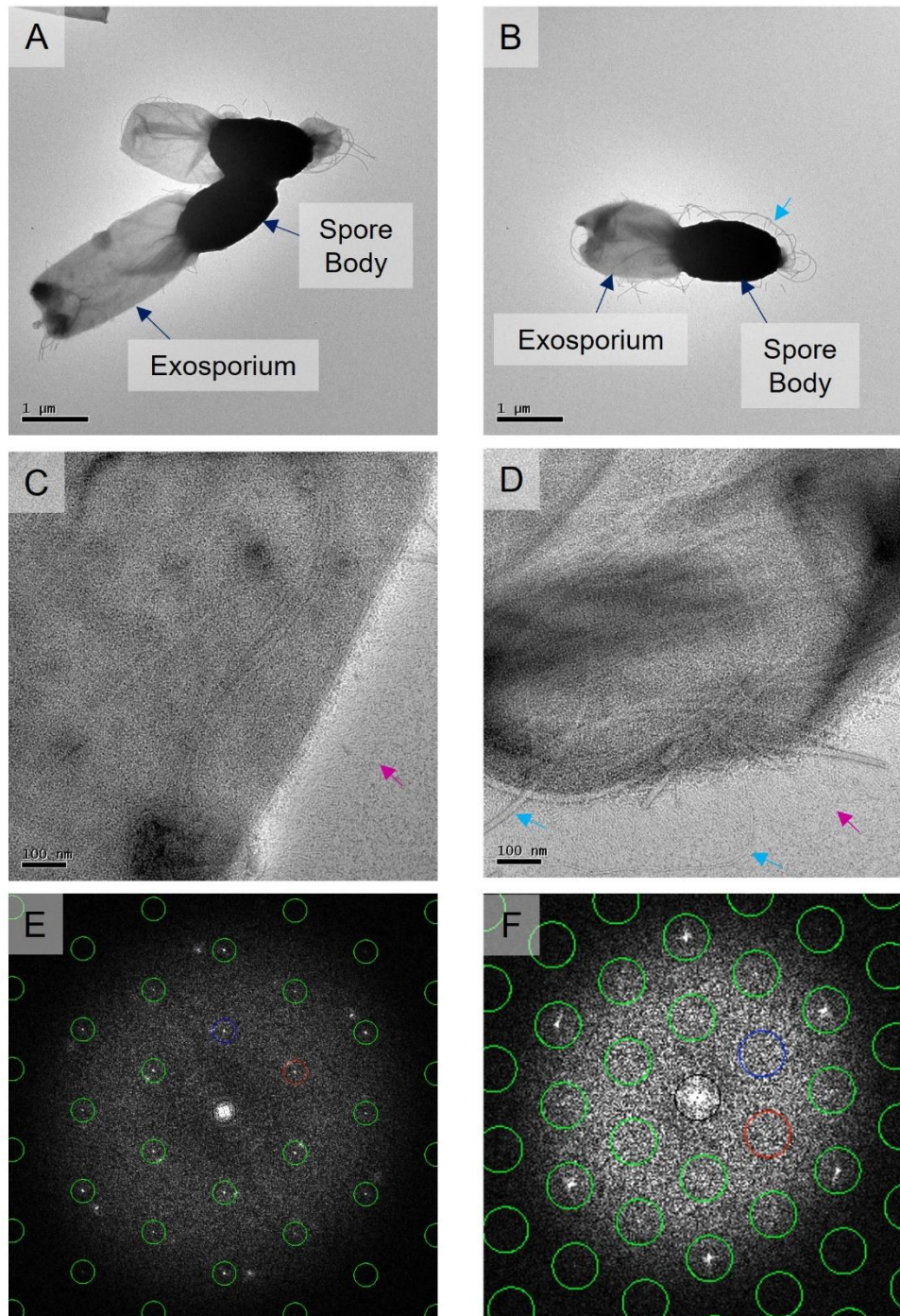
Figure 4.4: Negative Stain TEM of *csxC* Spores

A+B) Low magnification micrographs of negatively stained *csxC* spores show a hyper extension to one pole of the exosporium. C+D) Higher magnification micrographs showing the exosporium. The hairy nap can be seen decorating the surface of the exosporium (pink arrow) as well as large appendages and beaded fibrils (light blue arrow). E and F) Indexed FFTs of the crystalline exosporium layer surrounding the spore corresponding to Type I crystal, unit cell $a = b = 105$ Å and $y = 118°$ F) An indexed FFT where the first order spots are not visible.
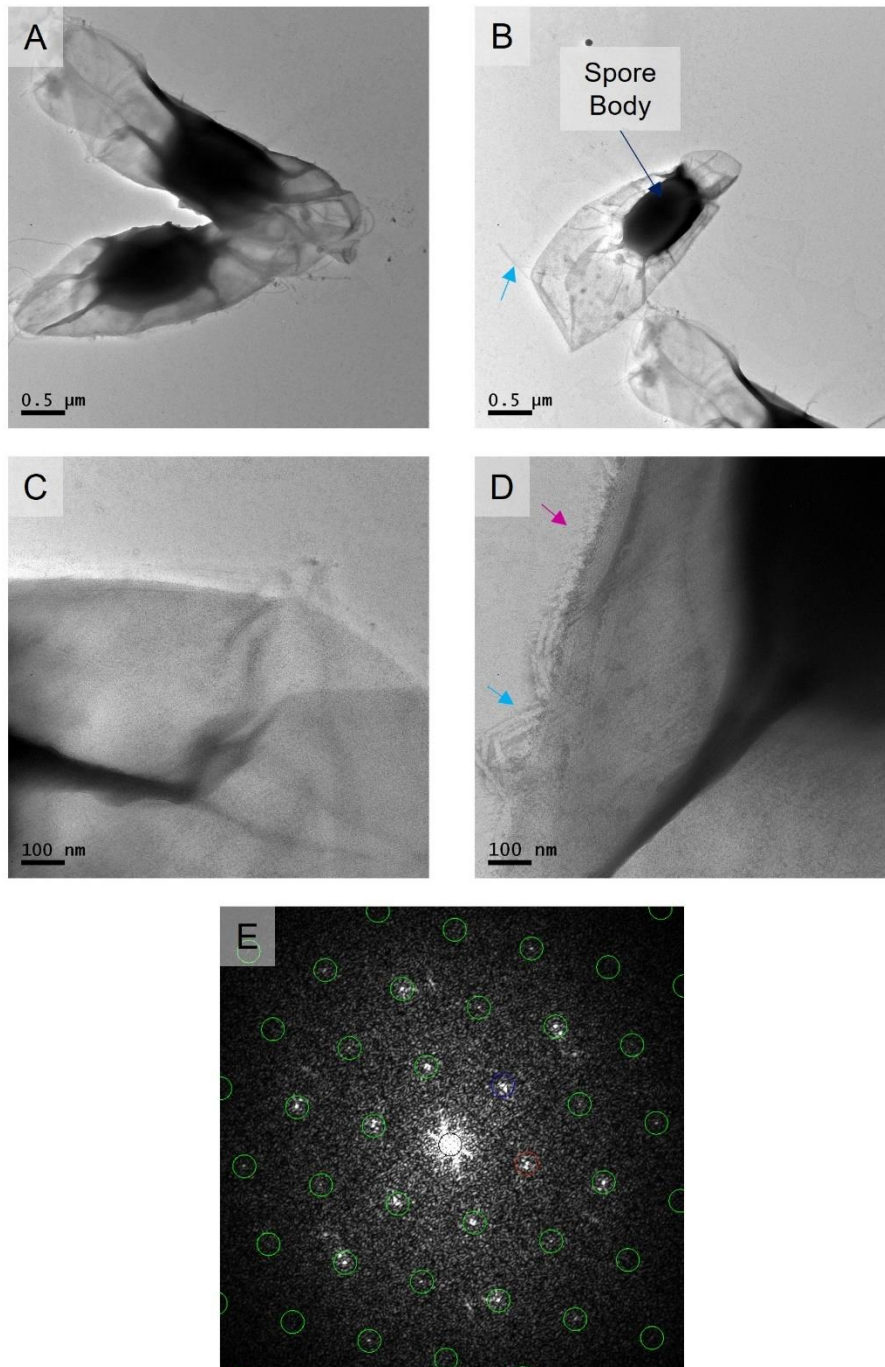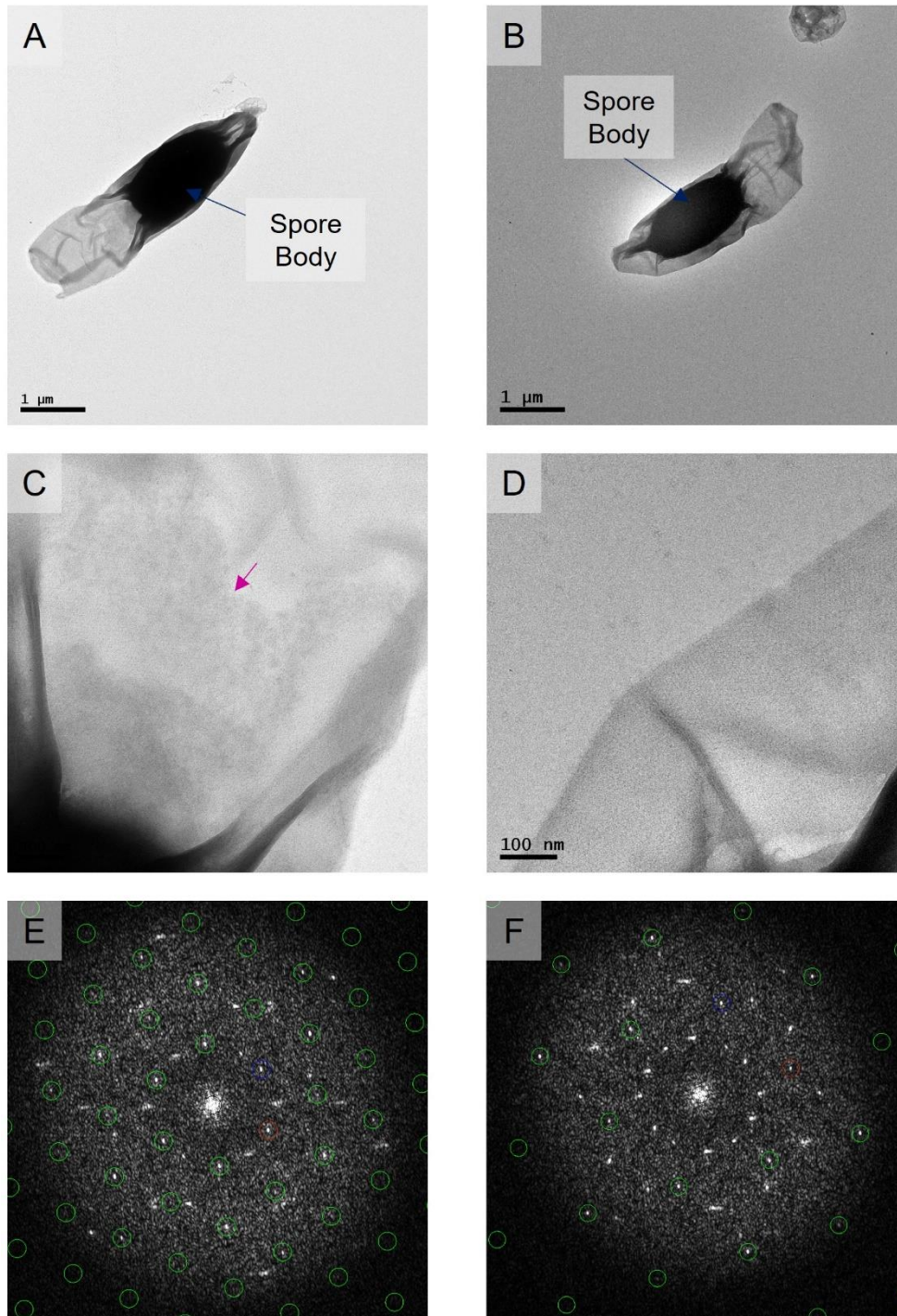
Figure 4.5: Negative Stain TEM of *bclA* Spores

A+B) Low magnification micrographs of negatively stained *bclA* spores show a baggy exosporium surrounding the spore dense spore body C+D) Higher magnification micrograph showing the exosporium and an area of darker staining (pink arrow) indicating a layer beneath the exosporium. No hairy nap was visible on the surface of the exosporium. E+F) Indexed FFTs of the crystalline layers present on *bclA* spores. E) Type I crystal, unit cell $a = b = 110$ Å and $y = 118°$ and F) Type II crystal, unit cell $a = b = 64$ Å and $y = 118°$.
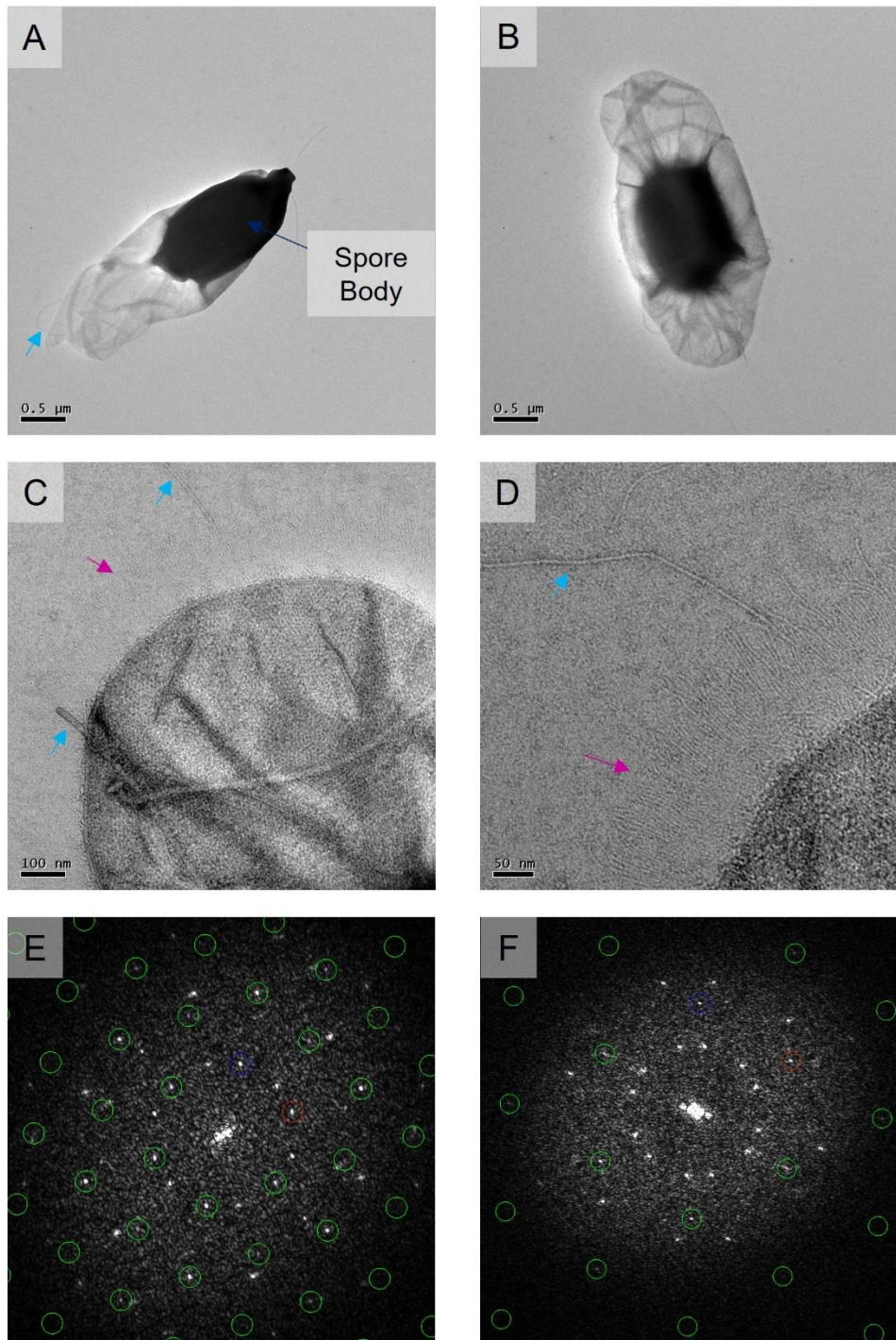
Figure 4.6: Negative Stain TEM of *bclB* Spores

A+B) Low magnification micrographs of negatively stained *bclB* spores show a baggy exosporium surrounding the spore dense spore body. C+D) Higher magnification micrograph showing the crystalline exosporium decorated in a hairy nap (pink arrows) including the presence of beaded fibrils and large appendages (light blue arrows). E+F) Indexed FFTs of the crystalline layers present on bclB spores. E) Type I crystal, unit cell $a = b = 106$ Å and $y = 120°$ and F) Type II crystal, unit cell $a = b = 65$ Å and $y = 119°$.

4.3.2.5   *bclB*

Micrographs of *bclB* mutant spores showed spores with no clear morphological differences. The exosporium layer completely surrounded the main spore body (Fig: 4.6A and B). In many cases the exosporium was extended from one pole as seen in WT spores. High magnification micrographs showed the clear presence of a hairy nap on the surface of the exosporium (Fig: 4.6C and D pink arrows). Beaded fibrils were also observed along with large appendages (Fig: 4.6 light blue arrows). Processing of crystalline areas of the exosporium confirmed the presence of a crystal type with unit cell length of $a = b = 106 \pm 3$ Å, $y = 120° \pm 2°$ identical to Type I crystal found in WT spores (Indexed FFT Fig: 4.6E). On one spore there was evidence of a second lattice with a unit cell length of $a = b = 65$ Å $y = 119°$ similar to the Type II crystal seen on *csxA* and *bclA* mutants (Indexed FFT Fig: 4.6F).

4.3.3   Electron Crystallography of Layers Present in Mutant Spores

Two distinct crystal lattice types were observed across the mutant spores, putatively Type I and Type II. These were processed using *2dx* (Gipson et al. 2007) to generate 2D projection maps. Processing proved to be challenging due to the highly disordered nature of the crystal patches across the spores. This meant that only a low number of images were suitable for merging for each putative crystal type.

4.3.3.1   Type I

Type I crystal was found in *csxB*, *csxC*, *bclA* and *bclB* spores and resembled native exosporium. Space group analysis of Type I crystals were consistent with *p6* symmetry, having a phase residual of 28.6° with a target of 31.4°. Therefore, 2D projection maps with *p6* symmetry imposed were produced from images of each mutant (Fig: 4.7B, C, D and F). For *csxB* and *bclA* the maps showed a central ring with an area of low density in the core. Each ring was connected to adjacent rings by a threefold

linker (Fig: 4.7B and D). In the case of *bclB* the projection map appears slightly different but shows the same features just less clearly defined, likely due to a lower SNR and lower resolution (Fig: 4.7F).

Processing of *csxC* crystals was notably more challenging than for the other mutants. Many areas of crystal had strong second order diffraction but completely absent or very weak first order spots (Fig: 4.4F). An example 2D projection map from a single image is shown in Fig: 4.7C which depicts a hexagonal ring structure with a central pore. Threefold linker regions were not seen in this map.

4.3.3.2   Type II

The second crystal type, Type II, was observed in *csxA*, *bclA* and *bclB* spores (Fig: 4.7A, E and G). In the case of *csxA* spores it was the only crystal type present. For *bclA* and *bclB* spores it was present in low abundance located in close proximity to the spore body in addition to Type I crystal. Space group analysis for Type II crystal suggested *p3* symmetry, giving a phase residual of 4.1° with a target of 14.9° for *csxA* spores, 2.9° with a target of 22.8° for *bclA* spores and 4.8° with a target of 18.9° for *bclB* spores. 6 images from *csxA* and 2 from *bclA* spores were merged to produce 2D projection maps with imposed *p3* symmetry. A single image example is shown for *bclB* spores. These all showed a threefold subunit surrounded by areas of low density (Fig: 4.7A, E and G).

A   Type II

csxA

65Å

B   Type I

csxB

105Å

C   Type I

csxC

105Å

D   Type I

E   Type II

bclA

110Å   64Å

F   Type I

G   Type II

bclB

106Å   65Å

120
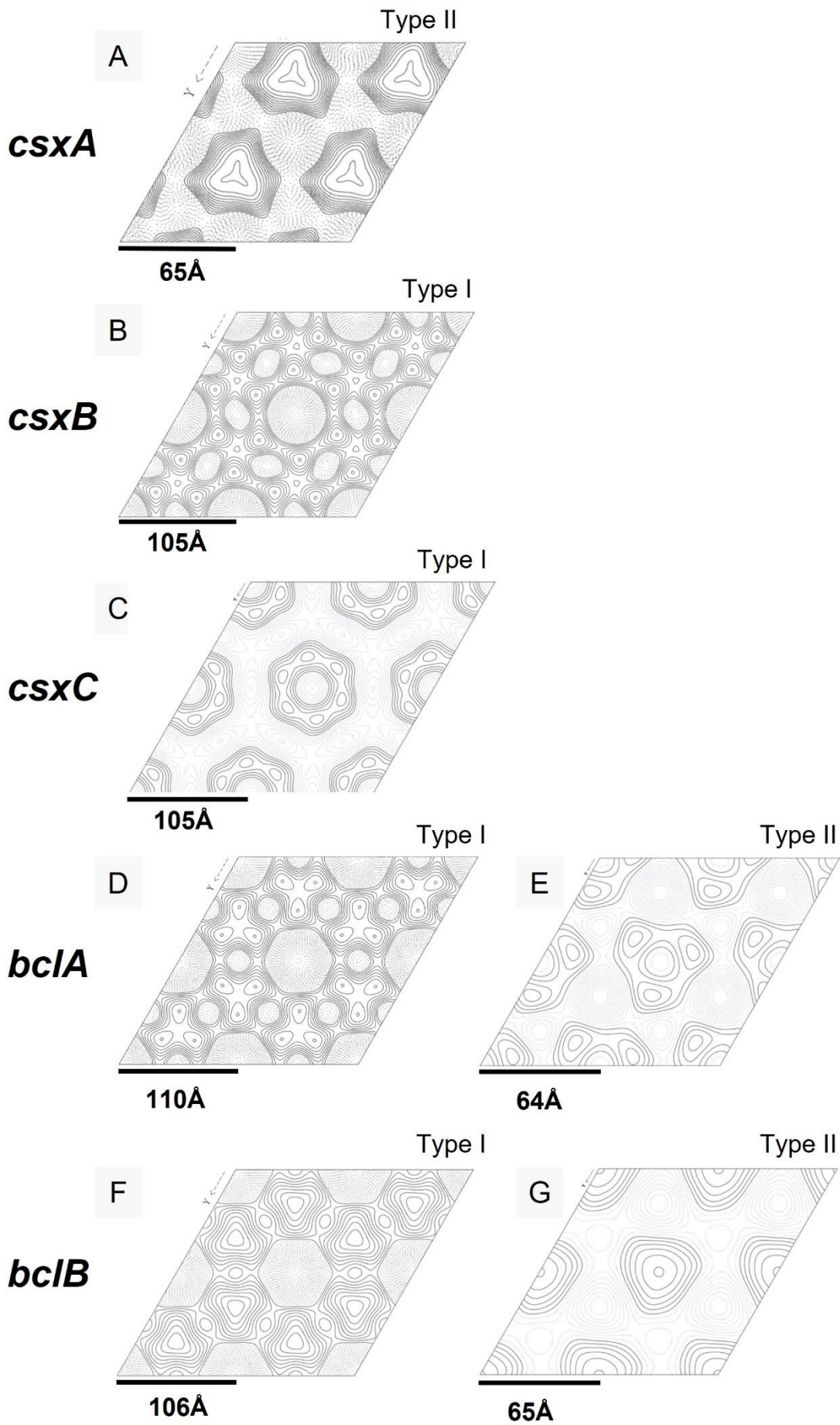
Figure 4.7: 2D Projection Maps of Crystal Types Found Across *C. sporogenes* Mutant Spores

The solid contour lines display stain excluding areas and therefore high-density areas, whilst dashed lines display low density areas. Potential subunits are indicated with black squares while 3-fold linker regions are indicated by black arrows. A) *csxA* mutant Type II crystal lattice with *p3* symmetry imposed. 6 images merged, unit cell *a* = *b* = 65 Å *y* = 120° B) *csxB* mutant Type I crystal lattice with *p6* symmetry imposed. 13 images merged, unit cell *a* = *b* = 105 Å *y* = 120° C) *csxC* mutant Type I crystal lattice with p6 symmetry imposed. Single image, unit cell *a* = *b* = 105 Å *y* = 120° D) *bclA* mutant Type I crystal lattice with p6 symmetry imposed. 6 images merged, unit cell *a* = *b* = 110 Å *y* = 120° E) *bclA* mutant Type II crystal lattice with *p3* symmetry imposed. 2 images merged, unit cell *a* = *b* = 64 Å *y* = 120° F) *bclB* mutant Type I crystal lattice with p6 symmetry imposed. 14 images merged, unit cell *a* = *b* = 106 Å *y* = 120° G) *bclB* mutant Type II crystal lattice with *p3* symmetry imposed. Single image, unit cell *a* = *b* = 65 Å *y* = 120°.

4.3.4   Probing the Internal Spore Structure of Mutants

Chemical fixation was carried out as detailed in Section 2.6.1.3 and thin sections (70-90 nm) were prepared and imaged by TEM.

4.3.4.1   *csxA*

Sections of *csxA* mutant spores showed that they were clearly devoid of a defined exosporium (Fig: 4.8). The spore body appeared intact, with the spore coat clearly visible as a darkly stained layer. The internal layers of the spore body were not clearly defined, probably due to poor stain infiltration, however the paler region is likely to correspond to the cortex layer with the densely stained core in the centre. Surrounding the spore body were discontinuous sheets of material which in some places appeared to be made up of multiple laminations (Fig: 4.8 pink arrows). The exterior surface of these sheets appeared to attract the accumulation of osmium particulates giving them a grainy appearance. In some places the laminated layers were in contact with the spore coat but generally an interspace appeared to be maintained between the outermost layers and the spore coat. This interspace varied in thickness but on average the interspace seen in transverse sections had a thickness of 85 nm ± 20 nm compared to 160 nm ± 40 nm in WT.
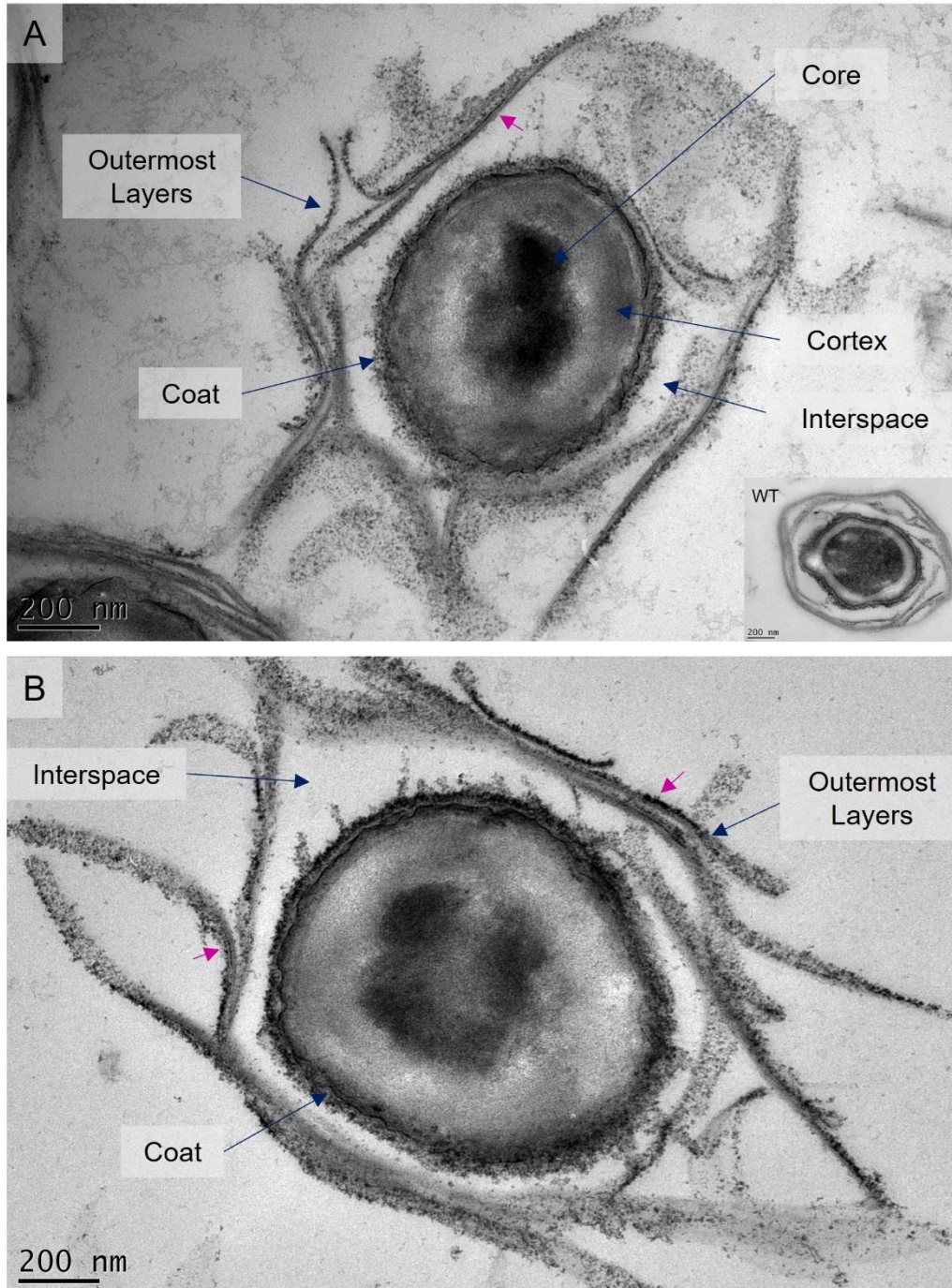
Figure 4.8: Thin Sectioning of *csxA* Spores

Micrographs depict *csxA* spore sections showing the outermost layers separated from the spore body by an interspace region. Pink arrows indicate laminations of the outer layers. Inlay shows WT spore section for comparison.

4.3.4.2 *csxB*

Thin sections of *csxB* mutant spores were similar to that of WT (Section 3.3.1.2). The exosporium clearly surrounded the entire spore body and had a smoother, more uniform shape when compared with WT, where the exosporium was more varied, particularly in longitudinal sections (Fig: 4.9). The parasporal layers within the interspace at the extended pole of the exosporium appeared to be curved at the edges forming concave sheets from the perspective of the exterior of the spore. The proteinaceous spore coat was darkly stained and on ~75% of spores, blebs were seen within the coat surface (Fig: 4.9 pink arrows). A paler region corresponding to the spore cortex was present beneath the coat and in some cases a thin darker stained unknown layer could be seen within (Fig: 4.9C light blue arrow). The dense spore core was present in the centre of the spore body.

4.3.4.3 *csxC*

Sections of *csxC* mutant spores showed an array of differing spore morphologies. Of particular interest was that the interspace was completely devoid of parasporal layers (Fig: 4.10). In the majority of cases the *csxC* spores showed a hyper extended exosporium at one pole (Fig: 4.10B and C) consistent with the negative stain images (Fig: 4.4A and B). For several spores the furthest pole of the exosporium appeared to be open with the edges of the exosporium curled back in on itself (Fig: 4.10B pink arrows). A small subset of spores showed a distorted exosporium where instead of a smooth rounded appearance the exosporium appeared far more angular (Fig: 4.10B light blue arrow). Around the lateral sides of the main spore body the exosporium was in close association with the spore coat and ripples were observed in the exosporium layer in these areas (Fig: 4.10C purple arrows). The spore coat of the *csxC* spores also appeared frayed or improperly assembled.
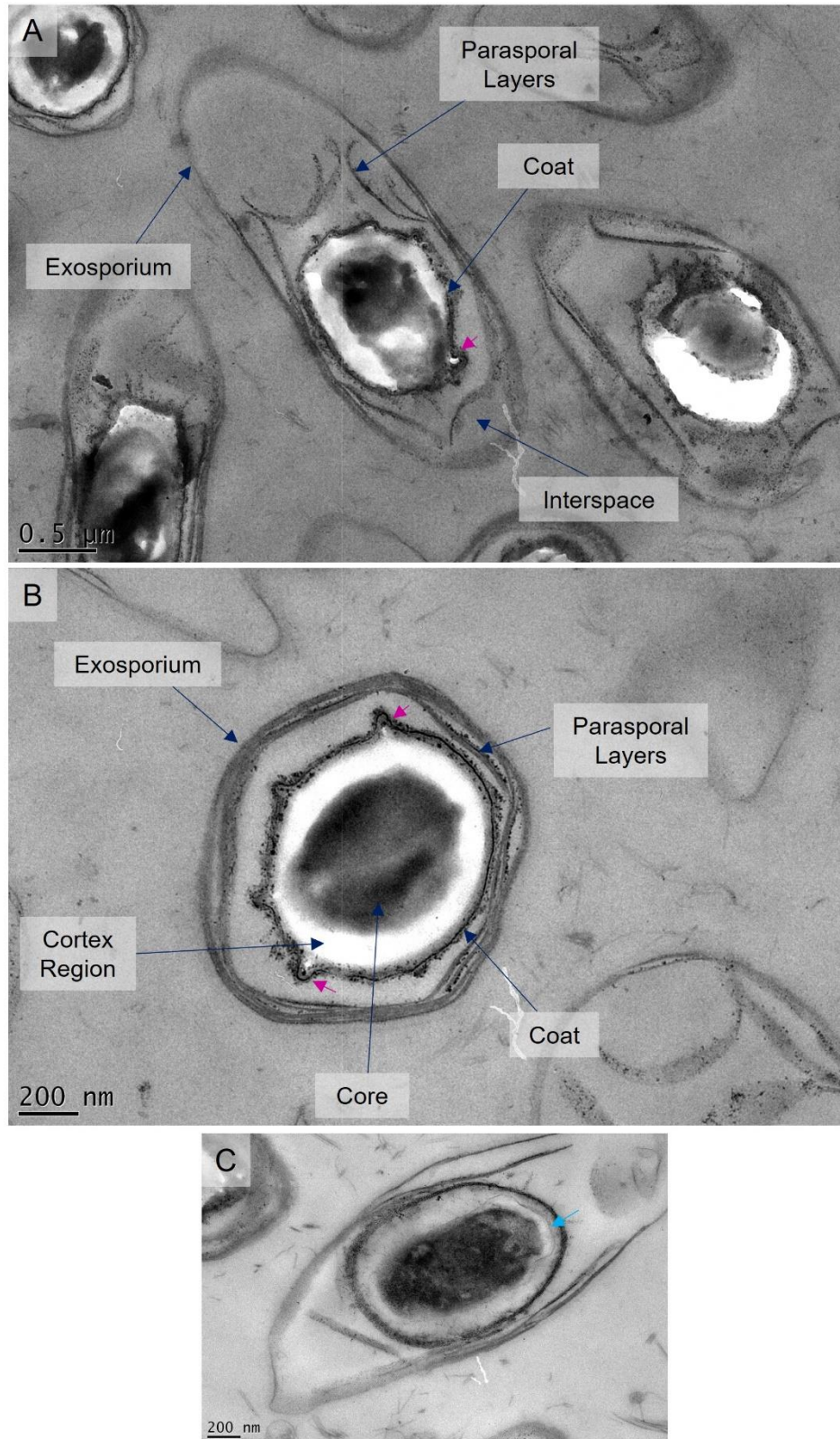
Figure 4.9: Thin Sectioning of *csxB* Spores

A-C) Micrographs of *csxB* spore thin sections show the presence of concave parasporal layers within the interspace (A) and 'blebs' within the spore coat (pink arrows). C) An additional darkly stained layer seen within the cortex (light blue arrow).
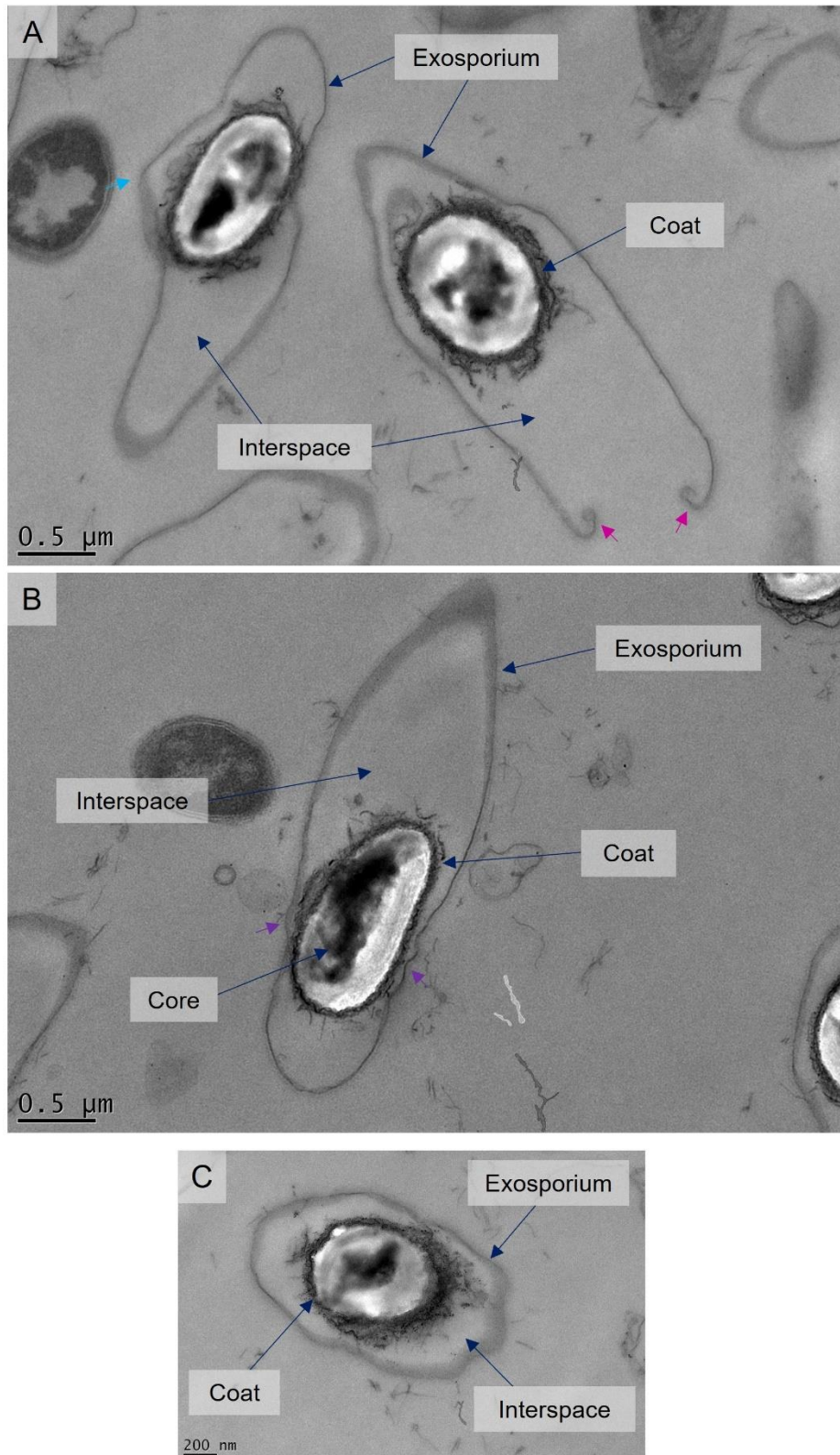
Figure 4.10: Thin Sectioning of *csxC* Spores

A-C) Micrographs of *csxC* spore thin sections. A+B) longitudinal sections show the hyper extended pole of the exosporium. Pink arrows (A) indicate open pole of the exosporium with edges curled back. Light blue arrow (A) angular region of the exosporium. Purple arrows (B) ripples in the exosporium where it is in association with the spore coat. C) transverse thin section of *csxC* spore shows the disordered nature of the spore coat.

4.3.4.4 *bclA*

Sections of *bclA* mutant spores appeared much the same as WT spores (Fig: 4.11). The exosporium clearly surrounded the entire spore and the interspace contained parasporal layers, often forming laminations against the outer exosporium layer. The spore coat was darkly stained and appeared intact. In some cases one pole of the exosporium appeared open with the edges of the exosporium folded back on itself (Fig: 4.11A pink arrows). The internal details of the spore body were only visible in a small number of spores due to inconsistent staining, however, those that allowed, showed a pale region of cortex along with a darkly stained spore core.

4.3.4.5 *bclB*

Thin sections of *bclB* mutant spores revealed no obvious differences in their ultrastructure. A clear exosporium was seen surrounding the spore body (Fig: 4.12). Parasporal layers were present within the interspace region of the spores and occasionally appeared to have a more concave like form than those seen in WT. The spore coat was darkly stained and appeared intact, however, the internal structures of the spore body were poorly stained.
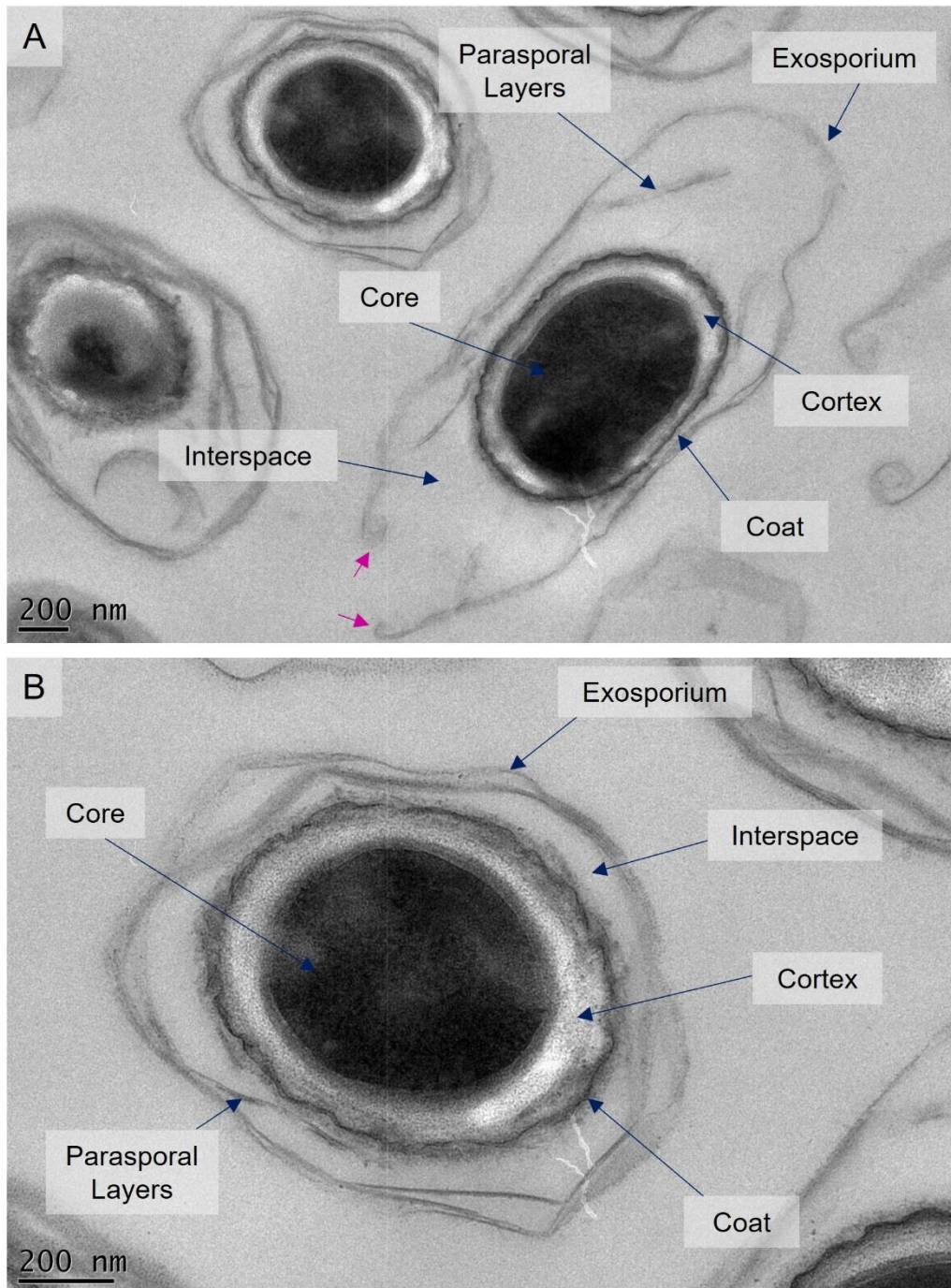
Figure 4.11: Thin Sectioning of *bclA* Spores

A+B) Micrographs of *bclA* spores A) longitudinal section with an open pole to the exosporium where the edges are curled back (pink arrows). B) transverse section. All distinguishable layers are labelled.
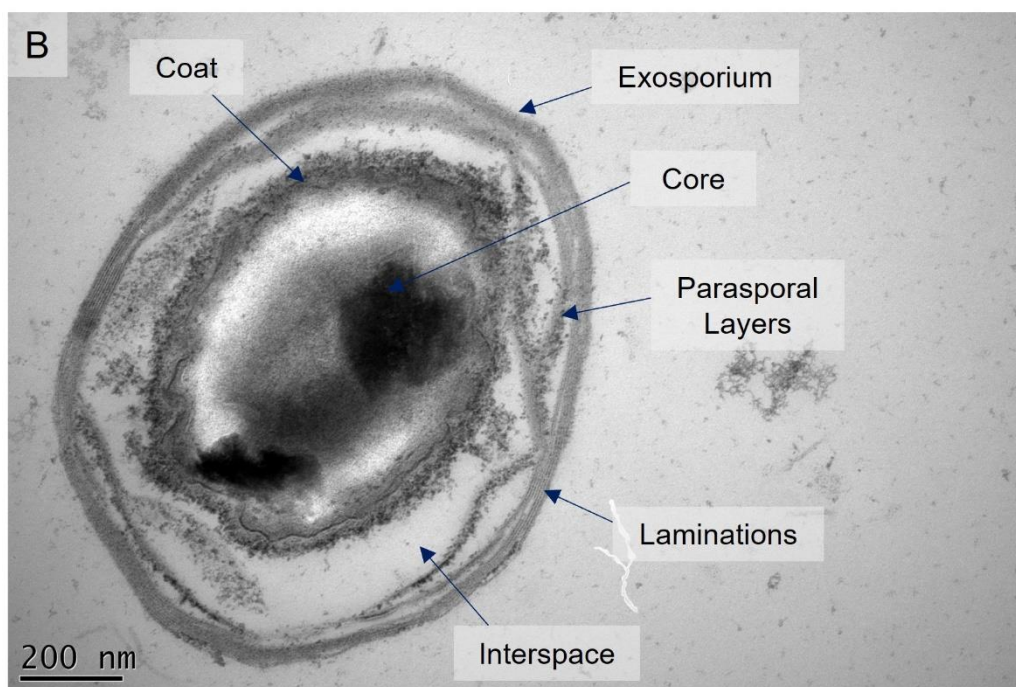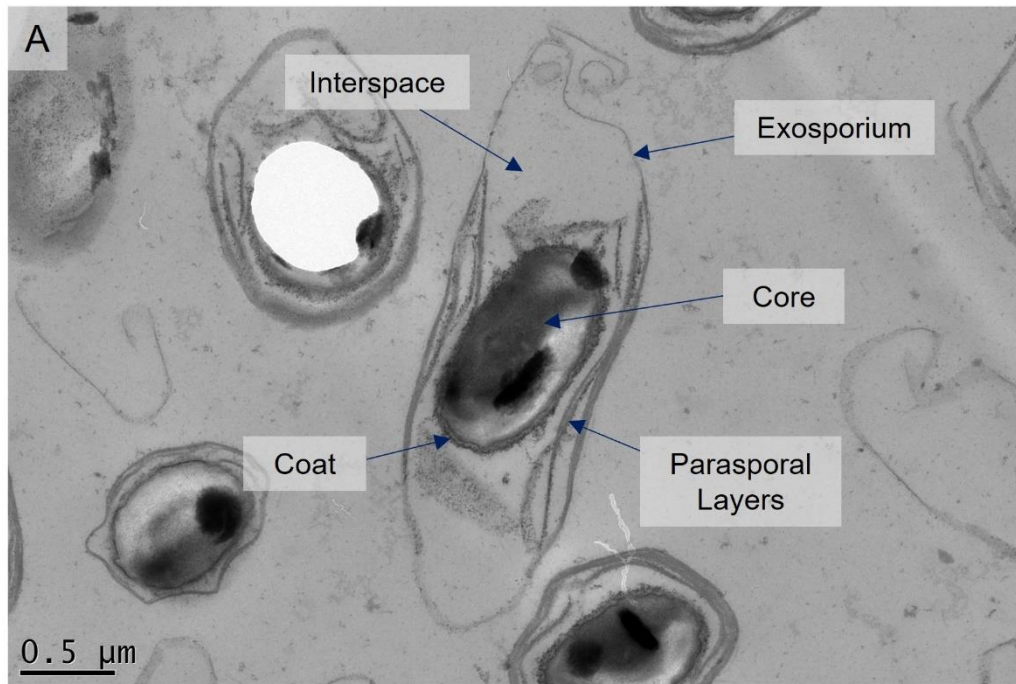
Figure 4.12: Thin Sectioning of *bclB* Spores

A) Micrographs of longitudinal thin section of *bclB* spore B) transverse thin section of *bclB* spore. All distinguishable layers are labelled.

4.3.5 Understanding the Surface Characteristics of Mutants

To understand the surface properties of the mutant spores, particularly the *bclA* and *bclB* mutants, AFM was carried out by Dr Nicholas Mullin (Department of Physics and Astronomy, University of Sheffield). Mutant spores were adhered to a glass slide coated with a thin film of poly-d-lysine. All samples were imaged in air.

4.3.5.1 *csxA*

The AFM data from *csxA* spores were consistent with observations seen by EM (Fig: 4.13A). The spores had patches of crystal surrounding the main spore body. The lattice spacing measured by AFM was 62 Å which is consistent with the electron crystallography data. The surface of the spores appeared to be devoid of a hairy nap, however, large appendages were still present (Fig: 4.13A light blue arrows).

4.3.5.2 *csxB*

csxB spores showed a generally rounded appearance with the spore body more centrally located within the exosporium than for WT (Fig: 4.13B). A clear hairy nap could be seen on the surface of the exosporium (Fig: 4.13B black arrow) as well as large appendages (Fig: 4.13B light blue arrows). The large appendages could also be seen across the surface of the spore body, potentially being located beneath the exosporium (Fig: 4.13B yellow arrow), an observation not seen by TEM due to the thickness of the spore body. Ridges and folds were also observed in the exosporium layer as it surrounded the spore body.

4.3.5.3 *csxC*

Two different spore morphologies were seen across the *csxC* AFM data. Most of the spores imaged had an elongated exosporium at one pole (Fig: 4.13C). Some spores appeared to have an exosporium that fanned out around the spore body in a manner reminiscent of flower petals (Fig: 4.13D). A clear

hairy nap was present on the surface of the exosporium of both morphologies (Fig: 4.13C and D

black arrows) along with large appendages and beaded fibrils (Fig: 4.13C and D light blue arrows).
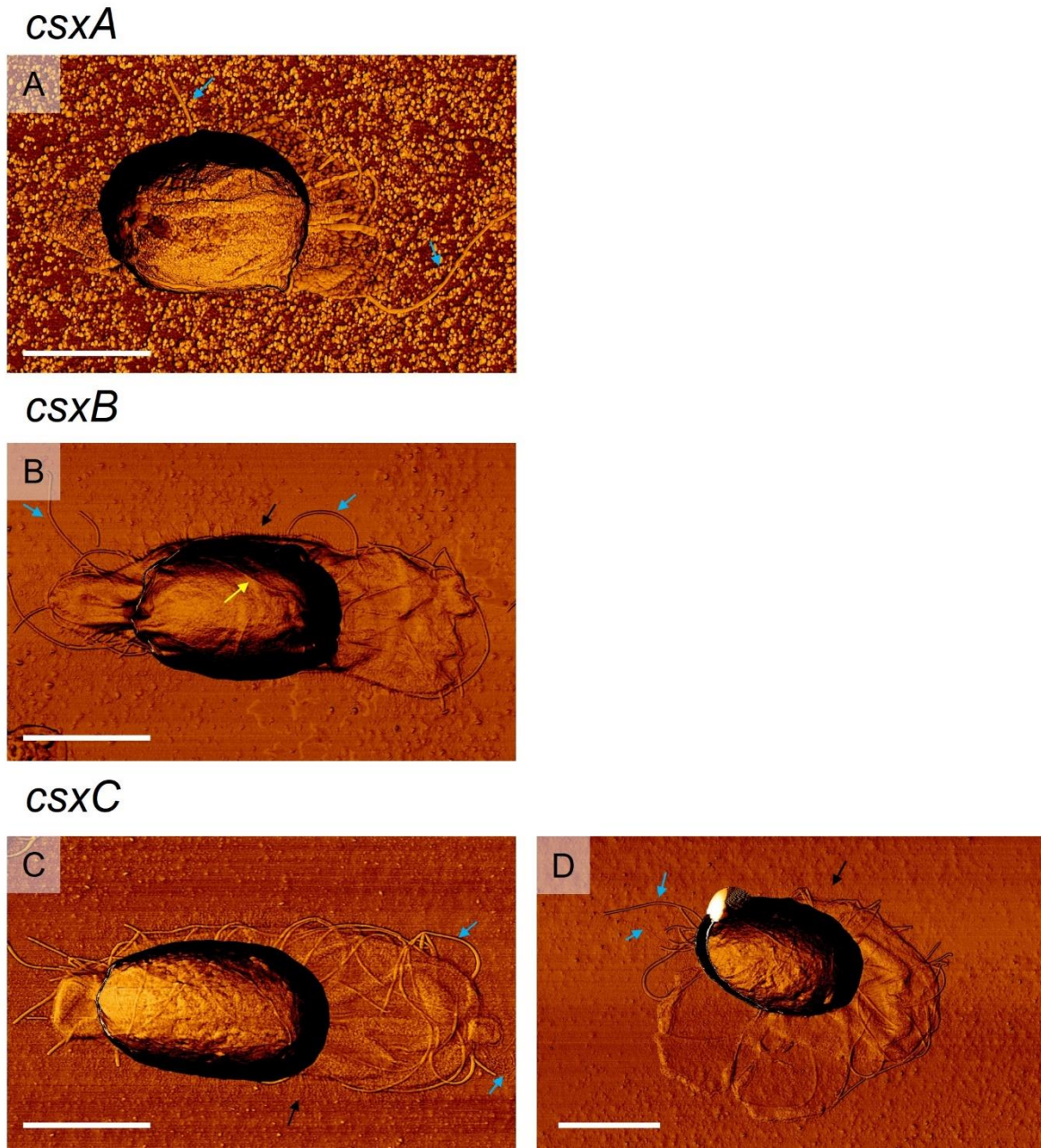
csxA

csxB

csxC

Figure 4.13: AFM of *csx* Mutant Spores

A) *csxA* mutant shows spore body with small regions of crystalline material around the edges B) *csxB* mutant shows spore body surrounded by exosporium C) *csxC* mutant spore with hyper extension to the exosporium D) *csxC* mutant spore with a fanned out exosporium. Arrows indicate large appendages and beaded fibrils (light blue arrows), hairy nap (black arrows), large appendage across the spore body (yellow arrow). Scale bars = 1 μm

4.3.5.4   *bclA*

For many of the *bclA* spore examples the exosporium appeared to be adhered to itself (Fig: 4.14A) suggesting that *bclA* spores had an altered surface compared to WT. It was clear from *bclA* spore data that the fringe on the exosporium surface was not present (Fig: 4.14A and B) suggesting that BclA is a key component of the nap. Large appendages and beaded fibrils were seen associated with the exosporium (Fig: 4.14A and B light blue arrows). Where thickness measurements were possible, a double layer of exosporium was found to be approximately 20 nm thick. A small region of material still appeared to be present on the exosporium surface forming a halo around the spore (Fig: 4.14B yellow arrows).

4.3.5.5   *bclB*

No obvious differences between *bclB* and WT spores could be ascertained from the AFM data (Fig: 4.14C). The exosporium surrounded the spore body and was decorated by a hairy nap (Fig: 4.14C black arrow). Beaded fibrils and large appendages were also present (Fig: 4.14C light blue arrows), the latter of which could be seen across the surface of the spore body (Fig: 4.14C yellow arrow).
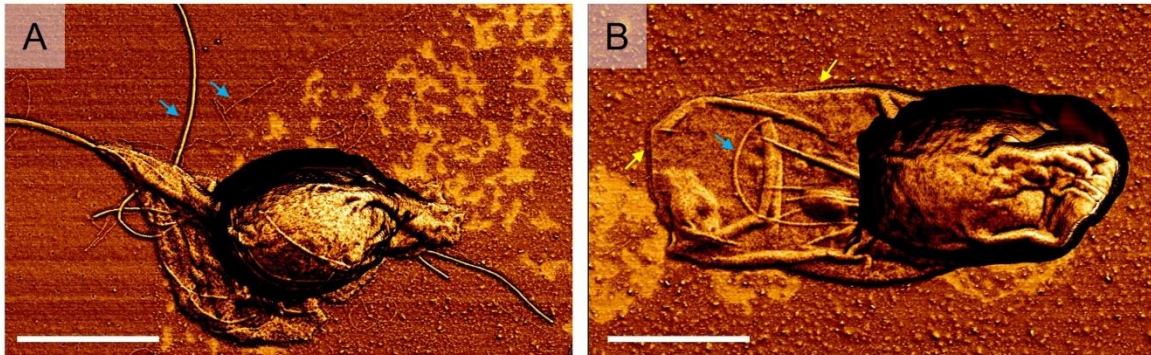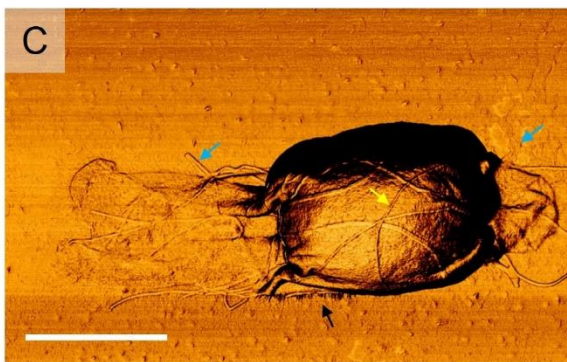
Figure 4.14: AFM of *bcl* Mutant Spores

A) *bclA* spore where the exosporium is adhered to itself and folded over. Large appendages and beaded fibrils were present (light blue arrows) B) *bclA* spore where the exosporium is lying flat across the surface. No fringe was seen around the edge of the exosporium but a smaller halo remained (yellow arrows). C) *bclB* spore shows the spore body surrounded by exosporium and the presence of a hairy nap on the spore surface (black arrow). Large appendages and beaded fibrils were also present (light blue arrows) including several that can be seen across the spore body (yellow arrow). Scale bars = 1 µm

4.3.6   Heterologous Expression of CsxB and CsxC Proteins

It has previously been shown that heterologous expression of the cysteine rich proteins in *E. coli* can lead to spontaneous formation of crystalline sheets (Janganan et al. 2020; Jiang et al. 2015; Terry et al. 2017). As CsxB and CsxC are also cysteine rich proteins heterologous expression was conducted to determine if a similar phenomenon is observed.

The genes encoding CsxB and CsxC were amplified from the *C. sporogenes* genome using primer pairs RF2074/2075 and RF2077/2078 respectively. The resulting fragments were inserted into

pET21a for CsxB expression and pET28a for CsxC expression via restriction ligation. The resulting constructs contained the *csxB* or *csxC* gene C-terminally tagged with His$_6$. pET21a had to be used for CsxB due to the presence of a NcoI restriction site located within the *csxB* gene required for cloning into pET28a. Plasmid constructs for over expression of CsxB and CsxC were transformed into Rosetta BL21 *E. coli* cells and expression was induced by addition of IPTG. CsxA was also over expressed in a similar manner using a plasmid construct previously used in (Janganan et al. 2020). Samples of cells pre- and post-induction were sonicated and soluble and insoluble fractions were analysed by SDS-PAGE (Fig: 4.15).
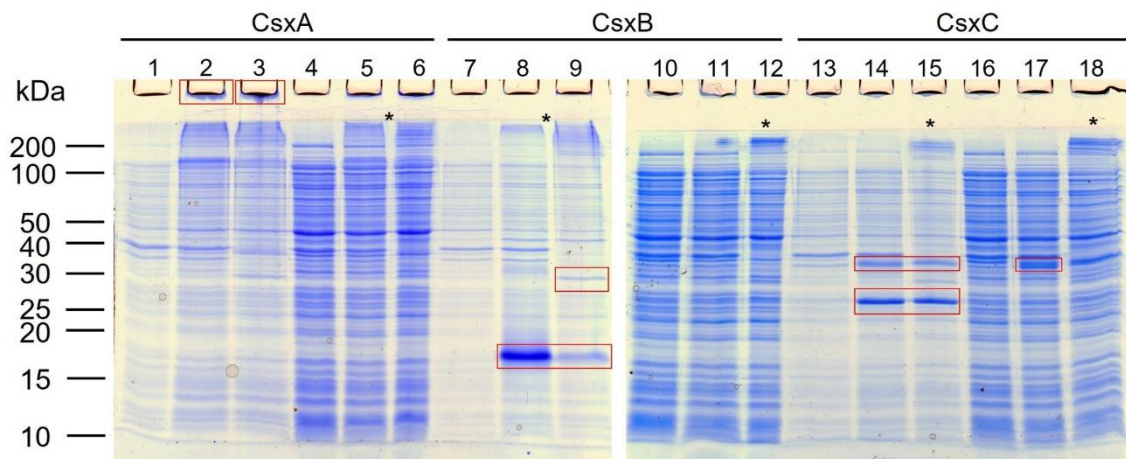
Figure 4.15: SDS-PAGE Analysis of Csx Protein Overexpression

CsxA, CsxB and CsxC proteins were over expressed in *E. coli*. Cells pre and post induction were lysed and the soluble and insoluble fractions analysed by SDS-PAGE. Samples were loaded in the same order for each overexpression consisting of: (1) pre-induction insoluble fraction boiled, (2) post induction insoluble fraction boiled, (3) post induction insoluble fraction not boiled, (4) pre-induction soluble fraction boiled, (5) post induction soluble fraction boiled, (6) post induction soluble fraction not boiled. Bands corresponding to each protein are highlighted in red. For CsxA this was within the wells of lanes 2 and 3. For CsxB bands were seen in the insoluble fractions, lanes 8 and 9. For CsxC bands were seen in the insoluble fraction, lanes 14 and 15 and in the soluble faction after boiling, lane 17. * Indicate possible high oligomeric states of overexpressed Csx proteins.

As expected from prior work on CsxA (Janganan et al. 2016), no clear band was seen around 35 kDa that would correspond to a CsxA monomer. A smear of high molecular weight bands was seen at the top of the resolving gel suggesting high oligomeric states. Heavy staining was also seen within the

well of the insoluble fractions (Fig: 4.15 lanes 2 and 3) which corresponded to protein unable to enter the gel.

For CsxB over-expression, the insoluble fraction contained a strong band at approximately 17 kDa that corresponded to that expected for monomeric CsxB (predicted MW = 16.6 kDa)(Fig: 4.15 lane 8). As with CsxA some evidence of high molecular weight complexes was also seen at the top of the resolving gel in both the soluble and insoluble fractions post induction (Fig: 4.15 lanes 8, 9 and 12 marked *).

CsxC had an expected molecular weight of 30 kDa. SDS-PAGE analysis showed strong expression bands within the insoluble fraction at approximately 32 kDa and at 28 kDa (Fig: 4.15 lane 14).

E. coli cells post induction were chemically fixed, thin sectioned (70-90 nm) and imaged by TEM. Within *E. coli* cells over expressing CsxA clear laminations of protein crystal could be seen (Fig: 4.16A pink arrow), as had been seen previously (Janganan et al. 2020). The cells over-expressing CsxB appeared to have dense inclusion bodies within them (Fig: 4.16B light blue arrows). CsxC over-expressing cells showed no clear evidence of inclusion bodies or crystals within the cytoplasm (Fig: 4.16C).
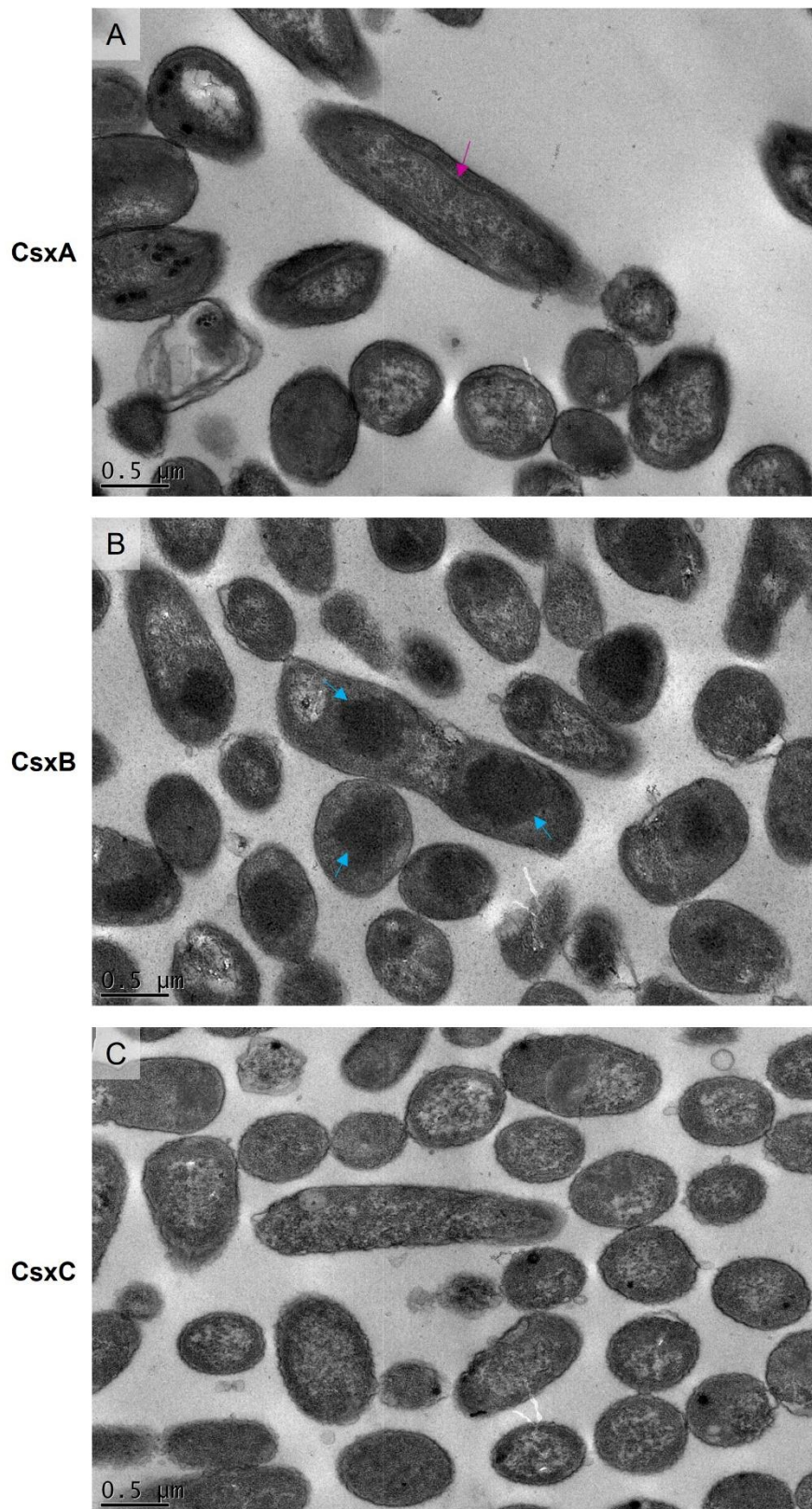
Figure 4.16: Thin Sectioning of *E. coli* Cells Overexpressing Csx Proteins

A) Sections of CsxA overexpressing cells show sheets of self-assembled crystals within the cytoplasm (pink arrow). B) Sections of CsxB overexpressing cells show darkly stained inclusion bodies (light blue arrows). C) Sections of CsxC overexpressing cells show no obvious signs of crystals or inclusion bodies within the cytoplasm.

4.3.7   AlphaFold Predictions for CsxC

As CsxC is a candidate structural protein for the composition of the parasporal layers we decided to predict the structure of CsxC using Alphfold2 (Jumper et al. 2021). Given appearance and threefold symmetry of the 2D projection map produced for Type II crystal, a trimer of CsxC was also predicted to determine if this would likely fit within the unit cell density.

The predicted monomer structure contained a high confidence beta barrel structure, an extended loop region and an N-terminal unstructured region of low confidence (Fig: 4.17). A number of cysteine residues were found to be in positions that would allow for the formation of up to 3 intramolecular disulphide bonds within the monomer structure (Fig: 4.17Ai and ii). There were also several cysteines located on more external facing regions that could potentially interact with other monomers to stabilise oligomers.

The predicted trimer structure formed a clear triangular shape with imperfect threefold symmetry. When viewed along the threefold axis one edge of the triangle measured 85Å (Fig: 4.18A). Each monomer substantially interacts with both neighbouring monomers with intercalating strands completing the beta barrel structure within the neighbouring monomer. This also results in the formation of an additional disulphide bond between Cys152 of one monomer and Cys39 of the adjacent monomer (Highlighted in Fig: 4.17A). The three intramolecular disulphides predicted within the monomer structure are also maintained within the trimer structure (Fig: 4.18Ai and ii). Viewed from the side the predicted trimer has a domed shape with the beta barrels bending down from the central apex (Fig: 4.18B). Viewing the structure coloured by confidence (Fig: 4.19) the central apex of the trimer and the beta barrels have the highest confidence whilst the loop regions and N-terminal ribbons have the lowest confidence.
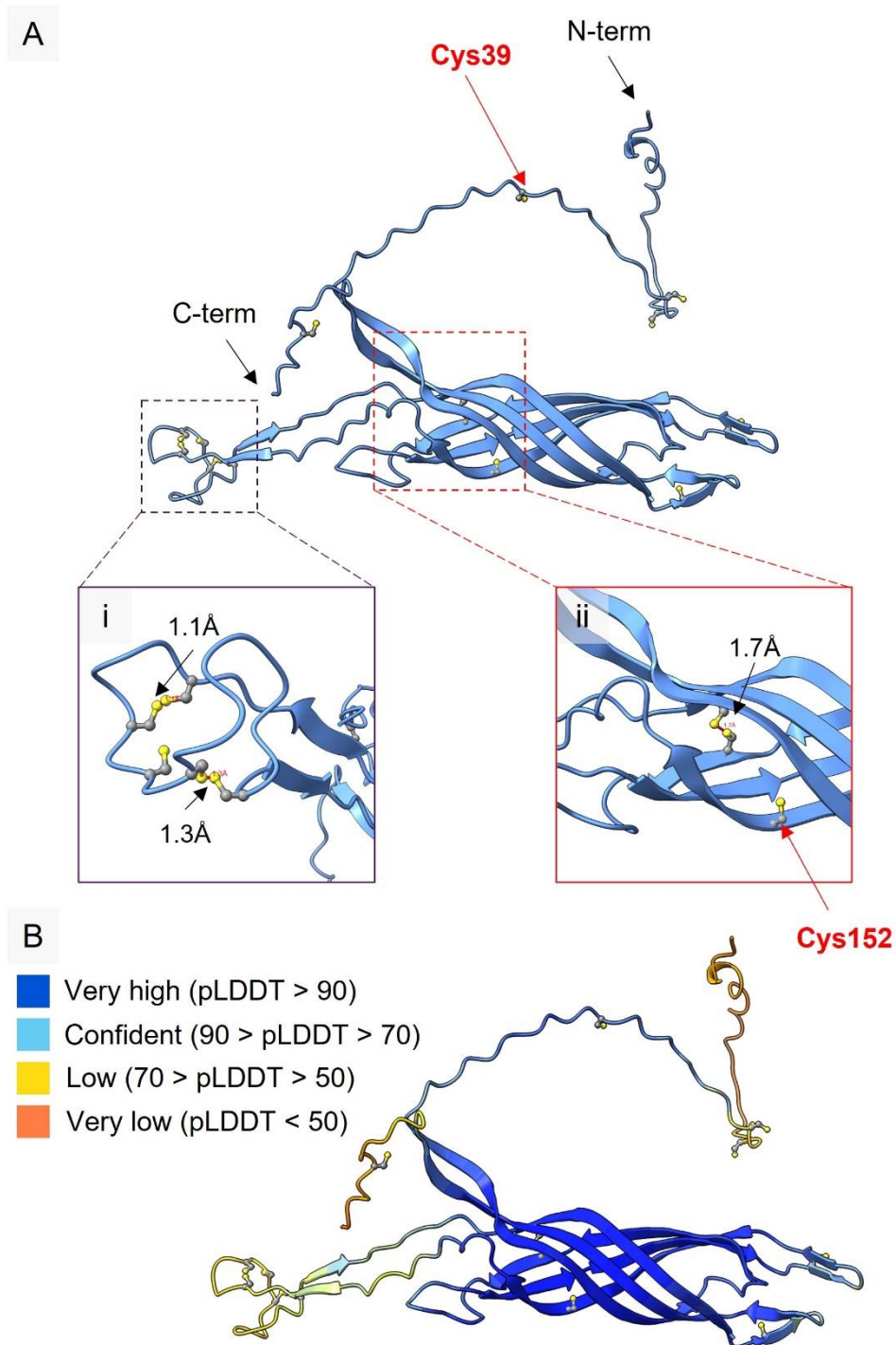
Figure 4.17: Alphafold2 Prediction of CsxC Monomer

A) The predicted monomer contains a beta barrel structure with an extended loop region. A large portion of the N-terminal is unstructured as is a small region of the C terminal. i+ii) Regions containing potential disulphide bonds between cysteine residues within the monomer. Cysteine residues involved in disulphide bond interactions within the trimer are labelled in red. B) Predicted monomer structure of CsxC coloured by pLDDT value to show confidence of prediction. The higher the pLDDT value the more confident the prediction. Shows high confidence in the beta-barrel region of the monomer.
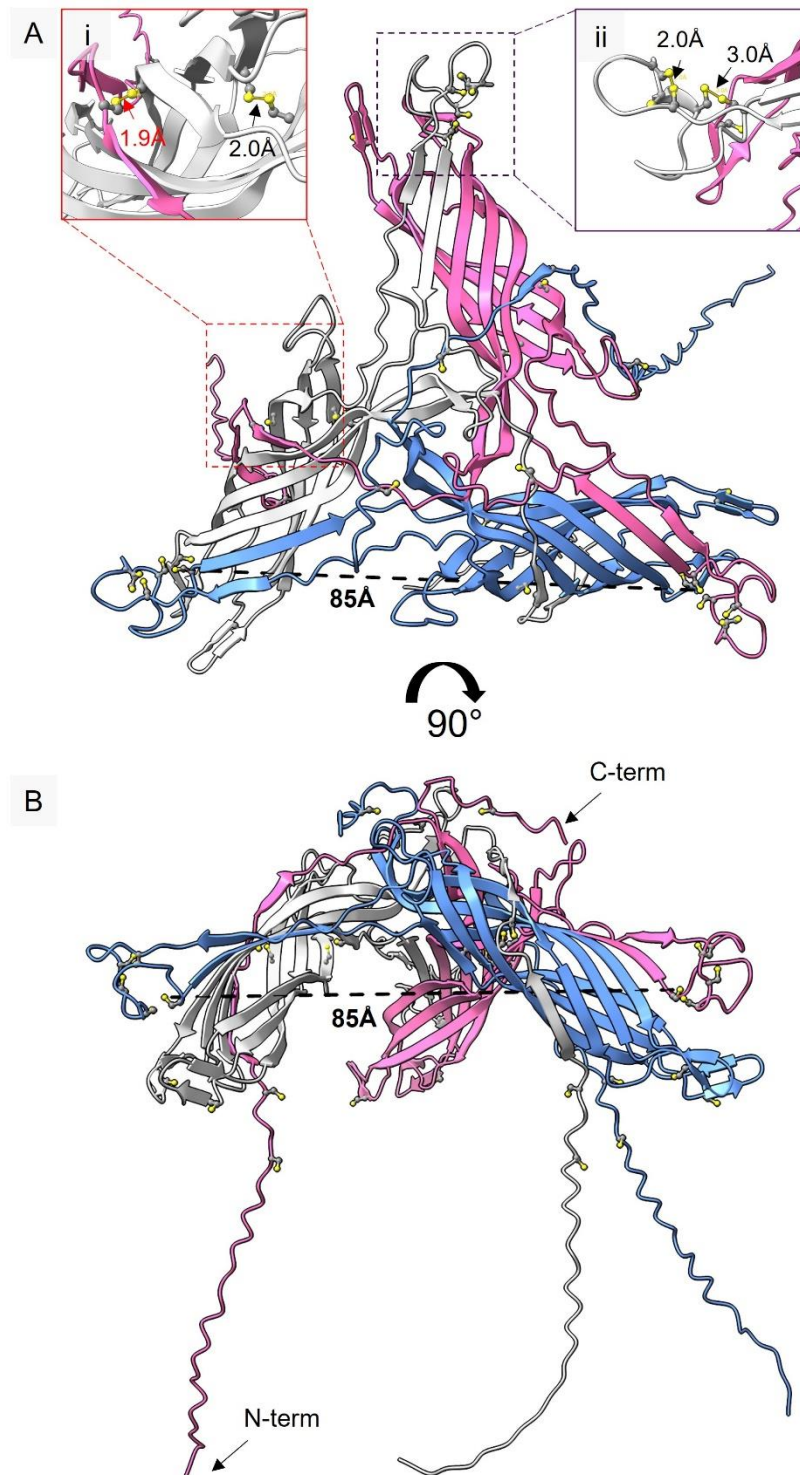
Figure 4.18: Alphafold2 Prediction of CsxC Trimer

A) Trimer prediction looking down the threefold axis shows a triangular structure with one side of the triangle measuring 85Å. Each monomer interacts with both neighbouring monomers with intercalating strands completing the beta barrel structure the neighbouring monomer. i+ii) Regions containing potential disulphide bonds including the formation of an additional disulphide between Cys152 of one monomer and Cys39 of another monomer. B) Side view of the CsxC trimer showing the beta barrels are orientated on an angle to form the domed nature of the structure.
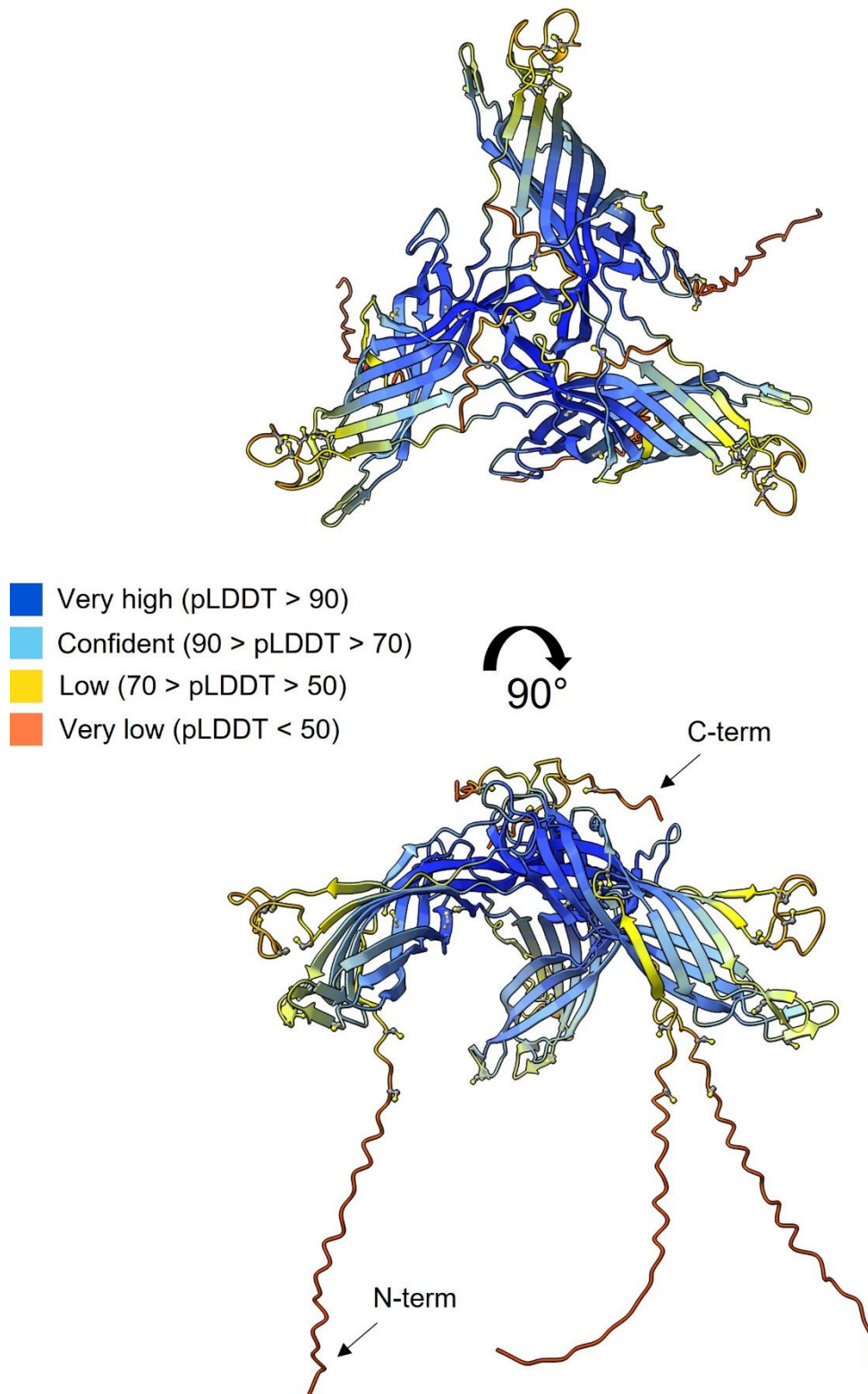
Figure 4.19: Predicted Trimer Structure of CsxC Coloured by Confidence

pLDDT values show confidence of prediction where the higher the pLDDT value the more confident the prediction. The central apex and the beta-barrel structure shows high confidence whilst the N-terminal regions are predicted with very low confidence hence their ribbon-like appearance.

4.4 Discussion

4.4.1 Phenotypic Analysis of Mutants

CsxA, CsxB, CsxC, BclA and BclB were all previously identified as being associated with the exosporium in *C. sporogenes* (Janganan et al. 2016). Based on previous findings in Bacillus species showing that cysteine rich proteins play a key role in the structure of both the exosporium and the coat (Jiang et al. 2015; Terry et al. 2017), the three cysteine rich proteins, CsxA, CsxB and CsxC were of particular interest as potential structural components of the exosporium. BclA and BclB are both putative collagen-like proteins similar to the proteins found to decorate the surface of *B. anthracis* (Boydston et al. 2005; Sylvestre et al. 2002; Thompson et al. 2012).

csxA, *csxB* and *csxC* mutants were previously constructed in the ATCC 15579 strain of *C. sporogenes* and their phenotypes were screened by negative stain TEM (Dafis-Sagarmendi, 2021). These previous mutants were produced using ClosTron technology (Heap et al. 2007) that utilises the addition of an insertion within the target gene to disrupt expression. The *csxA*, *csxB* and *csxC* mutants produced here in strain NCIMB 70179 were produced using allelic exchange mutagenesis which completely removes the target gene and therefore produces true knockouts. In addition, it was important to have exosporium mutants in the strain that we were using to carry out germination studies. Negative stain TEM showed the general spore phenotypes to be identical to those seen previously, confirming the knockout phenotypes of ATCC 15579. *csxA* spores showed a lack of baggy exosporium but the presence of other crystal patches associated with the spore body (Fig: 4.2). *csxB* spores appeared very similar to WT with no clear impact on the gross spore morphology (Fig: 4.3). On the other hand, the lack of CsxC had a major impact on spore phenotype. Negative stain TEM showed a hyper extension to one pole of the exosporium with a small protrusion sometimes present at the opposite pole (Fig: 4.4). It was unclear from the negative stain data whether the exosporium on *csxC* spores surrounded the entire spore body.

Having ascertained that the general spore morphologies were consistent between the strains further in-depth ultrastructural analysis was carried out on the mutants in NCIMB 70179. Thin sectioning of the *csxA* spores confirmed the presence of crystalline patches around the spore and showed that these patches were separated from the spore body by a small interspace region (Fig: 4.8). The spore coat appeared to be intact suggesting that the crystalline sheets present on the surface of *csxA* spores were not layers sloughed off from the coat but more likely parasporal layers seen localised within the interspace of WT spores (Chapter 3.3.1.2).

Ultrastructural analysis of *csxB* spores found the presence of blebs within the spore coat (Fig: 4.9), a feature that was not possible to identify by negative stain TEM and is discussed further in Section 4.4.2.5.

Thin sectioning of *csxC* spores confirmed that the exosporium did indeed surround the entire spore body but was very closely associated with the spore coat (Fig: 4.10). It also revealed that there were no parasporal layers within *csxC* spores suggesting CsxC plays a major role in their assembly (Discussed below).

Whole spore AFM for all of these mutants confirmed the gross spore phenotypes seen by EM and confirmed the presence of a hairy nap on the surface of both *csxB* and *csxC* spores (Fig: 4.13). Interestingly, spores of the *csxC* spores did not appear to have the ridges and folds seen within the exosporium layer for WT spores (Chapter 3.4.1). Perhaps this suggests that these features are the result of the parasporal layers present beneath the exosporium surface.

The addition of *bclA* and *bclB* mutant strains provided an insight into the structure of the hairy nap decorating the surface of the exosporium of *C. sporogenes*. Although no obvious differences in spore morphology were seen by TEM for either mutant, high magnification images from the edge of the exosporium of *bclA* spores did suggest a lack of a hairy nap. AFM data collected from these mutants provided a clearer understanding of the nap structure, in particular the role of BclA, and is discussed further in section 4.4.3.

4.4.2   The Roles of Cysteine Rich Proteins in *C. sporogenes* Spore Ultrastructure

4.4.2.1   Type I crystal corresponds the basal layer of exosporium

The Type I crystal, with a unit cell of approximately *a* = *b* = 110 Å, *y* = 120°, observed in *csxB*, *csxC*, *bclA* and *bclB* mutants is identical to that obtained from native exosporium basal layer(Janganan et al. 2020). The projection maps from *csxB*, *bclA* and *bclB* exosporium show a hexagonal ring structure connected by threefold linkers. A central region of low density can be seen in the middle of the ring, likely corresponding to a pore within the crystal structure. 6 smaller pores can also be seen between each of the points of the hexagonal ring. This structure is identical to what is seen for both native exosporium and 2D projections from CsxA crystal (Janganan et al. 2020) (Fig: 4.20). These projection maps were all produced from negative stain data and therefore have limited resolution to around 20Å. Despite this, the major structural details of the crystalline layer are clearly visible. This further confirms Type I crystal as the basal layer of the exosporium in *C. sporogenes*.

Whilst processing the data from *csxC* mutant spores the crystalline patches were found to be more disordered and in many cases the first order diffraction spots were absent or very faint. All crystalline areas that were amenable to processing gave unit cell parameters and phases consistent with Type I crystal from other mutants and WT. Despite this the final merged 2D projection map showed an electron dense hexagonal ring structure with a central pore but no indications of a threefold linker region (Fig: 4.7C). One explanation for this could be that there is incomplete stain penetration of the crystal lattice that produces a high contrast feature with a pseudo first order repeat. This would produce diffraction patterns missing first order spots and explain the slightly altered 2D projection map. This could be a reflection on a potential role of CsxC in aiding the formation of the exosporium layer resulting in increased crystal disorder and perhaps in a more sealed exosporium that does not readily allow for stain penetration. To probe the structure of the exosporium further in this mutant, fragments of the exosporium could be isolated and imaged by

cryoEM to produce a higher resolution projection map of the exosporium structure. This might

reveal any small structural differences that could account for the difference in crystallinity observed.
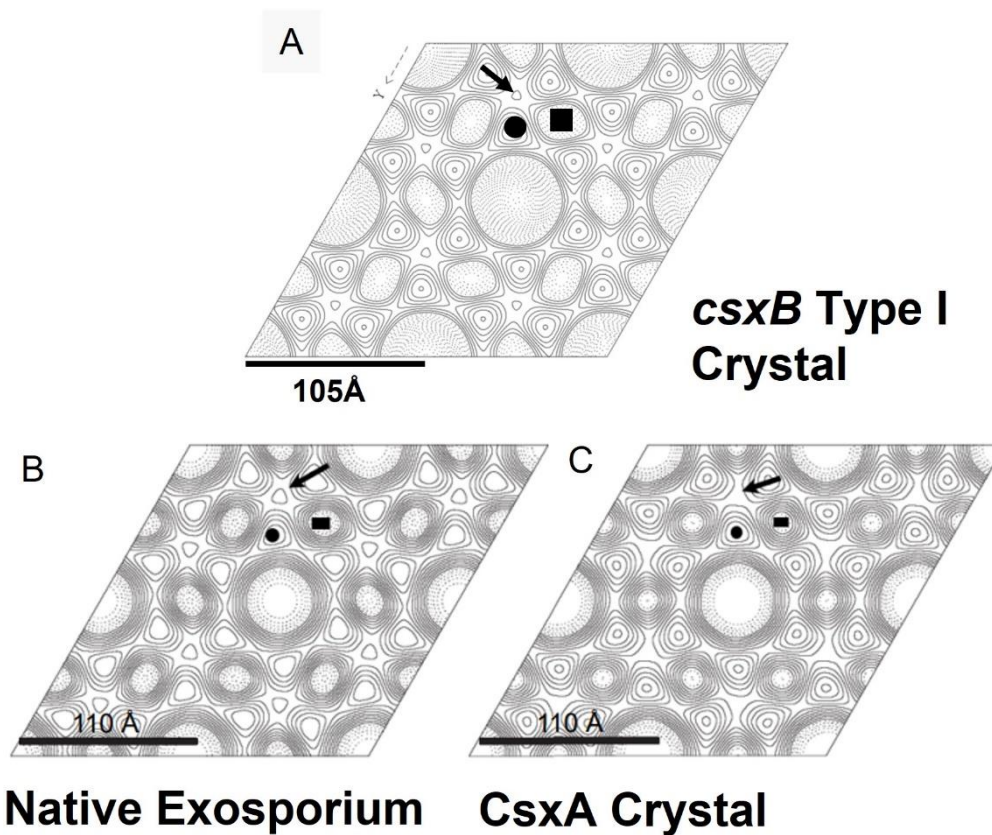
Figure 4.20: Comparison of *csxB* Type I Crystal and Native Exosporium

A) 2D projection map from *csxB* Type I crystal B) 2D projection map of negatively stained dormant spore exosporium from (Janganan et al. 2020). C) 2D projection map of negatively stained heterologously expressed CsxA crystal from (Janganan et al. 2020) Black circles indicates potential subunits, black squares indicate a peripheral pore, and the black arrows indicate a 3-fold linker.

B and C reproduced with permission (Janganan et al. 2020)

4.4.2.2 The Exosporium Basal Layer is Composed of CsxA

It has been established that Type I crystal corresponds to the basal layer of *C. sporogenes*

exosporium. Type I crystal is also structurally identical to heterologously expressed CsxA crystals

(Janganan et al. 2020). Because of this, CsxA has been proposed as the major structural component

of the exosporium basal layer in *C. sporogenes*. In addition, the classical exosporium structure

surrounding *C. sporogenes* spores is absent in the *csxA* mutant spores, seen both here and

previously (Janganan et al. 2020). The *csxA* spores still possessed fragments of crystalline material around the spore body, however, there was no evidence that any of these fragments had a crystal type that corresponded to Type I crystal. This further confirms that CsxA is essential for exosporium formation in *C. sporogenes*. The data from *csxB*, *csxC*, *bclA* and *bclB* mutants suggest that these exosporium associated proteins do not play a crucial role in the fundamental assembly of the exosporium basal layer in *C. sporogenes*.

In addition, *csxB*, *csxC* and *bclB* spores all possessed a clear hairy nap associated with Type I crystal. CsxA has been shown to form a complex with BclA, thought to be a major component of the hairy nap (Janganan et al. 2016). In *B. anthracis* interaction between BclA and the exosporium is mediated through EsxFA and EsxFB proteins that form the threefold linker regions between the hexagonal basal layer of the exosporium (Kailas et al. 2011; Steichen, Kearney, and Turnbough 2005; Terry et al. 2017). Projection maps of Type I crystal (Fig: 4.7B, D and F) and CsxA crystal (Janganan et al. 2020) clearly show the presence of these threefold linker regions, suggesting that additional proteins are not required to form these regions of the basal layer in *C. sporogenes*. This further cements the hypothesis that CsxA is the major structural protein of the exosporium basal layer.

Further to this the *csxA* spores showed no evidence of a cap structure remaining associated with the surface of the spore. This differs from *B. cereus* where the exosporium basal layer is formed of at least two proteins EsxY and CotY, with CotY forming the initial cap region of the exosporium (Johnson et al. 2006; Terry et al. 2017). This was confirmed in *esxY* mutant spores where the CotY cap region remains associated with the spore (Boydston et al. 2006). This could suggest that even the potential cap region of the exosporium in *C. sporogenes* is composed of CsxA and that the caps structural differences lie within the surface decoration rather than the fundamental basal layer. This phenomenon has been previously seen in *B. anthracis* where the distribution of BclA and BclB decoration across the surface of the exosporium is not uniform (Thompson et al. 2012). Alternatively, the cap region may simply not be able to stay adhered to the spore surface without

the presence of CsxA and so is not seen in *csxA* spores, or is composed of a non-crystalline region that is not amenable to structural study by EC.

4.4.2.3 Type II Crystal Corresponds to Parasporal Layers and is Likely Composed of CsxC

Type II crystal was observed predominantly in *csxA* mutant spores and was found to have a unit cell of $a = b \approx 65$ Å, $\gamma \approx 120°$ with phases consistent with *p3* symmetry. It was also found in very low abundance on spores of *bclA* and *bclB* mutants. Measurements obtained by AFM from crystal patches on *csxA* spores were also consistent with Type II crystal, with a lattice spacing of 62 Å. It is possible that Type II crystal corresponds to parasporal layers within the interspace of *C. sporogenes* spores. Perhaps coincidentally, crystalline layers thought to correspond to parasporal layers identified in *B. thuringiensis* and *B. cereus* were shown to not possess a hairy nap and also had *p3* symmetry with a unit cell side of ~65 Å (Ball et al. 2008; Kailas et al. 2011). The Type II crystal shown here displays remarkable structural similarities to those seen in *Bacillus* spp. including the lack of a hairy nap and the *p3* symmetry. Furthermore, the location of Type II crystal as layers on the outside of *csxA* spores, as well as the close proximity to the spore body in *bclA* and *bclB*, would correspond with the location of parasporal layers seen in the thin sectioning data. Together this evidence suggest that Type II crystal corresponds to parasporal layers located within the interspace of *C. sporogenes*.

There was no evidence of Type II crystals being present on both *csxB* and *csxC* spores. Therefore, these two proteins are the most likely candidates for forming the parasporal layers. It was clear from the thin sectioning of *csxB* spores that parasporal layers were present within the interspace. Therefore it is unlikely that CsxB forms the crystalline layers associated with Type II crystal. Perhaps the reason Type II crystals were not readily observed on *csxB* spores was due to the presence of the hairy nap on the surface of the spores which could potentially obscure the crystal layers present

within the exosporium. This is likely also the reason for the absence of this crystal type on WT spores.

On the other hand, thin sections of *csxC* spores showed that the interspace was completely devoid of parasporal layers. This could be because CsxC is a major constituent protein of the parasporal layers in *C. sporogenes* or at least is involved in their assembly. Given that CsxC is a cysteine rich protein, similar to CsxA, it would be reasonable to suggest that CsxC may also be able to self-assemble to form crystalline sheets. To this end, heterologous expression of CsxC in *E. coli* has thus far been inconclusive. Clear bands corresponding to monomeric CsxC (~30 kDa) were present after SDS-PAGE analysis at 32 kDa and 28 kDa (Fig: 4.15). The expression band at 28kDa could correspond with a monomer of CsxC that has not been completely unfolded due to the presence of disulphide bonds that are not fully reduced under these conditions, a phenomenon that can occur when folding is very cooperative (Chau and Nelson 1992). Alpha fold predictions of the CsxC monomer structure highlight 3 potential disulphide bonds within the structure (Fig: 4.17) which could be responsible for incomplete unfolding. No higher molecular weight bands were seen that could correspond with higher order oligomers, as was seen for CsxA, suggesting that large stable oligomers of CsxC able to withstand the reducing conditions of SDS-PAGE were not produced. Furthermore, thin sectioning of the expression cells did not reveal any indication of crystalline layers forming within the cytoplasm suggesting that large crystalline sheets of CsxC are not produced. However, the absence of inclusion bodies, yet the strong presence of CsxC within the insoluble fraction could suggest that a smaller multimeric state is formed within *E. coli* which is subsequently broken down in the reducing conditions of sample preparation for SDS-PAGE. This would suggest that the interactions between monomers is not as strong as those between monomers of CsxA that are not broken down under the same conditions.

Based on the *p3* symmetry of the parasporal layers, predictions for the structure of a trimer of CsxC were run through Alphafold2 (Fig: 4.18). This produced a structure that when viewed along the threefold access was not dissimilar in appearance to the threefold densities seen in the 2D projection map from Type II crystal on *csxA* spores (Fig: 4.21). Measurements of the predicted trimer structure suggested a unit cell of ~85 Å which is 20 Å larger than what was measured by electron crystallography. Side views of the predicted trimer show a domed appearance and it could be that when the trimers are packed together to form a crystal lattice that this dome is accentuated and or adjacent trimers are tucked underneath each other resulting in a smaller overall unit cell. The trimer prediction also showed the N-terminal region of each monomer to be disordered which could suggest they have a role in interactions with neighbouring trimers. These regions also contain two cysteine residues which could participate in disulphide bond interactions within neighbouring subunits to form a crystal lattice.
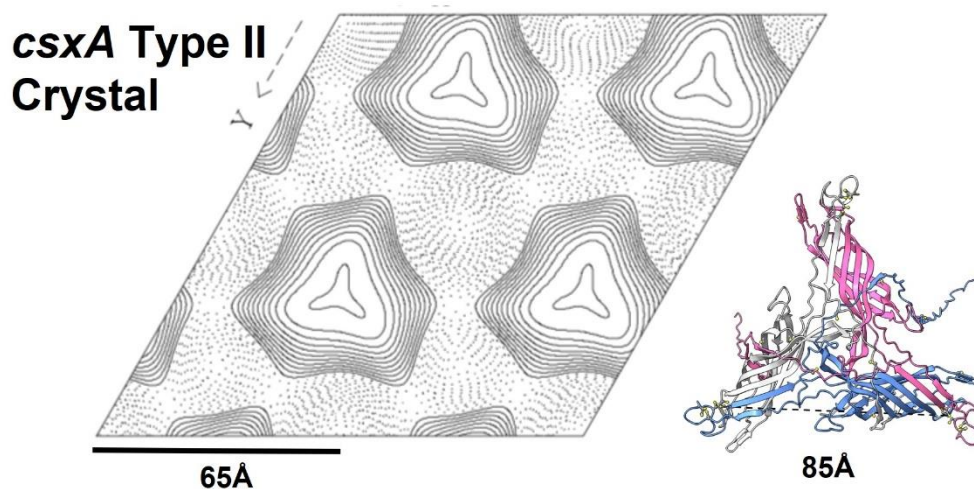
Figure 4.21: Type II Crystal Lattice Comparison to CsxC Predicted Trimer Structure

Predicted trimer structure scaled to match the *csxA* Type II crystal 2D projection map. Although slightly larger in unit cell the predicted timer structure could easily correspond to the regions of high density in the 2D projection map.

Together these observations suggest that CsxC is likely the major protein constituent of the parasporal layers within *C. sporogenes*. It is possible that other proteins are required for their

complete assembly, hence why higher order oligomeric states and crystalline sheets were not observed during overexpression in *E. coli*. Cell lysis and purification of heterologously expressed CsxC needs to be conducted to confirm if there are any crystals present within the sample. Additionally, it may be possible to dissociate the layers from the surface of the *csxA* mutant spores in a method similar to that conducted for WT spores in Janganan et al., 2016. This would allow for mass spectroscopy analysis to determine the protein composition of these layers as well as cryo electron crystallography which would provide a higher resolution crystal structure.

4.4.2.4 The Wider Role of CsxC Within the Spore

It appears that the primary role of CsxC is likely the composition of parasporal layers within the spores. The specific role of the parasporal layers is not abundantly clear but they could act as a scaffold onto which other proteins can adhere. These could include enzymes that protect the spore against oxidative stresses such as those found in the mass spectroscopy analysis of exosporium fragments (Janganan et al. 2016). Additionally, the parasporal layers could add rigidity to the spore and provide a physical barrier between the coat and the exosporium particularly during desiccation. AFM of WT spores compared to *csxC* spores suggest that the ridges and folds seen within the exosporium on WT spores likely correspond to the parasporal layers present beneath the surface. Without them the exosporium appears to sit flush against the spore coat. This physical barrier could aid in protecting the spore body from molecules diffusing through the pores in the exosporium layer.

csxC spores also showed multiple ultrastructural differences, when compared to WT, in addition to the lack of parasporal layers. Firstly, the exosporium of *csxC* spores is often hyper extended at one pole and often has a more irregular shape than seen in WT, particularly around the spore body. This could suggest that CsxC plays a role in regulating the formation of the complete exosporium and is responsible for its regularity in shape and assembly. In WT spores the parasporal layers are seen to stack against the exosporium forming lamellae which could provide support for the assembling

148

exosporium structure. However, in *csxC* spores no parasporal layers are present which could result in the unregulated assembly of the exosporium leading to the hyper extended exosporium pole. This could also lead to increased disorder in the crystalline lattice which was observed during processing of Type I crystal from *csxC* spores (discussed in section 4.4.2.1). Additionally, the interspace of *B. anthracis* has been proposed to contain two layers of polysaccharide that aid the formation of the exosporium (Lehmann et al. 2022). *B. anthracis* is not known to have parasporal layers present within the interspace, however, it could be that in *C. sporogenes* the parasporal layers act as a scaffold for proteins involved in polysaccharide production. The malformation of the exosporium could therefore be due to the mislocalisation of proteins involved in polysaccharide formation resulting in a misshaped exosporium.

Secondly the coat of *csxC* spores appears to be frayed. Again this could be due to the lack of parasporal layers and therefore the absence of any interactions that are made between the parasporal layers and the coat. However, it is also possible that CsxC could be involved in coat assembly or even be a constituent of the outer coat layers as is seen in *B. cereus* where the CotY protein is present within both the coat and the exosporium (Johnson et al. 2006). Pinpointing the exact location of CsxC within the spores would significantly aid our understanding of the role of CsxC within *C. sporogenes*. This could be done by raising antibodies against CsxC which can subsequently be used for immune-gold labelling of thin sections to identify the locality of CsxC within the spore ultrastructure.

4.4.2.5   The Role of CsxB

The occurrence of Type I crystal in *csxB* spores suggests that CsxB is not a fundamental component of the exosporium basal layer and is not essential for exosporium formation. The main feature of *csxB* spores is the presence of 'blebs' in the spore coat suggesting a potential role for CsxB in the assembly of the spore coat. The 'blebs' could be in indication of incomplete maturation of the spore

coat which in turn could lead to a lack of, or inefficient interactions, occurring between the spore

coat and other components of the spore. This in turn could lead to the mislocalisation of the spore

body which is found to be more central within the exosporium. In addition, the parasporal layers

seen within the interspace of *csxB* spores were more concave than those seen in WT which could

implicate CsxB in a role in parasporal layer formation or their interaction with the spore coat.

Over-expression of CsxB was successful, therefore some obvious next steps would be the

purification of CsxB followed by crystallisation trials in an attempt to obtain a protein structure.

Alternatively if larger oligomers of CsxB are formed it may be possible to determine the structure by

single particle cryoEM. Further to this, understanding the localisation of CsxB within the spores will

be hugely beneficial in determining its role. Tagging the protein with a fluorescent marker might be

possible, however, a better approach may be to raise an antibody against CsxB which can then be

used in combination with immuno-gold beads for localisation studies within thin sections.

4.4.3   BclA and the Hairy Nap

BclA has been extensively researched in Bacillus species and is found to compose the hairy nap on

the surface of spores belonging to the *B. cereus* group along with BclB (Kailas et al. 2011; Sylvestre et

al. 2002, 2005; Tan and Turnbough 2010; Terry et al. 2017). In *B. anthracis* and *B. cereus* BclA binds

to the surface of the exosporium through accessory proteins EsxFA or EsxFB which form the

threefold linkers between the hexagonal units of the exosporium basal layer (Kailas et al. 2011; Terry

et al. 2017). In *C. sporogenes* CsxA is the major structural protein of the exosporium basal layer,

including the threefold linker region (Janganan et al. 2020) and Section 4.4.2.2). BclA and CsxA have

been previously seen to form complexes (Janganan et al. 2016) and therefore it appears likely that

BclA adheres to the exosporium surface via direct interactions with CsxA, perhaps at the threefold

linker region, analogous to how BclA binds the surface in *B. anthracis*. In *B. anthracis* BclA trimers are

anchored to the exosporium through covalent interaction with ExsFA (BxpB) (Tan and Turnbough 2010).

In *C. sporogenes* the hairy nap on the surface of the spores proved challenging to consistently observe by negative stain TEM and relied heavily on good quality staining. Additionally in thin sectioning the hairy nap was not visible on the surface of the exosporium. In future imaging by TEM it may be possible to use Ruthenium red staining which allows for better visualisation of these surface features (Waller et al. 2004). A better understanding of the surface decoration present on the spores was obtained from AFM. This clearly showed the dense fringe visible on WT (Chapter 3.3.1.1), *csxB*, *csxC* and *bclB* spores. *bclA* spores were completely devoid of this fringe on the surface of the exosporium suggesting that BclA is a core component of the hairy nap on *C. sporogenes*. Further analysis of the data suggested that BclA composes the intermediate fibrils identified by Janganan et al (Janganan et al. 2016). The BclA fibres in *B. anthracis* were found to be 0.6 nm in length and contain 76 XXG repeats within the collagen-like domain (Boydston et al. 2005). The *C. sporogenes* BclA protein contains 186 XXG repeats, which, based on the length of BclA in *B. anthracis,* would correspond to a length of around 150 nm. The intermediate fibrils were measured to be 160 nm ± 15 nm on *C. sporogenes* spores which suggests that they are composed of BclA.

Intermediate fibrils are not the only decoration present on the surface of the exosporium composing the hairy nap. An additional halo of material was observed by AFM on the surface *bclA* spores (Fig: 4.14B). While it is possible that this feature corresponds to a tip artefact where the edge of the tip creates a shadow, the uniformity of the halo around multiple edges of the spores suggests that this is not the case. Furthermore, thickness measurements from regions of seemingly flat exosporium on *bclA* spores are found to be around 20 nm which is far thicker than estimates for a double layer of bare exosporium, suggested to be around 14 nm (Janganan et al. 2020). This additional material could correspond to the second collagen-like protein found in *C. sporogenes*, BclB.

In *B. anthracis* BclB was found to be localised to the surface of the exosporium but was notably absent from the cap region (Thompson et al. 2012). It is not possible to determine from the AFM data of *bclA* spores whether there is a region of the exosporium that is devoid of additional material which could correspond with a similar localisation of BclA and BclB between the species. Imaging of areas close to the edge of the exosporium at higher resolution could provide an insight into the structural nature of the additional material surrounding the surface of the spores and whether there are any differences in its composition across the length of the exosporium. Negative stain TEM, thin sectioning and AFM of *bclB* spores showed no obvious differences compared to WT. However, any subtle differences to the spore decoration would be challenging to characterise due to the presence of the dense mass of intermediate fibrils of BclA. To probe this hypothesis further, fluorescence microscopy could be used to locate BclB on the surface of spores.

In order to really harness the power of AFM it would be beneficial to obtain fragments of the exosporium, particularly for *bclA* and *bclB* mutants, in order to acquire accurate measurements of exosporium thickness. This would give a clear indication of the level of decoration left on the surface of the mutant spores without having to account for multiple layers of exosporium as well as potential parasporal layers within the spore. This will enable higher resolution imaging of the surface and potentially help to identify the more subtle changes in decoration that may be associated with these mutants.

4.4.4   The Role of the Hairy Nap

The exosporium of *bclA* spores when imaged by AFM was frequently seen to adhere to itself and roll up on the slide surface. The altered behaviour of the exosporium in the absence of the hairy nap suggests that BclA could play a role in spore surface adherence. This has previously been suggested for *B. anthracis* spores where the hydrophobicity of *bclA* mutant spores was seen to be increased indicating a difference in surface properties and adherence capability of the strain (Brahmbhatt et al.

2007). To explore this further for *C. sporogenes* hydrophobicity assays should be conducted to ascertain if there are differences in the surface properties of the *bclA* mutant spores. The ability of spores to adhere to surfaces is vitally important for their role in colonisation and therefore BclA and the hairy nap could play an important role.

5 Germination of Exosporium Mutants

5.1 Introduction

Sporulation is an important process for Clostridia and Bacillus species as it allows them to survive through harsh conditions and crucially, being anaerobes, the presence of oxygen. Spores are highly resistant to both chemical and physical threat and notably heat resistant. Heat resistance properties are thought to mostly be provided by the dehydrated state of the spore core (Setlow et al. 2006) which is maintained in part by the cortex and protected by the multi-layered spore coat (Mckenney, Driks, and Eichenberger 2012; Warth 1978). In addition, it has been suggested that in *C. botulinum* the thickness of the exosporium may contribute to the heat resistance properties of the spores (Portinha et al. 2022). As a model for Group I *C. botulinum*, probing the heat resistant properties of *C. sporogenes* spores and associated exosporium mutants may provide insights into the resistance properties conferred by the exosporium. The exosporium crystal structure has already been shown to be stable up to temperatures of 95°C without showing signs of degradation (Janganan et al. 2020).

As the outermost layer of the spores, the exosporium is thought to play an important role in modulating germination (reviewed in (Henriques & Moran, Jr., 2007)). In *B. anthracis* the exosporium incorporates an alanine racemase responsible for converting L-alanine to D-alanine, a competitive inhibitor of germinant receptors located within the inner membrane of the spore and thereby preventing premature germination (Chesnokova et al. 2009). More generally the exosporium is thought to act as a semipermeable barrier slowing down the passage of small molecules through the outer layers of the spore and preventing larger complexes from getting through (Janganan et al. 2020; Terry et al. 2017). This could act to slow down the passage of germinant molecules to the inner membrane thereby preventing premature germination. The true impact the exosporium has on the germination process has yet to be established. The effect the lack of key exosporium proteins has on the germination process may also provide insights into the important processes that occur in WT germination.

5.2   Aims

The work outlined in this chapter aimed to gain an insight into the influence of the exosporium on sporulation, germination and spore heat resistance. The mutants produced and discussed in Chapter 4 were therefore used in a series of experiments to probe the roles of these proteins, and the exosporium as a whole, in both heat resistance and the germination process. Further to this ultrastructural changes during the germination process of the mutant strains were explored through the imaging of thin sections.

5.3   Results

5.3.1   No Difference in Sporulation Efficiency of Mutants

The ability of mutants to sporulate whilst lacking key exosporium proteins was assessed by conducting sporulation assays. The assay involved taking two samples from a sporulating culture every day for 5 days. One of these aliquots was heat treated at 65°C to kill all vegetative cells and the other was left untreated before enumeration of CFUs on TY agar. Colonies were counted the following day to provide total counts (untreated) and spore counts (heat treated).

Over the course of the 5 day experiment there was no apparent difference in the sporulation efficiency of any of the mutant strains when compared to WT (Fig: 5.1). All strains showed a rapid population transition from cells to spores within 3 days.
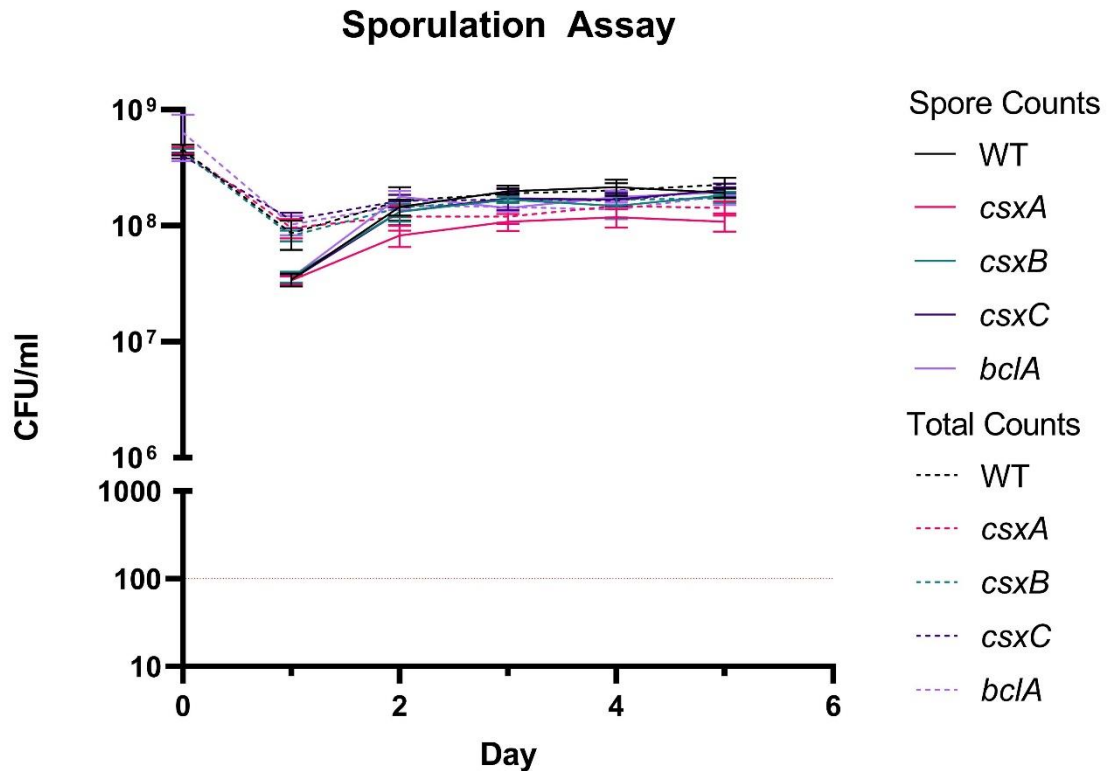
Sporulation Assay

Figure 5.1: Sporulation Assay of WT *C. sporogenes* and Exosporium Mutants

csxA (pink), *csxB* (teal), *csxC* (dark purple), and *bclA* (light purple) mutants were compared to WT. Total cell numbers were determined by counting CFUs on TY agar. Spore number were determined by the same method following incubation at 65°C for 30 min. Experiments were conducted in triplicate on biological duplicates. The means ± standard deviations (error bars) are shown.

5.3.2   Exosporium and Spore Heat Resistance

The spores of *C. sporogenes* tolerate high temperatures (Schill et al. 2016) and the exosporium itself is stable up to 95°C (Janganan et al. 2020). In *C. botulinum* the presence or thickness of the exosporium has been suggested to play a role in spore heat resistance (Portinha et al. 2022). *C. sporogenes* WT and exosporium mutant strains were tested for spore viability after heat treatment for 30 minutes across a range of temperatures (Fig: 5.2C).
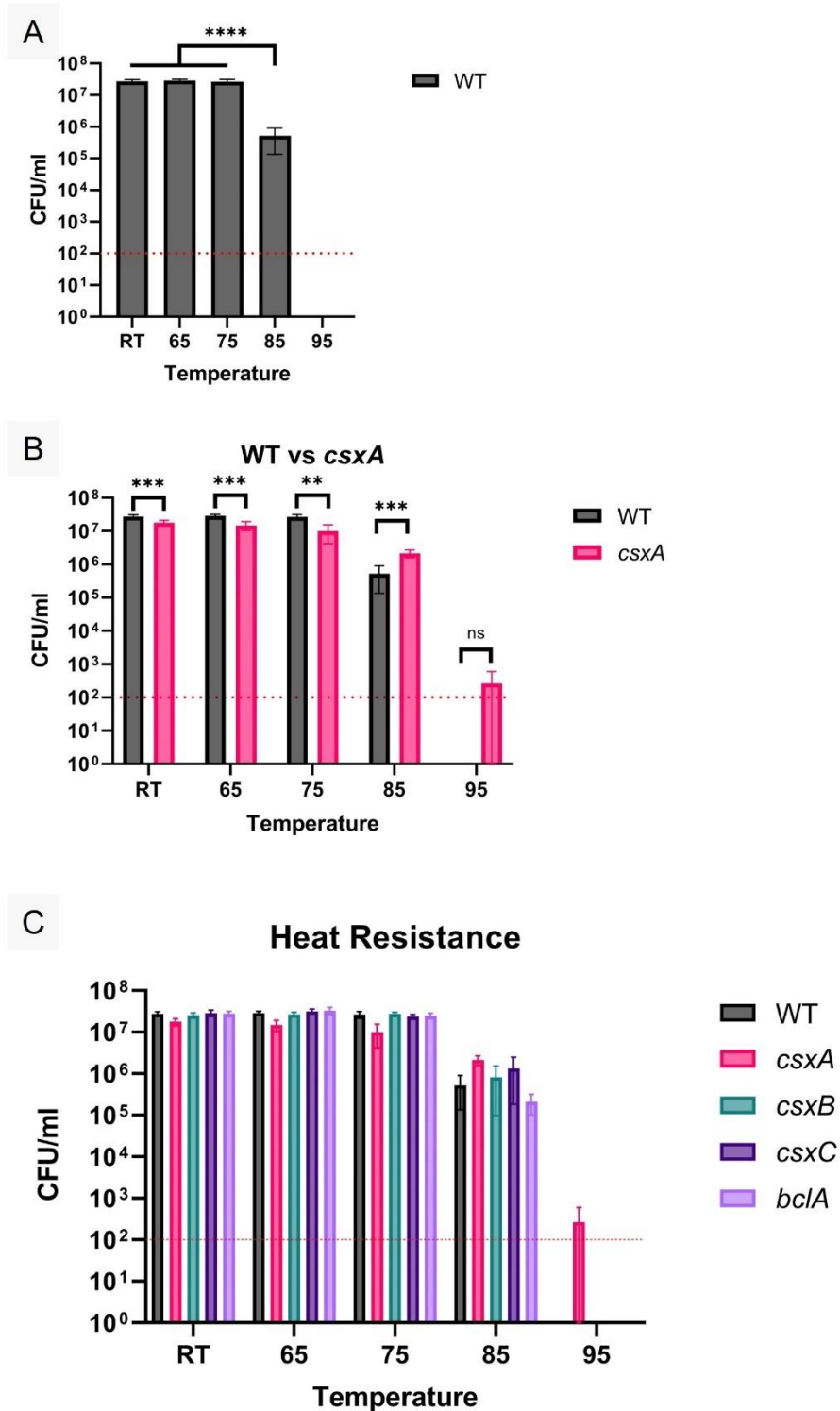
Figure 5.2: Heat Resistance of WT and Exosporium Mutants

A) *C. sporogenes* WT spores viability after heat treatment showing a 50-fold decrease in spore viability after heat treatment at 85°C. B) *csxA* spore viability after heat treatment compared to WT. C) *csxA*, *csxB*, *csxC*, *bclA* and WT spore viability after heat treatment. CFUs were enumerated following incubation at each temperature for 30 min. Experiments were conducted in triplicate on biological duplicates. The means ± standard deviations (error bars) are shown. Dotted red line depicts detection limit of the experiment. **** $P \leq 0.0001$, *** $P \leq 0.001$, ** $P \leq 0.01$ * $P \leq 0.05$, ns $P > 0.05$

For the WT strain (Fig: 5.2A) no drop in viability was seen after treatment at 65°C or 75°C. Heat treatment at 85°C saw an ~50-fold drop in viability. Spore viability dropped below the detection level of the experiment after heating to 95°C.

Generally, all the mutant strains tested appeared to behave in a similar fashion to WT and showed no difference in spore viability after treatment at 65°C and 75°C and a similar drop in viability after treatment at 85°C. *csxA* spores appeared to have a marginally lower viability than WT across the three lowest temperatures tested; RT, 65°C and 75°C (Fig: 5.2B).

The viability of spores was most varied across the strains after heat treatment at 85°C. There was no significant difference between the viability of *csxB*, *csxC* and *bclA* spores compared to WT (Fig: 5.2C). On the other hand, *csxA* spores showed a significantly higher viability after heat treatment at 85°C than for WT (Fig: 5.2B). Additionally, *csxA* was the only one to survive treatment at 95°C. However, the values were very close to the limit of detection for the experiment.

5.3.3   Exosporium Mutants Show Outgrowth Defects During Germination

Having already ascertained the conditions required for WT germination (Chapter 3), spore populations of each exosporium mutant strain were subjected to germination assays to determine whether these proteins play a role in facilitating the germination process. All assays were carried out in TY media in biological duplicate and technical triplicate.

csxA spores, which do not possess an exosporium, showed no clear initial drop in optical density usually associated with a decrease in the refractive index of the spore due to DPA release and core rehydration during the early stages of germination (Fig: 5.3A and F). After 125 min the OD_{600nm} began to increase suggesting the population had entered the outgrowth phase (Fig: 5.3A). This appeared to occur slightly earlier than for WT. By mid-exponential phase there was no discernible difference

between *csxA* and WT cultures and both reached stationary phase together with an identical final

OD.
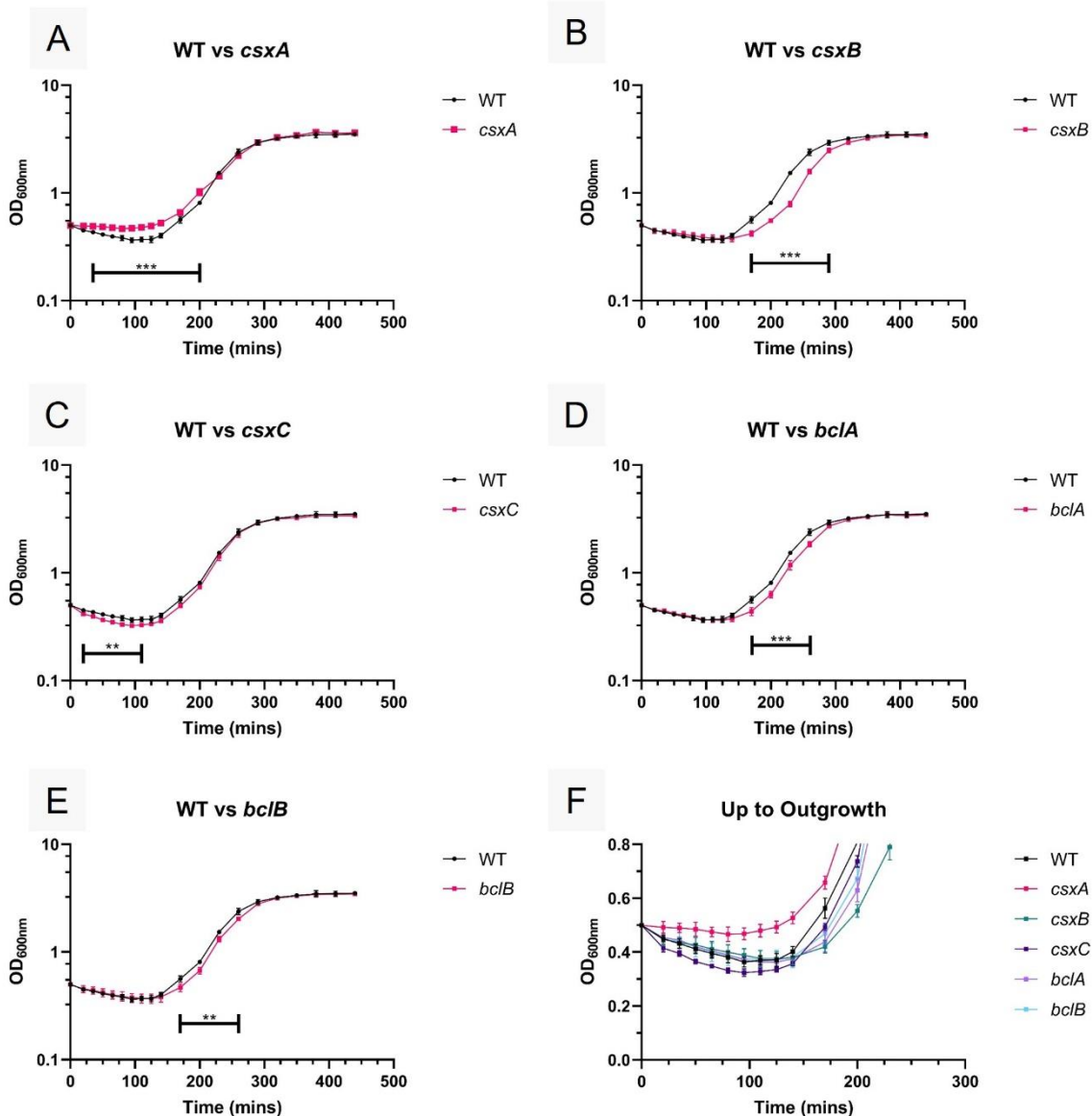
Figure 5.3: Germination Assays of Exosporium Mutants

A-E) Germination was monitored for each mutant strain by measuring the OD_{600nm} following germination initiation in TY media. Each strain is plotted for comparison to WT. A) *csxA* vs WT germination shows no initial drop in OD for csxA. B) *csxB* vs WT germination shows a lag in the outgrowth period for csxB spores. C) *csxC* vs WT shows a slight lower drop in OD for csxC D) *bclA* vs WT germination shows a small lag period in outgrowth E) *bclB* vs WT germination. F) Zoom in on the initial 200 min of germination showing the drop in OD_{6000nm} for all strains except *csxA* and the slightly lower drop for *csxC*. Experiments were conducted in triplicate on biological duplicates. The means ± standard deviations (error bars) are shown. Within the ranges highlighted all points have a significant P-value of at least the value shown when compared to WT. **** $P \leq 0.0001$, *** $P \leq 0.001$, ** $P \leq 0.01$ * $P \leq 0.05$, ns $P > 0.05$

Germination of *csxB* spores showed a clear initial drop in optical density as seen for WT. However, this was followed by a significant lag in the outgrowth phase from *csxB* spores and the population took ~30 min longer to reach exponential phase than WT (Fig: 5.3B). Following exponential phase, *csxB* reached stationary phase with a final OD identical to that of WT.

csxC spore germination was the most similar to that of WT (Fig: 5.3C). There was a slight, but statistically significant, difference in the initial OD drop, with *csxC* dropping to a slightly lower OD than WT (Fig: 5.3F). There was no significant difference between *csxC* and WT during outgrowth or stationary phase with both cultures reaching an identical final OD.

bclA and *bclB* germination had very similar profiles (Fig: 5.3D and E). They both showed an initial OD drop identical to WT during the early stages of germination. Both then showed a small lag going into the outgrowth phase when compared to WT. For *bclA* this lag phase appeared to be around 30 min while for *bclB* it was a little shorter, only around 15 min. Both cultures reached stationary phase with an OD identical to that of WT.

5.3.3.1 Mutant Strains Show No Evidence of Growth Defects

Growth of all strains was assayed in order to confirm that the differences seen between strains during the gemination assays corresponded to differences in the germination process rather than growth defects. Growth was carried out in TY media and was done in biological duplicate and technical triplicate (Fig: 5.4). All mutant strains showed identical growth to WT ruling out possible growth defects.

Growth Curve
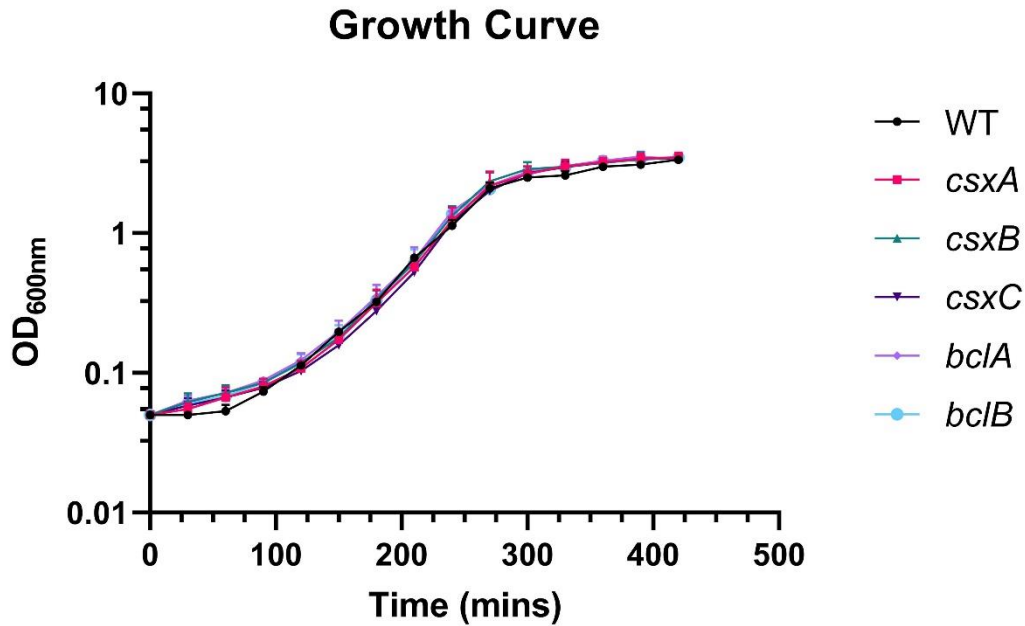
Figure 5.4: Growth Analysis of Exosporium Mutants

Growth of mutant and WT strains was monitored by measuring OD$_{600nm}$ until cultures reached stationary phase. Shows no difference in growth between strains. Experiments were conducted in triplicate on biological duplicates. The means ± standard deviations (error bars) are shown.

5.3.4 Ultrastructure of Mutants During Germination

In order to visualise what was occurring at the individual spore level during the germination process spores of *csxA*, *csxB* and *csxC* strains were chemically fixed 2 h post germination to allow for higher resolution imaging by TEM of thin sections (70-90 nm). Similar to what was seen in WT, the resulting micrographs for each mutant showed several clear morphological changes throughout the germination process. For ease of comparison these changes have been categorised into four distinct phases; early, mid, late and post germination.

5.3.4.1 *csxA*

Early Germination

csxA spores seen in the early phases of germination had two distinct forms (Fig: 5.5). Form 1 had unevenly stained spore bodies where no clear distinction could be made between the spore cortex

and the core (Fig: 5.5A). The second form had a clearly defined spore core and cortex layer (Fig: 5.5B and C) and could correspond to rehydrated spores. Both forms clearly showed a spore body that is surrounded discontinuously by parasporal layers. These can be seen to form laminations in some areas and appear to have both concave and flat arrangements (Fig: 5.5C). A small region of interspace was present between the parasporal layers and the darkly stained spore coat. The spore coat itself appeared intact. The cortex had an average thickness of 90 nm ± 20 nm at this stage and the core could be seen in form 2 spores as a darkly stained central region.

Mid Germination

Micrographs of *csxA* spores in the mid phase of germination showed a darkly stained developing cell within a paler region of expanded cortex (Fig: 5.6), with an average thickness in transverse spores of 180 nm ± 50 nm. The cortex region often contained darker stained rings or striations (Fig: 5.6A pink arrows). The spore coat was darkly stained and showed no signs of degradation. The interspace region between the coat and the parasporal layers was no longer distinguishable. In most cases the parasporal layers were still present around the outside of the spore body and in several places laminations could be seen. In some cases the spore body appeared to have shed the majority of the parasporal layers with only a few small fragments left associated with the spore coat (Fig: 5.6A).

Late Germination

Cells can be seen emerging from one pole of the spore body during the late gemination phase (Fig: 5.7). The coat was darkly stained and, other than the pole from which cell emergence is occurring, no obvious signs of degradation were seen. The coat can be seen adhering to the cell surface as the cell emerges (Fig: 5.7C). The cortex region remains within the spore coat and in some cases the striations seen in mid germination remain (Fig: 5.7C pink arrow). Parasporal layers were still present on the majority of spores, however, some spores appeared to have shed a significant proportion of them.

Figure 5.5: Thin Sections of *csxA* Spores in Early Germination

A-C) High magnification micrographs of *csxA* spores in early germination with all distinguishable layers labelled. No exosporium can be seen surrounding the spores and an interspace region is present between the coat and the parasporal layers B) Example of early germination spore with clear staining of internal spore layers possibly reflecting rehydration.
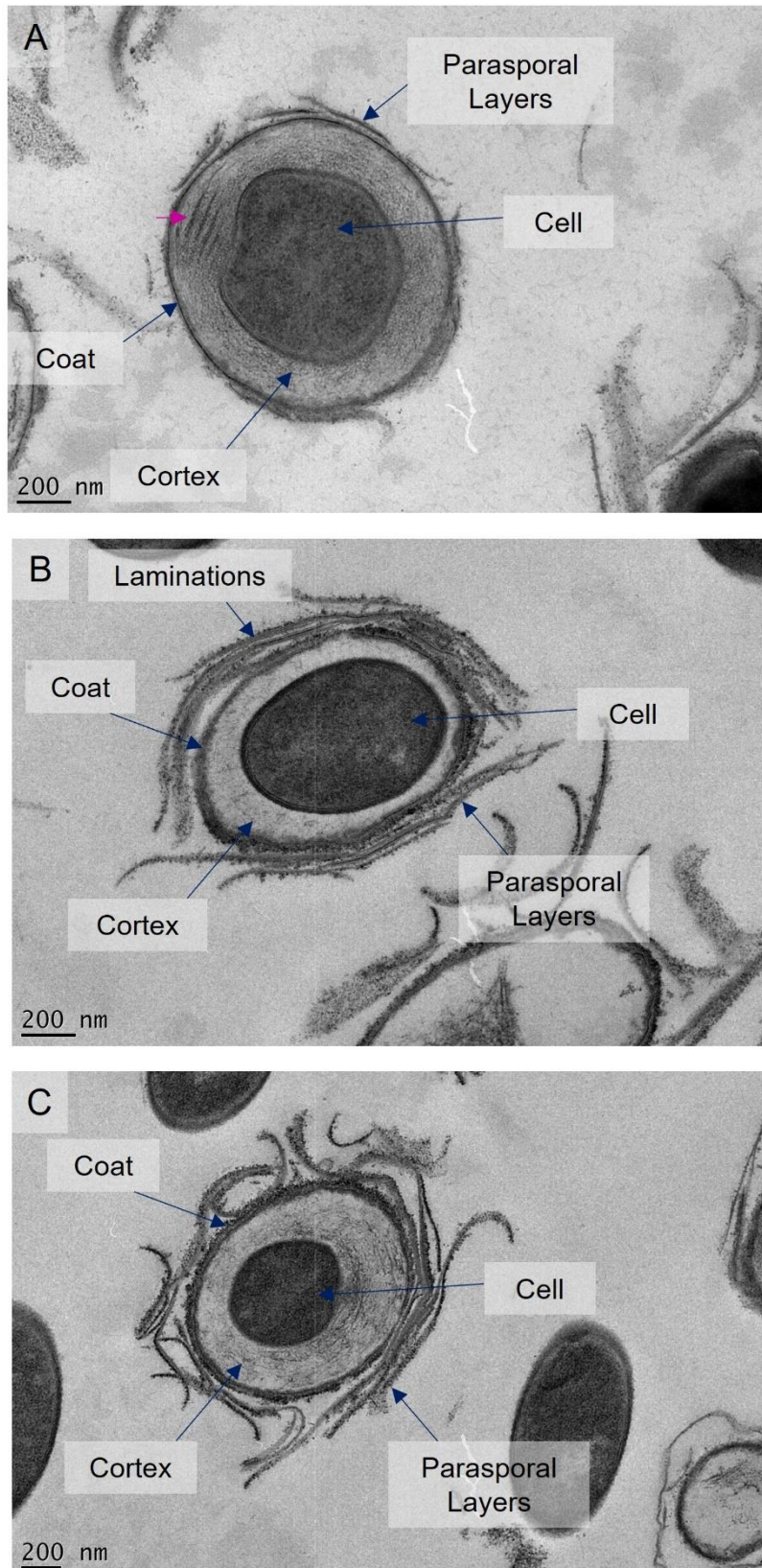
Figure 5.6: Thin Sections of *csxA* spores in Mid Germination

A-C) *csxA* spores in mid stages of germination showing an enlarged cortex region. Pink arrow (A) indicates striations within the cortex region. In A the parasporal layers appear to be mostly dissociated from the spore.
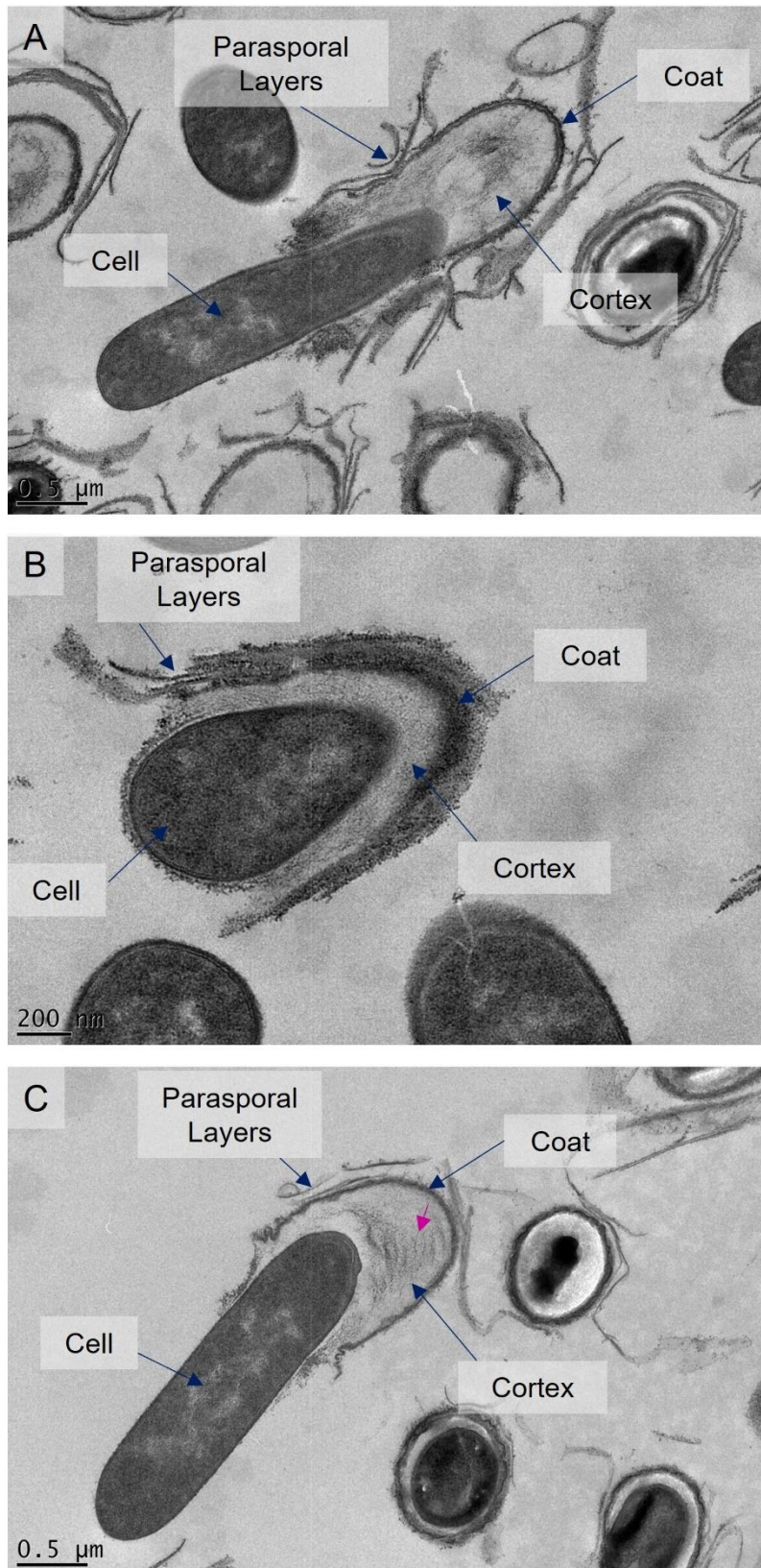
Figure 5.7: Thin Sections of *csxA* Spores in Late Germination

A-C) *csxA* spores in late germination show vegetative cells emerging from the spore with all distinguishable layers labelled. Pink arrow (C) indicates striations within the cortex.
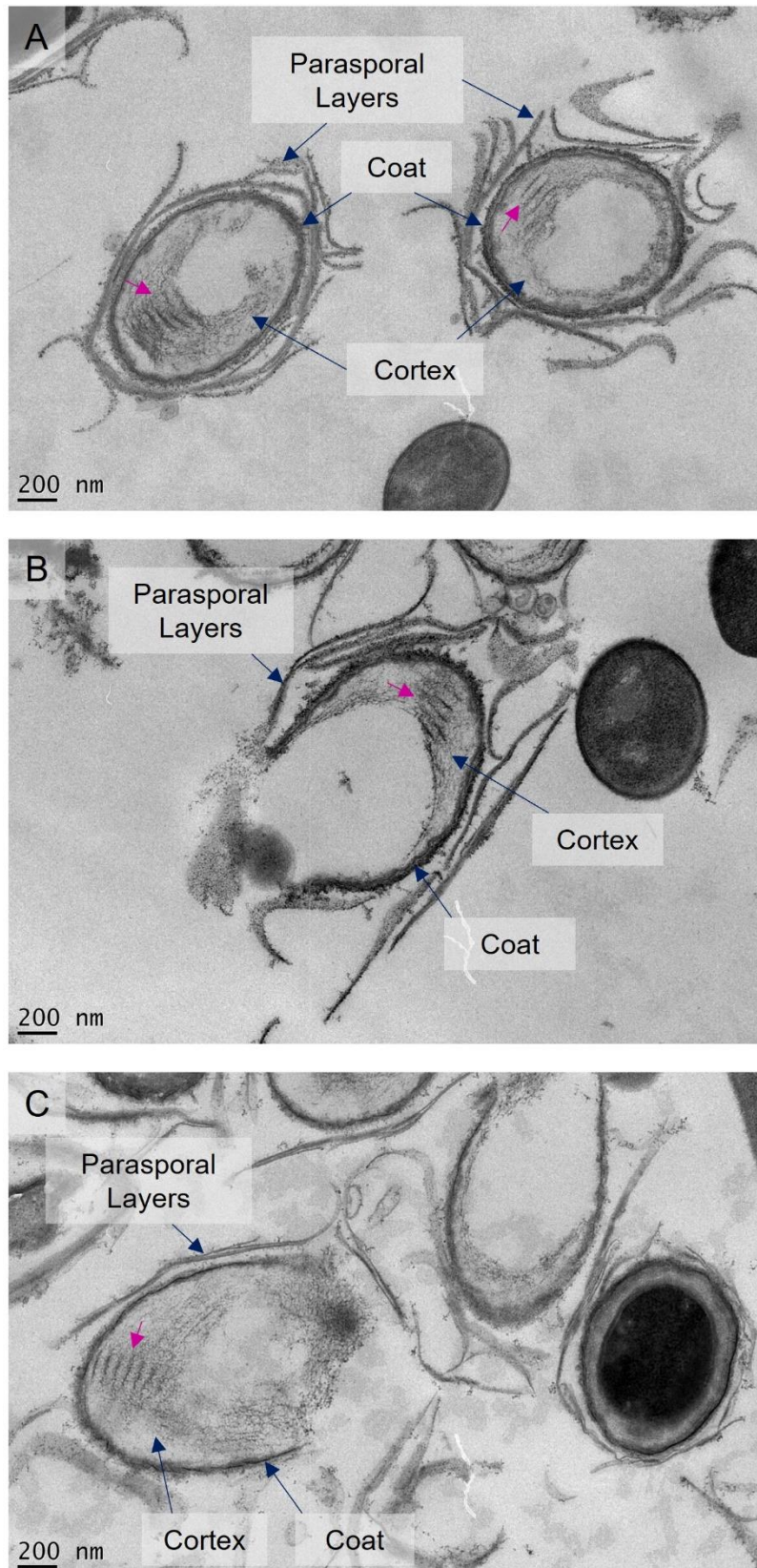
Figure 5.8: Thin Sections of *csxA* Spores Shells Post Germination

A-C) *csxA* spore shells composed of spore coat containing remnants of the cortex and parasporal layers associated with the surface. Pink arrows indicate the remains of striations seen within the cortex in earlier stages of germination.

Post Germination

Spore shells left behind after the germination process remained remarkably intact displaying a clear void left by the departed vegetative cell (Fig: 5.8). The darkly stained spore coat appeared predominantly unchanged apart from a small opening from where the cell had emerged. Within the coat remnants of the spore cortex were observed and clear darkly stained striations could be seen within the region opposite to cell emergence in longitudinal thin sections (Fig: 5.8 pink arrows). Parasporal layers were present associated with the spore coat. It is noted that layers seen in longitudinal sections associated with the longer edge of the spore often appeared straight when compared with those towards the poles that had a more concave appearance (Fig: 5.8B).

5.3.4.2   *csxB*

Early Germination

Micrographs depicting the early stages of germination for *csxB* spores, as for *csxA* spores, had two distinct forms (Fig: 5.9). There were examples of spores where the spore body was unevenly stained (Form 1) (Fig: 5.9A) and further examples were the spore body was clearly stained allowing for details of the spore core and cortex layers to be seen (Form 2) (Fig: 5.9B and C). Both forms displayed features clearly seen in dormant *csxB* spores (Section 4.3.4.2) including the presence of blebs in the spore coat on some spores (80%). The spore body is separated from the exosporium by a clear interspace, within which parasporal layers were present, often stacking to form clear laminations.

The exosporium of several spores appeared to be open at one pole with the ends of the para-crystalline layer folded back on itself (Fig: 5.9 A pink arrow). In addition, spores of form 2, that had the clear staining within the spore body, showed a thin pale region between the cortex and the coat that was not present in WT samples (Fig: 5.9B and C light blue arrows).

Mid Germination

csxB spores in the mid stages of the germination process showed a darkly stained cell developing within the spore body (Fig: 5.10). The cortex region appeared to be expanded with an average thickness of 140 nm ± 70 nm. Dark striations within the cortex layer were present (Fig: 5.10B pink arrow), however, unlike in WT these were not always localised to the pole opposite to the open exosporium. The darkly stained spore coat was pushed up against the exosporium layer with parasporal layers pressed between the two layers. The interspace at the open exosporium pole was devoid of parasporal layers and the coat and exosporium appeared to be deformed (Fig: 5.10B light blue arrow).

Late Germination

During late germination cells could be seen emerging from one pole of the outer layers of the spore (Fig: 5.11). The exosporium was closely associated with the emerging cell and had a rippled appearance (Fig: 5.11 pink arrows). Parasporal layers were present between the coat and the exosporium. Within the coat, lightly stained remnants of the cortex layer could be seen along with darker stained striations (Fig: 5.11B light blue arrows).

Post Germination

Several examples of shells left behind post germination were seen (Fig: 5.12). These consisted of darkly stained exosporium that was open at one end but otherwise intact. The exosporium surrounded parasporal layers and an open-ended coat. The centres of the shells contained remnants of the cortex region of the spore and in some cases the striations seen during germination were still present (Fig: 5.12 pink arrows). These striations were not constrained to the pole opposite the emergence site.
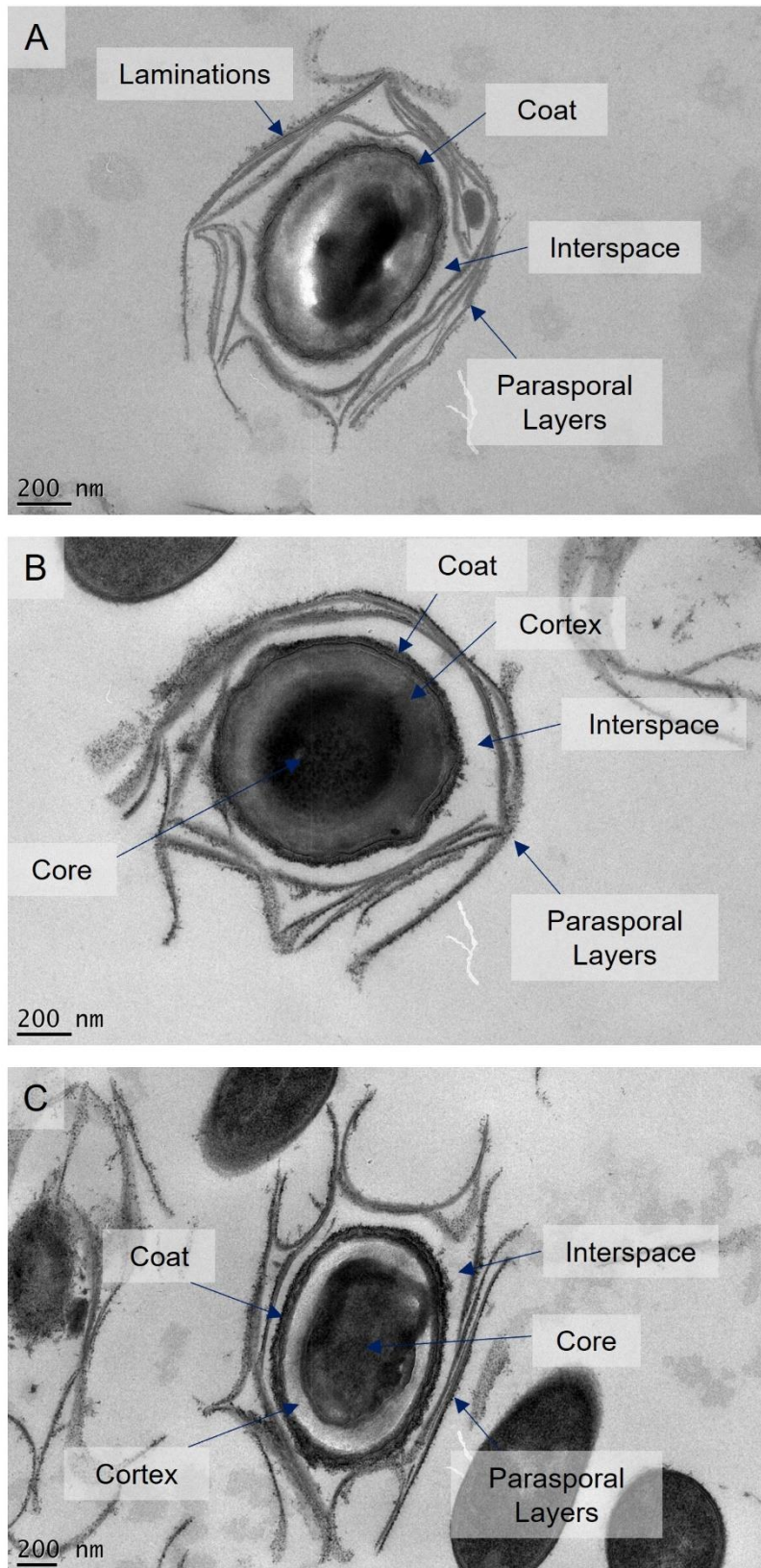
Figure 5.9: Thin Sections of *csxB* Spores in Early Germination

A-C) High magnification micrographs of *csxB* spores in early germination with all distinguishable layers labelled. Pink arrow indicates open pole of the exosporium. B+C) Examples of spores in early germination which clear staining of internal spore layers. Light blue arrow indicates separation between cortex and the coat.

Figure 5.10: Thin Sections of *csxB* Spores in Mid Germination

A+B) *csxB* spores in the mid stages of germination showing an enlarged spore body and cortex region. Pink arrow (B) indicates mislocalised striations within the cortex region. Light blue arrow indicates open pole of the exosporium.

Figure 5.11: Thin Sections of *csxB* Spores in Late Germination

A+B) *csxB* spores in late germination show vegetative cells emerging from the spore with all distinguishable layers labelled. Pink arrows indicate ripples in the exosporium associated with the emerging cell. Light blue arrow (B) indicates striations present within the cortex region.
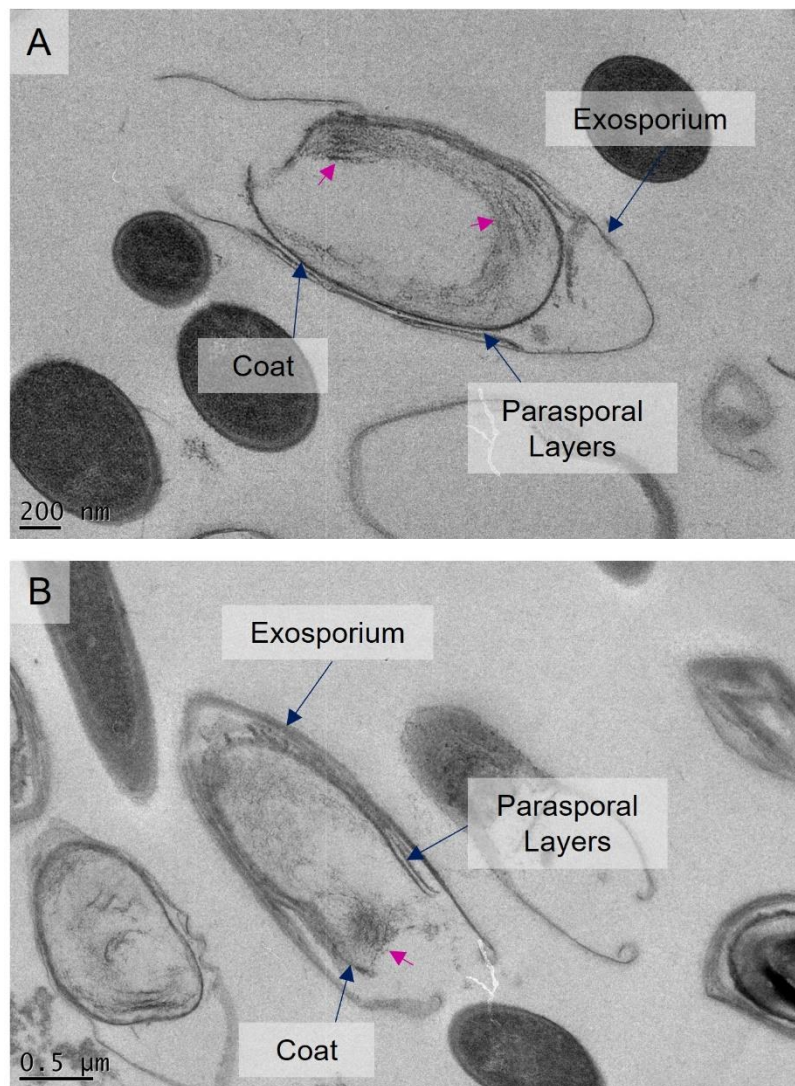
Figure 5.12: Thin Sections of *csxB* Spore Shells Post Germination

A+B) *csxB* spore shells composed of exosporium, parasporal layers, spore coat and remnants of the cortex. Pink arrows indicate remains of striations within the cortex region.

5.3.4.3   *csxC*

Early Germination

Similar to that seen for the *csxB* and *csxA* mutants, the *csxC* spores in the early stages of germination had two distinct forms (Fig: 5.13). Form 1 that had poor spore body staining (Fig: 5.13A) and form 2 which had a clear darkly stained core and a lightly stained cortex region (Fig: 5.13B and C). In both cases the spore coat was visible as a darkly stained layer, often frayed at the edges as seen in

dormant spores. The exosporium surrounded the spore body, was elongated at one pole and then was closely associated laterally with the coat around the spore body forming ripples in the exosporium layer (Fig: 5.13B and C light blue arrows). As in the dormant *csxC* spores no parasporal layers were present.

Mid Germination

Micrographs showing spores during mid germination showed a darkly stained cell developing within the spore body surrounded by an expanded cortex region with an average thickness of 160 nm ± 40 nm (Fig: 5.14). The cortex region showed darkly stained rings running throughout the layer seemingly surrounding the spore core (Fig: 5.14C purple arrow). Regular striations were present within the cortex, as seen in WT germination, that were localised to the opposite pole to cell emergence (Fig: 5.14 light blue arrows). The coat of the spores was pushed up against the exosporium and appeared to be degraded at one pole. This degradation coincided with the pole of the exosporium that was open and in some cases the edges of the exosporium appeared to be folded back on themselves forming curls (Fig: 5.14A pink arrows). The exosporium in close contact with the spore coat no longer appeared rippled as it did in dormant spores or in early germination.

Late Germination

Spores in the late germination phase showed cells emerging from the pole of the spores (Fig: 5.15). The exosporium was associated closely with the emerging cell and formed ripples along the sides of the cell (Fig: 5.15 pink arrows). In several cases, a darkly stained flat layer was seen along the edge of the emerging cell (Fig: 5.15B purple arrow). Within the remnants of the cortex region clear striations were seen located at the non-emerging pole (Fig: 5.15B light blue arrow).

Post Germination

Micrographs of spore shells post germination showed a clear open ended exosporium containing the remnants of the spore coat and the cortex region (Fig: 5.16). The coat was also open at one pole but

appeared to be much more disordered than in other strains, post germination. The open end of the exosporium also appeared to be curled like it was rolled back on itself.
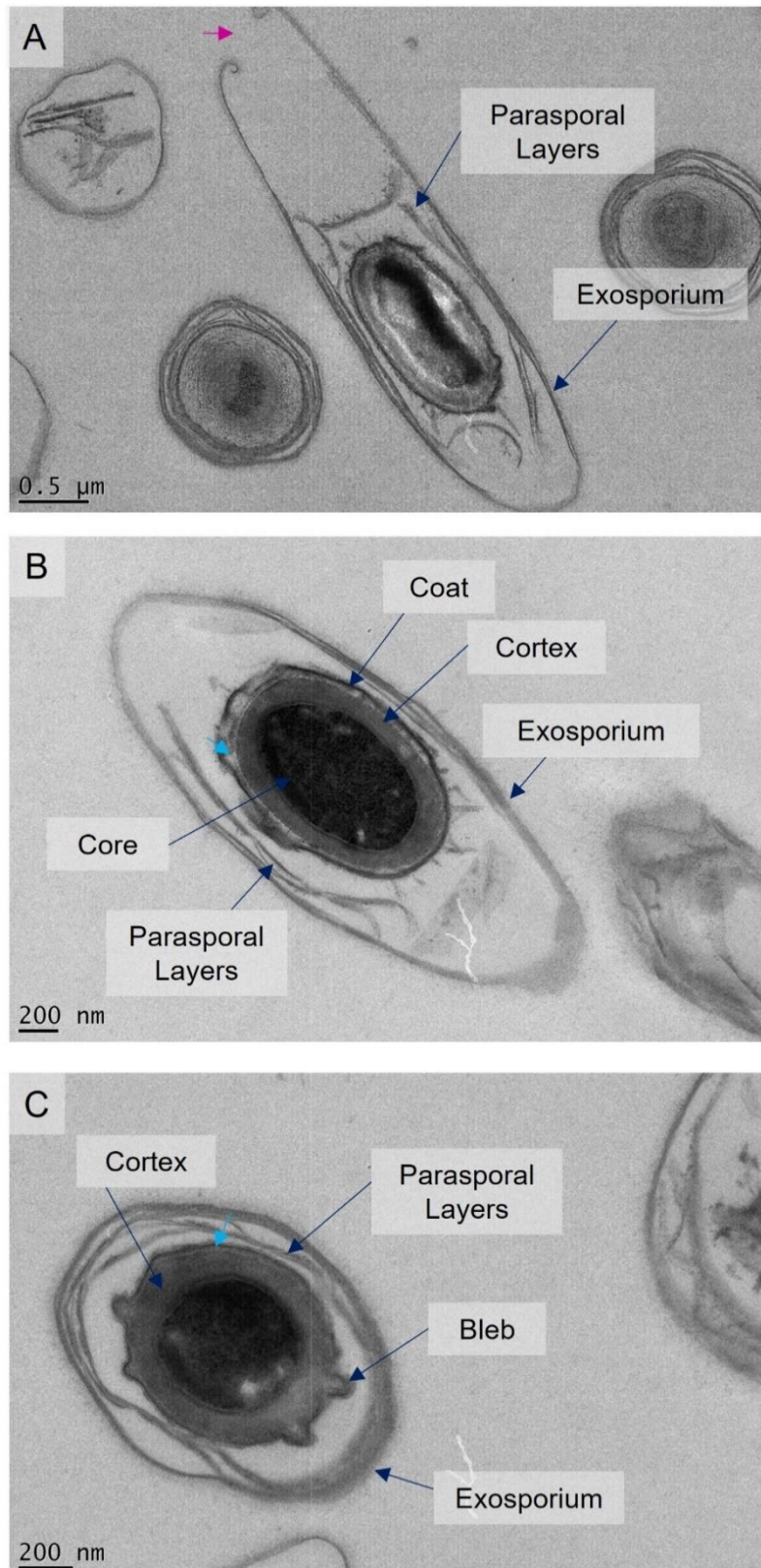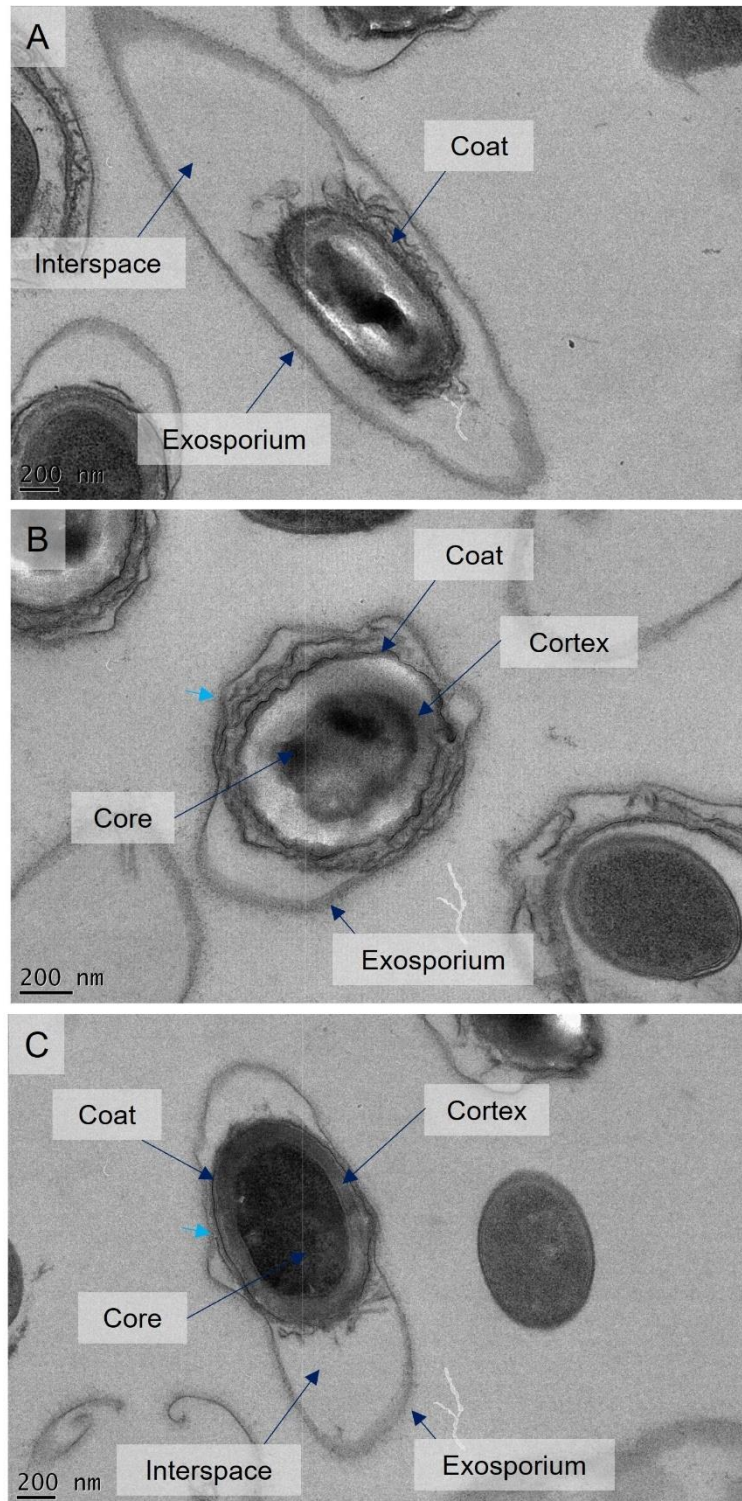

Figure 5.13: Thin Sections of *csxC* Spores in Early Germination

A-C) High magnification micrographs of *csxC* spores in the early stages of germination with all distinguishable layers labelled. Longitudinal sections show the extended exosporium. B+C) Examples of spores in early germination which clear staining of internal spore layers. Light blue arrows indicate ripples in the exosporium where it is associated with the spore coat.
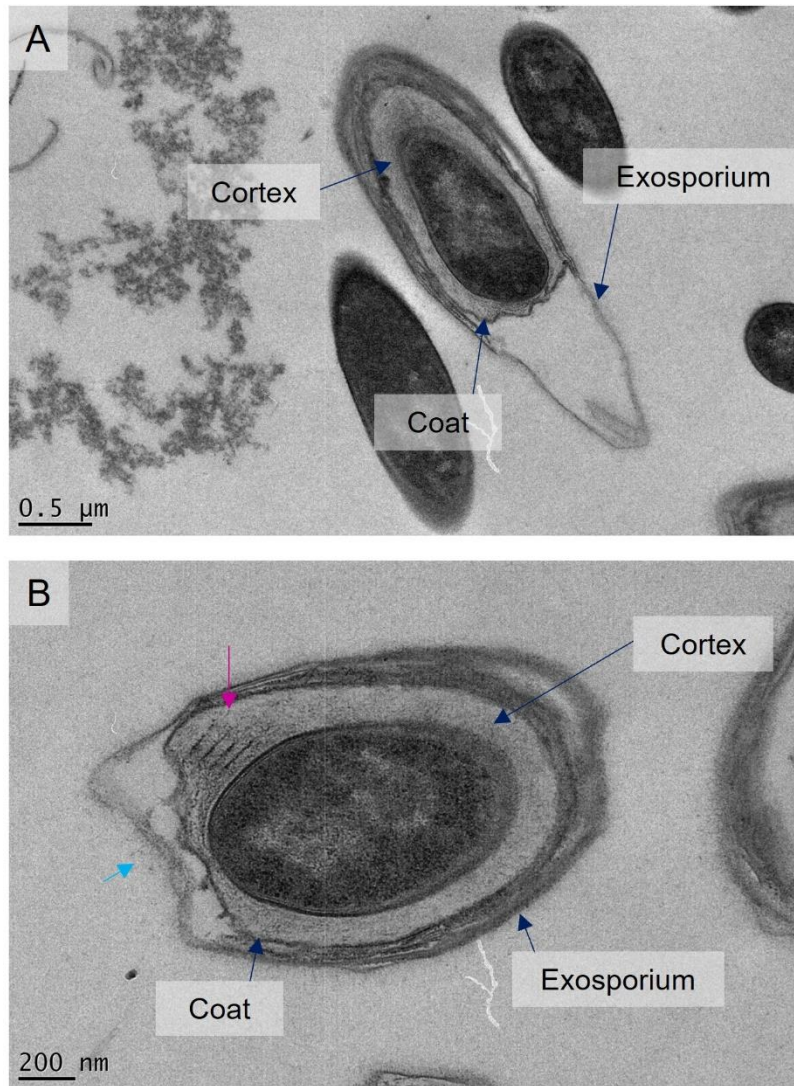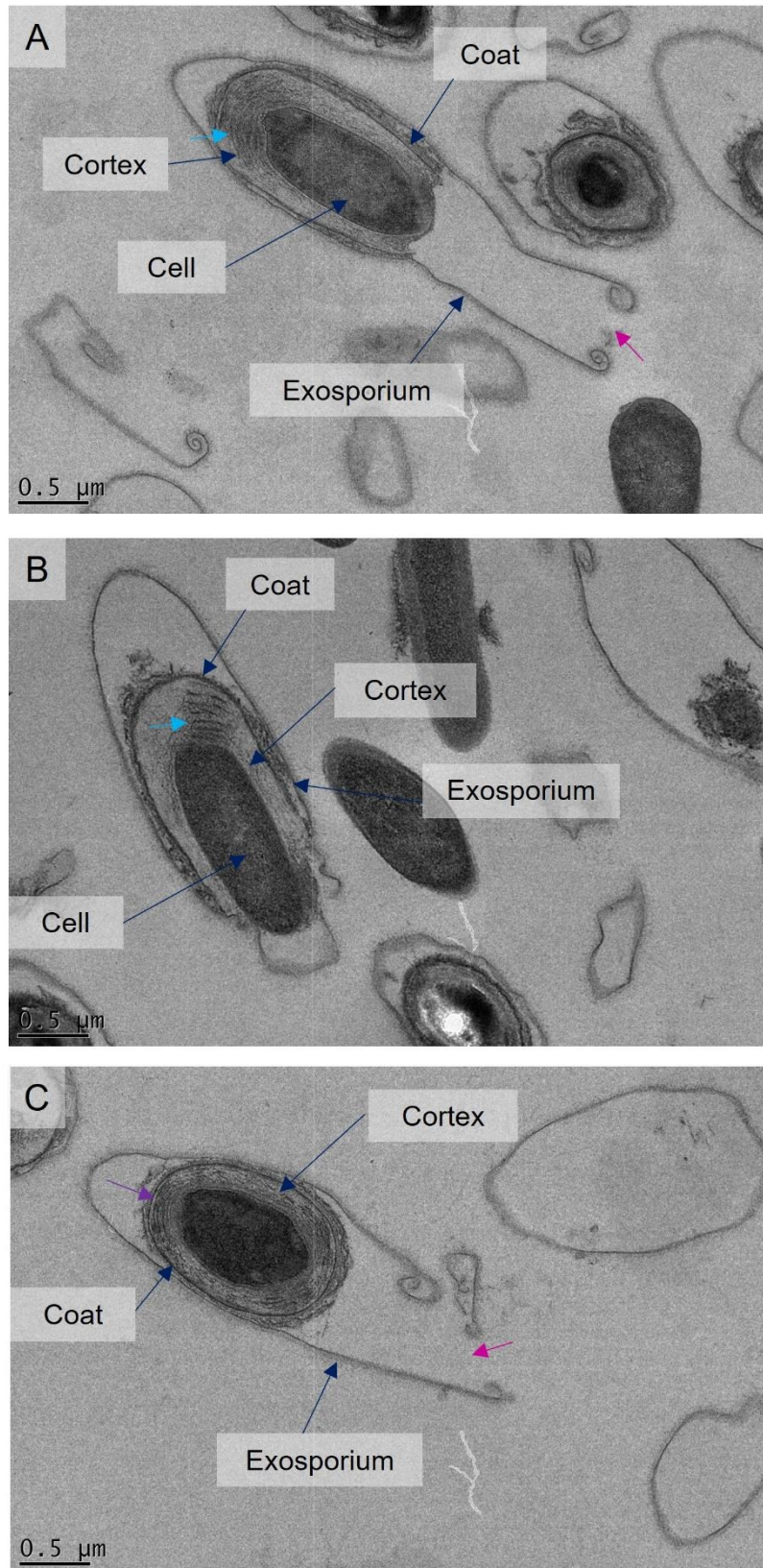
Figure 5.14: Thin Sections of *csxC* Spores in Mid Germination

A-C) *csxC* spores in the mid stages of germination showing an enlarged spore body and cortex region. Pink arrows indicate open pole to the exosporium. Light blue arrows indicate striations within the spore cortex. Purple arrow (C) indicates darkly stained rings in the cortex.
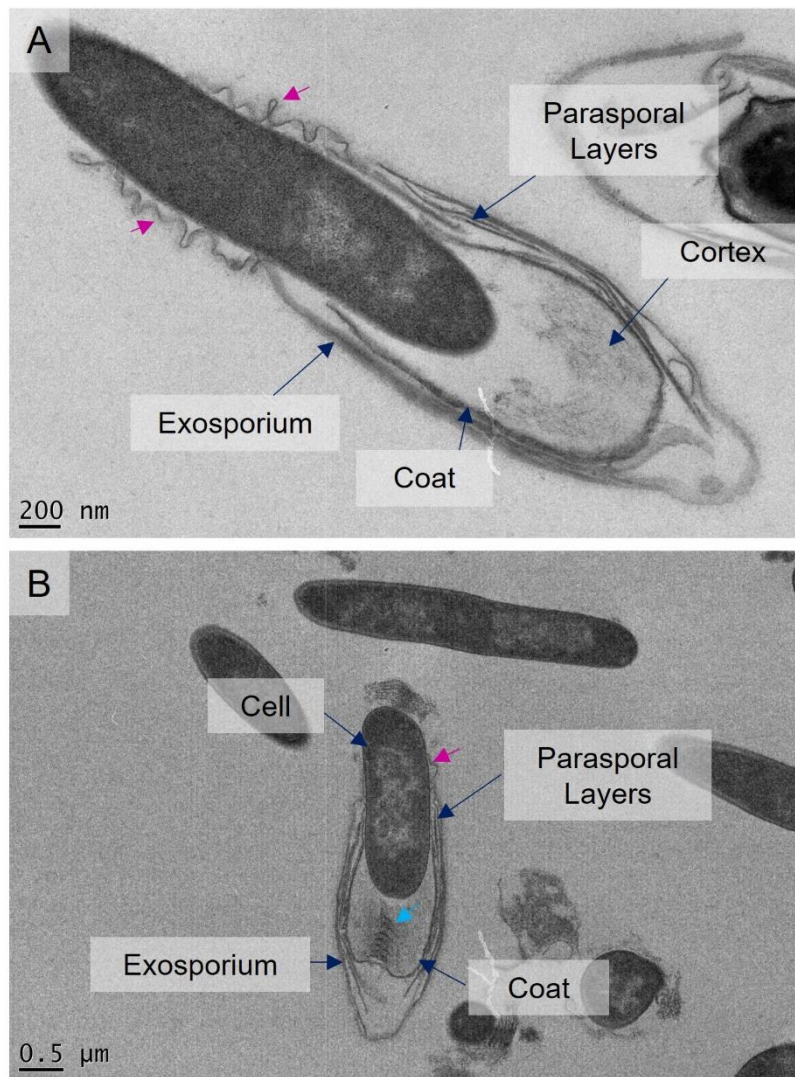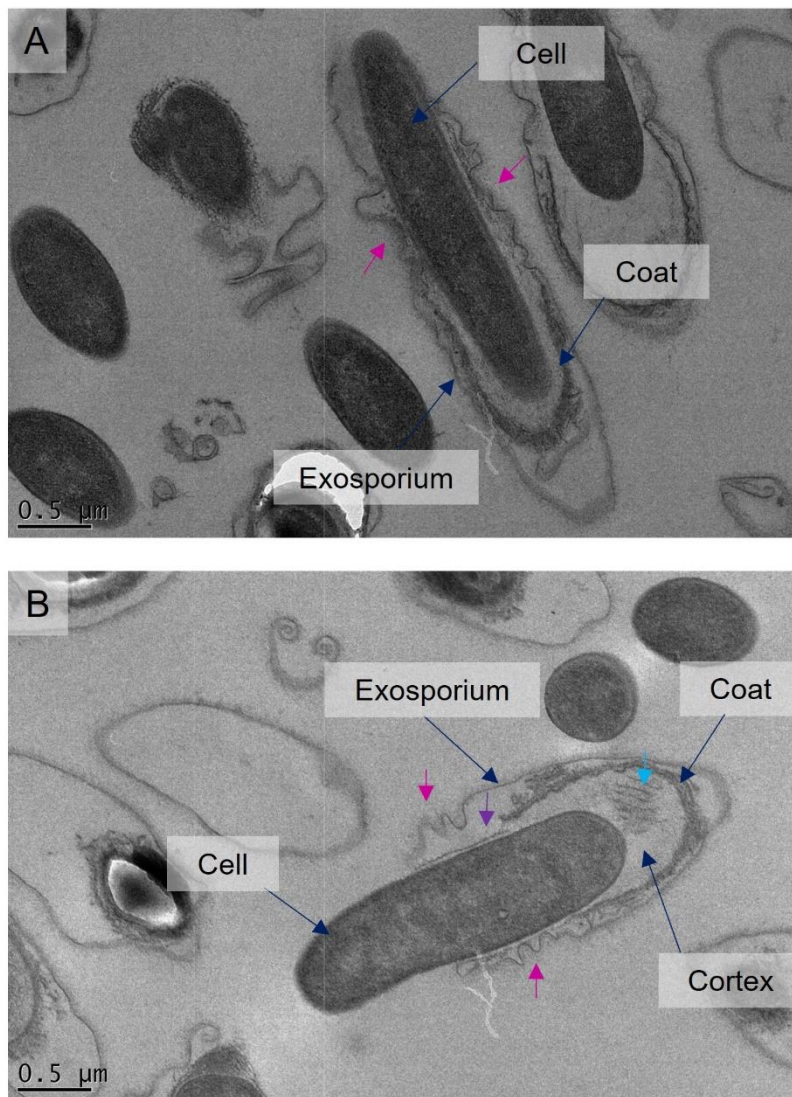
Figure 5.15: Thin Sections of *csxC* Spores in Late Germination

A+B) *csxC* spores in late germination show vegetative cells emerging from the pole of the spore with all distinguishable layers labelled. Pink arrows indicate ripples in the exosporium layer as it associates with the emerging cell. Light blue arrow (B) indicates striations within the cortex of the spore. Purple arrow (B) indicates a layer associated with the surface of the emerging cell.
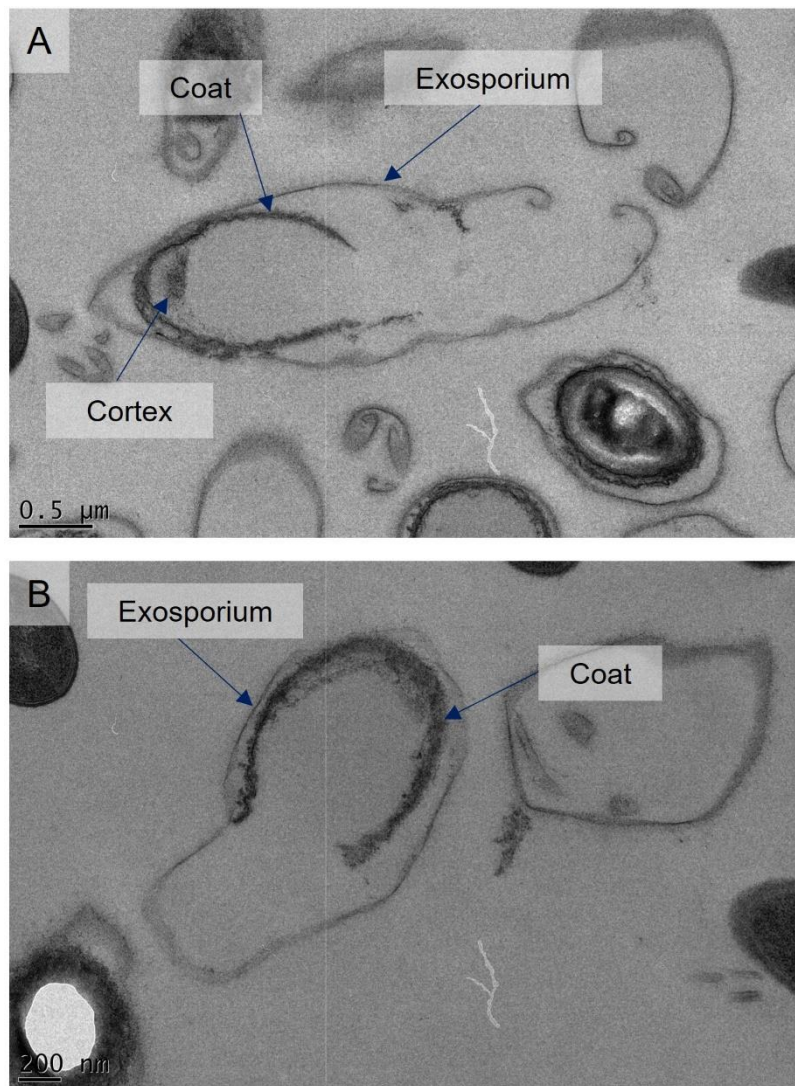
Figure 5.16: Thin Sections of *csxC* Spore Shells Post Germination

A+B) *csxC* spore shells composed of exosporium, spore coat and remnants of the cortex. The spore coat appears more disrupted compared to the coat post germination in WT.

5.4   Discussion

The structural roles of the cysteine rich proteins CsxA, CsxB, and CsxC and the collagen-like proteins

BclA and BclB within *C. sporogenes* were discussed in Chapter 4. Here we set out to determine if the

lack of these key exosporium proteins and the disruption to major structural components of the

spore ultrastructure had an affect on several key processes and properties of *C. sporogenes* spores.

These included sporulation, germination and spore heat resistance.

5.4.1   Exosporium Proteins and Sporulation

The sporulation process across the Bacilli and Clostridia is relatively well understood(Al-Hinai et al. 2015; Piggot and Hilbert 2004), although the specifics of *C. sporogenes* sporulation are not well characterised. Group I *C. botulinum*, for which *C. sporogenes* is a model, has a delayed release of the spores from the mother cell in comparison to Groups II and III (Portinha et al. 2022). *C. sporogenes* sporulation was seen here to be very rapid with the vast majority of the population becoming spores within 3 days (Fig: 5.1). The proportion of the population sporulating is also much higher than seen for other species such as *C. difficile* within the same time period (Dembek et al. 2015). Additionally and more surprisingly, there was no impact on sporulation efficiency of *C. sporogenes* strains lacking any of the exosporium-associated proteins tested. This suggests that the exosporium of *C. sporogenes* is not essential for spore viability and that defects, or indeed the complete lack of an exosporium in the case of *csxA* spores, has little effect on the efficiency of spore production.

However, this is unlikely to be the full story. The sporulation assay used here does not take into account whether the spores have been released from the mother cell, only that the developing spore is resistant enough to withstand heat treatment at 65°C for 30 min. 65°C is quite a moderate temperature for *C. sporogenes* spores and therefore, it is likely that a large number of the spore counts actually come from immature spores that are released from the confines of their mother cell during the heat treatment process. In order to test this, phase contrast microscopy should be carried out on samples from the sporulation culture to go along with the counts. This would allow for a distinction to be made between the percentage of the spore population that are still enclosed in the mother cell and those that are free within the environment.

Further to this it would also be interesting to observe the sporulation process, not only for WT but also for the exosporium mutants, at higher resolution, perhaps through thin sectioning or by CryoFIB-ET. Previous work looking at the sporulation process in *B. subtilis* by CryoFIB-ET showed immense detail of the sporulation process (Khanna et al. 2019). This kind of detail would allow

observation of the exosporium assembly process and the determination of potential roles of the cysteine rich exosporium proteins in modulating exosporium formation.

5.4.2 The Exosporium and Heat Resistance

Heat resistance of *C. sporogenes* spores varies between strains with the highest tolerance lying on average around 95-100°C (Schill et al. 2016). In *C. botulinum* it has been proposed that the exosporium plays a role in the heat resistance properties of the spore (Portinha et al. 2022). Observations across the three groups of *C. botulinum* showed that the strains within each group with the lowest heat resistance generally had thinner or no exosporium (Portinha et al. 2022). *C. sporogenes* is an established model for Group I *C. botulinum* and work on exosporium fragments has shown the exosporium itself remains crystalline up to temperatures of 95°C (Janganan et al. 2020). However, this is not necessarily a reflection on the heat tolerance of *C. sporogenes* spores as a whole.

When tested, WT *C. sporogenes* spores showed a 50-fold decrease in viability after heat treatment at 85°C and dropped below detection after treatment at 95°C. This suggests that the threshold for *C. sporogenes* spore heat tolerance lies somewhere between 85°C and 95°C. This would be slightly lower than that reported for Group I *C. botulinum* where spores tolerated heat treatment up to 98°C (Portinha et al. 2022). It is important to note however, that the experimental conditions for the two species were not identical. Heat treatment for *C. sporogenes* was for 30 min followed by enumeration of surviving CFUs whilst, for *C. botulinum,* heat exposure was for much shorter periods of time. It is possible that *C. sporogenes* spores might be able to survive higher temperatures providing the exposure time was of shorter duration.

In *C. sporogenes* it appears that the lack of an exosporium does not have a significant effect on the heat resistance properties of the spores over this sustained time duration. In fact, the lack of CsxA

appears to marginally improve the heat resistant properties of spores subjected to heat treatment at 85°C compared to WT (Fig: 5.2B). Additionally, the *csxA* mutant was the only strain to show any growth after heat treatment at 95°C, although this result may not be significant and requires further investigation (Fig: 5.2B). The improved heat resistance properties of *csxA* spores could be due to *csxA* spores being more susceptible to aggregation and therefore forming larger entities that could improve heat distribution. By washing the spores in a low percentage detergent before conducting heat resistance studies it may be possible to limit the auto aggregation of the spores.

Currently this work suggests that the exosporium does not have a significant role in protecting spore viability at sustained high temperatures, however, it is still possible that over shorter time periods the exosporium plays a more important role in heat resistance. Fine tuning of the experimental procedure to include a larger variety of temperatures and heat exposure times would provide valuable additional information about the heat resistance properties of these spores. This would allow for the threshold of *C. sporogenes* heat tolerance to be accurately determined and establish whether the exosporium has a role in the short term heat tolerance of the spores. Further to this, exosporium fragments are stable up to temperatures of 95°C (Janganan et al. 2020) and therefore it would be interesting to see if the *in situ* exosporium also remains crystalline after whole spore heat treatment at high temperatures. This could be done by conducting negative stain TEM and EC on whole spores after heat treatment.

Protection of the cortex layer is thought to be vital for maintaining the low water content of the spore core and the heat resistance properties of the spores (Reviewed in Mckenney et al., 2012). This protection is thought to be provided by the multi-layered coat surrounding the spore cortex that protects the cortex from degradation (Mckenney et al. 2012). Thin sectioning showed the frayed nature of the spore coat in dormant *csxC* spores (Fig: 5.17C) and the presence of blebs in the spore coat that could be an indication of incomplete coat formation in *csxB* spores (Fig: 5.17B) yet neither of these mutant spores appeared to show any heightened sensitivity to heat treatment (Fig:

5.2C). Again, this could be due to the prolonged heat treatment process used in this experimental procedure and heightened sensitivity may be revealed when tested using shorter heat exposures over a larger variety of temperatures. It would also be interesting to carry out thin sectioning on the heat treated spores of both the *csxB* and *csxC* mutants as well as WT to determine if there are any structural differences seen within the spores post heat treatment. This might reveal disruption to the spore coat or the cortex layers that could be responsible for the loss in spore viability.
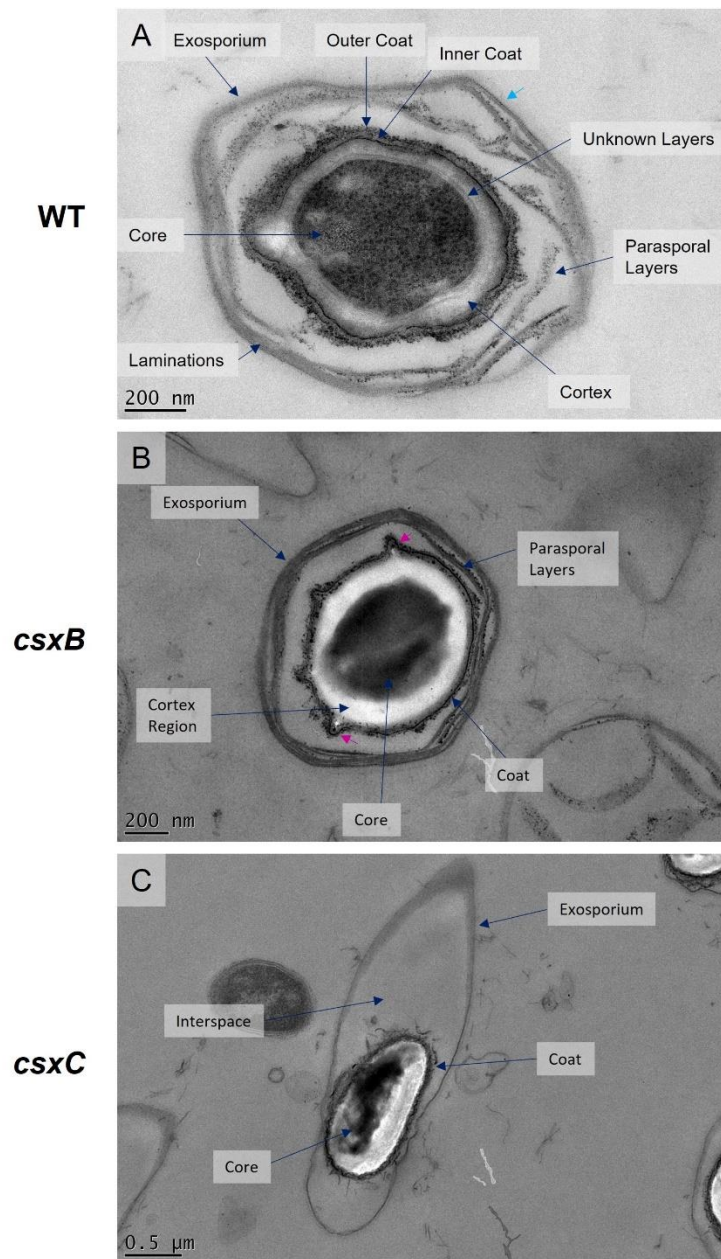
Figure 5.17: Summary of Sectioning of Dormant WT, *csxB* and *csxC* Spores

A) Thin section of dormant WT spore. B) *csxB* spore showing blebs in the spore coat (pink arrows) C) *csxC* spore showing the frayed nature of the spore coat.

5.4.3 The Role of the Exosporium and Csx Proteins in Germination

5.4.3.1 CsxA

It has been established that CsxA composes the basal layer of the exosporium in *C. sporogenes* and without it an exosporium is unable to form around the spore. The exosporium has been suggested to modulate the germination process in a variety of different ways. In *B. anthracis* the exosporium houses alanine racemase that converts L-alanine to D-alanine in order to prevent premature germination (Chesnokova et al. 2009). The porous nature of the exosporium layer may also act as a molecular sieve restricting the flow of molecules into and out of the spore and preventing larger complexes from passing through to the internal spore layers (Janganan et al. 2020; Terry et al. 2017).

Based on these proposed roles one might expect that spores lacking an exosporium would germinate more rapidly than those with an exosporium due to the spore being more accessible to germinant molecules. In response to germinants, DPA is released from the spore core and the spores become rehydrated reducing the refractive properties of the spores. A more rapid germination process would therefore manifest as a dramatic drop in OD as the refractive properties of the spore population decreased. Interestingly, for *csxA* spores, which lacked an exosporium, an initial OD drop was not observed during germination assays (Fig: 5.3F). Evidence of potential rehydration was seen in the thin sectioning data of *csxA* spores (Discussed for WT in Chapter 3) suggesting that the rehydration process is a key early process that occurs in these spores. However, this appeared not to be accompanied by an OD drop at the population level. A possible explanation for this is that a subset of the population transitions rapidly into the outgrowth phase of germination, thereby increasing the OD which would mask any drop in OD. To investigate these early stages of germination further live cell phase contrast microscopy should be used to observe in real time the changes that occur during the germination process of *csxA* spores. This would provide temporal information on the initial phase change and rehydration of *csxA* spores as well as the dynamics of cell emergence. The *csxA* population was seen to reach the outgrowth phase earlier than WT spores

which could be an indication of a more rapid germination process due to emerging cells not having

to navigate exit from the confines of the exosporium layer and therefore being released more

readily from the spore shell into the environment. Again, live cell phase contrast microscopy should

provide more information about this process.

The thin sectioning data from *csxA* spores showed that the parasporal layers were initially separated

from the spore coat by a small interspace region which measured 85 nm ± 20 nm. From mid

germination onwards this interspace region was no longer apparent; from this point parasporal

layers often became disassociated from the spore surface (Fig: 5.6). Based on the observations in *B.*

anthracis, the interspace is proposed to be composed of two polysaccharide layers (Lehmann et al.

2022). It is possible that the small interspace region seen in *csxA* spores is an indication of the

presence of the inner polysaccharide layer seen in *B. anthracis*. The disappearance of the interspace

during the germination process indicates that breakdown of these polysaccharide layers must occur

early in germination. The breakdown of the polysaccharide layers could also disrupt the interactions

between the parasporal layers and the spore coat which would explain the dissociation of the

parasporal layers from the surface of the spores during the germination process. The polysaccharide

layer has been proposed to provide energy for the developing cell (Lehmann et al. 2022) and its

breakdown early during the germination process would be important for this role.

In WT germination and in *csxB* mutant germination it was noted that the parasporal layers within the

interspace at one pole disappear. Although parasporal layers are seen to dissociate from the spore

body during the germination process of *csxA* spores there is no evidence that this occurs specifically

from one pole. This could suggest that the disappearance of parasporal layers seen prior to cell

emergence is modulated in some way by the polarity introduced by the exosporium. Furthermore, in

longitudinal sections of *csxA* spores late in germination and in spore shells it was apparent that the

parasporal layers still associated laterally with the spores, and were less curved (Fig: 5.8B). A similar

observation was made within WT spores, however, with the parasporal layers being sandwiched

between the coat and the exosporium it was assumed that their morphology was forced due to the confines of the spore. It would seem, however, that the change in parasporal layer morphology during germination is not dependent on the presence of the exosporium and is a fundamental process that occurs during germination.

5.4.3.2 CsxB

Germination of *csxB* spores appeared to occur in a very similar fashion to WT with a short lag period observed during the outgrowth phase. Thin sectioning of the germination process appeared to show the same overall structural changes as seen for WT, however, there were a few small differences observed. During early germination thin sections showed that the spore coat continued to show the presence of blebs across the surface as observed in dormant *csxB* spores. These blebs were not apparent in any of the latter stages of germination, perhaps suggesting that they correspond to folds in the coat that are stretched during the rehydration of the spore core and the expansion of the cortex region. This would be analogous to the expansion process suggested to occur in dormant *B. thuringiensis* on exposure to high humidity conditions (Driks 2003; Westphal et al. 2003). There is also an additional gap between the coat and the cortex observed in thin sections of early germination likely to further indicate the poor structural integrity of the spore coat. Together this would point to CsxB having a role in spore coat formation or possibly being a constituent coat protein. The location of the gap between the cortex and the coat could indicate that CsxB plays a role in anchoring the coat to the cortex layer or in maintaining coat cortex interaction. To investigate this further, localisation of CsxB within the spore structure will be required. Methods to do this could involve using immuno-gold labelling, discussed previously in Chapter 4 (Section 4.4.2.4), or the use of fluorescently tagged CsxB to map its location within the spore, as was done previously for *B. subtilis* coat proteins (McKenney and Eichenberger 2012).

During WT germination, striations within the expanded cortex region were observed and were seen to localise to the pole distal from cell emergence. In *csxB* spores the striations are also present within the cortex region, however, they appear to be located at different points around the developing cell and in some cases post germination, multiple sets of striations can be seen (Fig: 5.10B and 5.12A). It was suggested in section 3.4.5.3 in WT spores that these features could play a role in facilitating cell emergence from the outer layers of the spore. The mislocalisation of the striations in *csxB* spores could therefore account for the delay in the outgrowth phase seen during the germination assays. This also suggests that CsxB is important for the localisation of material within the expanding cortex during germination.

5.4.3.3   CsxC

Germination assay data for *csxC* spores showed that the initial OD drop was lower than for WT. It was apparent from thin sectioning of dormant *csxC* spores that the spore coat was markedly disrupted compared to WT (Fig: 5.17). This could allow both germinant molecules and water molecules to pass through the coat more readily, leading to a more rapid rehydration process accounting for the lower drop in OD seen at a population level in the initial stages of the germination assay.

During mid germination, striations were visible within the expanded cortex region of *csxC* spores as in WT spores. These were located towards the pole distil from cell emergence. Unlike WT spores, *csxC* spores contained additional darker stained rings within the expanded cortex region. These were mostly evident in mid germination but a hint of their presence could also be seen in late germination as the cells were emerging from the outer layers of the spore (Fig: 5.14 and 5.15). The rings could be an indication of regular structure within the cortex region which would be a further indication that the putative cortex-lytic enzymes, CwlJ and SleB, do not in fact degrade the cortex but are instead involved in restructuring the cortex during the germination process. Why these rings are not

185

observed in WT germination remains unclear. It could purely be down to the staining of the samples and the frayed coat allowing for increased stain penetration to the cortex layer. Another explanation for the presence of rings within the cortex could be that proteins from the seemingly unstable coat disassociate from the under layers of the spore coat and become associated with layers of the cortex during the expansion. This does not appear to have any major impact on the ability of the spore to germinate or the developing cell to emerge. It is possible that the thin layer associated with the emerging cell in late germination (Fig: 5.15B purple arrow) is a remnant of these rings. Higher resolution 3D information on the cortex layer would provide a better understanding of the make up of this layer.

It was noted in Chapter 4 that *csxC* spores have a large extended pole to the exosporium. From the thin sectioning data it is clear that this pole is more often than not the site for cell emergence. There was no evidence of any lag to the outgrowth phase of *csxC* spores in the germination assays which suggests that there is no impact at a population level. The thin sectioning data do suggest that the exosporium associates with the cell as it emerges from the outer layers of the spore (Fig: 5.15). In some cases an additional layer is also seen between the cell as it emerges and the exosporium. The lack of parasporal layers within these spores indicates that it cannot be a parasporal layer. As suggested above, it could be a part of one of the rings found in the cortex during mid germination. Alternatively it could be a fragment of the coat that has adhered to the cell surface as the cell is manoeuvring its way out of the spore shell. The coat already appearing frayed in this mutant would make this a likely explanation.

csxC spores were found not to have any parasporal layers present within the interspace of the spore and it was further established in Chapter 4 that CsxC is likely the major structural component of the parasporal layers in *C. sporogenes*. From the germination data it is apparent that CsxC and therefore the parasporal layers are not essential for the germination process in *C. sporogenes* and that the lack of parasporal layers appears to have very little impact on the germination process. The parasporal

layers could act as a scaffold for other proteins within the interspace, in particular for proteins involved in the modelling and breakdown of the potential polysaccharide layers that compose the interspace. The breakdown of the interspace polysaccharide has been proposed to occur during early germination to provide energy for the developing cell (Lehmann et al. 2022). Although not clear from the thin sectioning data here, it would be interesting to see if this degradation occurs in the absence of the parasporal layers, given their possible role as a protein scaffold.

Post germination the spore coat of *csxC* spores is far more disordered than that seen in WT. Despite the increased disorder there is clear polar degradation of the coat layer suggesting that the targeted approach to coat degradation is not disrupted by the immature nature of the spore coat in *csxC* spores. This also points further to CsxC having a role in maintaining the structural integrity of the spore coat. Whether this is a direct role in coat composition or a more accessory role remains to be determined and localisation studies through fluorescent labelling or immune-gold labelling may provide an indication as to what the role of CsxC in coat formation may be.

5.4.3.4   BclA and BclB

The lack of BclA and BclB appeared to have very little impact on the germination of *C. sporogenes* spores. It has been established that BclA composes the intermediate fibrils, a major component of the hairy nap in *C. sporogenes* (Section 4.4.3). BclB is also likely a decorative element on the surface of the exosporium.

Thin sectioning of these mutant strains during the germination process may provide a clearer picture as to why a lag was seen in the outgrowth phase. As suggested in previous chapters it appears likely that the germination process in *C. sporogenes* is dependent on a cap region in the exosporium from which the new vegetative cell emerges. This is analogous to the bottle cap model of germination developed in *B. anthracis* (Steichen et al. 2007). The exosporium basal layer appears to be composed

entirely of CsxA suggesting that any cap region present involves differences in the decoration on the surface of the exosporium. As key decoration proteins BclA and BclB could be involved in cap formation and subsequent opening during the germination process. It would therefore be interesting to look at these mutants in more detail with a particular focus on when an opening appears in the exosporium and if there is any delay in the emergence of vegetative cells from these spores. To better understand the distribution of the Bcl proteins and their functions a combination of techniques will likely need to be used including fluorescence microscopy for localisation studies and AFM to look at high resolution at the surface properties of both WT and mutant exosporium.

Overall it seems that the exosporium associated proteins investigated here are not essential for the germination and outgrowth process. However, it does appear that the exosporium is important in modulating the germination process and that subtle changes in the ultrastructure of the spores can have an impact on *C. sporogenes* germination and outgrowth. There is a lot of work still to be done to fully understand this complex process and the roles played by these and other proteins within the spores.

6 General Discussion

6.1 The Exosporium and Associated Proteins in *C. sporogenes*

Spores are crucial to the lifecycle of firmicutes including Bacilli and Clostridia species. This thesis has focused on *C. sporogenes,* a significant threat posed to the food industry and an important model for the study of Group I *C. botulinum* strains, the causative agent of botulism (Peck et al. 2011). The highly resilient spore state is key to the survival of these species and is vital for the transmission and persistence of infection, particularly in aerobic environments. The resilient properties of dormant spores are conferred by the multiple layers that compose the spore ultrastructure (Henriques and Moran 2000). Of particular interest is the outermost layer of *C. sporogenes* spores, the exosporium. It forms the first point of contact between the spore and the environment and has been implicated in providing heat resistance properties to the spores (Portinha et al. 2022) as well as modulating the germination process (Henriques and Moran, Jr. 2007).

The structural nature of the exosporium has been extensively examined in species of Bacillus as well as in *C. sporogenes*. Within the *B. cereus* group and *C. sporogenes* (Chapter 1.3.6) the exosporium basal layer is composed of a hexagonal para-crystalline array of cysteine rich proteins (Ball et al. 2008; Janganan et al. 2020; Kailas et al. 2011; Terry et al. 2017). Mass spectroscopy of *C. sporogenes* exosporium fragments identified three cysteine rich proteins, CsxA, CsxB, and CsxC (Janganan et al. 2016). Overexpression of CsxA yielded 2D crystals identical in structure to the native exosporium (Janganan et al., 2020), suggesting that CsxA is the major structural component of the exosporium basal layer. The roles of the other two cysteine rich proteins, CsxB and CsxC, remained unclear. It follows then that one of the key aims of this research was to elucidate the roles of the additional Csx proteins, CsxB and CsxC in the ultrastructure of the spore.

6.1.1 Roles of Cysteine Rich Proteins in Spore Ultrastructure

In order to determine the roles of the cysteine rich proteins in spore ultrastructure a series of knockout strains were produced using a novel allelic exchange mutagenesis process. *csxA*, *csxB* and *csxC* spores were structurally analysed by a range of microscopy techniques.

CsxA had already been established as the major structural protein of the exosporium (Janganan et al. 2020). This was further confirmed by the data presented here showing that *csxA* spores completely lacked an exosporium structure and that *csxB* and *csxC* spores appeared to assemble a complete exosporium (Fig: 4.8, 4.9 and 4.10).

The role of CsxB remained challenging to determine as *csxB* mutant spores display a very similar phenotype to WT consisting of a dense spore body surrounded by a baggy exosporium that is extended at one pole (Fig: 4.3, 4.9 and 4.13B). Despite this, thin sections of germinating *csxB* spores displayed a mislocalisation of the striated cortex feature suggesting that CsxB could be responsible for the localisation of these structures during germination. In addition, sectioning of dormant *csxB* spores did reveal some disruption to the spore coat in the form of blebs, possibly suggesting a role for CsxB in the maturation of the coat layer. Thin sectioning during the sporulation process of *csxB* spores would improve our structural understanding of coat assembly in *C. sporogenes* and allow us to further investigate the potential role of CsxB in coat maturation.

Thin sections of *csxC* spores revealed them to be completely devoid of parasporal layers suggesting that CsxC is either fundamental in orchestrating the formation of parasporal layers or that CsxC is the major structural component of these layers. Being a cysteine rich protein it seems more likely to be the latter as prior work on other cysteine rich proteins in Bacillus and *C. sporogenes* has revealed their structural importance in outer spore layers (Janganan et al. 2020; Jiang et al. 2015; Terry et al. 2017). This was further supported by the fit of the predicted Alphafold trimer when superimposed onto the 2D projection map of type II crystal which, as discussed in 4.4.2.3, likely corresponds to the parasporal layers (Fig: 4.21). Although just a prediction, pLDDT values suggest high confidence in the

majority of the predicted structure. In addition, the intercalated nature of the monomers and the formation of convincing disulphide bonds lends further confidence to the prediction. To confirm the composition of the parasporal layers it may be possible to dissociate the surface layers from *csxA* spores and analyse their composition by mass spectroscopy. This may also reveal proteins associated with these layers which could provide an insight into their function. Overexpressed CsxC has yet to be purified; its potential to self-assemble into 2D crystals analogous to native Type II crystals should be tested, as demonstrated for other cysteine rich spore proteins (Janganan et al. 2020; Jiang et al. 2015; Terry et al. 2017).

This does not rule out the possibility that other proteins are involved in the composition of the parasporal layers or that CsxC may have other roles and be found in other locations within the spore. Localisation studies of CsxC using immuno-gold labelling would provide an insight into the distribution of CsxC across the spore. For example, CsxC appears to have some role in coat formation given that the structural integrity of the spore coat was also seen to be disrupted in thin sectioning of *csxC* spores.

The role of the parasporal layers within the spore is not clear. They may act as a scaffold onto which other proteins and enzymes can adhere. These could include enzymes responsible for the synthesis and degradation of the polysaccharide layers proposed to be within the interspace region of the spore (Lehmann et al. 2022). It could also be the location of enzymes that play an active role in the protection of the spore against toxic compounds and oxidative stress found during the mass spectroscopy analysis of exosporium fragments (Janganan et al. 2016). To further investigate the role of parasporal layers it may be possible to utilise *csxC* spores in additional experiments to probe their resistant properties, such as exposure to oxidative stress and dry heat.

6.1.2 Collagen-Like Proteins and the Hairy Nap

In addition to the basal layer, the surface of the exosporium is often decorated with a hairy nap. In the *B. cereus* group this is composed of fibrils of collagen-like proteins (Boydston et al. 2005; Sylvestre, Couture-Tosi, and Mock 2003; Sylvestre et al. 2005; Todd et al. 2003). Similar proteins with collagen-like repeats were also identified within *C. sporogenes* (Janganan et al. 2016), however, their specific involvement in forming the hairy nap is yet to be established. The surface of *C. sporogenes* was also seen to possess several longer appendages including beaded fibrils, intermediate fibrils, and 'large appendages' (Janganan et al. 2016). To ascertain whether the collagen-like proteins identified in *C. sporogenes* fulfil a similar role to those seen in Bacillus, structural analysis of *bclA* and *bclB* spores was conducted.

AFM of *bclA* spores showed the absence of a fringe surrounding the exosporium suggesting that BclA composes the intermediate fibrils identified in Janganan et al., 2016. Additionally, length analysis of the intermediate fibrils in negative stain TEM images further indicates that BclA composes these structures due to the correlation between the number of XXG repeats present within the sequence and the measured width of the fringe (Discussed in 4.4.3). The surface of *bclA* spores was not completely bare suggesting that additional proteins are present on the surface, decorating the exosporium. One such protein could be BclB, however, this requires further investigation, particularly as little could be gained from the AFM imaging of *bclB* spores due to the dominating presence of BclA. The role of BclB could thus be tested through imaging of a *bclA*:*bclB* double mutant. Higher resolution AFM imaging on fragments of exosporium from *bclA*, *bclB* and a double mutant would provide a more detailed understanding of the surface properties as well as allowing for more reliable thickness measurements of the exosporium.

6.1.3   The Role of the Exosporium

The exosporium has been suggested to play a role in protection, adhesion, and germination (Henriques and Moran, Jr. 2007). In *C. botulinum* the exosporium has also been implicated in spore heat resistance, with strains possessing a thinner exosporium being more susceptible to heat treatment (Portinha et al. 2022). The production of *csxA* spores, that lacked an exosporium, provided the opportunity to investigate the role of the exosporium in carrying out these proposed functions. In addition, *csxB*, *csxC*, *bclA* and *bclB* mutants were also probed to ascertain if these proteins also contributed to these spore properties.

As discussed in Chapter 5 (Section 5.4.2), the exosporium does not appear to play a role in the heat resistant properties of *C. sporogenes* spores (Fig: 5.2). This is in contrast to *C. botulinum* where strains possessing a thinner exosporium were less heat tolerant (Portinha et al. 2022). However, it is noted that the experimental approach varied considerably in that *C. sporogenes* spores were subjected to a prolonged heat treatment of 30 min whilst *C. botulinum* spores were only subjected to heat treatment for several minutes (Portinha et al. 2022). This investigation into heat resistance of *C. sporogenes* spores would benefit from a more refined experimental procedure where more temperatures and exposure times could be investigated. This would provide a more robust analysis of the heat resistant properties of *C. sporogenes* providing an indication of the threshold of heat tolerance and establish whether the exosporium or its associated proteins contribute to the short term heat tolerance of the spores. It would also be interesting to compare the viability of spores after exposure to wet versus dry heat to explore any differences that might occur in the behaviour of spores in a dehydrated state.

In terms of the germination and subsequent outgrowth of *C. sporogenes* it is clear that the exosporium is not essential and more likely plays a more minor role in modulating these processes (Chapter 5). There are small, yet significant, differences seen between each of the mutants and WT when subjected to germination assays. *csxA* spores showed no initial drop in OD usually associated

with the rehydration of the spore core early in germination (Fig: 5.3A), however, thin sectioning data showed clear evidence of core rehydration occurring (Fig: 5.5). This suggests that the initial drop in OD was likely masked at the population level, perhaps by a subset of the population transitioning early into the outgrowth phase. As a whole, the *csxA* population transitioned into the outgrowth phase slightly more rapidly than WT (Fig: 5.5) which could suggest either more rapid germination initiation or easier exit for vegetative cells from the spore without the presence of the exosporium. *csxB* spores showed a lag in the outgrowth phase compared to WT, possibly indicating a delay in vegetative cell emergence (Fig: 5.3B). *csxC* spores showed a slight but significant lower initial OD drop when compared with WT (Fig: 5.3C), perhaps suggesting a more rapid rehydration process which could be due to the disrupted nature of the spore coat seen within thin sectioning data (Fig: 4.10). It was not possible to conclusively determine the specific stage of the germination and outgrowth process that was affected by the lack of each protein. Carrying out live phase contrast microscopy of germination for each mutant will provide temporal data at the individual spore level. This will give an indication as to what, if any, stages of the germination process are affected by the lack of each specific protein. Thin sectioning of the *csx* mutants provided some structural details of the germination process which will be discussed below.

With regard to the protection and adhesion properties of the exosporium these are yet to be investigated in detail. During the AFM analysis of *bclA* spores it was noted that the exosporium was more often folded in on itself rather than laying flat on the imaging surface as was seen for WT and other mutants (Fig: 4.13 and 4.14). This could point to BclA having a role in the surface adhesion properties of the spore. To investigate this further, hydrophobicity assays should be conducted to determine the adhesion properties of spores with altered surfaces. For *B. anthracis* the lack of BclA changed the surface properties of the spores and was suggested to impact the spores ability to adhere to surfaces which could further impact on the spores ability for colonisation (Brahmbhatt et al. 2007; Faille et al. 2010).

6.2   Germination in *C. sporogenes*

Whilst there have been a number of studies into the biochemical nature of the germination process there has been comparatively little done to enhance our structural understanding of this remarkable process.

Some initial thin sectioning of *C. sporogenes* showed the gross morphological changes associated with spores as they undergo germination (Hoeniger and Headley 1969). However, since then there have been major advances in EM and sample preparation that allow for higher resolution imaging and the observation of much finer details. The work presented here provides in-depth ultrastructural analysis of the germination process in *C. sporogenes* (Chapter 3) including important additional information from analysis of germination in exosporium mutant spores (Chapter 5). With the temporal information from the live cell imaging and the ultrastructural detail from the thin sectioning data it was possible to produce a model for spore restructuring during the germination process in *C. sporogenes.*

6.2.1   Ultrastructural Model for Germination

A schematic showing the germination process can be seen in Figure 6.1 the evidence for which is laid out below.

The early stages of germination are characterised by the rehydration of the spore, seen clearly in the phase contrast microscopy as a change from phase bright to phase dark (Movie 3.1). Additionally, within the thin sectioning data, two subclasses of spores in the early stages of germination were seen. One class showed comparatively poor staining of the internal structures of the spore body whilst the other possessed clear details of the inner spore layers. This phenomenon was more pronounced in the sectioning data from germinating mutant spores (Fig: 3.9, 5.5, 5.9,and 5.13) and could correspond to the rehydration of the core as discussed in Chapters 3 and 5.

As the spores continue to undergo the germination process the interspace region becomes indiscernible, possibly due to degradation of polysaccharide layers that may be present within the interspace (Lehmann et al. 2022). The spore body increases in size to the point where the parasporal layers are stacked against each other between the coat and the exosporium (Fig: 3.10 and 5.10). Spore body expansion appears to be coupled to the expansion of the spore cortex region rather than the spore core itself. This is in contrast to what is observed in other species such as *C. difficile* (Baloh et al. 2022). The exosporium often appeared open at one pole by this stage and the opening was seen to be at the extended pole of the exosporium. This was seen most clearly in *csxC* mutants that possess a hyper-extended exosporium (Fig: 5.14). Within the expanded cortex region striations were observed at the pole distal from the exosporium opening. Although the composition and role of these striations remains unclear, their locality and overall appearance might suggest a potential molecular spring mechanism acting to assist in the emergence of the vegetative cell in the latter stages of outgrowth. As discussed in 5.4.3.2 these striations were mislocalised within *csxB* spores perhaps accounting for the lag seen in the outgrowth phase of the germination assay (Fig: 5.3).

Micrographs depicting spores in the late stages of outgrowth clearly showed the vegetative cell emerging through the spore coat and through the opening in the exosporium layer (Fig: 3.11, 5.7, 5.11, 5.15). This suggests that coat degradation is targeted to the spore pole to align with the opening already present in the exosporium. The mechanism by which this occurs is yet to be determined but could involve the action of localised proteases already present within the coat that become activated during germination. Alternatively, coat degradation enzymes could be associated with the surface of the emerging cell which then gradually degrade the coat as the cell is propelled towards the pole potentially through the molecular spring action of the striated region within the cortex. Looking for the expression of potential coat proteases during the sporulation process may identify enzymes that could be assembled into the coat during spore maturation. Alternatively, proteases expressed during early cell development could indicate that coat degradation is enabled by the emerging cell. This process is interesting because it appears to occur differently from

previously studied species such as *B. subtilis* and *B. atrophaeus* where no clear directionality in coat degradation is observed (Plomp et al. 2007; Santo and Doi 1974). In these species the coat appears to breakdown at various points around the spore in order for the vegetative cell to be released (Plomp et al. 2007; Santo and Doi 1974).

Eventually the emerging cell completely leaves the confines of the spore outer layers, leaving behind a shell composed of the exosporium, parasporal layers, coat, and cortex remnants (Fig: 3.12, 5.8, 5.12, 5.16).
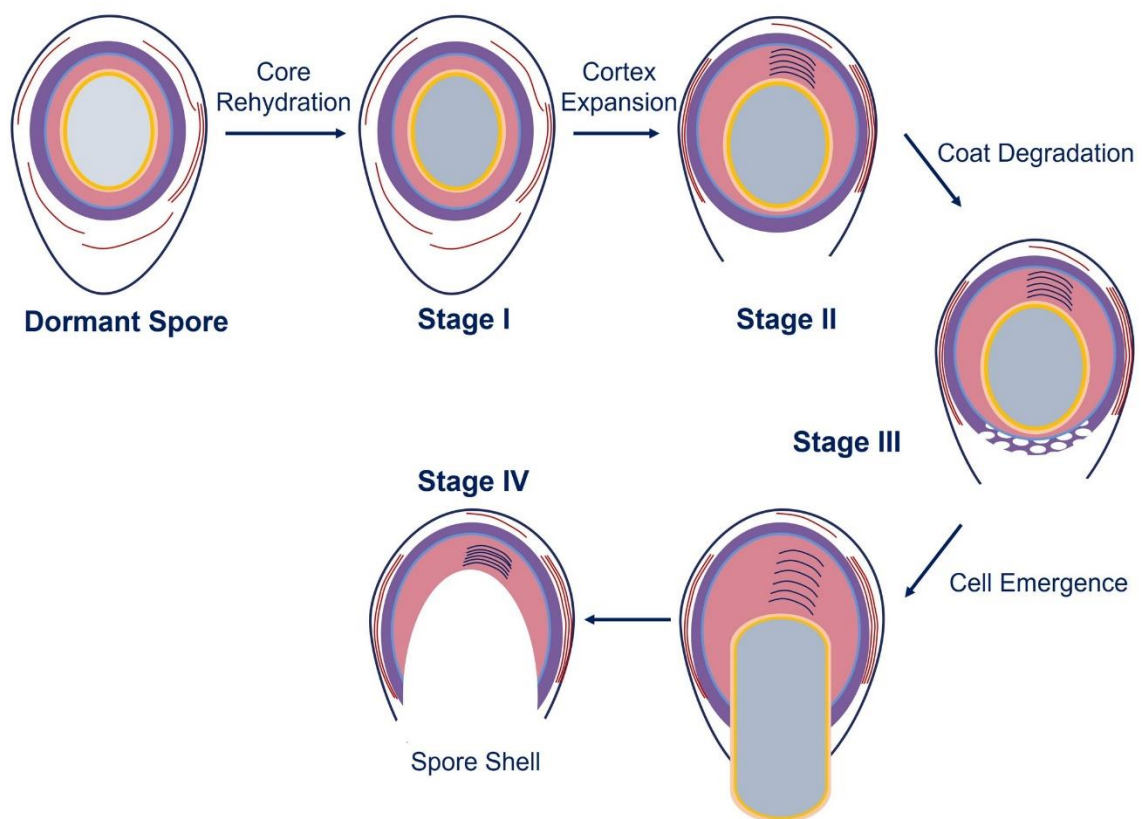
Figure 6.1: Model of Spore Restructuring During Germination and Outgrowth

The germination process begins with the rehydration of the spore core (Stage I). The spore body then swells, a process that is coupled with the expansion of the spore cortex. The expansion of the spore body sandwiches the parasporal layers between the exosporium and the coat. The exosporium is often open at one pole and striations can be seen within the expanded cortex region (Stage II). The coat of the spore is degraded in line with the opening at the pole of the exosporium allowing the vegetative cell to begin emerging (Stage III). The vegetative cell emerges through the open pole into the environment, possibly mediated by the striations within the cortex, leaving behind the outer spore layers as a spore shell (Stage IV).

6.2.2   The Bottle Cap Model

Analysis of the exosporium in *B. anthracis* revealed the presence of a structurally distinct polar cap through which the new vegetative cell is seen to emerge during germination (Steichen et al. 2007). This led to the idea of the bottle cap model of germination where the weakened polar cap facilitates the emergence of the vegetative cell. Therefore a key question was whether a similar mechanism of emergence exists within *C. sporogenes*.

A potential cap was observed at the pole of the extended region of the exosporium in AFM imaging of WT spores (Fig: 3.2). This correlated with the location of apertures seen in the exosporium layer in previous imaging by SEM (Brunt et al. 2015), the location of the open exosporium pole seen in thin sections of *csxC* spores during germination (Fig:5.14), and the location of later cell emergence (Fig: 5.15). Together this suggests that the mechanical properties of this polar exosporium region are different and could correspond to a structurally distinct polar cap. High resolution imaging of these regions by AFM would provide information regarding their structural composition and could provide an insight into their possible role in facilitating germination.

Live cell imaging of the germination process (Movie 3.1) clearly depicted polar germination of *C. sporogenes* spores and even confirmed that the majority of cells emerged from the extended pole region of exosporium. Thin sectioning of germinating spores also appeared to show the new vegetative cell emerging through the extended pole of exosporium (Fig: 3.11, 5.11, 5.15). In many cases the pole of the exosporium was seen to be open prior to the cell leaving the confines of the spore coat (Fig: 5.14A and C) and that coat degradation is targeted to the pole aligned with the opening in the exosporium (discussed 3.4.5.4). This complements the observations of a polar cap and opening seen by AFM and the apertures seen by SEM (Brunt et al. 2015). To investigate the emergence of the new vegetative cell from the spore further it would be beneficial to have high resolution live cell imaging. Time lapse AFM imaging of the germination process could provide this high resolution information, however, whether it is possible to secure germinating spores to a

surface well enough for imaging to be conducted whilst also allowing for the physical changes associated with germination to take place remains to be seen. Alternatively, it may be possible to obtain 3D structural information of the emergence process through CryoET. Initial attempts at obtaining tomography data were discussed in 3.4.7 and with further optimisation or the use of FIB-milling it may be possible to obtain higher resolution 3D structural information on germinating spores which may provide further structural insights into the potential cap structure of the exosporium.

Despite these observations no structural basis for the presence of an exosporium cap in *C. sporogenes* has yet been found. The crystalline structure of the exosporium seen previously in dormant spores (Janganan et al. 2020) was maintained post germination (Discussed in 3.3.5). Additionally, in *csxA* spores that lack the major protein component of the exosporium, no initial cap region was seen associated with the spore. This suggests that any cap region is either, also composed of a CsxA basal layer and that accessory proteins are responsible for an altered cap structure, that the cap is not formed of an ordered crystalline array and is therefore not amenable to structural study by EC, or that the cap region requires CsxA and the rest of the exosporium to remain adhered to the spore surface. Further investigation of the surface of the exosporium by AFM could help to ascertain if there is a structural difference in the pole of the exosporium. In addition, localisation of surface exposed proteins such as BclA and possibly BclB could indicate if there are any patterns in their distribution across the exosporium as seen in *B. anthracis* (Thompson et al. 2012).

6.3 Further work

6.3.1 Cryo-ET

Throughout this work thin sectioning was used to obtain ultrastructural details of both dormant mutant spores and the germination process. In chapter 3 initial attempts at cryo-ET were carried out

on germinating *C. sporogenes* spores which yielded promising results for the future use of this technique to understand the physical changes occurring within the spores. It also provided additional detail on the exosporium surface decoration, particularly the beaded fibrils that are not readily observed by traditional EM. Further studies should consider the use of cryo-FIB-ET, particularly for the study of dormant spores and those early in germination which proved too thick for reliable tomography data collection. This would provide higher resolution and 3D structural information and allow for further analysis of structures such as the striations seen in the cortex region and the parasporal layers. It may even be possible to conduct subtomogram averaging on some of the layers within the structure. This may also prove useful for the study of exosporium decoration proteins, allowing for structures of the large appendages and beaded fibrils to be determined.

6.3.2   Localisation of Csx Proteins

Thin sectioning of mutant spores provided extraordinary detail of the ultrastructure of the spores and provided insights into the possible location and role of the Csx proteins within the spores. To further understand the distribution of CsxA, CsxB and CsxC it would be beneficial to carry out immuno-gold labelling on WT and mutant spores. Using anti-CsxC on *csxA* spores would be particularly interesting to confirm the composition of the parasporal layers. Moreover, it may be possible to fluorescently label these proteins and conduct correlated light and electron microscopy to determine the locality of these proteins within the spore (Koning et al. 2018).

6.3.3   Overexpression of CsxB and CsxC

Heterologous expression of CsxB and CsxC was successful, giving clear over expression bands when analysed by SDS-PAGE (Fig: 4.15). Unfortunately, there was insufficient time to conduct any purification of these proteins. This would confirm whether self-assembly to form crystals occurs for either of these two cysteine rich proteins. If crystals are formed then these could be used for cryo-EC studies to determine their structure and may provide confirmation that CsxC composes the

parasporal layers. If not, the proteins could be used for laying down crystal trials for X-ray crystallography, or if oligomers are formed single particle cryoEM could be used to determine the structure of these proteins.

6.3.4 Surface Adhesion Studies

As the first point of contact between the spore and the environment the exosporium is thought to play a key role in adhesion (Henriques and Moran, Jr. 2007), in particular the BclA proteins on the surface of *B. anthracis* spores have been shown to increase the hydrophobicity properties of the spores (Brahmbhatt et al. 2007). It would therefore be interesting to conduct hydrophobicity assays with the exosporium mutant spores, particularly the two bcl mutants to ascertain if they could play a role in the surface adhesion properties of *C. sporogenes* spores.

Bibliography

Al-Amoudi, Ashraf, Jiin Ju Chang, Amélie Leforestier, Alasdair McDowall, Laurée Michel Salamin, Lars P. O. Norlén, Karsten Richter, Nathalie Sartori Blanc, Daniel Studer, and Jacques Dubochet. 2004. 'Cryo-Electron Microscopy of Vitreous Sections'. *The EMBO Journal* 23(18):3583–88. doi: 10.1038/SJ.EMBOJ.7600366.

Al-Hinai, Mohab A., Shawn W. Jones, and Eleftherios T. Papoutsakis. 2015. 'The Clostridium Sporulation Programs: Diversity and Preservation of Endospore Differentiation'. *Microbiology and Molecular Biology Reviews* 79(1):19–37. doi: 10.1128/MMBR.00025-14/ASSET/43B2750B-38CC-4EC0-8B19-F7A44CE198D9/ASSETS/GRAPHIC/ZMR0011523800007.JPEG.

Amos, L. A., Richard Henderson, and P. N. T. Unwin. 1982. 'Three-Dimensional Structure Determination by Electron Microscopy of Two-Dimensional Crystals'. *Progress in Biophysics and Molecular Biology* 39(C):183–231. doi: 10.1016/0079-6107(83)90017-2.

Atrih, Abdelmadjid, and Simon J. Foster. 1999. 'The Role of Peptidoglycan Structure and Structural Dynamics during Endospore Dormancy and Germination'. *Antonie van Leeuwenhoek, International Journal of General and Molecular Microbiology* 75(4):299–307.

Bagyan, Irina, and Peter Setlow. 2002. 'Localization of the Cortex Lytic Enzyme CwlJ in Spores of Bacillus Subtilis'. *Journal of Bacteriology* 184(4):1219. doi: 10.1128/JB.184.4.1219-1224.2002.

Ball, David A., Robert Taylor, Sarah J. Todd, Caroline Redmond, Evelyne Couture-Tosi, Patricia Sylvestre, Anne Moir, and Per A. Bullough. 2008. 'Structure of the Exosporium and Sublayers of Spores of the Bacillus Cereus Family Revealed by Electron Crystallography'. *Molecular Microbiology* 68(4):947–58. doi: 10.1111/j.1365-2958.2008.06206.x.

Baloh, Marko, Hailee N. Nerber, and Joseph A. Sorg. 2022. 'Imaging Clostridioides Difficile Spore Germination and Germination Proteins' edited by T. M. Henkin. *Journal of Bacteriology* 204(7). doi: 10.1128/JB.00210-22.

Barlass, Paul J., Christopher W. Houston, Mark O. Clements, and Anne Moir. 2002. 'Germination of Bacillus Cereus Spores in Response to L-Alanine and to Inosine: The Roles of GerL and GerQ Operons'. *Microbiology* 148(7):2089–95. doi: 10.1099/00221287-148-7-2089/CITE/REFWORKS.

Bharat, Tanmay A. M., Danguole Kureisaite-Ciziene, Gail G. Hardy, Ellen W. Yu, Jessica M. Devant, Wim J. H. Hagen, Yves v. Brun, John A. G. Briggs, and Jan Löwe. 2017. 'Structure of the Hexagonal Surface Layer on Caulobacter Crescentus Cells'. *Nature Microbiology* 2:17059. doi: 10.1038/NMICROBIOL.2017.59.

Bisson-Filho, Alexandre W., Yen Pang Hsu, Georgia R. Squyres, Erkin Kuru, Fabai Wu, Calum Jukes, Yingjie Sun, Cees Dekker, Seamus Holden, Michael S. VanNieuwenhze, Yves v. Brun, and Ethan C. Garner. 2017. 'Treadmilling by FtsZ Filaments Drives Peptidoglycan Synthesis and Bacterial Cell Division'. *Science* 355(6326):739–43. doi: 10.1126/SCIENCE.AAK9973/SUPPL_FILE/AAK9973_BISSON-FILHO_SM.PDF.

Biyani, Nikhil, Ricardo D. Righetto, Robert McLeod, Daniel Caujolle-Bert, Daniel Castano-Diez, Kenneth N. Goldie, and Henning Stahlberg. 2017. 'Focus: The Interface between Data Collection and Data Processing in Cryo-EM'. *Journal of Structural Biology* 198(2):124–33. doi: 10.1016/J.JSB.2017.03.007.

Black, Elaine P., Kasia Koziol-Dube, Dongsheng Guan, Jie Wei, Barbara Setlow, Donnamaria E. Cortezzo, Dallas G. Hoover, and Peter Setlow. 2005. 'Factors Influencing Germination of Bacillus Subtilis Spores via Activation of Nutrient Receptors by High Pressure'. *Applied and Environmental Microbiology* 71(10):5879–87. doi: 10.1128/AEM.71.10.5879-5887.2005.

Boland, Fiona M., Abdelmadjid Atrih, Haridasan Chirakkal, Simon J. Foster, and Anne Moir. 2000. 'Complete Spore-Cortex Hydrolysis during Germination of Bacillus Subtilis 168 Requires SleB and YpeB'. *Microbiology* 146(1):57–64. doi: 10.1099/00221287-146-1-57.

Boone, Tyler J., Michael Mallozzi, Alex Nelson, Brian Thompson, Mark Khemmani, Dörte Lehmann, Alexis Dunkle, Paul Hoeprich, Amy Rasley, George Stewart, Adam Driks, Citation TJ Boone, and Alberta Canada. 2018. 'Coordinated Assembly of the Bacillus Anthracis Coat and Exosporium during Bacterial Spore Outer Layer Formation Downloaded From'. doi: 10.1128/mBio.01166-18.

Boydston, Jeremy A., Ping Chen, Christopher T. Steichen, and Charles L. Turnbough. 2005. 'Orientation within the Exosporium and Structural Stability of the Collagen-Like Glycoprotein BclA of Bacillus Anthracis'. *Journal of Bacteriology* 187(15):5310. doi: 10.1128/JB.187.15.5310-5317.2005.

Boydston, Jeremy A., Ling Yue, John F. Kearney, and Charles L. Turnbough. 2006. 'The ExsY Protein Is Required for Complete Formation of the Exosporium of Bacillus Anthracis'. *Journal of Bacteriology* 188(21):7440–48. doi: 10.1128/JB.00639-06/ASSET/5AA52E57-C0C9-4E97-982E-42202D6E9BAD/ASSETS/GRAPHIC/ZJB0210662050007.JPEG.

Bradford, Marion M. 1976. 'A Rapid and Sensitive Method for the Quantitation of Microgram Quantities of Protein Utilizing the Principle of Protein-Dye Binding'. *Analytical Biochemistry* 72(1–2):248–54. doi: 10.1016/0003-2697(76)90527-3.

Brahmbhatt, Trupti N., Brian K. Janes, E. Scott Stibitz, Stephen C. Darnell, Patrick Sanz, Susan B. Rasmussen, and Alison D. O'Brien. 2007. 'Bacillus Anthracis Exosporium Protein BclA Affects Spore Germination, Interaction with Extracellular Matrix Proteins, and Hydrophobicity'. *Infection and Immunity* 75(11):5233. doi: 10.1128/IAI.00660-07.

Breedijk, R. M. P., J. Wen, V. Krishnaswami, T. Bernas, E. M. M. Manders, P. Setlow, N. O. E. Vischer, and S. Brul. 2020. 'A Live-Cell Super-Resolution Technique Demonstrated by Imaging Germinosomes in Wild-Type Bacterial Spores'. *Scientific Reports* 10(1):1–12. doi: 10.1038/s41598-020-62377-1.

Brenner, S., and R. W. Horne. 1959. 'A Negative Staining Method for High Resolution Electron Microscopy of Viruses'. *Biochimica et Biophysica Acta* 34(C):103–10. doi: 10.1016/0006-3002(59)90237-9.

Brunt, Jason, Kathryn L. Cross, and Michael W. Peck. 2015. 'Apertures in the Clostridium Sporogenes Spore Coat and Exosporium Align to Facilitate Emergence of the Vegetative Cell'. *Food Microbiology* 51:45–50. doi: 10.1016/j.fm.2015.04.013.

Brunt, Jason, June Plowman, Duncan J. H. Gaskin, Manoa Itchner, Andrew T. Carter, and Michael W. Peck. 2014. 'Functional Characterisation of Germinant Receptors in Clostridium Botulinum and Clostridium Sporogenes Presents Novel Insights into Spore Germination Systems' edited by A. L. Sonenshein. *PLoS Pathogens* 10(9):e1004382. doi: 10.1371/journal.ppat.1004382.

Callaway, Ewen. 2015. 'The Revolution Will Not Be Crystallized: A New Method Sweeps through Structural Biology'. *Nature* 525(7568):172–74. doi: 10.1038/525172A.

Cartman, Stephen T., Michelle L. Kelly, Daniela Heeg, John T. Heap, and Nigel P. Minton. 2012. 'Precise Manipulation of the Clostridium Difficile Chromosome Reveals a Lack of Association between the TcdC Genotype and Toxin Production'. *Applied and Environmental Microbiology* 78(13):4683–90. doi: 10.1128/AEM.00249-12.

Chau, Mei Hing, and Jeffrey W. Nelson. 1992. 'Cooperative Disulfide Bond Formation in Apamin'. *Biochemistry* 31(18):4445–50. doi: 10.1021/BI00133A009/ASSET/BI00133A009.FP.PNG_V03.

Chesnokova, Olga N., Sylvia A. McPherson, Christopher T. Steichen, and Charles L. Turnbough. 2009. 'The Spore-Specific Alanine Racemase of Bacillus Anthracis and Its Role in Suppressing Germination during Spore Development'. *Journal of Bacteriology* 191(4):1303–10. doi: 10.1128/JB.01098-08.

Chirakkal, Haridasan, Michele O'Rourke, Abdelmadjid Atrih, Simon J. Foster, and Anne Moir. 2002. 'Analysis of Spore Cortex Lytic Enzymes and Related Proteins in Bacillus Subtilis Endoscope Germination'. *Microbiology* 148(8):2383–92. doi: 10.1099/00221287-148-8-2383.

Cortezzo, D. E., and P. Setlow. 2005. 'Analysis of Factors That Influence the Sensitivity of Spores of Bacillus Subtilis to DNA Damaging Chemicals'. *Journal of Applied Microbiology* 98(3):606–17. doi: 10.1111/J.1365-2672.2004.02495.X.

Cowan, Ann E., Elizabeth M. Olivastro, Dennis E. Koppel, Charles A. Loshon, B. Setlow, and Peter Setlow. 2004. 'Lipids in the Inner Membrane of Dormant Spores of Bacillus Species Are Largely Immobile'. *Proceedings of the National Academy of Sciences* 101(20):7733–38. doi: 10.1073/pnas.0306859101.

Crowther, R. A., R. Henderson, and J. M. Smith. 1996. 'MRC Image Processing Programs'. *Journal of Structural Biology* 116(1):9–16. doi: 10.1006/JSBI.1996.0003.

Dafis-Sagarmendi, Ainhoa. 2021. 'Ultrastructure of Clostridial Endospores'. University of Sheffield.

Dembek, Marcin, Lars Barquist, Christine J. Boinett, Amy K. Cain, Matthew Mayho, Trevor D. Lawley, Neil F. Fairweather, and Robert P. Fagan. 2015. 'High-Throughput Analysis of Gene Essentiality and Sporulation in Clostridium Difficile'. *MBio* 6(2). doi: 10.1128/MBIO.02383-14.

Diebolder, C. A., F. G. A. Faas, A. J. Koster, and R. I. Koning. 2015. 'Conical Fourier Shell Correlation Applied to Electron Tomograms'. *Journal of Structural Biology* 190(2):215–23. doi: 10.1016/J.JSB.2015.03.010.

Driks, Adam. 2003. 'The Dynamic Spore'. *Proceedings of the National Academy of Sciences of the United States of America* 100(6):3007–9. doi: 10.1073/PNAS.0730807100/ASSET/DEDC7DF9-A4DF-4810-A9CE-79DE1F15A58B/ASSETS/GRAPHIC/PQ0730807001.JPEG.

Driks, Adam, and Patrick Eichenberger. 2016. 'The Spore Coat'. *Microbiology Spectrum* 4(2). doi: 10.1128/MICROBIOLSPEC.TBS-0023-2016.

Dubochet, J., M. Adrian, J. J. Chang, J. C. Homo, J. Lepault, A. W. McDowall, and P. Schultz. 1988. 'Cryo-Electron Microscopy of Vitrified Specimens'. *Quarterly Reviews of Biophysics* 21(2):129–228. doi: 10.1017/S0033583500004297.

Ebersold, H. R., P. Lüthy, J. L. Cordier, and M. Müller. 1981. 'A Freeze-Substitution and Freeze-Fracture Study of Bacterial Spore Structures'. *Journal of Ultrasructure Research* 76(1):71–81. doi: 10.1016/S0022-5320(81)80051-2.

Faille, Christine, Yannick Lequette, Annette Ronse, Christian Slomianny, Estelle Garénaux, and Yann Guerardel. 2010. 'Morphology and Physico-Chemical Properties of Bacillus Spores Surrounded or Not with an Exosporium: Consequences on Their Ability to Adhere to Stainless Steel'. *International Journal of Food Microbiology* 143(3):125–35. doi: 10.1016/J.IJFOODMICRO.2010.07.038.

Gerhardt, P., and E. Ribi. 1964. 'Ultrastructure Of The Exosporium Enveloping Spores Of Bacillus Cereus.' *Journal of Bacteriology* 88(6):1774–89. doi: 10.1128/jb.88.6.1774-1789.1964.

Ghosh, Sonali, and Peter Setlow. 2009. 'Isolation and Characterization of Superdormant Spores of Bacillus Species'. *Journal of Bacteriology* 191(6):1787–97. doi: 10.1128/JB.01668-08/ASSET/580B9935-58F1-4B23-B158-78762FBD518F/ASSETS/GRAPHIC/ZJB0060985700007.JPEG.

Gibson, Daniel G., Lei Young, Ray-Yuan Chuang, J. Craig Venter, Clyde A. Hutchison, and Hamilton O. Smith. 2009. 'Enzymatic Assembly of DNA Molecules up to Several Hundred Kilobases'. *Nature Methods* 6(5):343–45. doi: 10.1038/nmeth.1318.

Gilbert, Peter. 1972. 'Iterative Methods for the Three-Dimensional Reconstruction of an Object from Projections'. *Journal of Theoretical Biology* 36(1):105–17. doi: 10.1016/0022-5193(72)90180-4.

Gipson, Bryant, Xiangyan Zeng, Zi Yan Zhang, and Henning Stahlberg. 2007. '2dx-User-Friendly Image Processing for 2D Crystals'. *Journal of Structural Biology* 157(1):64–72. doi: 10.1016/j.jsb.2006.07.020.

Glaeser, R. M., J. Baldwin, T. A. Ceska, and R. Henderson. 1986. 'Electron Diffraction Analysis of the M412 Intermediate of Bacteriorhodopsin'. *Biophysical Journal* 50(5):913–20. doi: 10.1016/S0006-3495(86)83532-9.

Harris, J. Robin. 2007. 'Negative Staining of Thinly Spread Biological Samples'. *From: Methods in Molecular Biology* 369:107–42. doi: 10.1007/978-1-59745-294-6_7.

Hashimoto, T., and S. F. Conti. 1971. 'Ultrastructural Changes Associated with Activation and Germination of Bacillus Cereus T Spores.' *Journal of Bacteriology* 105(1):361–68. doi: 10.1128/jb.105.1.361-368.1971.

Heap, John T., Oliver J. Pennington, Stephen T. Cartman, Glen P. Carter, and Nigel P. Minton. 2007. 'The ClosTron: A Universal Gene Knock-out System for the Genus Clostridium'. *Journal of Microbiological Methods* 70(3):452–64. doi: 10.1016/J.MIMET.2007.05.021.

Henderson, R., J. M. Baldwin, T. A. Ceska, F. Zemlin, E. Beckmann, and K. H. Downing. 1990. 'Model for the Structure of Bacteriorhodopsin Based on High-Resolution Electron Cryo-Microscopy'. *Journal of Molecular Biology* 213(4):899–929. doi: 10.1016/S0022-2836(05)80271-2.

Henderson, R., J. M. Baldwin, K. H. Downing, J. Lepault, and F. Zemlin. 1986. 'Structure of Purple Membrane from Halobacterium Halobium: Recording, Measurement and Evaluation of Electron Micrographs at 3.5 Å Resolution'. *Ultramicroscopy* 19(2):147–78. doi: 10.1016/0304-3991(86)90203-2.

Henderson, R., and P. N. T. Unwin. 1975. 'Three-Dimensional Model of Purple Membrane Obtained by Electron Microscopy'. *Nature 1975 257:5521* 257(5521):28–32. doi: 10.1038/257028a0.

Henriques, Adriano O., and Charles P. Moran. 2000. 'Structure and Assembly of the Bacterial Endospore Coat'. *Methods* 20(1):95–110. doi: 10.1006/METH.1999.0909.

Henriques, Adriano O., and Charles P. Moran, Jr. 2007. 'Structure, Assembly, and Function of the Spore Surface Layers'. *Annual Review of Microbiology* 61(1):555–88. doi: 10.1146/annurev.micro.61.080706.093224.

Hoeniger, J. F., and C. L. Headley. 1969. 'Ultrastructural Aspects of Spore Germination and Outgrowth in Clostridium Sporogenes.' *Canadian Journal of Microbiology* 15(9):1061–65. doi: 10.1139/m69-189.

Ihekwaba, Adaoha E. C., Ivan Mura, John Walshaw, Michael W. Peck, and Gary C. Barker. 2016. 'An Integrative Approach to Computational Modelling of the Gene Regulatory Network Controlling Clostridium Botulinum Type A1 Toxin Production' edited by N. D. Price. *PLOS Computational Biology* 12(11):e1005205. doi: 10.1371/journal.pcbi.1005205.

Janganan, Thamarai K., Nic Mullin, Ainhoa Dafis-Sagarmendi, Jason Brunt, Svetomir B. Tzokov, Sandra Stringer, Anne Moir, Roy R. Chaudhuri, Robert P. Fagan, Jamie K. Hobbs, and Per A. Bullough. 2020. 'Architecture and Self-Assembly of Clostridium Sporogenes and Clostridium Botulinum Spore Surfaces Illustrate a General Protective Strategy Across Spore Formers'. *MSphere* 5(4):424–44. doi: 10.1128/mSphere.00424-20.

Janganan, Thamarai K., Nic Mullin, Svetomir B. Tzokov, Sandra Stringer, Robert P. Fagan, Jamie K. Hobbs, Anne Moir, and Per A. Bullough. 2016. 'Characterization of the Spore Surface and Exosporium Proteins of Clostridium Sporogenes; Implications for Clostridium Botulinum Group I Strains'. *Food Microbiology* 59:205–12. doi: 10.1016/j.fm.2016.06.003.

Jiang, Shuo, Qiang Wan, Daniela Krajcikova, Jilin Tang, Svetomir B. Tzokov, Imrich Barak, and Per A. Bullough. 2015. 'Diverse Supramolecular Structures Formed by Self-Assembling Proteins of the Bacillus Subtilis Spore Coat'. *Molecular Microbiology* 97(2):347–59. doi: 10.1111/mmi.13030.

Johnson, Matt J., Sarah J. Todd, David A. Ball, Andrew M. Shepherd, Patricia Sylvestre, and Anne Moir. 2006. 'ExsY and CotY Are Required for the Correct Assembly of the Exosporium and Spore Coat of Bacillus Cereus'. *Journal of Bacteriology* 188(22):7905–13. doi: 10.1128/JB.00997-06.

Jumper, John, Richard Evans, Alexander Pritzel, Tim Green, Michael Figurnov, Olaf Ronneberger, Kathryn Tunyasuvunakool, Russ Bates, Augustin Žídek, Anna Potapenko, Alex Bridgland, Clemens Meyer, Simon A. A. Kohl, Andrew J. Ballard, Andrew Cowie, Bernardino Romera-Paredes, Stanislav Nikolov, Rishub Jain, Jonas Adler, Trevor Back, Stig Petersen, David Reiman, Ellen Clancy, Michal Zielinski, Martin Steinegger, Michalina Pacholska, Tamas Berghammer, Sebastian Bodenstein, David Silver, Oriol Vinyals, Andrew W. Senior, Koray Kavukcuoglu, Pushmeet Kohli, and Demis Hassabis. 2021. 'Highly Accurate Protein Structure Prediction with AlphaFold'. *Nature 2021 596:7873* 596(7873):583–89. doi: 10.1038/s41586-021-03819-2.

Kailas, Lekshmi, Cassandra Terry, Nicholas Abbott, Robert Taylor, Nic Mullin, Svetomir B. Tzokov, Sarah J. Todd, B. A. Wallace, Jamie K. Hobbs, Anne Moir, and Per A. Bullough. 2011. 'Surface Architecture of Endospores of the Bacillus Cereus/Anthracis/ Thuringiensis Family at the Subnanometer Scale'. *Proceedings of the National Academy of Sciences of the United States of America* 108(38):16014–19. doi: 10.1073/pnas.1109419108.

Khaneja, R., L. Perez-Fons, S. Fakhry, L. Baccigalupi, S. Steiger, E. To, G. Sandmann, T. C. Dong, E. Ricca, P. D. Fraser, and S. M. Cutting. 2010. 'Carotenoids Found in Bacillus'. *Journal of Applied Microbiology* 108(6):1889–1902. doi: 10.1111/j.1365-2672.2009.04590.x.

Khanna, Kanika, Javier Lopez-Garrido, and Kit Pogliano. 2020. 'Shaping an Endospore: Architectural Transformations During *Bacillus Subtilis* Sporulation'. *Annual Review of Microbiology* 74(1):361–86. doi: 10.1146/annurev-micro-022520-074650.

Khanna, Kanika, Javier Lopez-Garrido, Joseph Sugie, Kit Pogliano, and Elizabeth Villa. 2021. 'Asymmetric Localization of the Cell Division Machinery during Bacillus Subtilis Sporulation'. *ELife* 10. doi: 10.7554/ELIFE.62204.

Khanna, Kanika, Javier Lopez-Garrido, Ziyi Zhao, Reika Watanabe, Yuan Yuan, Joseph Sugie, Kit Pogliano, and Elizabeth Villa. 2019. 'The Molecular Architecture of Engulfment during Bacillus Subtilis Sporulation'. *ELife* 8:498220. doi: 10.7554/elife.45257.

Kirk, David G., Elias Dahlsten, Zhen Zhang, Hannu Korkeala, and Miia Lindström. 2012. 'Involvement of Clostridium Botulinum ATCC 3502 Sigma Factor K in Early-Stage Sporulation'. *Applied and Environmental Microbiology* 78(13):4590–96. doi: 10.1128/AEM.00304-12/SUPPL_FILE/AEM-AEM00304-12-S01.PDF.

Kirk, David G., Zhen Zhang, Hannu Korkeala, and Miia Lindström. 2014. 'Alternative Sigma Factors SigF, SigE, and SigG Are Essential for Sporulation in Clostridium Botulinum ATCC 3502'. *Applied and Environmental Microbiology* 80(16):5141. doi: 10.1128/AEM.01015-14.

Kirk, Joseph A., and Robert P. Fagan. 2016. 'Heat Shock Increases Conjugation Efficiency in Clostridium Difficile'. *Anaerobe* 42:1–5. doi: 10.1016/J.ANAEROBE.2016.06.009.

Koning, Roman I., Abraham J. Koster, and Thomas H. Sharp. 2018. 'Advances in Cryo-Electron Tomography for Biology and Medicine'. *Annals of Anatomy - Anatomischer Anzeiger* 217:82–96. doi: 10.1016/J.AANAT.2018.02.004.

Kühlbrandt, Werner. 2014. 'The Resolution Revolution'. *Science* 343(6178):1443–44. doi: 10.1126/SCIENCE.1251652/ASSET/71F1CC4C-5202-4323-A43C-1F8F1197BD97/ASSETS/GRAPHIC/343_1443_F1.JPEG.

Laemmli, U. K. 1970. 'Cleavage of Structural Proteins during the Assembly of the Head of Bacteriophage T4'. *Nature 1970 227:5259* 227(5259):680–85. doi: 10.1038/227680a0.

Lanzoni-Mangutchi, Paola, Oishik Banerji, Jason Wilson, Anna Barwinska-Sendra, Joseph A. Kirk, Filipa Vaz, Shauna O'Beirne, Arnaud Baslé, Kamel el Omari, Armin Wagner, Neil F. Fairweather, Gillian R. Douce, Per A. Bullough, Robert P. Fagan, and Paula S. Salgado. 2022. 'Structure and Assembly of the S-Layer in C. Difficile'. *Nature Communications 2022 13:1* 13(1):1–13. doi: 10.1038/s41467-022-28196-w.

Laue, Michael, Hong Mei Han, Christin Dittmann, and Peter Setlow. 2018. 'Intracellular Membranes of Bacterial Endospores Are Reservoirs for Spore Core Membrane Expansion during Spore Germination'. *Scientific Reports* 8(1):11388. doi: 10.1038/s41598-018-29879-5.

Lehmann, Dörte, Margaret Sladek, Mark Khemmani, Tyler J. Boone, Eric Rees, and Adam Driks. 2022. 'Role of Novel Polysaccharide Layers in Assembly of the Exosporium, the Outermost Protein Layer of the *Bacillus Anthracis* Spore'. *Molecular Microbiology*. doi: 10.1111/MMI.14966.

Lopez-Garrido, Javier, Nikola Ojkic, Kanika Khanna, Felix R. Wagner, Elizabeth Villa, Robert G. Endres, and Kit Pogliano. 2018. 'Chromosome Translocation Inflates Bacillus Forespores and Impacts Cellular Morphology'. *Cell* 172(4):758-770.e14. doi: 10.1016/j.cell.2018.01.027.

Lorenzo, Jose M., Paulo E. Munekata, Ruben Dominguez, Mirian Pateiro, Jorge A. Saraiva, and Daniel Franco. 2018. 'Main Groups of Microorganisms of Relevance for Food Safety and Stability: General Aspects and Overall Description'. *Innovative Technologies for Food Preservation* 53. doi: 10.1016/B978-0-12-811031-7.00003-0.

Lyumkis, Dmitry. 2019. 'Challenges and Opportunities in Cryo-EM Single-Particle Analysis'. *The Journal of Biological Chemistry* 294(13):5181. doi: 10.1074/JBC.REV118.005602.

Marko, Michael, Chyongere Hsieh, Richard Schalek, Joachim Frank, and Carmen Mannella. 2007. 'Focused-Ion-Beam Thinning of Frozen-Hydrated Biological Specimens for Cryo-Electron Microscopy'. *Nature Methods 2007 4:3* 4(3):215–17. doi: 10.1038/nmeth1014.

Mastronarde, David N. 1997. 'Dual-Axis Tomography: An Approach with Alignment Methods That Preserve Resolution'. *Journal of Structural Biology* 120(3):343–52. doi: 10.1006/JSBI.1997.3919.

Mastronarde, David N., and Susannah R. Held. 2017a. 'Automated Tilt Series Alignment and Tomographic Reconstruction in IMOD'. *Journal of Structural Biology* 197(2):102–13. doi: 10.1016/J.JSB.2016.07.011.

Mastronarde, David N., and Susannah R. Held. 2017b. 'Automated Tilt Series Alignment and Tomographic Reconstruction in IMOD'. *Journal of Structural Biology* 197(2):102–13. doi: 10.1016/J.JSB.2016.07.011.

Matias, Valério R. F., and Terry J. Beveridge. 2007. 'Cryo-Electron Microscopy of Cell Division in Staphylococcus Aureus Reveals a Mid-Zone between Nascent Cross Walls'. *Molecular Microbiology* 64(1):195–206. doi: 10.1111/J.1365-2958.2007.05634.X.

McDonald, Kent L., and Manfred Auer. 2006. 'High-Pressure Freezing, Cellular Tomography, and Structural Cell Biology'. *BioTechniques* 41(2):137–43. doi: 10.2144/000112226/ASSET/IMAGES/LARGE/FIGURE2.JPEG.

Mckenney, Peter T., Adam Driks, and Patrick Eichenberger. 2012. 'The Bacillus Subtilis Endospore: Assembly and Functions of the Multilayered Coat'. *Nature Reviews Microbiology 2012 11:1* 11(1):33–44. doi: 10.1038/nrmicro2921.

McKenney, Peter T., and Patrick Eichenberger. 2012. 'Dynamics of Spore Coat Morphogenesis in Bacillus Subtilis'. *Molecular Microbiology* 83(2):245–60. doi: 10.1111/J.1365-2958.2011.07936.X.

McMullan, G., S. Chen, R. Henderson, and A. R. Faruqi. 2009. 'Detective Quantum Efficiency of Electron Area Detectors in Electron Microscopy'. *Ultramicroscopy* 109(9):1126–43. doi: 10.1016/J.ULTRAMIC.2009.04.002.

Meador-Parton, Jennifer, and David L. Popham. 2000. 'Structural Analysis of Bacillus Subtilis Spore Peptidoglycan during Sporulation'. *Journal of Bacteriology* 182(16):4491. doi: 10.1128/JB.182.16.4491-4499.2000.

Moir, A., B. M. Corfe, and J. Behravan. 2002. 'Spore Germination'. *Cellular and Molecular Life Sciences CMLS 2002 59:3* 59(3):403–9. doi: 10.1007/S00018-002-8432-8.

Nuyts, Sandra, L. Van Mellaert, J. Theys, W. Landuyt, P. Lambin, and J. Anné. 2002. 'Clostridium Spores for Tumor-Specific Drug Delivery'. *Anti-Cancer Drugs* 13(2):115–25.

Olguín-Araneda, Valeria, Saeed Banawas, Mahfuzur R. Sarker, and Daniel Paredes-Sabja. 2015. 'Recent Advances in Germination of Clostridium Spores'. *Research in Microbiology* 166(4):236–43.

Paidhungat, M., K. Ragkousi, and P. Setlow. 2001. 'Genetic Requirements for Induction of Germination of Spores of Bacillus Subtilis by Ca2+-Dipicolinate'. *Journal of Bacteriology* 183(16):4886–93. doi: 10.1128/JB.183.16.4886-4893.2001.

Panessa-Warren, B. J., G. T. Tortora, and J. B. Warren. 1997. 'Exosporial Membrane Plasticity of Clostridium Sporogenes and Clostridium Difficile'. *Tissue and Cell* 29(4):449–61. doi: 10.1016/S0040-8166(97)80031-6.

Panessa-Warren, Barbara J., George T. Tortora, and John B. Warren. 1994. 'Electron Microscopy of C. Sporogenes Endospore Attachment and Germination'. *Scanning* 16(4):227–40. doi: 10.1002/sca.4950160408.

Paredes-Sabja, Daniel, Peter Setlow, and Mahfuzur R. Sarker. 2011. 'Germination of Spores of Bacillales and Clostridiales Species: Mechanisms and Proteins Involved'. *Trends in Microbiology* 19(2):85–94.

Peck, Michael W. 2009. 'Biology and Genomic Analysis of Clostridium Botulinum'. *Advances in Microbial Physiology* 55:183–320.

Peck, Michael W., Sandra C. Stringer, and Andrew T. Carter. 2011. 'Clostridium Botulinum in the Post-Genomic Era'. *Food Microbiology* 28(2):183–91.

Piggot, Patrick J., and David W. Hilbert. 2004. 'Sporulation of Bacillus Subtilis'. *Current Opinion in Microbiology* 7(6):579–86. doi: 10.1016/J.MIB.2004.10.001.

Plomp, Marco, Terrance J. Leighton, Katherine E. Wheeler, Haley D. Hill, and Alexander J. Malkin. 2007. 'In Vitro High-Resolution Structural Dynamics of Single Germinating Bacterial Spores.' *Proceedings of the National Academy of Sciences of the United States of America* 104(23):9644–49. doi: 10.1073/pnas.0610626104.

Popham, D. L. 2002. 'Specialized Peptidoglycan of the Bacterial Endospore: The Inner Wall of the Lockbox'. *Cellular and Molecular Life Sciences CMLS 2002 59:3* 59(3):426–33. doi: 10.1007/S00018-002-8435-5.

Portinha, Inês M., François P. Douillard, Hannu Korkeala, and Miia Lindström. 2022. 'Sporulation Strategies and Potential Role of the Exosporium in Survival and Persistence of Clostridium Botulinum'. *International Journal of Molecular Sciences* 23(2):754. doi: 10.3390/ijms23020754.

Punjani, Ali, John L. Rubinstein, David J. Fleet, and Marcus A. Brubaker. 2017. 'CryoSPARC: Algorithms for Rapid Unsupervised Cryo-EM Structure Determination'. *Nature Methods 2017 14:3* 14(3):290–96. doi: 10.1038/nmeth.4169.

Purdy, Des, Triona A. T. O'Keeffe, Michael Elmore, Mike Herbert, Anne McLeod, Monika Bokori-Brown, Anna Ostrowski, and Nigel P. Minton. 2002. 'Conjugative Transfer of Clostridial Shuttle Vectors from Escherichia Coli to Clostridium Difficile through Circumvention of the Restriction Barrier'. *Molecular Microbiology* 46(2):439–52. doi: 10.1046/J.1365-2958.2002.03134.X.

Radermacher, Michael. 1988. 'Three-Dimensional Reconstruction of Single Particles from Random and Nonrandom Tilt Series'. *Journal of Electron Microscopy Technique* 9(4):359–94. doi: 10.1002/JEMT.1060090405.

Ragkousi, Katerina, Patrick Eichenberger, Christiaan Van Ooij, and Peter Setlow. 2003. 'Identification of a New Gene Essential for Germination of Bacillus Subtilis Spores with Ca2+-Dipicolinate'. *Journal of Bacteriology* 185(7):2315–29. doi: 10.1128/JB.185.7.2315-2329.2003.

Ransom, Eric M., Craig D. Ellermeier, and David S. Weiss. 2015. 'Use of MCherry Red Fluorescent Protein for Studies of Protein Localization and Gene Expression in Clostridium Difficile'. *Applied and Environmental Microbiology* 81(5):1652–60. doi: 10.1128/AEM.03446-14.

Redmond, Caroline, Leslie W. J. Baillie, Stephen Hibbs, Arthur J. G. Moir, and Anne Moir. 2004. 'Identification of Proteins in the Exosporium of Bacillus Anthracis'. *Microbiology* 150(2):355–63. doi: 10.1099/mic.0.26681-0.

Renault, Ludovic, Hui Ting Chou, Po Lin Chiu, Rena M. Hill, Xiangyan Zeng, Bryant Gipson, Zi Yan Zhang, Anchi Cheng, Vinzenz Unger, and Henning Stahlberg. 2006. 'Milestones in Electron Crystallography'. *Journal of Computer-Aided Molecular Design* 20(7–8):519–27. doi: 10.1007/S10822-006-9075-X/FIGURES/3.

Riemann, Hans, and Z. John Ordal. 1961. 'Germination of Bacterial Endospores with Calcium and Dipicolinic Acid'. *Science* 133(3465):1703–4. doi: 10.1126/science.133.3465.1703.

Rode, L. J., and J. W. Foster. 1961. 'Germination of Bacterial Spores with Alkyl Primary Amines'. *Journal of Bacteriology* 81(5).

de Rosier, D. J., and A. Klug. 1968. 'Reconstruction of Three Dimensional Structures from Electron Micrographs'. *Nature 1968 217:5124* 217(5124):130–34. doi: 10.1038/217130a0.

Santo, L. Y., and R. H. Doi. 1974. 'Ultrastructural Analysis during Germination and Outgrowth of Bacillus Subtilis Spores.' *Journal of Bacteriology* 120(1):475–81.

Sarker, Mahfuzur R., Saeed Akhtar, J. Antonio Torres, and Daniel Paredes-Sabja. 2015. 'High Hydrostatic Pressure-Induced Inactivation of Bacterial Spores'. *Critical Reviews in Microbiology* 41(1):18–26. doi: 10.3109/1040841X.2013.788475.

Scheres, Sjors H. W. 2012. 'RELION: Implementation of a Bayesian Approach to Cryo-EM Structure Determination'. *Journal of Structural Biology* 180(3):519–30. doi: 10.1016/J.JSB.2012.09.006.

Schill, Kristin M., Yun Wang, Robert R. Butler, Jean François Pombert, N. Rukma Reddy, Guy E. Skinner, and John W. Larkin. 2016. 'Genetic Diversity of Clostridium Sporogenes PA 3679 Isolates Obtained from Different Sources as Resolved by Pulsed-Field Gel Electrophoresis and High-Throughput Sequencing'. *Applied and Environmental Microbiology* 82(1):384–93. doi: 10.1128/AEM.02616-15/SUPPL_FILE/ZAM999116835SO1.PDF.

Setlow, Barbara, Swaroopa Atluri, Ryan Kitchel, Kasia Koziol-Dube, and Peter Setlow. 2006. 'Role of Dipicolinic Acid in Resistance and Stability of Spores of Bacillus Subtilis with or without DNA-Protective α/β-Type Small Acid-Soluble Proteins'. *Journal of Bacteriology* 188(11):3740–47. doi: 10.1128/JB.00212-06.

Setlow, P. 2006. 'Spores of Bacillus Subtilis: Their Resistance to and Killing by Radiation, Heat and Chemicals'. *Journal of Applied Microbiology* 101(3):514–25. doi: 10.1111/j.1365-2672.2005.02736.x.

Setlow, P. 2013. 'Summer Meeting 2013 - When the Sleepers Wake: The Germination of Spores of Bacillus Species'. *Journal of Applied Microbiology* 115(6):1251–68.

Setlow, Peter. 2007. 'I Will Survive: DNA Protection in Bacterial Spores'. *Trends in Microbiology* 15(4):172–80.

Setlow, Peter. 2014. 'Germination of Spores of Bacillus Species: What We Know and Do Not Know'. *Journal of Bacteriology* 196(7):1297–1305.

Setlow, Peter, Shiwei Wang, and Yong-Qing Li. 2017. 'Germination of Spores of the Orders *Bacillales* and *Clostridiales*'. *Annual Review of Microbiology* 71(1):459–77. doi: 10.1146/annurev-micro-090816-093558.

Stahlberg, Henning, Nikhil Biyani, and Andreas Engel. 2015. '3D Reconstruction of Two-Dimensional Crystals'. *Archives of Biochemistry and Biophysics* 581:68–77. doi: 10.1016/J.ABB.2015.06.006.

Steichen, Christopher, Ping Chen, John F. Kearney, and Charles L. Turnbough. 2003. 'Identification of the Immunodominant Protein and Other Proteins of the Bacillus Anthracis Exosporium'. *Journal of Bacteriology* 185(6):1903–10. doi: 10.1128/JB.185.6.1903-1910.2003.

Steichen, Christopher T., John F. Kearney, and Charles L. Turnbough. 2005. 'Characterization of the Exosporium Basal Layer Protein BxpB of Bacillus Anthracis'. *Journal of Bacteriology* 187(17):5868. doi: 10.1128/JB.187.17.5868-5876.2005.

Steichen, Christopher T., John F. Kearney, and Charles L. Turnbough. 2007. 'Non-Uniform Assembly of the Bacillus Anthracis Exosporium and a Bottle Cap Model for Spore Germination and Outgrowth'. *Molecular Microbiology* 64(2):359–67. doi: 10.1111/j.1365-2958.2007.05658.x.

Stevenson, K. E., R. H. Vaughn, and E. v. Crisan. 1972. 'Fixation of Mature Spores of Clostridium Botulinum'. *Journal of Bacteriology* 109(3):1295. doi: 10.1128/JB.109.3.1295-1297.1972.

Stewart, George C. 2015. 'The Exosporium Layer of Bacterial Spores: A Connection to the Environment and the Infected Host'. *Microbiology and Molecular Biology Reviews* 79(4):437–57. doi: 10.1128/mmbr.00050-15.

Sylvestre, Patricia, Evelyne Couture-Tosi, and Michele Mock. 2002. 'A Collagen-like Surface Glycoprotein Is a Structural Component of the Bacillus Anthracis Exosporium'. *Molecular Microbiology* 45(1):169–78. doi: 10.1046/j.1365-2958.2000.03000.x.

Sylvestre, Patricia, Evelyne Couture-Tosi, and Michèle Mock. 2003. 'Polymorphism in the Collagen-like Region of the Bacillus Anthracis BclA Protein Leads to Variation in Exosporium Filament Length'. *Journal of Bacteriology* 185(5):1555–63. doi: 10.1128/JB.185.5.1555-1563.2003/ASSET/E92E8E7C-545D-4938-A831-953FC506BE3A/ASSETS/GRAPHIC/JB0531218006.JPEG.

Sylvestre, Patricia, Evelyne Couture-Tosi, and Michèle Mock. 2005. 'Contribution of ExsFA and ExsFB Proteins to the Localization of BclA on the Spore Surface and to the Stability of the Bacillus Anthracis Exosporium'. *Journal of Bacteriology* 187(15):5122–28. doi: 10.1128/JB.187.15.5122-5128.2005/ASSET/C1F9CE99-2E14-43C0-8F1E-36B04F51FC82/ASSETS/GRAPHIC/ZJB0150549200005.JPEG.

Tan, Li, and Charles L. Turnbough. 2010. 'Sequence Motifs and Proteolytic Cleavage of the Collagen-Like Glycoprotein BclA Required for Its Attachment to the Exosporium of Bacillus Anthracis'. *Journal of Bacteriology* 192(5):1259–68. doi: 10.1128/JB.01003-09.

Terry, Cassandra, Shuo Jiang, David S. Radford, Qiang Wan, Svetomir Tzokov, Anne Moir, and Per A. Bullough. 2017. 'Molecular Tiling on the Surface of a Bacterial Spore – the Exosporium of the Bacillus Anthracis/Cereus/Thuringiensis Group'. *Molecular Microbiology* 104(4):539–52. doi: 10.1111/mmi.13650.

Thompson, Brian M., Bryce C. Hoelscher, Adam Driks, and George C. Stewart. 2012. 'Assembly of the BclB Glycoprotein into the Exosporium and Evidence for Its Role in the Formation of the Exosporium "cap" Structure in Bacillus Anthracis'. *Molecular Microbiology* 86(5):1073–84. doi: 10.1111/mmi.12042.

Thompson, Rebecca F., Matt Walker, C. Alistair Siebert, Stephen P. Muench, and Neil A. Ranson. 2016. 'An Introduction to Sample Preparation and Imaging by Cryo-Electron Microscopy for Structural Biology'. *Methods* 100:3–15. doi: 10.1016/J.YMETH.2016.02.017.

Todd, Sarah J., Arthur J. G. Moir, Matt J. Johnson, and Anne Moir. 2003. 'Genes of Bacillus Cereus and Bacillus Anthracis Encoding Proteins of the Exosporium'. *Journal of Bacteriology* 185(11):3373–78. doi: 10.1128/JB.185.11.3373-3378.2003.

Tovar-Rojo, F., M. Chander, B. Setlow, and P. Setlow. 2002. 'The Products of the SpoVA Operon Are Involved in Dipicolinic Acid Uptake into Developing Spores of Bacillus Subtilis'. *Journal of Bacteriology* 184(2):584–87. doi: 10.1128/JB.184.2.584-587.2002.

Unwin, P. N. T., and R. Henderson. 1975. 'Molecular Structure Determination by Electron Microscopy of Unstained Crystalline Specimens'. *Journal of Molecular Biology* 94(3):425–40. doi: 10.1016/0022-2836(75)90212-0.

Valpuesta, José María, José L. Carrascosa, and Richard Henderson. 1994. 'Analysis of Electron Microscope Images and Electron Diffraction Patterns of Thin Crystals of Ø29 Connectors in Ice'. *Journal of Molecular Biology* 240(4):281–87. doi: 10.1006/JMBI.1994.1445.

Vepachedu, Venkata Ramana, and Peter Setlow. 2007. 'Role of SpoVA Proteins in Release of Dipicolinic Acid during Germination of Bacillus Subtilis Spores Triggered by Dodecylamine or Lysozyme'. *Journal of Bacteriology* 189(5):1565–72. doi: 10.1128/JB.01613-06.

Waller, Lashanda N., Nyssa Fox, Karen F. Fox, Alvin Fox, and Robert L. Price. 2004. 'Ruthenium Red Staining for Ultrastructural Visualization of a Glycoprotein Layer Surrounding the Spore of Bacillus Anthracis and Bacillus Subtilis'. *Journal of Microbiological Methods* 58(1):23–30. doi: 10.1016/J.MIMET.2004.02.012.

Walz, Jochen, Dieter Typke, Michael Nitsch, Abraham J. Koster, Reiner Hegerl, and Wolfgang Baumeister. 1997. 'Electron Tomography of Single Ice-Embedded Macromolecules: Three-Dimensional Alignment and Classification'. *Journal of Structural Biology* 120(3):387–95. doi: 10.1006/JSBI.1997.3934.

Wang, Shiwei, Jason Brunt, Michael W. Peck, Peter Setlow, and Yong Qing Li. 2017. 'Analysis of the Germination of Individual Clostridium Sporogenes Spores with and without Germinant Receptors and Cortex-Lytic Enzymes'. *Frontiers in Microbiology* 8(OCT):2047. doi: 10.3389/fmicb.2017.02047.

Wang, Yanyu, Sarah A. Jenkins, Chunfang Gu, Ankita Shree, Margarita Martinez-Moczygemba, Jennifer Herold, Marina Botto, Rick A. Wetsel, and Yi Xu. 2016. 'Bacillus Anthracis Spore Surface Protein BclA Mediates Complement Factor H Binding to Spores and Promotes Spore Persistence'. *PLoS Pathogens* 12(6). doi: 10.1371/JOURNAL.PPAT.1005678.

Warth, A. D. 1978. 'Molecular Structure of the Bacterial Spore'. *Advances in Microbial Physiology* 17(C):1–45. doi: 10.1016/S0065-2911(08)60056-9.

Wehrli, E., P. Scherrer, and O. Kuebler. 1980. 'The Crystalline Layers in Spores of Bacillus Cereus and Bacillus Thuringiensis Studied by Freeze-Etching and High Resolution Electron Microscopy.' *European Journal of Cell Biology* 20(3):283–89.

Westphal, Andrew J., P. Buford Price, Terrance J. Leighton, and Katherine E. Wheeler. 2003. 'Kinetics of Size Changes of Individual Bacillus Thuringiensis Spores in Response to Changes in Relative Humidity'. *Proceedings of the National Academy of Sciences of the United States of America* 100(6):3461–66. doi: 10.1073/PNAS.232710999/ASSET/12488712-3EDF-4106-9961-A29866176C2E/ASSETS/GRAPHIC/PQ0237109006.JPEG.

Wu, Ling Juan, and Jeffery Errington. 1994. 'Bacillus Subtilis SpoIIIE Protein Required for DNA Segregation During Asymmetric Cell Division'. *Science* 264(5158):572–75. doi: 10.1126/SCIENCE.8160014.

Wu, Ling Juan, and Jeffery Errington. 1998. 'Use of Asymmetric Cell Division and SpoIIIE Mutants to Probe Chromosome Orientation and Organization in Bacillus Subtilis'. *Molecular Microbiology* 27(4):777–86. doi: 10.1046/J.1365-2958.1998.00724.X.

Yi, Xuan, and Peter Setlow. 2010. 'Studies of the Commitment Step in the Germination of Spores of Bacillus Species'. *Journal of Bacteriology* 192(13):3424–33. doi: 10.1128/JB.00326-10.

Zeng, Gengsheng L. 2012. 'A Filtered Backprojection Algorithm with Characteristics of the Iterative Landweber Algorithm'. *Medical Physics* 39(2):603. doi: 10.1118/1.3673956.

Appendices

Appendix 1: List of Oligos and Plasmids Used in this Study

Name	Sequence 5'-3'	Restriction Site
RF311	TAGGGTAACAAAAAACACCG	
RF312	CCTTTTTGATAATCTCATGACC	
RF1686	AATACGGTGTTTTTTGTTACCCTAGAGCTCGATTGCTCTTAGGATTTTATAAT AATATATTAATTG	
RF1687	GGAAAAATCATGAGTTAATATTTAAAAATAATTGTTTGAAATG	
RF1688	TATTTTTAAATATTAACTCATGATTTTTCCCCC	
RF1689	TTGGTCATGAGATTATCAAAAAGGGGATCCTTATTGAAGAGGCTTTTATTG	
RF1825	TAATATTTAAAAATAATTGTTTGAAATGAATCTTAAC	
RF1877	GCTACG <u>GAGCTC</u> GTAATTAAGAAGGAGTGATTACATGAAC	SacI
RF1878	GCTACG <u>GGATCC</u> TTATTTCCTCCCGTTAAATAATAGATAAC	BamHI
RF1885	TTCTATGAGTCGCTTTTGTAAATTTG	
RF1886	TCAAACAATTATTTTTAAATATTAGCGGCCGCATTATTAAAAAAAATTAC	
RF1887	CAAAAGCGACTCATAGAATTATTTCCTCCCGTTAAATAATAGATAAC	
RF2074	GATC <u>CTCGAG</u> ATTGCATGGATGAGTATAGTTAGC	XhoI
RF2075	GATC <u>CATATG</u> ATGAGTAAATCTTCAGAAGAAAGATGG	NdeI
RF2077	GATC <u>CTCGAG</u> GTGTTCCTTTGATCTACATCCCAAGCCACCAGC	XhoI
RF2078	GATC <u>CCATGG</u> ATGATGTCAATGGATGAAATGAGAGG	NcoI

List of Plasmids

Plasmid Name	Description	Source
pJAK014	Plasmid containing P_{cwp2}	Dr Joseph Kirk
pJAK184	Mutagenesis plasmid for KO of *slpA* in *C. difficile* containing *mazF* under the inducible P_{xyl} promotor for counter selection	Dr Joseph Kirk
pJAK188	pJAK184 with additional terminator sequence to prevent readthrough into homology arms	Dr Joseph Kirk
pHF001	Mutagenesis plasmid for KO of *csxB*	This study
pHF007	pJAK014 with *ermB* inserted under P_{cwp2}	This study
pHF009	Mutagenesis plasmid for KO of *csxB*. pHF001 with P_{cwp2}-*ermB* inserted between homology arms	This study
pHF010	Mutagenesis plasmid for KO of *csxA*	This study
pHF012	pJAK188 with insertion between P_{xyl} promoter and *mazF* corrected	This study

pHF013	Mutagenesis plasmid for KO of *csxC*	This study
pHF014	Mutagenesis plasmid for KO of *bclB*	This study
pHF015	Mutagenesis plasmid for KO of *bclA*	This study
pTER001	Overexpression plasmid for expressing C-terminally His tagged CsxC	This study
pTER003	Overexpression plasmid for expressing C-terminally His tagged CsxB	This study

Appendix 2: Composition of Gibson Assembly Master Mix

2X Gibson Assembly Master Mix

Prepare Isothermal Start Mix

1.5 g PEG_{8000}

3 ml 1 M Tris-HCl, pH 8.0

150 µl 2 M $MgCl_2$

2X Gibson Assembly Master Mix

405 µl Isothermal Start Mix

25 µl 1 M DTT

20 µl 25 mM dNTPs

50 µl NAD+ (NEB Cat. B9007S)

1 µl T5 exonuclease (NEB Cat. M0363S – 10 units/µl)

31.25 µl Phusion High Fidelity DNA Polymerase (NEB Cat. M0530S – 2 units/µl)

250 µl Taq Ligase (NEB Cat. M0208S – 40 units/µl)

467.75 µl H_2O

Makes 100 µl aliquots.

Appendix 3: Timelapse of Phase Contrast Live Cell Imaging of *C. sporogenes* Germination

Appendix 4: Emergence Behaviours of Spores in Timelapse

Spores are colour coded according to the emergence behaviour of the vegetative cell from the spore outer layers. Red indicates cell emerges from the extended pole of the exosporium, light blue from the non-extended exosporium pole, light green polar emergence but no clear extended pole to the exosporium, purple no distinguishable exosporium but polar germination, orange no outgrowth, and black no phase change.
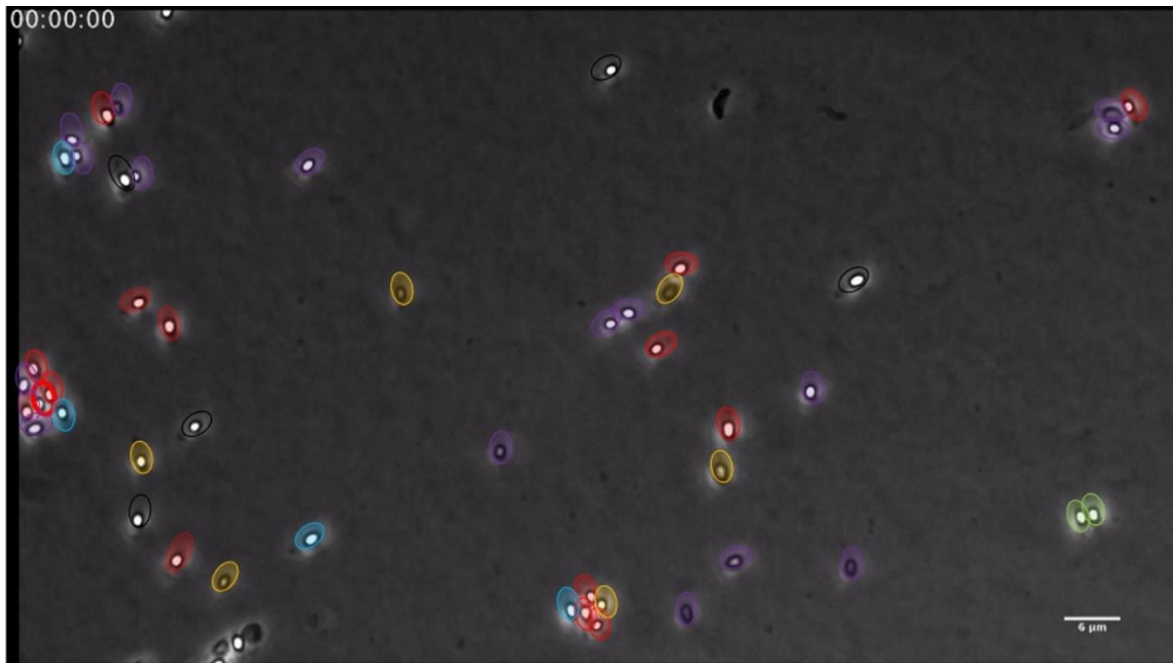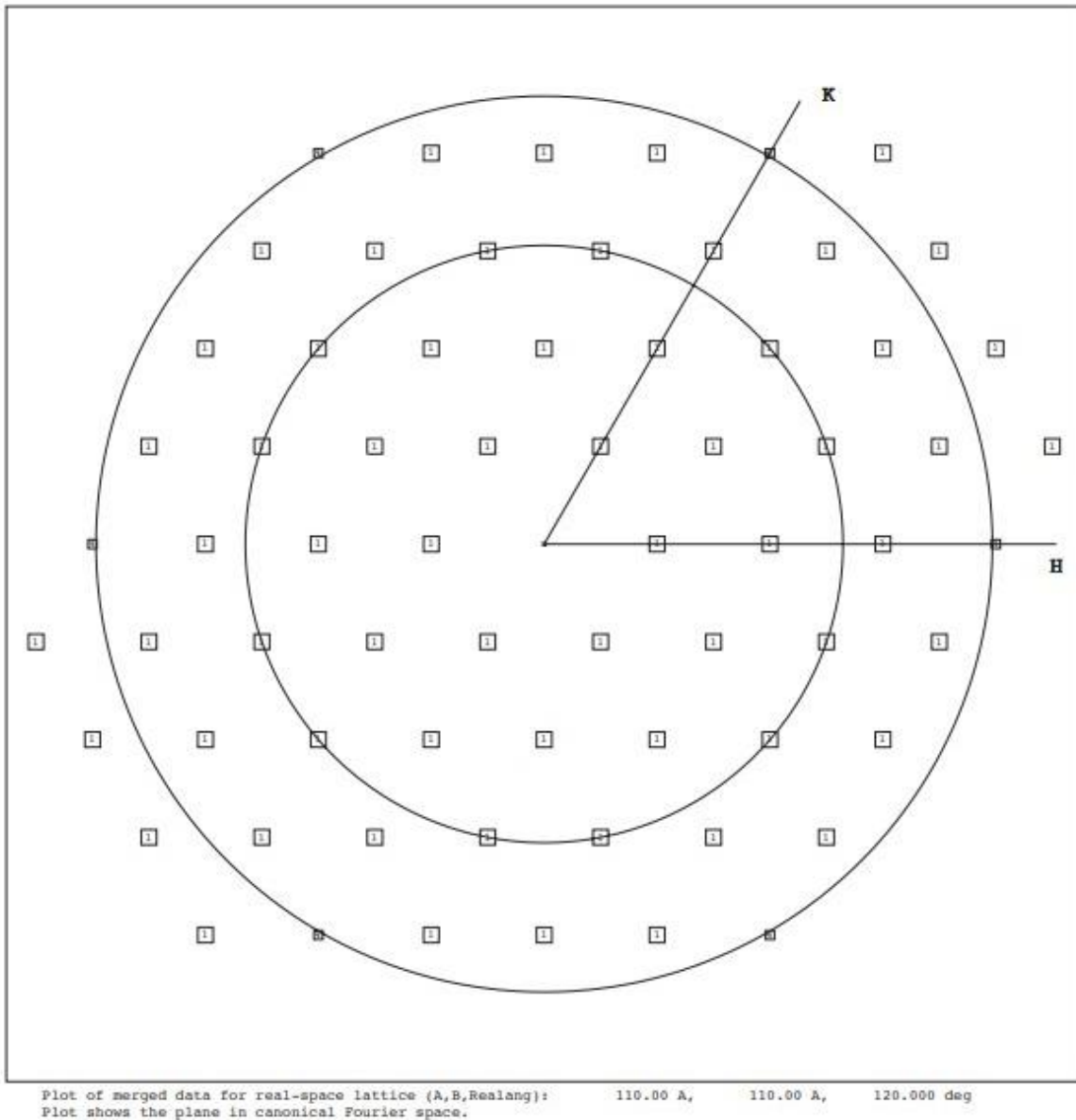

■ Extended Pole

■ Non-extended Pole

■ Even Poles

■ Polar Germination – No clear extended pole

■ No Outgrowth

■ Phase Bright

Appendix 5: Resolution Circle Plot for Merged 2D Projection Map of Post Germination Exosporium. The reflections are indicated in squares with the numbers representing the IQ values. Resolution rings at 36Å and 24Å are shown.

Symbols based on FOM:

Symbol:	1	2	3	4	5	6	7	8	9
FOM:	>95	>90	>85	>80	>75	>70	>65	>60	<60

Resolution Max (Nyquist of plot) at   20.00 A

Resolution Ring at   36.00 A
Resolution Ring at   24.00 A

Plot of merged data for real-space lattice (A,B,Realang):   110.00 A,   110.00 A,   120.000 deg
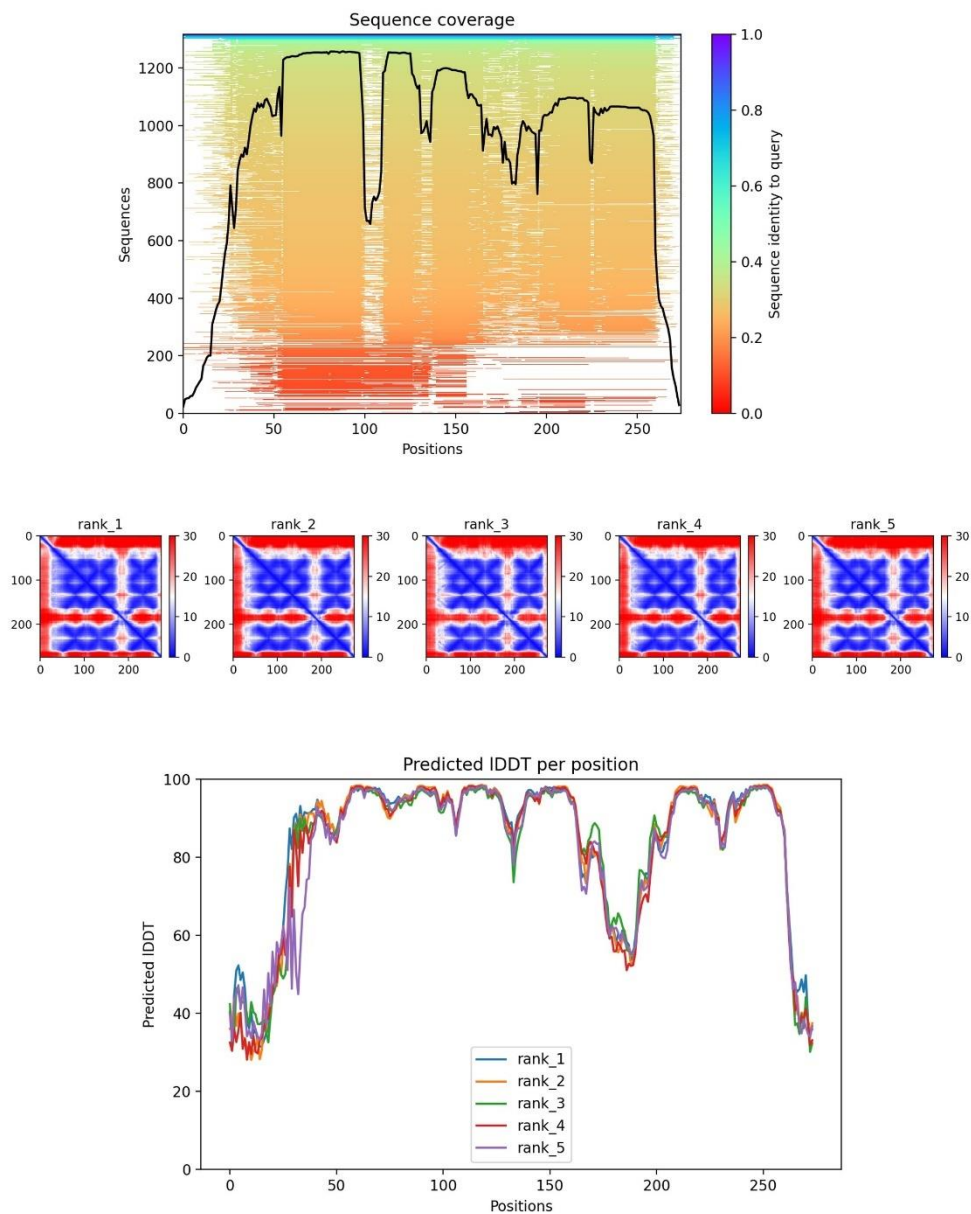Plot shows the plane in canonical Fourier space.

Appendix 6: Alphafold2 Confidence Outputs for CsxC Monomer Structure

A) Sequence Coverage plot shows how many homologous sequences have been identified with structures available in the PDB database and are colour coded by their sequence identity.

B) Predicted Aligned Error (PAE) plot shows the confidence in the alignment between individual residues within the structure. Residues within the same domain structure tend to have a higher confidence i.e. a lower PAE value.

C) Amino acid position vs confidence of prediction at that position. A value of 80 or above indicates a confident prediction.

Appendix 7: Alphafold2 Confidence Outputs for CsxC Trimer Structure

A) Sequence Coverage plot shows how many homologous sequences have been identified with structures available in the PDB database and are colour coded by their sequence identity.

B) Predicted Aligned Error (PAE) plot shows the confidence in the alignment between individual residues within the structure. Residues within the same domain of the structure tend to have a higher confidence i.e. a lower PAE value. For the rank 1 model there was also high confidence between residues from multiple monomer domains.

C) Amino acid position vs confidence of prediction at that position. A value of 80 or above indicates a confident prediction.